

Soils and Rocks

An International Journal of Geotechnical
and Geoenvironmental Engineering



Volume 42, N. 2
May-August 2019

SOILS and ROCKS

An International Journal of Geotechnical and Geoenvironmental Engineering

Editor Paulo Scarano Hemsí - Aeronautics Institute of Technology, Brazil

Co-editor José Couto Marques - University of Porto, Portugal

Executive Board

Waldemar Coelho Hachich
University of São Paulo, Brazil
António Topa Gomes
University of Porto, Portugal

Renato Pinto Cunha
University of Brasília, Brazil
Rafaela Cardoso
University of Lisbon, Portugal

José Antonio Schiavon (*Secretary*)
Aeronautics Institute of Technology, Brazil

Associate Editors

H. Einstein
MIT, USA
John A. Hudson
Imperial College, UK
Kenji Ishihara
University of Tokyo, Japan
Michele Jamiolkowski
Studio Geotecnico Italiano, Italy
Willy A. Lacerda
COPPE/UFRJ, Brazil

E. Maranha das Neves
Lisbon Technical University, Portugal
Nielen van der Merve
University of Pretoria, South Africa
Paul Marinos
NTUA, Greece
James K. Mitchell
Virginia Tech., USA
Lars Persson
SGU, Sweden

Harry G. Poulos
University of Sidney, Australia
Niek Rengers
ITC, The Netherlands
Fumio Tatsuoka
Tokyo University of Science, Japan
Luiz González de Vallejo
UCM, Spain
Roger Frank
ENPC-Cermes, France

Editorial Board Members

Roberto F. Azevedo
Federal University of Viçosa, Brazil
Milton Kanji
University of São Paulo, Brazil
Kátia Vanessa Bicalho
Federal University of Espírito Santo, Brazil
Omar Y. Bitar
IPT, Brazil
Lázaro V. Zuquette
University of São Paulo at São Carlos, Brazil
Fabio Taioli
University of São Paulo, Brazil
Tarcisio Celestino
University of São Paulo at São Carlos, Brazil
Edmundo Rogério Esquivel
University of São Paulo at São Carlos, Brazil
Nilo C. Consoli
Federal Univ. Rio Grande do Sul, Brazil
Sandro S. Sandroni
Consultant, Brazil
Sérgio A.B. Fontoura
Pontifical Catholic University, Brazil
Ennio M. Palmeira
University of Brasília, Brazil
Luciano Décourt
Consultant, Brazil
Façal Massad
University of São Paulo, Brazil
Marcus Pacheco
University of the State of Rio de Janeiro, Brazil
Paulo Maia
University of Northern Rio de Janeiro, Brazil
Renato Cunha
University of Brasília, Brazil

Orencio Monje Vilar
University of São Paulo at São Carlos, Brazil
Maria Eugenia Boscov
University of São Paulo, Brazil
Eda Freitas de Quadros
BGTECH, Brazil
Tácio de Campos
Pontifical Catholic University of Rio de Janeiro, Brazil
Richard J. Bathurst
Royal Military College of Canada
Robert Mair
University of Cambridge, UK
Serge Leroueil
University of Laval, Canada
Mario Manassero
Politécnico di Torino, Italy
Luis Valenzuela
Consultant, Chile
Jorge G. Zornberg
University of Texas/Austin, USA
Andrew Whittle
MIT, USA
Pierre Bérest
LCPC, France
Peter Kaiser
Laurentian University, Canada
He Manchao
CUMT, China
Teruo Nakai
Nagoya Inst. Technology, Japan
Claudio Olalla
CEDEX, Spain
Frederick Baynes
Baynes Geologic Ltd., Australia

R. Kerry Rowe
Queen's University, Canada
R. Jonathan Fannin
University of British Columbia, Canada
Laura Caldeira
LNEC, Portugal
António S. Cardoso
University of Porto, Portugal
José D. Rodrigues
Consultant, Portugal
António G. Coelho
Consultant, Portugal
Luís R. Sousa
University of Porto, Portugal
Rui M. Correia
LNEC, Portugal
João Marcelino
LNEC, Portugal
António C. Mineiro
University of Lisbon, Portugal
António P. Cunha
LNEC, Portugal New
António G. Correia
University of Minho, Portugal
Carlos D. Gama
Lisbon Technical University, Portugal
José V. Lemos
LNEC, Portugal
Nuno Grossmann
LNEC, Portugal
Luís L. Lemos
University of Coimbra, Portugal
Ricardo Oliveira
COBA, Portugal

“Ad hoc” Reviewers (2019)

Soils and Rocks is indebted to all “ad hoc” reviewers.

A complete list of reviewers that contributed to the current volume of Soils and Rocks will be published here in the December issue.

Soils and Rocks publishes papers in English in the broad fields of Geotechnical Engineering, Engineering Geology and Geoenvironmental Engineering. The Journal is published in April, August and December. Subscription price is US\$ 90.00 per year. The journal, with the name “Solos e Rochas”, was first published in 1978 by the Graduate School of Engineering, Federal University of Rio de Janeiro (COPPE-UFRJ). In 1980 it became the official magazine of the Brazilian Association for Soil Mechanics and Geotechnical Engineering (ABMS), acquiring the national character that had been the intention of its founders. In 1986 it also became the official Journal of the Brazilian Association for Engineering Geology and the Environment (ABGE) and in 1999 became the Latin American Geotechnical Journal, following the support of Latin-American representatives gathered for the Pan-American Conference of Guadalajara (1996). In 2007 the journal acquired the status of an international journal under the name of Soils and Rocks, published by the Brazilian Association for Soil Mechanics and Geotechnical Engineering (ABMS), Brazilian Association for Engineering Geology and the Environment (ABGE) and Portuguese Geotechnical Society (SPG). In 2010, ABGE decided to publish its own journal and left the partnership.

Soils and Rocks

1978,	1 (1, 2)
1979,	1 (3), 2 (1,2)
1980-1983,	3-6 (1, 2, 3)
1984,	7 (single number)
1985-1987,	8-10 (1, 2, 3)
1988-1990,	11-13 (single number)
1991-1992,	14-15 (1, 2)
1993,	16 (1, 2, 3, 4)
1994-2010,	17-33 (1, 2, 3)
2011,	34 (1, 2, 3, 4)
2012-2018,	35-41 (1, 2, 3)
2019,	42 (1, 2,

ISSN 1980-9743

CDU 624.131.1

SOILS and ROCKS

An International Journal of Geotechnical and Geoenvironmental Engineering

Publication of**ABMS - Brazilian Association for Soil Mechanics and Geotechnical Engineering****SPG - Portuguese Geotechnical Society****Volume 42, N. 2, May-August 2019****Table of Contents****ARTICLES**

<i>Progressive Mapping and Urban Growth: The Construction of Urbanization Suitability Map of Pelotas-Southern Brazil</i>	
S.C. Xavier, L.A. Bressani	99
<i>Soil Elastic Modulus Determined by Ultrasound Tests</i>	
W.S. Sarro, G.C.S. Ferreira	117
<i>Geotechnical Behavior and Soil-Fiber Interaction of Clayey Soil Mixed with Randomly Dispersed Coconut Fibers</i>	
A.I. Oliveira Júnior, J.F.T. Jucá, J.A. Ferreira, L.C. Guilherme	127
<i>Geological-Geotechnical Characterization of Slopes Belonging to the Serra do Mar Paranaense, Brazil</i>	
A.A.M. González, L.B. Passini, R.B. Boszczowski, A.C.M. Kormann, A.P. Fiori	139
<i>Investigating the Differences between Various Deterministic Liquefaction Correlation Methods</i>	
E. El Kahi, M. Khouri	155
<i>Soil Classification System from Cone Penetration Test Data Applying Distance-Based Machine Learning Algorithms</i>	
L.O. Carvalho, D.B. Ribeiro	167
<i>An Alternative Method to Estimate the Effective Energy During Pile Driving Based on Set and Elastic Rebound Records</i>	
A. Querelli, F. Massad	179

TECHNICAL NOTES

<i>Biodegradation of Biodiesel in Laboratory and Field in a Clayey Residual Soil</i>	
A. Thomé, A.W.S. Trentin, I. Cecchin, C. Reginato	193
<i>Dynamic Cone Penetrometer (DCP) relative density correlations for sands</i>	
C.J. MacRobert, G.S. Bernstein, M.M. Nchabeleng	201

Articles

Soils and Rocks
v. 42, n. 2

Progressive Mapping and Urban Growth: The Construction of Urbanization Suitability Map of Pelotas-Southern Brazil

S.C. Xavier, L.A. Bressani

Abstract. Significant portions of Brazilian city populations are subjected to an imbalance of environmental systems and geological and geotechnical risks. Such factors can only be properly addressed through planning and actions that take into account both the potential and limitations of the physical environment to urban land use. In this sense, geotechnical mapping plays a vital role in confronting problems that are inherent to any land affected by human activity, since, at its core, involves the study of mapping methods and processes which focus on the urban environment. Geotechnical mapping allows for the production of information for management planning and sustainable growth of the city. This work describes the structure and application of a geotechnical mapping methodology that incorporates both the study of urban growth and progressive mapping techniques. Based on the use of pre-existing information, this methodology was applied to the city of Pelotas in Southern Brazil, generating information regarding the physical environment of the city. Such information was fundamental for the planning and the control of occupation and land use, as well as for the development of susceptibility mapping for geodynamic processes (floods and erosion), which served as the basis for the development of urbanization suitability map of the urban voids of the city.

Keywords: geotechnical mapping, map of susceptibility, territorial planning, urban growth.

1. Introduction

The physical and environmental systems of Brazilian cities were strongly impacted by the population growth that occurred after the first decades of the last century. Pollution, deforestation, biodiversity reduction, waste production and disposal, occupation of inadequate areas (such as hill slopes, environmental preservation areas and flood plains of watercourses) are some examples of the problems associated with city growth. From the second decade of the last century to the first decade of the twenty-first century, Brazilian urbanization increased from 10.7% (Santos, 1998) to 84.35% (IBGE, 2011): a transformation of profound qualitative consequences in terms of structuring the urban environment.

There is a consensus on the necessity of intervention in the process of growth and development of Brazilian cities, in order to ensure a more balanced socio-environmental space (Rolnik, 1994), as well as about the central role of urban planning in this process (Ferreira & Ferreira, 2011; Namur & Boeira, 2005; Oliveira, 2011). Notwithstanding, for planning to play its role in the sustainable organization and development of the city, it is imperative that the actors involved in this process have extensive knowledge of the physical and environmental characteristics of the planned environment.

An adequate knowledge of the local physical environment is indispensable for the development of urban plans. According to Ferreira dos Santos (2004), “planning is a

process that involves the collection, organization and systemic analysis of information to make decisions about the best alternatives for resources of the planned environment”. Thus, identification of an area’s suitability and weaknesses, as well as prediction of human impact, are fundamental for the proper planning and the urban legislation that follows, in order to prescribe relevant rules of use and occupation for the area. In this context, Geotechnical Charts are fundamental tools for analysis and integrated systematization of environmental processes, allowing for the understanding and handling of problems that can occur when implementing activities that significantly modify the environment.

Among the different types and styles of maps and geotechnical charts, process susceptibility maps and urbanization suitability maps are among the products of geotechnical cartography that have direct applications in land use planning and urban planning. Geotechnical susceptibility maps represent cartographically the pre-disposition of terrains, according to their characteristics, in order to develop a certain phenomenon and/or process of the physical environment in different forms and degrees (Fell *et al.*, 2008; Julião *et al.*, 2009; Sobreira & Souza, 2012; Diniz, 2012; Diniz & Freitas, 2013; Bressani & Costa, 2013). Sobreira & Souza (2012) define the suitability for urbanization as the capacity of the lands to support the different uses and practices of engineering and urbanism, with the least impact and highest level of safety possible. The urbanization suitability map is essential to an integrated approach to the physi-

Sinval Cantarelli Xavier, Dr., Associate Professor, Escola de Engenharia, Universidade Federal do Rio Grande, Rio Grande, RS, Brazil, e-mail: xavier.sinval@gmail.com.
Luiz Antônio Bressani, Ph.D., Full Professor, Programa de Pós-Graduação em Construção e Infraestrutura, Universidade Federal do Rio Grande do Sul, Porto Alegre, RS, Brazil, e-mail: bressani@ufrgs.br.
Submitted on January 16, 2018; Final Acceptance on July 8, 2019; Discussion open until December 31, 2019.
DOI: 10.28927/SR.422099

cal-environmental, legal and socio-economic-organizational axes of the areas available and/or intended for urban sprawl, on which analyses must be carried out in order to indicate their potentialities and restrictions (Sobreira & Souza, 2012).

With the development of geotechnical mapping in the world after World War II (Caballero, 1973) and in Brazil after the 1980's, several international methodologies were developed and published, such as the International Association for Engineering Geology and the Environment (IAEG), the Pattern Unit Component Evaluation System (PUCE), the French Methodology and the ZERMOS methodology (Zones Exposed to Risks of Movements of the Soils). Nationally, the methodologies of the Technological Research Institute of the State of São Paulo SA – IPT, of the School of Engineering of São Carlos - EESC/USP, the Progressive Detailing (UNESP/Rio Claro) and the Diniz & Freitas methodology (2013) were also developed. These and other classical methodologies of geotechnical mapping that largely focus on the execution of engineering works, prevention or resolution of geological-geotechnical problems, do not explicitly differentiate the constructed urban environment from the one built in the mapping processes. That is to say, they treat both in the same way, whether in obtaining attributes or in the procedures for the development of geotechnical cartographic products. Moreover, the methodologies do not incorporate the analysis of the urban morphology or the dynamics of its transformation into the mapping process. In this sense, there is room and pertinence for a better delimitation of the object of study, in this case the city, as well as a need for new investigations for better adaptations of existing environmental mapping techniques. Therefore, the present work reports the experience of applying a methodological proposal focusing on the environment of the city. The proposal is based on: a) the appropriation of concepts of mapping methods used in Brazil, especially the progressive mapping; b) the preponderant use of pre-existing data and; c) the technique of reducing the areas for analysis through morphological studies and

urban growth patterns. The main objective is to contribute to the development of tools to aid in the planning of sustainable growth of the city.

The study was developed in the city of Pelotas, State of Rio Grande do Sul, Brazil. Pelotas has a territorial area of 1,609 km² and is located in the coordinate quadrilateral 31°19'; 31°48' South latitude and 52°36'; 52°00' West longitude (Fig. 1). Its estimated population is 341,648 inhabitants (IBGE, 2018), with an urbanization index of 93.27%.

The municipality is divided into two large geomorphological regions: the plains and lowland areas, which make up an overlapping landscape (Coastal Plain), and the undulating area, which constitutes a tectonic relief (Plateau). The Northwest half of the municipality includes shield border formations and colluvial deposits, or crystalline plateau dissected with fractures, with or without unevenness. The Southeast portion, where the urban zone is inserted, corresponds to the flat and low area of the municipality, which is a fluvial-lacustrine plain with stretches of floodplains, especially the regions of the São Gonçalo Channel and the Patos Lagoon (Rosa, 1985) (Fig. 2 and Table 1).

2. Materials and Methods

A literary review of geotechnical cartography and accumulated Brazilian scientific knowledge allows us to verify a solid base for the investigation and proposition of new forms of mapping. In order to shape the present methodology, concepts of the methods elaborated by Cerri *et al.* (1996), Dias (1995), Diniz & Freitas (2013), Sobreira & Souza (2012) and Souza & Sobreira (2014) were used in combination with techniques of analysis, studies of morphology and urban growth.

The basis of this methodology is progressive detailing, through which the geotechnical mapping is developed in three consecutive stages, at increasing levels of detail and scale (Cerri *et al.*, 1996). The progressive method focuses on the idea that more generic studies should point out the needs to the more specific ones, so as to obtain more de-



Figure 1 - Pelotas municipality location.

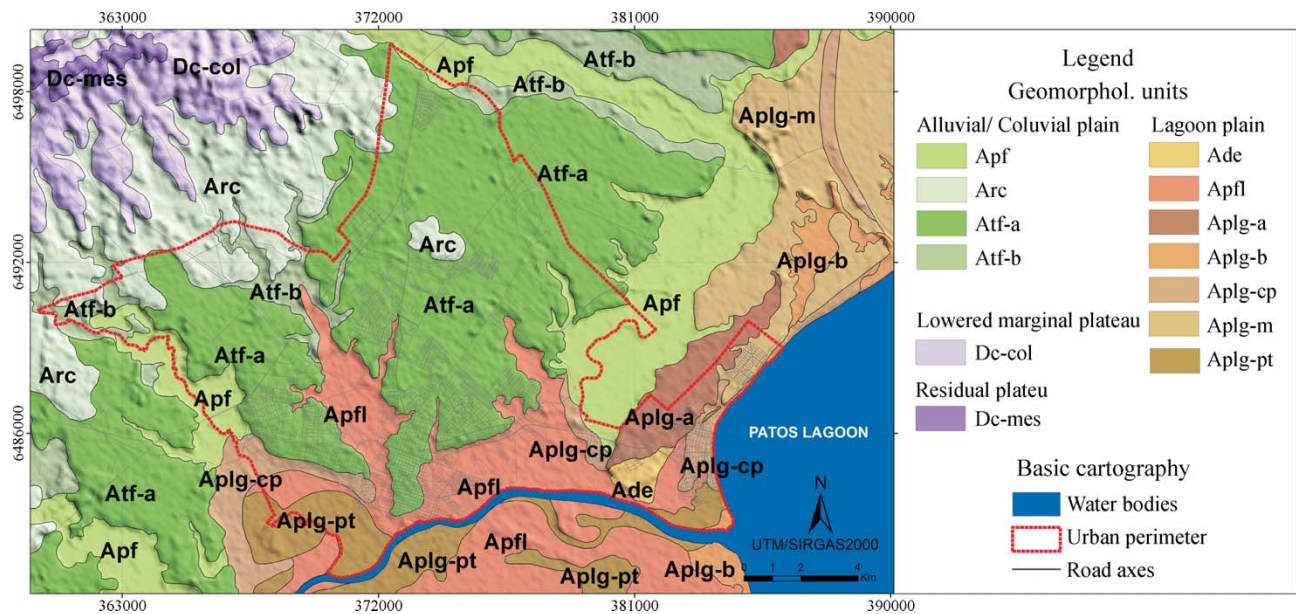


Figure 2 - Map of relief forms of the urban area of Pelotas and its surroundings.

Table 1 - Forms of reliefs with their main characteristics.

Morphological units	Forms of relief	Geological period	Average slope (%)	Local ampl. (m)	
Residual Plateau	Dc-mes	Hills with gentle slopes	Pre-Cambrian	11.25	95-185
Lowered marginal plateau	Dc-col	Hillock	Pre-Cambrian	8.70	50-120
Alluvial/colluvial plain	Arc	Deposits of colluvium	Neogene	5.60	25-85
	Apf	Fluvial deposits	Pleistocene/ Holocene	2.74	1.5-25
	Atf-a	Deposits of high alluvial terrace	Pliocene	2.56	7-35
	Atf-b	Deposits of low alluvial terrace	Pleistocene/ Holocene	2.78	7-15
Lagoon plain	Ade	Eolian deposits	Holocene	3.50	4-20
	Apfl	Deposits of fluviolake plain	Holocene	1.83	0-5
	Aplg-b	Deposits of low lagoonal plain	Holocene	1.86	0.5-10
	Aplg-m	Deposits of medium lagoonal plain	Holocene	1.90	4-12
	Aplg-a	Deposits of high lagoonal plain	Pleistocene	2.10	10-15
	Aplg-cp	Deposits of crest and lagoon beaches	Holocene	2.29	0.50-5
	Aplg-pt	Dep. of marshes and peats swamps of plain	Holocene	1.62	0-1

tailed and precise evaluations where necessary, while not losing the regional contours of the study and not wasting efforts. Sobreira & Souza (2012) argue that progressive detailing in planning and urban planning practices can be represented at their levels through only susceptibility (general stage) and suitability for urbanization (intermediate stage), thus in this work the mapping was developed for the first two stages of the progressive method: general and intermediate.

Mapping followed a sequence of four main stages: 1 - inventory; 2 - data preparation; 3 - general stage of the progressive method; 4 - semi-detail (intermediate) stage of the progressive method (Fig. 3). The use of the proposed method presupposes the existence of a minimum base of information of the physical environment, being necessary, at least: basic cartography; pedology; geology; geomorphology; altimetry; aerial imagery and geotechnical surveys. The lack of one or more of these basic pieces of information

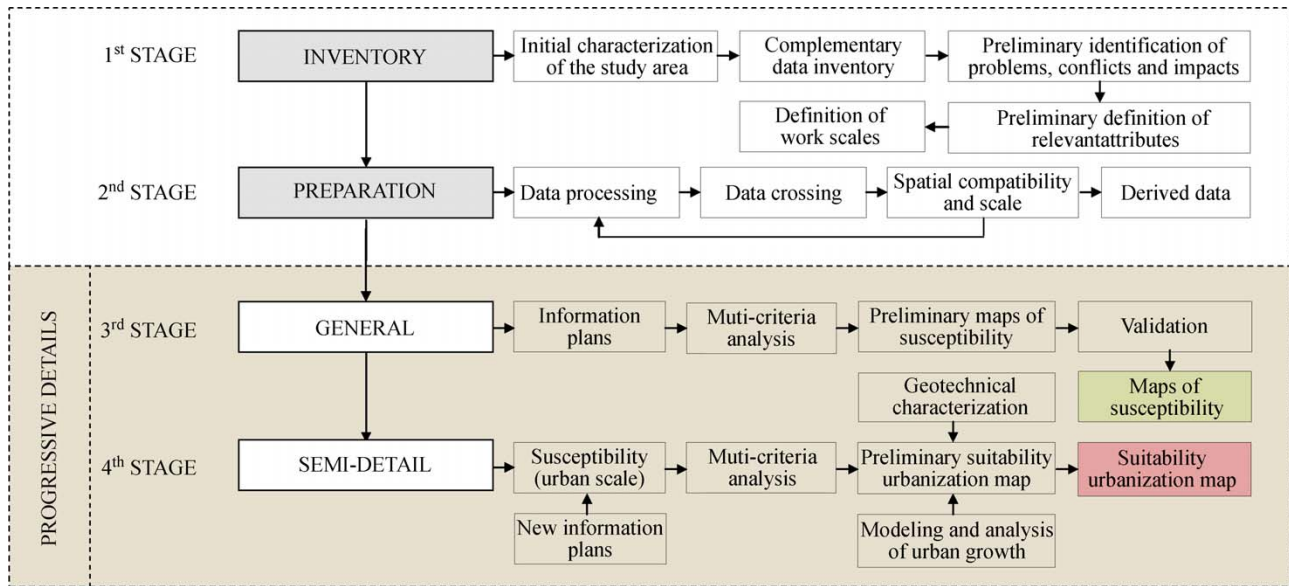


Figure 3 - Stages of development and sequence of the main mapping procedures.

determined whether specific techniques would be incorporated during the mapping process. Compatibility between scales of mapping and the scales of the basic themes was also essential, or where lacking, the possibility of their adaptation was considered.

2.1. Inventory stage

The inventory stage, with adaptations and additions, follows the proposal of Diniz & Freitas (2013), and is subdivided into the following steps: 1.1 - initial characterization of the study area; 1.2 - complementary data inventory; 1.3 - preliminary identification of problems, conflicts and impacts associated with the physical environment; 1.4 - preliminary definition of relevant attributes; 1.5 - definition of work scales.

The initial characterization of the study area (step 1.1) aims at a general and comprehensive understanding of the physical environment aspects fundamental to development, dealing with topics relevant to the geotechnical mapping and indispensable to the understanding of local processes. The “complementary data inventory” step (step 1.2) concerns the collection of environmental data and is dedicated to prospecting and systematizing available information, as well as analyses and classifications regarding the content, scale and potential for exploitation. Step 1.3 aims at preliminary identification of geological-geotechnical problems, conflicts and negative impacts of human action on the local physical environment, obtained through an initial characterization survey. The next step (step 1.4), is dedicated to the identification of attributes relevant to the geological-geotechnical mapping of the study area. The final step (step 1.5) is to define the compatibility scales of the basic maps and the final scales of the cartographic mapping products

(maps and charts), which are based on inventoried data, relevant attributes and available literature.

2.2. Preparation stage

The second general stage of the methodology corresponds to the preparation of data for mapping. In this stage, prospected data is processed and cross-checked, aiming at spatial and scalar compatibility and generation of derivative data. For the potential development of mapping operations, it is of paramount importance that the data produced be stored in the form of “Information Plans” and tables in a geographic database and processed using Geographic Information System (GIS) software. Geomorphological information constitutes the main basis for data integration, due both to its close relationship with the analysis themes and its relative importance in the geological-geotechnical mapping works, especially in countries with a tropical climate (Diniz, 2012).

2.3. General stage of the progressive method

In this stage of the method, the progressive detail is represented by susceptibility, that is, by the predisposition of the lands to the occurrence of geodynamic processes, which is represented by classes of occurrence possibilities. Although susceptibility is predominantly analyzed through the predisposing natural conditions, in the case of the urban environment, the anthropic action must be considered in some specific situations, such as in the cases of the relevant technogenic features that have decisively altered the natural processes and land use.

The elaboration of susceptibility map(s) is based on an integrated approach of the different environmental aspects that condition the development of the geodynamic processes previously detected in the first stage of mapping.

In data integration, each of the themes has a differentiated importance in relation to the analyzed process, being therefore open to the weighting of values or indices for the different units. Thus, in order to evaluate the attributes and themes, a multicriteria analysis (also known as decision tree or hierarchical analysis of weights), was used for mapping susceptibility (Sobreira & Souza, 2012). The multicriteria analysis is based on the mapping of variables (attributes) by information plane and on the definition of the pertinence degree of the plans and their legend components, in the construction of the final result. Among the different methods used to integrate factors based on the multicriteria approach, we opted for the Weighted Linear Combination, in which the factors are standardized for a common numerical scale, weighted and combined by means of a weighted average (Voogd, 1983). According to Torezan (2005), the method, besides allowing for the retention of the variability of the continuous data, offers the possibility for the environmental parameters to compensate with each other.

The distribution of weights is required in two hierarchical levels: in the first one for classes (attributes) that compose the legend of the information plans (themes); and in the second for the plans to be integrated by means of map algebra. At the level of plan classes, the weighting was carried out by data-driven evaluation, which refers to the knowledge of similar situations (Moura, 2005) achieved through previous analysis of existing works and field survey. In order to reduce the subjectivity associated with the distribution of weights, at this level, we selected portions of the territory where the result of the analyzed phenomenon is known (in its greater and lesser occurrence) and, thus, the study of the relations between the variables and the definition of their weights were validated, in comparison to the behavior of these samples. In the second level, the Analytic Hierarchy Process (AHP) (Saaty, 1977) method was used, which is one of the most used systems to aid multicriteria

decision making (Fernandes, 2016). The AHP method is based on the pairwise comparison of the analyzed attributes, allowing an evaluation their relative importance. AHP basically consists of prioritizing the relative importance of “n” decision-making elements against a pre-established goal. By means of comparative evaluations of the elements the method facilitates the analysis by the evaluator that, through the application of a consistency index, can verify if the values assigned to each pair of criteria are coherent (Rafaeli & Müller, 2007).

Figure 4 schematically represents the data and the sequence of procedures employed to create the susceptibility map. According to the schematic sequence, after the multicriteria analysis and integration of the plans, a preliminary map is produced to be validated through event history, process evidences and field work. The non-validation of the map determines whether the process will be repeated with new attribution of the weights, until the results can be confirmed. Following the recommendation of Cerri *et al.* (1996), the mapping territory of the general stage was defined as: urbanized areas, areas with medium-term urbanization prospects and adjacent areas. This is done with the intention of characterizing the environmental areas of influence, in relation to urban occupation both current and future.

2.4. Intermediate stage of the progressive method

The mapping of the intermediate stage of the progressive method (or semi-detail stage) is represented by the suitability of lands to urbanization, and utilizes the urban zones and legally established urban expansion zones as initial area of analysis. Susceptibility maps formed the initial database for urbanization suitability mapping. The use of these maps, however, requires the adjustment of their spatial resolution to the larger scale of suitability mapping. Furthermore, urbanization suitability mapping involves other aspects related to territory that surpass those used in

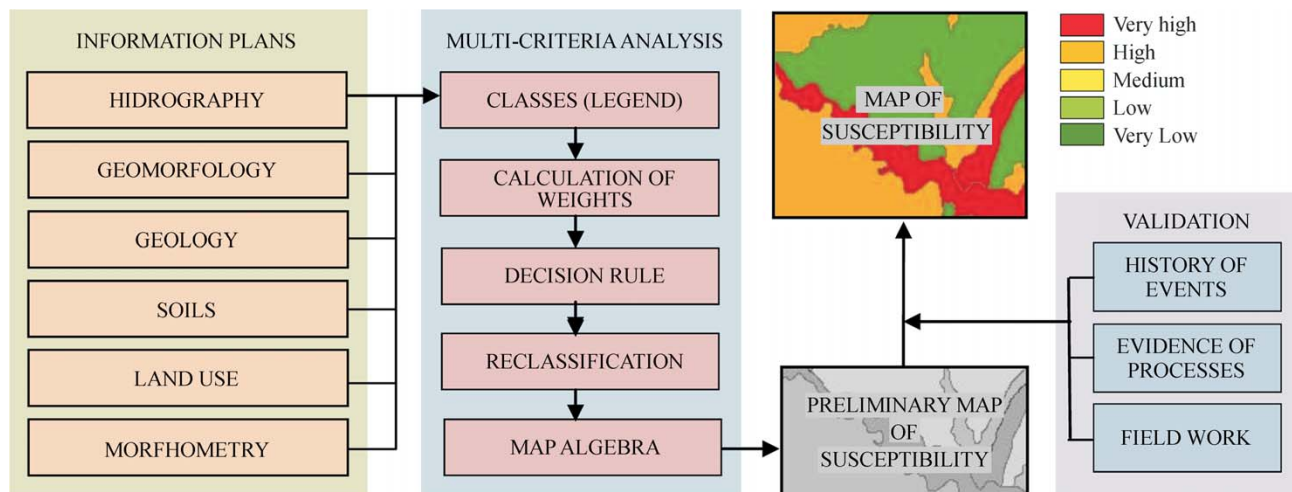


Figure 4 - Schematic sequence of procedures for the development of susceptibility maps for geodynamic processes.

the mapping of susceptibilities and it is therefore necessary to include more information plans involving other aspects of the environment (natural or anthropogenic), such as the geotechnical unit plan. For the mapping of geotechnical units, the methodology proposed by Dias (1995) was used, which is based on the cross-referencing of geological, pedological and relief information in the estimation of homogeneous units from a geotechnical point of view or, in other words, by soil profiles with similar behavior regarding use and occupation.

The development of the map initially follows the same procedures used to develop the susceptibility map, which are: integration of information plan by weighted linear combination, and multicriteria analysis supported by data-driven evaluation and AHP. Thus, after weighting, the plans were integrated by algebra in the production of the preliminary urbanization suitability map.

The preliminary suitability for urbanization map delimits territorial units of: (i) very high and high suitability, which correspond to the areas without restrictions to urbanization or already consolidated from the geological-geotechnical point of view, where the municipality can release the installment and the permanent occupation of the soil; (ii) moderate suitability, corresponding to areas that have one or more geotechnical constraints, but which can be parceled out and occupied according to certain technical criteria and guidelines; (iii) low suitability, which correspond to the areas with the most severe geotechnical restrictions, which can only be occupied and/or consolidated from the geotechnical point of view, through the undertaking of structural measures by the municipality and the entrepreneurs; (iv) very low suitability, corresponding to areas with severe occupancy restrictions and/or inapt to being consolidated from a geological-geotechnical point of view and for which other types of use are recommended, due to the high cost of urbanization and associated risk (Souza & Sobreira, 2014).

In the traditional process of urbanization suitability map production, the interpretation of results and definition

of guidelines and advice for the use and occupation of the soil is, in general, carried out for the total mapped area, including areas of consolidated occupation. In order to reduce mapping efforts, the current method included a stage for the delimitation of the analysis areas and subsequent conversion of the preliminary map into a suitability one. This was done with the assumption that it is possible to reduce areas with a previous analysis of urban voids and local growth dynamics. Figure 5 shows the sequence of procedures used in the development of the urbanization suitability map of the city of Pelotas.

2.4.1. Urban growth analysis

The urban growth analysis stage has the objective of delimiting the areas available to the city's growth (urban voids), as well as its future urban occupation potential. Therefore, the following general sequence of procedures was established: (i) prior delimitation of areas available for growth (urban voids); (ii) simulation of growth through a model based on Cellular Automata (Polidori, 2004); (iii) definition of the potential of future occupation of urban voids.

The study and simulation of urban growth for the city of Pelotas was carried out through the model based on Cellular Automata developed by Polidori (2004). The model utilizes the principles contained in Krafta's (1994) Centrality and Potential model and applies them to a computational environment, which integrates elements of the graph theory with Cellular Automata (CA), allowing for immediate neighborhood relations (achieved by CA) and remote neighborhood relationships (achieved by graph), to be treated together (Saraiva, 2013). In summary, the model is a CA environment, which integrates urban, natural and institutional factors. These factors can be defined by the user, both as attraction and as resistance to urbanization. It is also up to the user to define the relative weight of each feature, so as to best represent its degree of importance in the spatial growth process of the city. Between each cell pair that presents a charge, a voltage is developed, which is calculated by

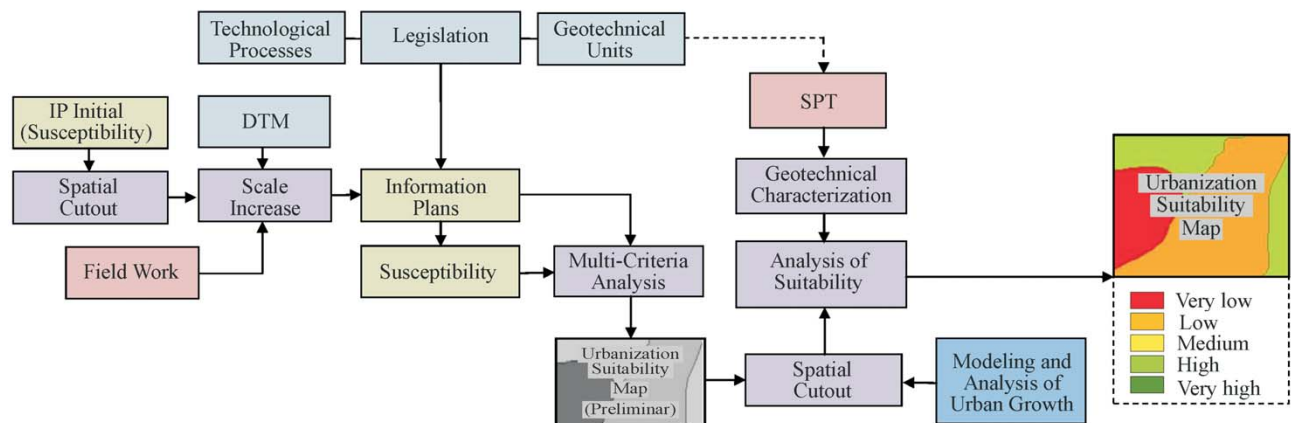


Figure 5 - Schematic of the urbanization suitability map development.

the product of the total charge of each cell by the total charge of each of the others that can be reached (with user-defined range limit). The tensions generated between a pair of cells are distributed by the system in three ways: (i) axial; (ii) polar; (iii) diffuse, each type intending to capture an aspect of urban locational dynamics. The partial result of the tensions calculation is accumulated in each cell, generating the measure of cellular centrality. Based on the difference of the centrality value of each cell with the maximum centrality of its neighborhood, we obtained the cell growth potential of each cell. At each stage of time (interaction), the growth potential of a cell is recalculated, which can result in the reduction of its resistance and the increase of its urban load. In this way, a cell initially defined as “non-urban” may have its state changed to urban, thus representing changes in the morphology of the city (urban growth).

3. Results of the Application of the Methodology

The application of the methodology and the mapping of susceptibility to geodynamic processes and the suitability of lands to urbanization followed the stages and procedures previously described. Its main results are described and discussed below.

3.1. Inventory stage results

The initial characterization of the study area produced a general and comprehensive understanding of its physical and environmental aspects, which served as guideline for the development of the work as a whole. We addressed aspects related to: biodiversity, climate, hydrography, geomorphology and relief, geology and soils. We also identified the geological and geotechnical problems that occurred: flooding, erosion and soft soils. In the sub-stage

of complementary inventory of available data, we were able to search an extensive list of geographic information. Findings were evaluated regarding their content, scale and applicability to work, among other attributes, and then cataloged. In the sub-stage of identification of conflicts and impacts on the physical environment, we identified flooding of urbanized areas due to flood phenomena; occupation of areas of natural plains; erosion and silting; differential settlements and low capacity to support foundations.

The attributes of the physical environment were defined according to the products (susceptibility and urbanization suitability maps) and the geodynamic processes occurring in the area. Using the available data and the possibility of producing new information as both a base and a limit, and following the indications of Sobreira & Souza (2012), Bitar (2014) and Zuquette & Gandolfi (2004), the following classes of attributes in Table 2 were defined as fundamental.

Defining the scale of work is one of the most important stages in the geotechnical mapping process, and in our study was based on relevant attributes in the analysis of the inventoried data and following the indications of Cerri (1990) Cerri *et al.* (1996), Sobreira & Souza (2012), Diniz & Freitas (2013) and Zuquette & Gandolfi (2004). When defining the scale, the objective was to reconcile the purpose of the mappings with the territorial extensions mapped in each one of the stages, using the scales of the basic data (and/or the possibility of their extension) as limitations. In the case of the study area, pedology and geology maps were below the values indicated in the literature for susceptibility and suitability mapping. With this in mind, it was crucial to adjust the scale of these documents, something that, in this study, was facilitated by the close relationship between the soils, their substrates and the forms of relief existing on

Table 2 - Attributes relevant to the mapping of susceptibility and suitability to urbanization.

Class	Sub-class	Attribute
Geomorphology		Terrain units (patterns)
Morphometry		Reliance amplitude; slope; concentration of flows; hierarchical order; curvature and orientation of the aspects
Hydrology	Superficial waters	Areas of water accumulation; soil potential infiltration; surface runoff; drainage net; water bodies; waterway density
	Underground waters	Depth of water table
Unconsolidated materials	Soil units	Texture; soil profile alteration
Structural and sedimentary geology	Geological units	Depositional system; lithology
Geotechnical	Geotechnical units	Resistance; consistency / compaction
Evidence of processes		Erosions; silting ; affected areas by floods
Vegetal cover		Vegetation index
Land use		Types of use; occupation intensity
Anthropogenic processes		Mining; drain channels; works that interfere in the flow of superficial and underground water

the site. Thus, the production of a geomorphology map at a suitable scale was the starting point for the improvement of the scale of the other two maps. The development of the geomorphological map, however, depends on the availability of compatible topographic data. Therefore, it is important to verify the limits of cartographic accuracy that can be reached through this data, represented in the case in question by the digital terrain and elevation models (DTM and DEM).

Thus, the first stage in defining the work scale was the evaluation of the models available for the general stage area: SRTM TOPODATA and ASTER GDEM (both with spatial resolution of 30 m); and the derived model of airborne laser profiling, made available by the municipal administration of Pelotas (with spatial resolution of 0.50 m), for the semi-detail stage. The planimetric and altimetric precision of the model were evaluated according to Cartographic Requirement Standard (CRS) for charts in Brazil, through 34 control points. Having defined the compatibility scales of the models for producing class A digital maps, the mapping scales were established following the indications of Cerri (1990), Cerri *et al.* (1996), Diniz & Freitas (2013) and Zuquette & Gandolfi (2004): 1:50,000 for regional susceptibility (general stage) and 1:25,000 for estimation of geotechnical units, urban susceptibility and suitability for urbanization (intermediate stage). More complete details on the evaluation of the models can be obtained in Xavier (2017). It should be noted that although the DTM of the intermediate stage (Urban DTM) has shown to be compatible with the 1:5,000 scale, the mapping of the intermediate stage in a scale larger than 1:25,000 (as recommended by Sobreira & Souza (2014)), stumbled in its limit of increase on the pedology scale, without the need for extensive investigation and field surveys (*in situ*).

3.2. Results of the data preparation stage

In this stage, the data were processed and cross-referenced in a GIS environment, aimed at their spatial and scalar compatibility, as well as tailored for producing data required for subsequent stages. The initial task was to produce the geomorphological map in which the relief compartments were organized and classified following the methodologies proposed by Ross (1992). In turn, the geomorphological map served as a basis for the production of maps of soils and geology, which, in the next stage, support the mapping of geotechnical units. The preparation stage also served to extract morphometric parameters of the drainage basins and to tabulate and systematize the data contained in the SPT-type survey bulletins. The maps of Hypsometry, Iso-declivities, Relief Curvatures, Soil Use and NVDI (Normalized Difference Vegetation Index) were also developed.

3.3. Results of the general stage of the progressive method

The susceptibility maps were predominantly developed using predisposing natural factors of greater relevance to the phenomenon under study (flooding and erosion). However, two anthropic features were also considered: the diversion and damming of Santa Bárbara stream and changes in soil cover.

To determine the predisposition of the lands to the occurrence of floods, the following information plans were selected: basin morphometry; pedology (soil); geology; iso-declivities; hypsometry; and land use (soil cover). It should be clarified that, although some scientific studies that apply the multivariate analysis to map the susceptibility floods use geomorphology as one of the themes of analysis, this can be replaced by iso-declivity and hypsometry, since it is the properties of the relief that best determine the phenomenon's possibility of occurrence. The selected information plans (PI) were submitted to the multicriteria analysis. For each of the different classes of attributes analyzed (PI), a weight was attributed to its degree of susceptibility to the occurrence of the process under analysis (first level). The weights, ranging from 1 to 5, indicate, respectively, very low, low, moderate, high and very high susceptibility to the phenomenon under study. Regarding the evaluation of the relative contribution of the plans to the susceptibility composition, the AHP method was applied (second level).

The morphometric susceptibility of the drainage basins to floods was defined based on the methodology proposed by Souza (2005), with a focus on coastal areas. According to the author, "any study of morphometric susceptibility in coastal areas should take into account that these basins have two distinct geomorphological compartments, which should be analyzed individually": their headwaters are mostly on basement land, with average to high slopes, and the remainder is situated in lowland coastal plains, with low to zero-height slopes.

The application of the Analytic Hierarchy Process (AHP) method determined the paired comparison between information plans, in which the weights of comparative judgment between each of the themes were established, following the scale of importance defined by Saaty (1977). Based on the paired comparison matrix, the percentages of contribution of each theme towards flood susceptibility of lands were established. Saaty (1977) establishes mathematical formulations to verify the consistency of the judgments. These mathematical calculations allowed for the determination of the so-called Consistency Ratio, which was within the limit of admissibility defined by the author.

The degree of predominance of one factor (conditioning) on the other is not universal and has to be analyzed in relation to the characteristics of the physical environment under analysis, mainly the formation of the relief. The importance of declivity in relation to other themes, in particu-

lar altimetry, is substantially higher in areas of rugged relief, but decreases in areas of the coastal plain. Thus, for the study area, iso-declivity has moderate importance in relation to hypsometry (Fig. 6), strong in relation to soil use and from strong to very strong importance in relation to pedology. The morphometry of the river basins, due to the low slope in all or most of them, has a diminished importance, being slightly superior to land use and moderately more relevant than pedology that, also due to relief, gains greater magnitude.

In this way, the information plans, already duly reclassified according to the weights assigned to each of the classes, were submitted to the algebraic map operation in GIS (with the contribution percentage of each plan defined by AHP). The Equation 1 served as the basis for the operation, where: *SEI* = flood susceptibility; *MBD* = watershed morphology; *P* = pedology; *G* = geology; *ID* = iso-declivities; *HP* = hypsometry; and *US* = land use.

$$SEI = [(MBD \times 0.113) + (P \times 0.070) + (G \times 0.033) + (ID \times 0.375) + (HP \times 0.280) + (US \times 0.129)] \quad (1)$$

The resulting raster grid was reclassified into five equal ranges of values, each corresponding to a susceptibility class. To validate the map, the mappings of affected areas in three large rainfall events (in 2004, 2019 and 2015), were analyzed. Field trips were carried out to survey and diagnose two specific situations where the influence of anthropic action and extrapolation was detected in the mapping, in an area hit by the event of 2015. Thus, the preliminary map was validated, becoming the map of susceptibility to floods (Fig. 7).

The same method was applied in the case of laminar erosions, from the selection of pedology information plans, geomorphology, declivities, relief curvature, land use and intensity of vegetation cover. The map algebra was carried out based on Equation 2, where: *SEL* = susceptibility to laminar erosion; *US* = soil use; *P* = pedology; *ID* = iso-de-

clivities; *CR* = relief curvature; *CV* = density of vegetation cover. The map produced (Fig. 8) was also validated, this time through field surveys in mapped areas with different susceptibilities.

$$SEL = [(US \times 0.170) + (P \times 0.398) + (ID \times 0.274) + (CR \times 0.050) + (CV \times 0.107)] \quad (2)$$

3.4. Results of the semi-detail stage of the progressive method

In the composition of the urbanization suitability of the lands, in addition to the information plans regarding the susceptibilities (initial database), two other themes were used: geotechnical units and a protection and drainage system against flooding, the latter being part of anthropic interventions on the natural environment. The geotechnical units were mapped using the methodology of Dias (1995), resulting in a map with 13 units with homogeneous geotechnical behavior regarding the use and occupation of the soil. These are identified on the map with the symbols “XYZxyz”, where the capital letters correspond to the pedological classification of the profile (considering the superficial horizons A and B), and the lower case letters represent the geology, characterized by the horizons C, RA, and R (Fig. 9). The drainage system and flood protection information plan, in turn, was drawn from the mapping and analysis of the drainage system (channels and galleries) and the system of dikes, polders and pumps that protect part of the urban area of the São Gonçalo Channel.

A preliminary map of urbanization suitability was created, covering the total urban area and urban expansion area of the municipality (Fig. 10). The map results from the crossing of susceptibility, geotechnical units, drainage system and flood protection plans. The development of the map followed the same sequence of procedures used to construct the susceptibility maps, namely: (i) attribution of weights to the classes of the plans; (ii) raster reclassification; (iii) definition of the percentages of contribution of

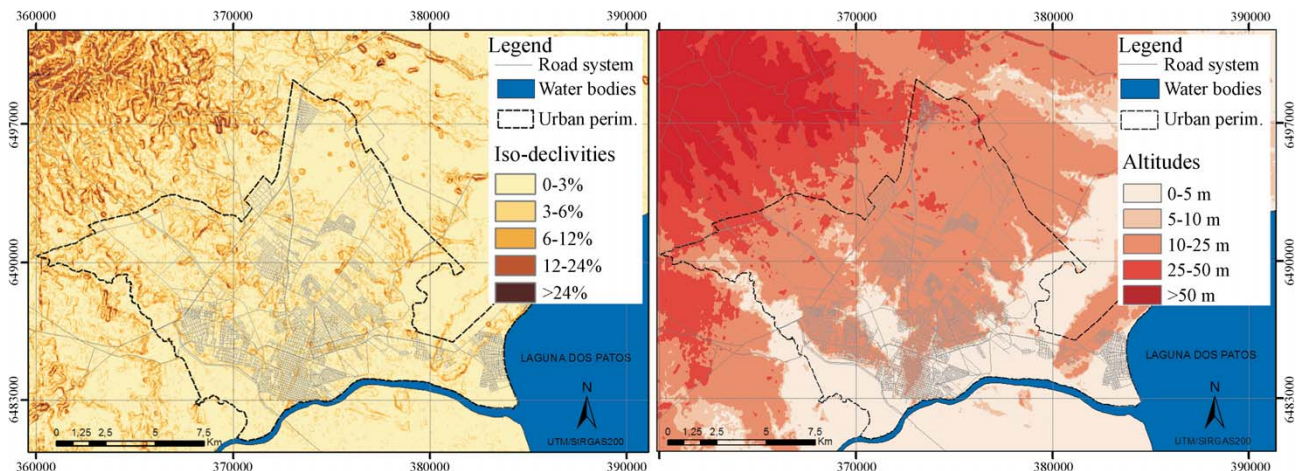


Figure 6 - Maps of iso-declivities (left) and Hipsometry of Pelotas (right) (UTM Zone 22S).

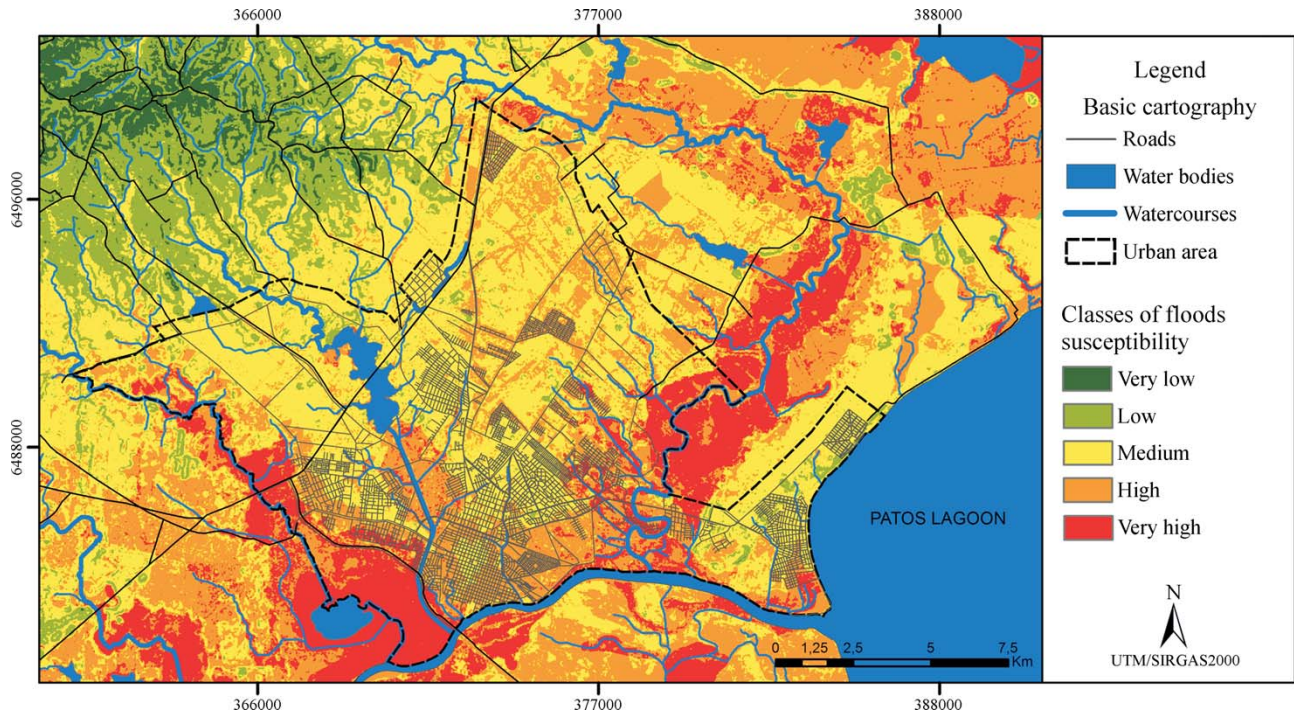


Figure 7 - Map of susceptibility to the flood of Pelotas (UTM Zone 22S).

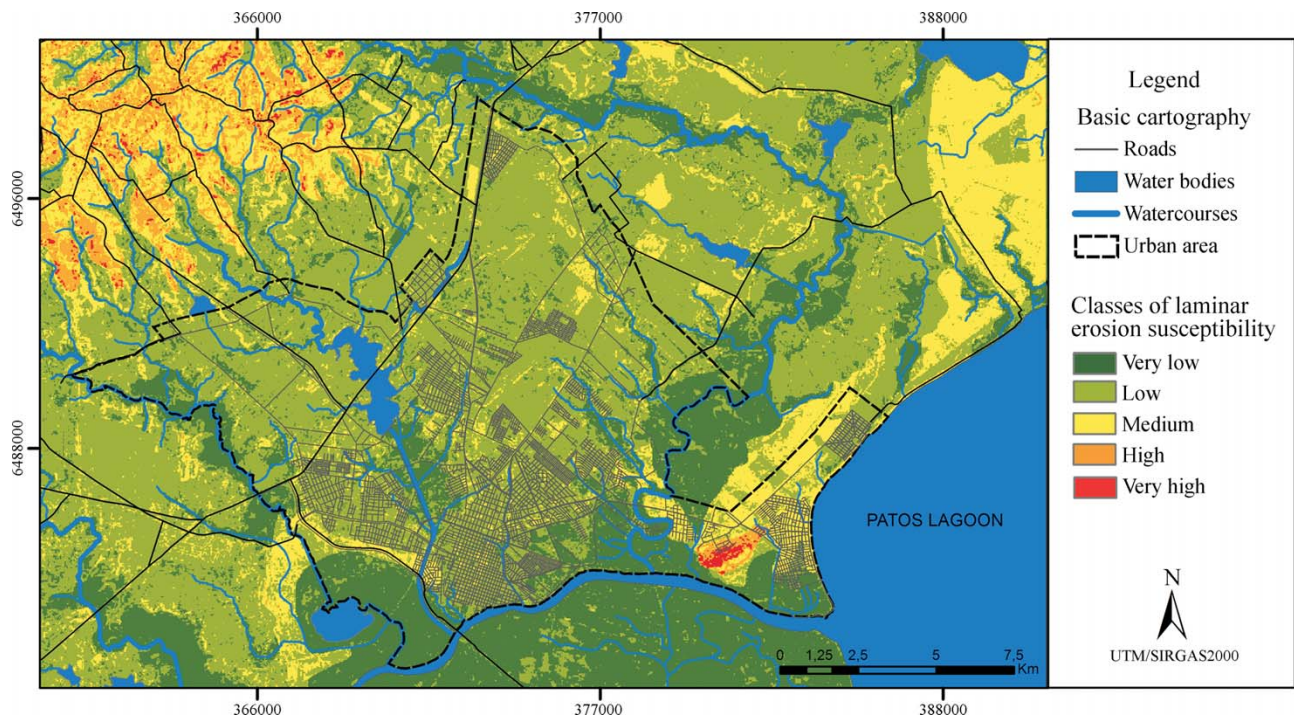


Figure 8 - Map of susceptibility to the erosion of Pelotas (UTM zone 22S).

each plan through the application of the AHP method; (iv) intersection of planes by map algebra (Eq. 3), where: APU = suitability to urbanization; SEI = susceptibility to floods; SE = susceptibility to laminar erosion; UG = geo-technical units; AP = protected areas (against floods).

$$APU = [(SEI \times 0.5129) + (SE \times 0.0594) + (UG \times 0.1478) + (AP \times 0.2799)] \quad (3)$$

After developing the preliminary urbanization suitability map, mapping of the urban voids and the simulation

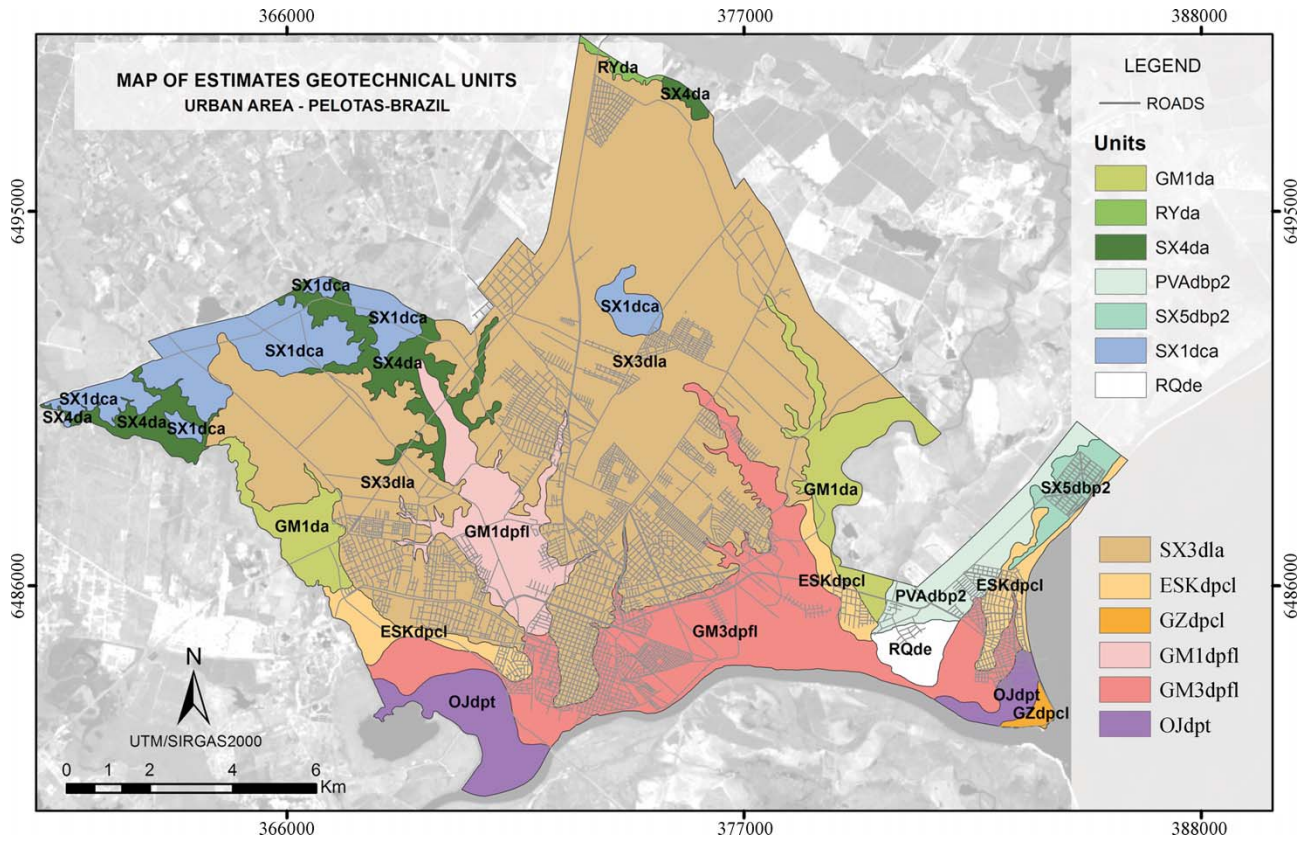


Figure 9 - Geotechnical Unit Estimation Map (UTM zone 22S).

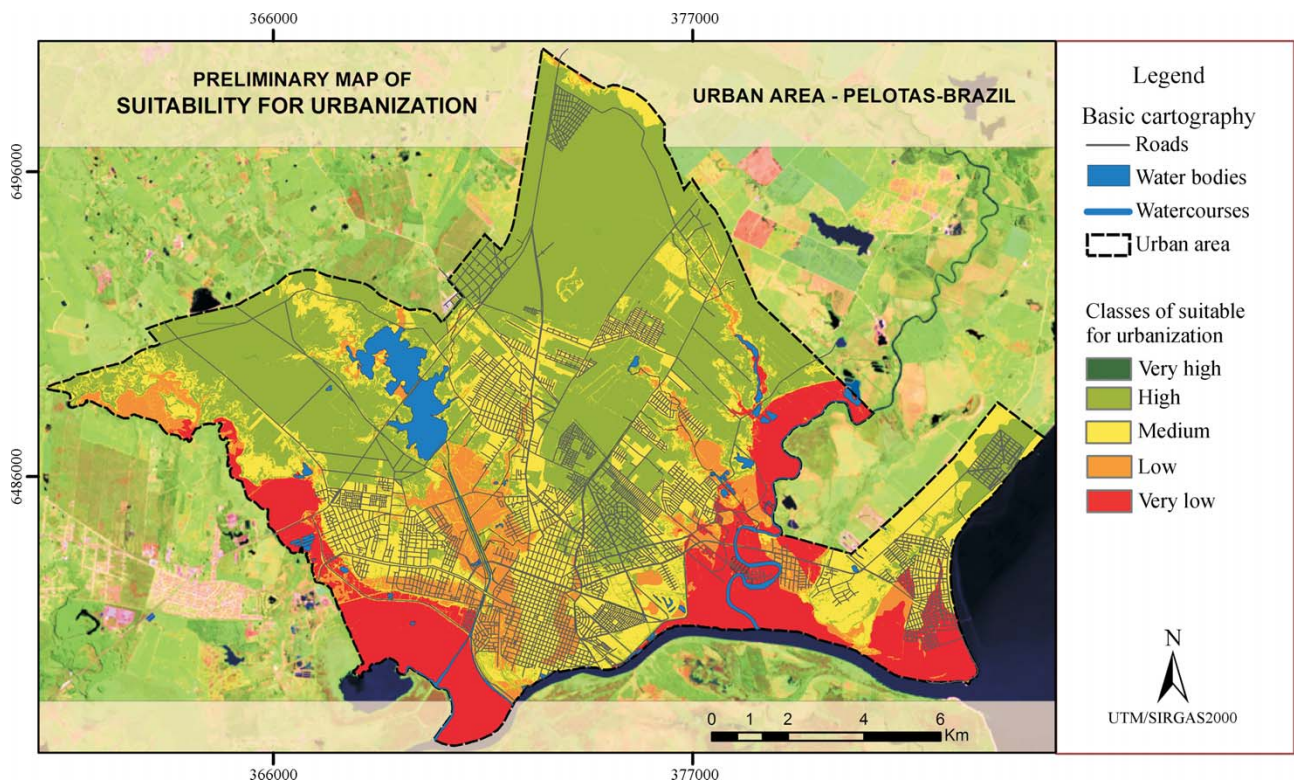


Figure 10 - Preliminary map of suitability for urbanization of Pelotas/RS (UTM zone 22S).

of urban sprawl spatial growth processes were carried out, aimed both at reducing the areas of analysis and characterizing suitability. This time, the urbanization suitability map was produced only for those portions of the territory that demand greater urgency for information pertaining to urban planning. The mapping of urban voids, considered here as areas available for urban growth, was based on the crossing of an orthophoto from 2015 with the cadastral base of lots provided by the city hall.

The study and simulation of urban growth, in turn, were carried out through the model based on Cellular Automata, implemented by CityCell software (Saraiva & Polidori, 2014). Since it is a pre-existing model, several conceptual and practical stages of modeling were already provided, leaving only calibration and validation of the model for the available input data (Liu, 2009). Besides the configuration of the model's internal parameters, the variables and their weights needed to be validated. A common way of validation is to compare the simulation results with historical data of past urban growth in the study area. In this way, the model was calibrated and validated through the simulation of city growth between the years 1965 and 2011. Through the calibration study, the attributes used and their respective weights were defined, which served as the basis for the growth simulation of Pelotas from the year 2015 to the year 2040 (Fig. 11). More complete details on the procedures for mapping the urban voids and simulation of the urban growth of Pelotas can be obtained in Xavier (2017).

Far from representing a future undeniable fact, the resulting information points to an effective probability, simulated based on the past and present conditions, and mechanisms of production and reproduction of the built urban environment studied and described by contemporary urban science. The simulation indicated urbanization pressure on the urban voids, which, in order to characterize the suitability for urbanization, were grouped in eight sets, having as criterion their spatial relationship and the constituent geotechnical units (Fig. 12).

Among the eight groups of voids mapped, we highlight those of group 7, due to their physical characteristics, location and urbanization pressure. Further description of

this group is given below as an example of the characterizations made.

Group 7 of urban voids is composed of 4 voids located in the Southeastern part of the urban zone, in the Administrative Regions of São Gonçalo (voids 29, 30 and 34) and Areal (void 33), with a total area of 3.12 km², and urban growth projection according to the graphs in Fig. 13. The group of voids is made up of lands of the geotechnical units GM3dpfl (98.43%) and SX3dla (1.57%).

Almost all of the land in Group 7 is located on the geomorphological unit of the fluvial-lacustrine plateaus, which form the main part of the floodplain of São Gonçalo Channel. They are lands with low altitude (0 to 5 m) with little or no relief. This group of voids has a predominance of suitability between very low (34.47%), low (26.38%) and moderate (30.54%), followed by high suitability (7.45%) and very high suitability (1.16%) (Fig. 14).

The voids of group 7, due to its proximity to the historical and commercial center of the city, are subject to great urban growth pressure. The simulation of growth indicates an occupation of 100% of voids 29, 30 and 33, in up to 12 years. This group covers naturally flooding land, but is currently partially protected by the flood control system in voids 29 and 30. Thus, despite having high and very high natural susceptibility to floods, these voids are typically at a moderate level of susceptibility. The very low suitability class is almost totally restricted to void 34 and the low suitability class is concentrated in void 33. Table 3 shows the percentage levels of susceptibility to flooding and soil erosion for this group of voids.

The GM3dpfl geotechnical unit, which encompasses almost all of this group of voids, presents variation in foundational support, due to the presence of soft to very soft clay in the vicinity of the Pelotas stream and the Santa Bárbara channel. Figure 15 shows the soil resistance drop, shown through the N_{spt} values of 3 probes of the GM3dpfl unit: the greater the distance of the SX3dla unit and the greater the São Gonçalo channel approximation, the lower the N_{spt} index of the soil with depth. It should be noted that due to the geological formation of these soils, there is a great heterogeneity in their texture and support capacity,



Figure 11 - Results of the simulation of urban growth in Pelotas: a) urban area in 2015; b) urban area in the year 2027; c) urban area in 2040.

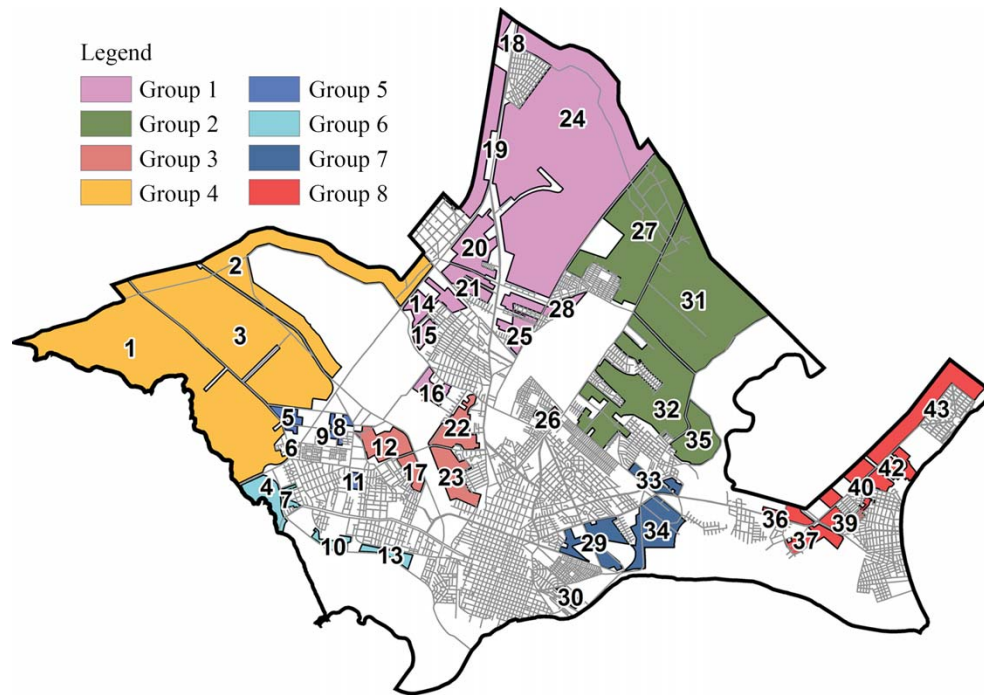


Figure 12 - Grouping of urban voids for analysis of urbanization suitability.

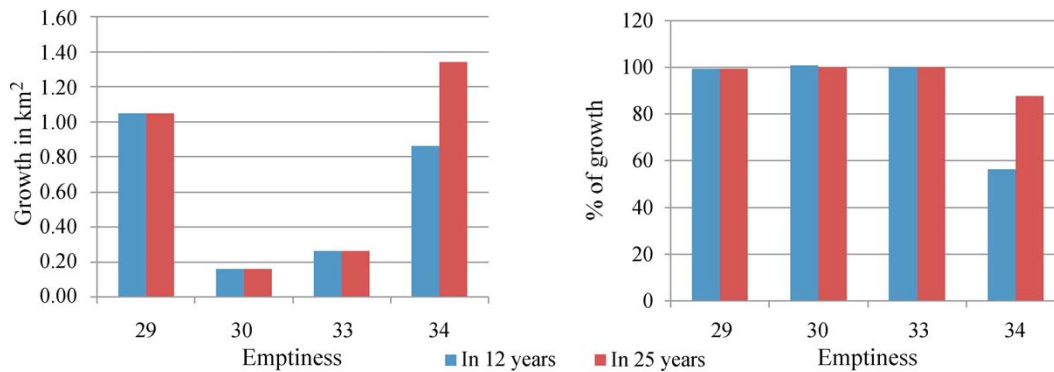


Figure 13 - Graphs of urban growth in the voids of group 7.

Table 3 - Percentages of occurrence of different levels of susceptibility in lands belonging to group 7 of urban voids.

Levels of susceptibility	Area susceptible to floods (km ²)	% susceptible to floods	Area susceptible to erosions (km ²)	% susceptible to erosions
Very low	0	0.00	2.918	93.63
Low	0.058	1.87	0.183	5.87
Moderate	0.276	8.84	0.014	0.46
High	1.434	45.96	0.001	0.03
Very high	1.352	43.33	0	0.00

and there may be a decrease or increase of resistance with depth and variable locations within the unit.

The urbanization conditions of the voids in group 7 are variable and dependent on the suitability level of each

area. In the areas with moderate and low suitability, urbanization can take place with due care for drainage, which includes raising the terrain's elevation by at least 1.50 m. In order to approve larger land parceling projects in

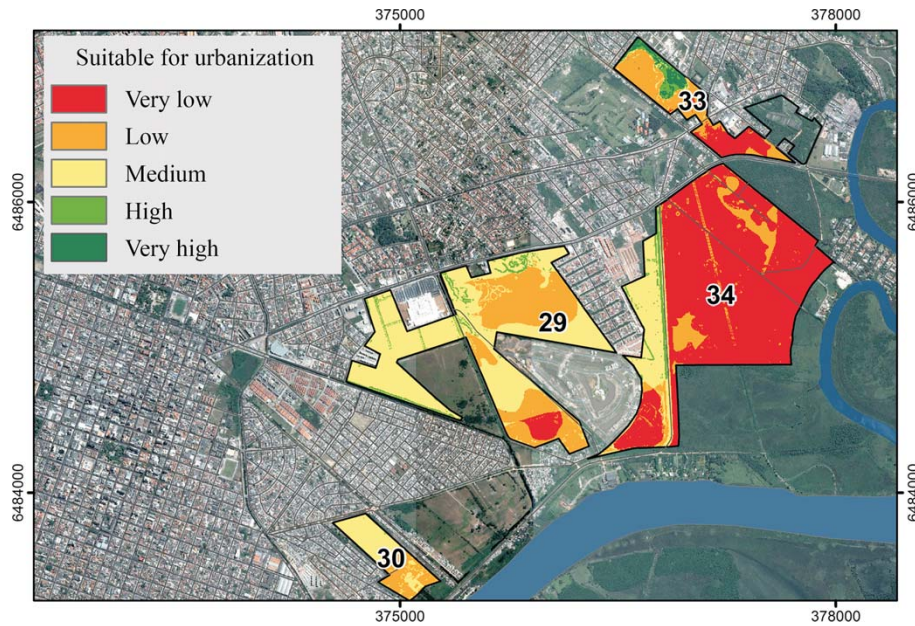


Figure 14 - Levels of suitability for urbanization in group 7 (UTM zone 22S).

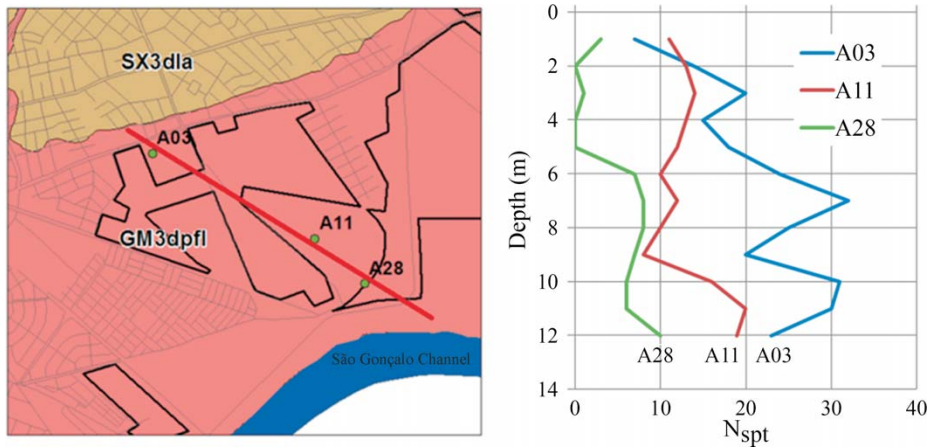


Figure 15 - Soil resistance variation of geotechnical unit GM3dpfl. Left: map showing the location of the probes A03, A11 and A28 in relation to the geotechnical units and the part of the voids in group 7. On the right: graph with the variation of the values of N_{spt} (axis x) with depth (y axis).

voids 29 and 30, a reservoir for holding or damping the peak precipitation deflation should be required, in order to relieve the channel and pump system that retains rainwater beyond the protective dam.

Urban void 33 is situated in a natural drainage area that, from ancient natural channels, directs part of the rainwater that reaches the high alluvial terraces into the Pelotas stream. With urbanization, the natural channels were replaced by artificial ones, with deviation from their natural course. Therefore, the occupation of void 33 by urban use requires firstly a verification of the capacity and the drainage conditions of the channels that drain into the Pelotas stream and/or opening of new channels, along with the inclusion of adequate local drainage measures. Finally, void

34 has very low suitability for urbanization. It is a low area that is subject to complete flooding in the event of large precipitations (Fig. 16), playing an important role in the retention, infiltration of rainwater and buffering the peak of rainfall precipitation. Therefore, the occupation of this area with denser urban uses should be deterred. However, because of its geographic location (near the São Gonçalo channel, Pelotas stream and not far from the city center), this void is favorable for very low density uses (leisure sites, parks, etc.), involving drainage solutions that allow for the maintenance of current levels of retention and infiltration of rainwater.

It should be noted that the safety against flooding of voids 29 and 30 is totally dependent on the correct design



Figure 16 - Photographic image of the area of the void 34 in the 2015 flood (PMPel, 2015).

and operation of the system of dikes, channels and booster pumps that protect the area. Therefore, the adequacy of its drainage capacities, as well as the improvement of its operating conditions, precede the liberation of larger projects in the area.

Due to the presence of low consistency organic clay in part of the area of group 7, it is essential that local prospecting surveys be carried out for the execution of civil work. In addition, it is recommended to increase the number and minimum density of drillings established in NBR 8036 (ABNT, 1983). Furthermore, it should be pointed out that not only buildings and structures have to be properly constructed, but the whole infrastructure (streets, sewage and water networks, among others) must be protected against the excessive settlements common in these areas.

4. Final Considerations

The continuous growth of Brazilian cities, their negative impact on the physical environment and the risk to which large portions of their populations are subjected, determines the planning of urban development in line with the limitations and potential of this environment. The need to use geological-geotechnical information in the planning process is unquestionable, since a broad knowledge about the planned area is essential in deciding or choosing the best alternatives for the use of available resources. Despite the reasonable state of Brazilian geotechnical cartography, there is a strong need for new studies on the optimization of mapping processes, a better adaptation to the urban environment and its applicability to the process of urban growth planning, in a way that is more sustainable and more adjusted to the physical-environmental characteristics of the territory. In this sense, based on a review of the main mapping methodologies used in Brazil, from the most generic to those directed to urban planning, it was possible to establish the theoretical framework for structuring the methodology in the city of Pelotas-South Brazil. The progressive method

of Cerri *et al.* (1996), together with the concepts and procedures of the methodologies of Diniz & Feitas (2013), Sobreira & Souza (2012) and the regional method of Dias (1995), were found to be the most adequate for the conditions and the objectives of the present study. The methodologies, rather than overlapping each other, in the way they were structured, complemented each other and formed a new procedure that generated data and products (maps and charts) aimed at planning and controlling the growth of the city. Among the products of Geotechnical Cartography, the maps of susceptibility to geodynamic processes and the urbanization suitability map were identified as instruments capable of providing information on physical aspects of the urban environment directly related to the occupation of the territory.

The multi-criteria approach, through the weighted linear combination of factors in the GIS environment through the AHP method, allowed for the integration of information plans and the mapping of different degrees of susceptibility and terrain suitability. Their use made possible the compensation between the physical-environmental factors employed and the hierarchical ordering of the plans, according to their relative importance in the occurrence of the phenomena studied, with results validated both by historical processes and the survey of the conditions present in the field, validating the use of the method in geological-geotechnical mapping.

The method of Dias (1995), chosen to produce the map of estimates of geotechnical units, proved to be capable to produce an information plan with geotechnical classes that can be evaluated and used in the composition of the suitability for urbanization, after the indispensable taxonomic generalizations, adjustments and validations. In relation to the geotechnical units, it was concluded that the SPT surveys, widely used in geotechnical mapping work, are excellent data sources that allow for an adequate geo-

technical characterization of the lands, when the objective of the work is to support urban planning.

The number of SPT tests required to characterize the geotechnical units depends on the characteristics of soil types and substrates, on the variation of their vertical profiles, on the spatial distribution of the surveys and on the purpose of the mapping, and should only be determined after preliminary analysis of each unit. In the case of the GM3dpfl (26.54 km²) unit, for instance, which features considerable variation in the vertical profile, 30 reports were sufficient to characterize the suitability for urbanization (for urban planning purposes), in the 1:25,000 scale of its urban voids.

A limitation detected is related to the inexistence of surveys in low urban areas. In these cases, the inference of the properties is required by means of correlation with the typological components common to other areas or, if the correlation is not feasible, the completion of new surveys. At this point, the municipal land use planning and control bodies should develop strategies for the collection, storage and systematization of geotechnical information in their territory. The requirement, for example, of the geotechnical survey report in the process of releasing building permits, could be a viable alternative, since they relate to the proof of the stability of the building.

The procedures applied to the cartography of the free areas and areas predisposed to the growth of the city made possible the spatial reduction and allowed a more detailed evaluation of urbanization suitability, avoiding the expenditure of effort in the characterization of consolidated areas in which the change of use is unlikely or very slow. On the other hand, the simulation of urban growth through the model implemented by the CityCell software presented results consistent with the historical process of spatial development of the city. However, it should be emphasized that the model, based on the past morphology and the mechanisms of production and reproduction of the urban environment, predicts probable future urban forms which may not be fully achieved. In this way, the model should be used with caution. In the present case, with the objective of assisting in the characterization of urban voids and identifying probable conflicts between growth and suitability to urbanization, the use of the model showed potential and relevance.

The application of the methodology, as a whole, presented important results of great relevance regarding the production of cartographic documents, both for a better understanding of the current state of urbanization of the study area, in relation to the characteristics of its physical environment, and to plan for future growth. Therefore, it is expected that the application of this methodology represents a contribution to geotechnical cartography with regard to the development of tools that aid in urban planning. The simplicity and ease of execution of the mapping methods and the results achieved indicate their potential for partial or to-

tal use in other physiographic realities and/or as a basis or part of new methodologies.

Compared to other methodologies, this method focuses almost exclusively on the use of pre-existing data, on reducing the areas of analysis and directing them to the planning of the city's growth. This method can be seen as less labor intensive, more appropriate for the instrumental and financial reality of Brazilian municipalities and finally, better adjusted to the urban physical environment. The application of this method, however, requires the availability of basic data on the area in question: geological maps, local pedology, and local geomorphology, as well as remote sensing images (satellite or orthophotos), numerical terrain models, and SPT probe reports.

References

- Associação Brasileira de Normas Técnicas (1983). NBR 8036: Programação de sondagens de simples reconhecimento dos solos para fundações de edifício. Rio de Janeiro, Brazil, 3 p.
- Bitar, O.Y. (Coord.) (2014). Cartas de suscetibilidade a movimentos gravitacionais de massa e inundações - 1:25.000: nota técnica explicativa. São Paulo: IPT (IPT Publicação 3016), 50 p.
- Bressani, L.A. & Costa, E.A. (2013). Mapeamento geotécnico: suscetibilidade, perigo, vulnerabilidade técnica, risco e risco instalado. In: Proc. 14^o Congresso Brasileiro de Geologia de Engenharia e Ambiental, 2013, ABGE, Rio de Janeiro, CD-ROM.
- Caballero, M. (1973). Evolución Histórica de los Mapas Geotécnicos. In: Boletín Geológico y Minero, IGME, Espanha, 84(1):55-68.
- Cerri, L.E.S. (1990). Carta Geotécnica: contribuições para uma concepção voltada as necessidades brasileiras. In: Proc. 6^o Congresso Brasileiro de Geologia de Engenharia, 1990, ABGE, Salvador, v. 1, p. 315.
- Cerri, L.E.S.; Akiossi, A.; Augusto Filho, O. & Zaine, J.E. (1996). Cartas e mapas geotécnicos de áreas urbanas: reflexões sobre as escalas de trabalho e proposta de elaboração com o emprego do método de detalhamento progressivo. Proc. 8^o Congresso Brasileiro de Geologia de Engenharia, ABGE, Rio de Janeiro, v. 2, p. 537-548.
- Dias, R.D. (1995). Proposta de metodologia de definição de carta geotécnica básica em regiões tropicais e subtropicais. Revista do Instituto Geológico, 16(número especial):51-55.
- Diniz, N.C. (2012). Cartografia geotécnica por classificação de unidades de terreno e avaliação de suscetibilidade e aptidão. Revista Brasileira de Geologia de Engenharia e Ambiental, 2(1):29-77.
- Diniz, N.C. & Freitas, C.G.L. (2013). Cartografia geotécnica. In: Coutinho, R.Q. (org.) Parâmetros para a Cartografia Geotécnica e Diretrizes para Medidas de Intervenção de Áreas Sujeitas a Desastres Naturais. Ministério das Cidades, Brasília e GEGEP, UFPE.

- Fell, R.; Corominas, J.; Bonnard, C.; Cascini, L.; Leroi, E. & Savage, W.Z. (2008). Guidelines for landslide susceptibility, hazard and risk zoning for land-use planning. *Engineering Geology*, 102(3-4):83-111.
- Fernandes, N.S. (2016). Mapeamento de Áreas Suscetíveis à Inundação em Santa Maria/RS. Dissertação de Mestrado em Geografia, Programa de Pós-Graduação em Geografia, UFSM, Santa Maria, 103 p.
- Ferreira Dos Santos, R.F. (2004). Planejamento Ambiental: Teoria e Prática. Oficina de Textos, São Paulo, 184 p.
- Ferreira, G.L.B.V. & Ferreira, N.B.V. (2011). Direito à Cidade: O Papel do Planejamento Urbano. *Revista Argumenta*, 14(1):35-50.
- Instituto Brasileiro de Geografia e Estatística (2011). Censo Demográfico 2010. Características da população e dos domicílios: resultados do universo. Rio de Janeiro: IBGE. Available at <http://www.ibge.gov.br> and downloaded on May 20th 2016.
- Instituto Brasileiro de Geografia e Estatística (2018). Estimativa Populacional 2018. Available at <http://www.ibge.gov.br/cidades-e-estados/rs/pelotas.html> and downloaded on May 15th 2019.
- Julião, R.P.; Nery, F.; Ribeiro, J.L.; Branco, M.C. & Zêzere, J.L. (2009). Guia Metodológico para a Produção de Cartografia Municipal de Risco e para a Criação de Sistemas de Informação Geográfica (SIG) de Base Municipal. Autoridade Nacional de Protecção Civil, Lisboa, Available at http://www.proteccaocivil.pt/Documents/guia_metodologico_SIG.pdf and downloaded on April 30th 2015.
- Krafta, R. (1994). Modelling intra-urban configurational development. *Environment and Planning B: Planning and Design*, London: Pion, 21(1):67-82.
- Liu, Y. (2009). Modelling Urban Development with Geographical Information Systems and Cellular Automata. CRC Press, Boca Raton, 188 p.
- Moretti, R.S. (2017). Responsabilidade municipal na aplicação da carta geotécnica de aptidão à urbanização. In: 1^o Workshop do Comitê Brasileiro de Cartografia Geotécnica e Geoambiental. Apresentação. Universidade Federal do ABC, São Bernardo do Campo.
- Moura, A.C.M. (2005). Geoprocessamento na Gestão e Planejamento Urbano. 2nded. Edição da Autora, Belo Horizonte, 294 p.
- Namur, M. & Boeira, J.G. (2005). Reflexões sobre o papel do Planejamento Urbano no Brasil. In: Proc. XI Encontro Nacional da Associação Nacional de Pós-Graduação e Pesquisa em Planejamento Urbano e Regional, 2005. ANPUR, Salvador.
- Oliveira, D.A.M. (2011). Discurso e Planejamento Urbano no Brasil. *Revista Geográfica da América Central*. Número Especial EGAL, 2011. EGAL, Costa Rica.
- Polidori, M.C. (2004). Crescimento Urbano e Ambiente – Um Estudo Exploratório sobre as Transformações e o Futuro da Cidade. Tese de Doutorado em Ecologia, Programa de Pós-graduação em Ecologia, Universidade Federal do Rio Grande do Sul, Porto Alegre. 328 p.
- Prefeitura Municipal de Pelotas (2015). Levantamento fotográfico aéreo da enchente de 2015. 1 Digital Photography, Pelotas/RS.
- Rafaeli, L. & Müller, C.J. (2007). Estruturação de um índice consolidado de desempenho utilizando o AHP. *Gestão e Produção*, 14(2):363-377.
- Rolnik, R. (1994). Planejamento Urbano nos anos 90: Novas perspectivas para velhos temas. Ribeiro, L.C.Q. & Santos Junior, O.A. (orgs.), *Globalização, Fragmentação e Reforma Urbana - O Futuro das Cidades Brasileiras na Crise*. Civilização Brasileira, Rio de Janeiro, 426 p.
- Rosa, M. (1985) *Geografia de Pelotas*. UFPel, Pelotas, 333p.
- Ross, J.L.S. (1992). O registro cartográfico dos fatos geomórficos e a questão da taxonomia do relevo. *Revista do Departamento de Geografia*, 6(1):17-29.
- Saaty, T.H.A. (1977). A scaling method for priorities in hierarchical structures. *Journal of Mathematical Psychology*, 15(3):234-281.
- Santos, M. (1998) *A Urbanização Brasileira*. 1^o Edição. Editora Hucitec, São Paulo, 157 p.
- Saraiva, M.V.P. (2013) *Simulação de Crescimento Urbano em Espaços Celulares com uma Medida de Acessibilidade: Método e Estudo de Caso em Cidades do Sul do Rio Grande do Sul*. Dissertação de Mestrado em Arquitetura, Programa de Pós Graduação em Arquitetura, Faculdade de Arquitetura, Universidade Federal de Pelotas, Pelotas, 87 p.
- Saraiva, M.V. & Polidori, M.C. (2014). CityCell - Urban Growth Simulator (software). LabUrb., Laboratório de Urbanismo da FAUrb. UFPel, Pelotas.
- Sobreira, F.G. & Souza, L.A. (2012). Cartografia geotécnica aplicada ao planejamento urbano. *Revista Brasileira de Geologia de Engenharia e Ambiental*, 2(1):79-97.
- Sobreira, F.G. & Souza, L.A. (2014). Guia para Elaboração de Cartas Geotécnicas de Aptidão à Urbanização Frente aos Desastres Naturais. Estudo de Caso de Ouro Preto - 2013. ABGE, Brasília, available at <http://www.abge.org.br/uploads/imgfck/file> and downloaded on March 30th, 2015.
- Souza, C.R.G. (2005). Suscetibilidade morfométrica de bacias de drenagem ao desenvolvimento de inundações em áreas costeiras. *Revista Brasileira de Geomorfologia*, 6(1):45-61.
- Souza, L.A. & Sobreira, F.G. (2014). Guia para Elaboração de Cartas Geotécnicas de Aptidão à Urbanização Frente aos Desastres Naturais. ABGE, Brasília, 68 p. Available at http://www.abge.org.br/uploads/imgfck/file/guia_aptidao_a_urbanizacao_souza_e_sobreira_2014.pdf and downloaded on September 15th 2015.

- Torezan, F.E. (2005). Proposta Metodológica para Subsidiar a Determinação do Grau de Impacto Ambiental em Empreendimentos Minerários na Região de Descalvado e Analândia. Tese de Doutorado, Programa de Pós-Graduação em Ecologia e Recursos Naturais, Universidade Federal de São Carlos, São Carlos, 149 p.
- Voogd, H. (1983). Multicriteria Evaluation for Urban and Regional Planning. Pion, London, 125 p.
- Xavier, S.C. (2017). Mapeamento Geotécnico Aplicado ao Planejamento do Uso e Ocupação do Solo na Cidade de Pelotas: Estudo Voltado à Expansão Urbana. Tese de Doutorado, Universidade Federal do Rio Grande do Sul, Escola de Engenharia, Programa de Pós-Graduação em Engenharia Civil, Porto Alegre, 338 p.
- Zuquette, L.V. & Gandolfi, N. (2004). Cartografia Geotécnica. Oficina de Textos, São Paulo, 190 p.

Soil Elastic Modulus Determined by Ultrasound Tests

W.S. Sarro, G.C.S. Ferreira

Abstract. The elastic constants obtained through conventional destructive (triaxial and resilience) tests can present great variability, even for soils with the same classification. Thus, a test is necessary to determine the elastic constants of soils in a reliable and replicable way. The ultrasonic technique is used to characterize rock and several construction materials (wood, cementitious matrices, metals), including the elastic parameters (elastic modulus, shear modulus, and Poisson's ratio). The aim of this study was to verify the correlation between the elastic modulus obtained through ultrasonic testing and through a simple unconfined compression test on compacted clayey soil. Test specimens were molded at normal compression energy with three moisture contents; the specimens were exposed to air and packed with plastic wrap for 120 days. After this period, we performed ultrasonic and compression tests. The technique presented great potential to study the mechanical behavior, with correlation coefficients over 0.97 for both parameters (compressive strength and static elastic modulus). We also verified that the ultrasonic testing is influenced mainly by the moisture content.

Keywords: geotechnical, mechanical characterization, nondestructive testing, soil elastic behavior, soil moisture content, ultrasound transmission method.

1. Introduction

Defining the elastic constants of compacted soil is crucial for its correct application in geotechnical works (pavements, landfills, dams). However, the elastic modulus and the Poisson's ratio are usually determined through empirical tests performed with laboratory specimens, which do not represent actual conditions of the material (Yang *et al.*, 2015). These conditions become even more complex since the behavior of the soil regarding its deflection is not perfectly linear, with residual deflections occurring even in the strain \times specific deflection curve (Dias, 2007). Thus, performing specific soil tests to determine the elastic modulus and Poisson's ratio (triaxial compression, resilience) are not feasible due to the number of repetitions required for a correct and reliable characterization. Moreover, elastic constants obtained by these methods can present great variability, even for soils with the same classification.

Recent research indicates that nondestructive in situ testing techniques called cross-hole, down-hole and up-hole allow to determine the propagation velocity and consequently the elastic constants of soils in depth under low strain (Choo *et al.*, 2018; Nejad *et al.*, 2017; Pegah *et al.*, 2017). Measurements are made inside the borehole and the technique is chosen depending on the position of the seismic sources in the holes. Although these tests can cover large volumes of soil, the preparation of the holes and the equipment have a high cost.

Champiré *et al.* (2016) and Miccoli *et al.* (2014) studied sandy samples through unconfined compression tests with determination of deflections; both studies achieved similar values of elastic modulus, between 2.20 and

2.80 GPa. In contrast, Bui *et al.* (2014a) and Lombillo *et al.* (2014) studied soils with the same classification and also used the unconfined compression test; their values were in the range 0.18 to 0.95 GPa. The contradiction in the literature reinforces the need for a test capable to determine the elastic constants of soils in a reliable and replicable way.

The ultrasonic testing is recommended to determine the elastic constants of compacted soils more easily. It is a nondestructive technique already applied in the characterization of several building materials (wood, cementitious matrices, metals). The velocity of longitudinal and transverse ultrasonic waves is required when ultrasonic testing is used to determine elastic constants. The application of elasticity theory to the longitudinal and transverse velocities determines the elements of the stiffness matrix, which, after their inversion, result in the flexibility matrix and consequently, in the values of the elastic modulus, of shear and of the Poisson's ratio (Bucur, 2006; Bucur & Archer, 1984; Gonçalves *et al.*, 2011a, 2014; Kohlhauser & Hellmich 2012; Vázquez *et al.*, 2015). Materials may present isotropic, anisotropic or orthotropic behavior, thus, it is necessary to know their elastic properties to determine the matrix (Bui & Morel, 2009; Bui *et al.*, 2014b; Christ & Park, 2009; Ferreira *et al.*, 2014; Maillard & Aubert, 2014; Miccoli *et al.*, 2015; Pietruszczak & Krucinski, 1989).

Some authors studied the application of the ultrasonic technique in compacted soil specimens and in constructive elements in soil. These studies involve the determination of preliminary data (ultrasonic velocity at the soil), the isotropy of the compacted soil (Christ & Park, 2009), the elastic constants (Cai *et al.*, 2015; Hammam & Eliwa, 2013;

Wélida de Sousa Sarro, M.Sc., Ph.D. Student, Departamento de Tecnologia, Universidade Estadual de Campinas, Limeira, SP, Brazil, e-mail: welidasarro@gmail.com.
Gisleiva Cristina dos Santos Ferreira, D.Sc., Associate Professor, Departamento de Tecnologia, Universidade Estadual de Campinas, Limeira, SP, Brazil, e-mail: gisleiva@ft.unicamp.br.
Submitted on January 28, 2018; Final Acceptance on June 11, 2019; Discussion open until December 31, 2019.
DOI: 10.28927/SR.422117

Wang *et al.*, 2006; Yu *et al.*, 2016) and the definition of factors that can interfere in the ultrasonic pulse (Dongqing *et al.*, 2016; Ferreira *et al.*, 2014; Sarro *et al.*, 2017; Teixeira *et al.*, 2015).

The factors that may interfere in the ultrasonic pulse on soil and must be considered are both those already determined for other materials and those considered during the determination of the elastic constants of the soil by destructive methods. Vanapalli & Adem, 2014 (Adem & Vanapalli, 2015 and Oh & Vanapalli, 2016) describe void ratio, compaction energy and soil structure as interfering factors to determine the elastic modulus, therefore, they should also be considered for ultrasonic tests. The porosity, a parameter related to the void ratio, directly interferes in velocity (Chen *et al.*, 2016; Luong *et al.*, 2014) and must be considered in ultrasonic testing, because of the absorption and scattering of the ultrasonic pulse (Bauer, 2000; Cultrone *et al.*, 2001; Lombillo *et al.*, 2014; Qasrawi, 2000; Sarro *et al.*, 2015).

Other studies indicate water content, soil density and type of transducer as factors that also interfere in ultrasonic velocity (Cardoso *et al.*, 2017; Champiré *et al.*, 2016; Chen *et al.*, 2017; Dongqing *et al.*, 2016; Ferreira *et al.*, 2014; Sarro *et al.*, 2017; Teixeira *et al.*, 2015). Thus, the aim of this study was to investigate the correlation between the elastic modulus obtained from ultrasonic testing and the modulus obtained through a simple unconfined compression test on clay soil specimens compressed at different moisture content.

2. Materials and Methods

2.1. Soil characterization and compaction

Deformed samples were collected from the deposits available in the region of Limeira (São Paulo, Brazil), a characteristic soil of the region (Fig. 1). The choice of deposit considered an area with minimum traffic of people where there was no need for deep excavations, guaranteeing the homogeneity of the material. After extraction, the



Figure 1 - Location of extraction of the soil sample.

sample was sieved and prepared (ABNT, 2016a) for characterization according to grain size distribution test (sieving and sedimentation) (ABNT, 2016b) and density.

To define the optimum moisture content and the maximum dry unit weight of the samples, we performed compaction tests using the Proctor method at normal compaction energy (ABNT, 2016c). Then, we molded specimens at 2% below the optimum moisture content (A1), at the optimum moisture content (A2), and 2% above the optimum moisture content (A3). Five cylindrical specimens (diameter 100 mm, height 127 mm) were molded for each moisture content and for each storage condition (packed and unpacked), totaling 30 specimens. All samples were exposed to the environment conditions of the laboratory for 120 days.

2.2. Ultrasonic testing

The nondestructive ultrasonic testing was performed 120 days after molding using the Epoch4 equipment (Panametrics, USA) with 500 kHz frequency transducers capable of measuring longitudinal and transverse waves. The compressional (V_p) and shear (V_s) velocities were calculated through the relation between the distance traveled by the wave (d), in millimeters, and the time of the course (t), in microseconds. In the tests with the shear transducer, a coupler gel (corn glucose) was required to minimize reflection and refraction of ultrasonic pulse. The aim of the ultrasonic testing was to determine the elastic modulus of the samples to compare with the results obtained from the destructive method (compression test).

$$V = \frac{d}{t} \quad (1)$$

2.3. Determination of the elastic modulus by ultrasonic test

The stiffness matrix (Eq. 3) was determined using the longitudinal (V_p) and shear (V_s) velocities and considering the soil as an isotropic material, where the parameters of the diagonal (C_{ii}) $C_{11} = C_{22} = C_{33}$ were calculated using an average of the V_p and likewise $C_{44} = C_{55} = C_{66}$ and using an average of the V_s (Eq. 2).

Through the inverse of stiffness matrix, the flexibility matrix (Eq. 4), we can determine the longitudinal elastic modulus (E_{US}) using the nondestructive ultrasonic testing (Eq. 5). Other elastic constants, such as the shear modulus (G_{US}) and Poisson's ratio (ν_{US}), can be determined using the matrices, S_{44} and S_{12} , respectively; however, this was not the focus of this study.

$$C_{ii} = \rho V_{ii}^2 \quad (2)$$

$$[C]_{Isotropic} = \begin{bmatrix} C_{11} & C_{12} & C_{12} & 0 & 0 & 0 \\ C_{12} & C_{11} & C_{12} & 0 & 0 & 0 \\ C_{12} & C_{12} & C_{11} & 0 & 0 & 0 \\ 0 & 0 & 0 & C_{44} & 0 & 0 \\ 0 & 0 & 0 & 0 & C_{44} & 0 \\ 0 & 0 & 0 & 0 & 0 & C_{44} \end{bmatrix} \quad (3)$$

$$[S]_{Isotropic} = \begin{bmatrix} S_{11} & S_{12} & S_{12} & 0 & 0 & 0 \\ S_{12} & S_{11} & S_{12} & 0 & 0 & 0 \\ S_{12} & S_{12} & S_{11} & 0 & 0 & 0 \\ 0 & 0 & 0 & S_{44} & 0 & 0 \\ 0 & 0 & 0 & 0 & S_{44} & 0 \\ 0 & 0 & 0 & 0 & 0 & S_{44} \end{bmatrix} \quad (4)$$

$$E_{US} = \frac{1}{S_{11}} \quad (5)$$

Christoffel (Bucur, 2006) developed the theoretical equations above and these have already been applied for wood by other researchers (Gonçalves *et al.*, 2011b, 2014; Kohlhauser & Hellmich, 2012; Vázquez *et al.*, 2015), in concrete (Gonçalves *et al.*, 2011a) and stabilized soil (Ferreira *et al.*, 2013; Hoffmann & Gonçalves, 2010; Milani, 2008).

2.4. Determination of the elastic modulus by compression test

After the ultrasonic test, the specimens were subjected to unconfined simple axial compression tests by the press EMIC 23-600 of the brand INSTRON/EMIC (Fig. 2), with deflection control to determine the static elastic modulus (E_{ST}). The method used was adapted according to the standards of resistance to unconfined compression of cohesive soils and elastic modulus of concrete (ABNT, 1992, 2008).

To validate the results between the moduli obtained by ultrasonic and by static testing, statistical tests (linear regression, confidence interval, t-test) were performed using the Origin 8.1 software to determine if there is a statistically significant correlation between the analysed variables.



Figure 2 - Compressive strength with deflection control.

3. Results and Discussion

3.1. Characterization

As shown in the particle size curve (Fig. 3), the soil used was classified as ML, according to the Unified Soil Classification System (USCS), composed of 55% clay, 23% sand and 22% silt, with a specific weight of the solids equal to 27.9 kN.m⁻³.

The results of optimum moisture content and maximum dry unit weight used to mold the specimens were obtained from the compaction curves. The specimens were molded according to the moisture conditions described in Table 1, 15 of them were packed and 15 exposed to laboratory air for 120 days.

The increase in compaction energy results in a decrease in the macroscopic and microscopic pores of granular materials (Caputo, 1988; Pinto, 2006) and the velocity can vary according to the propagation medium and the presence of voids. Due to this, it was decided to analyze the three compaction energies of the Proctor method (ABNT, 2016c). Mansour *et al.* (2016) points out that the variation in porosity and voids can interfere with the application of acoustic methods of investigation applied to compacted soil.

The purpose of the two types of storage (packed and unpacked) was to qualify the velocity differences of specimens with variations of moisture and density. Thus, we verified an average loss of approximately 17.0% in moisture and 17.0% in density in the unpacked specimens, in contrast to 2.9% and 2.6%, respectively, in those that remained packed, after 120 days.

Table 1 - Casting conditions based on moisture content.

Condition	Optimum moisture content (%)	Dry unit weight (kN.m ⁻³)	Porosity (%)	Voids ratio
A1	21.40	15.14	43	0.76
A2	23.40	15.89	40	0.68
A3	25.40	15.68	38	0.61

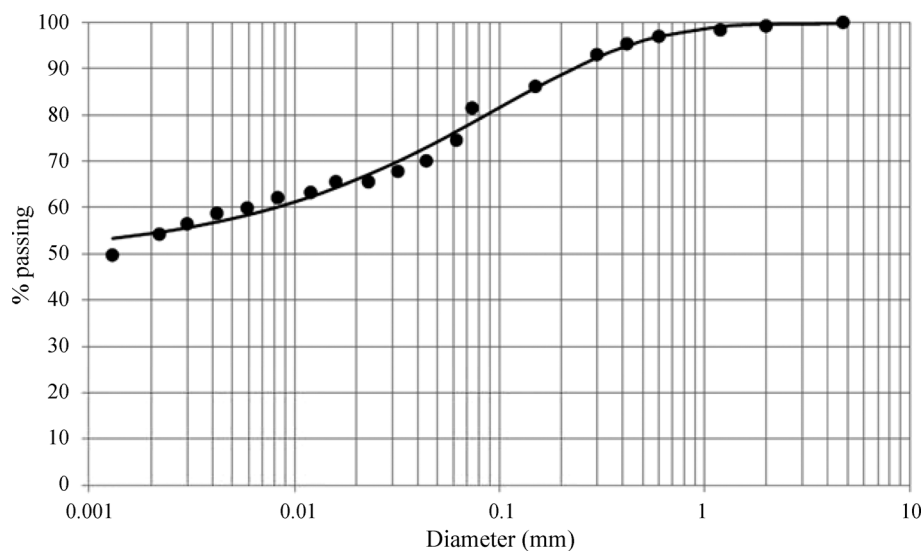


Figure 3 - Soil particle-size distribution.

3.2. Nondestructive testing

The final velocities obtained for the packed specimens were lower than on the exposed specimens by approximately 20% for longitudinal to compressive wave velocities (V_p) and 26% for shear wave (V_s) velocities. This behavior was expected due to the moisture content presence, which increases the dispersion of the ultrasonic pulse (Bernat-Maso *et al.*, 2017; Luong *et al.*, 2014). Additionally, we can consider the occurrence of a thixotropic behavior, which may increase the resistance in clayey samples with a high degree of saturation when kept at rest (Jeong *et al.*, 2015; Seng & Tanaka, 2012).

The V_p values obtained in this study ranged between 891 and 1407 $\text{m}\cdot\text{s}^{-1}$ (Figs. 4a and 5a), for the packed and unpacked specimens, respectively, and agree with values found in the literature. Studies that use soils classified as sandy are usually more common, with V_p located between 954 and 1376 $\text{m}\cdot\text{s}^{-1}$ (Ferreira *et al.*, 2013; Hoffmann & Gonçalves, 2010; Milani, 2008; Sarro *et al.*, 2015). For clayey and compacted soils at intermediate energy (the

same used in this research), Teixeira *et al.* (2015) obtained a mean V_p of 1444 $\text{m}\cdot\text{s}^{-1}$. Sarro *et al.* (2017) used normal compaction energy and obtained mean values of approximately 1500 $\text{m}\cdot\text{s}^{-1}$.

Regarding V_s , we obtained values between 491 and 837 $\text{m}\cdot\text{s}^{-1}$ (Figs. 4b and 5b), for the packed and unpacked specimens, respectively. There is not enough data on this type of velocity due to the lack of research on the application of ultrasonic testing in soil. Hoffmann & Gonçalves (2010) obtained mean values of 502 $\text{m}\cdot\text{s}^{-1}$ for samples of sandy soil molded at normal energy and kept in moist environment for seven days, while Milani (2008) obtained average V_s of 810 $\text{m}\cdot\text{s}^{-1}$ for stabilized soil with 7% Portland cement. Wang *et al.* (2006) studied frozen soil samples and obtained higher V_s values than other authors (mean of 1120 $\text{m}\cdot\text{s}^{-1}$). This behavior is expected due to increased water viscosity with decreasing temperature, which reduces the velocity of wave propagation (Bucur, 2006; IAEA, 2002).

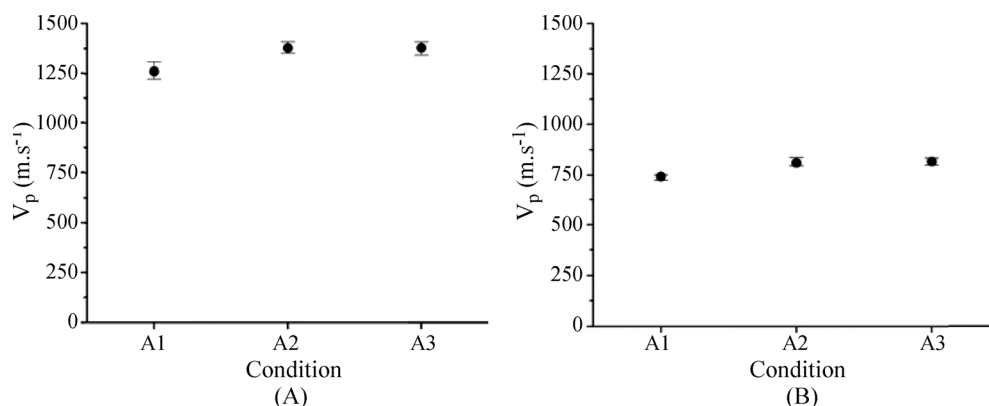


Figure 4 - Comparison between V_p (A) and V_s (B) of each condition for the unpacked specimens.

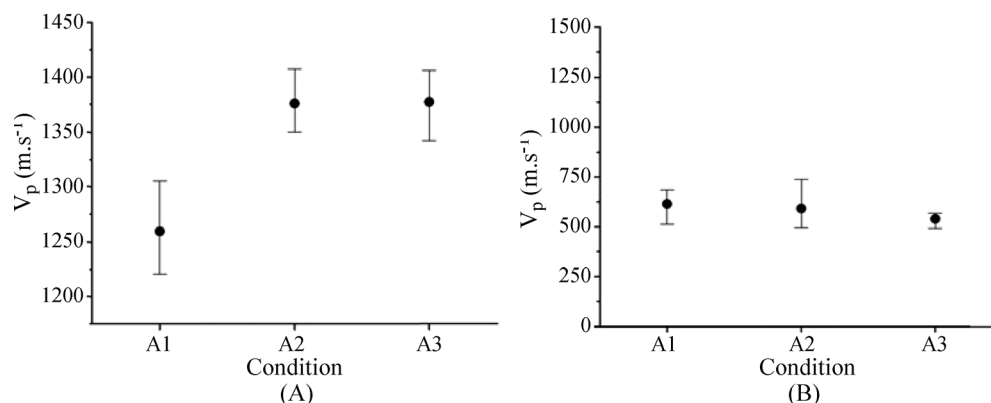


Figure 5 - Comparison between V_p (A) and V_s (B) of each condition for the packed specimens.

The high variation in the values of V_s and V_p is due to the storage difference of the samples. In the packed specimens, the velocities were lower because of the higher moisture content. This effect was also observed by Sarro (2017) and Sarro *et al.* (2017) when comparing samples with different moisture content. In addition, the presence of water in the pores of the material may still result in a decrease in the ultrasonic wave amplitude (Bernat-Maso *et al.*, 2017; Mansour *et al.*, 2016; Markov *et al.*, 2014).

When comparing the three moisture conditions of the unpacked specimens analyzed through Student's t-test and ANOVA, conditions A2 and A3 are statistically equal (p-value = 0.00), the only condition that showed same statistically significant difference was A1 (Fig. 4). Although these specimens lost moisture to the environment during the same period (120 days), the variations in compaction moisture caused differences in the microstructure. The ultrasonic testing identified this microstructural difference, which is more significant when moisture is above the optimum (Andrianatrehina *et al.*, 2018; Otálvaro *et al.*, 2015; Romero, 2013).

Regarding the specimens that were packed, the velocities of the three moisture contents presented significant statistical difference (Fig. 5). This difference is caused by

the higher water content, which differentiates the soil microstructure (Otálvaro *et al.*, 2015). This behavior corroborates the assertion that moisture content is the factor that most influences velocity (Sarro *et al.*, 2017; Teixeira *et al.*, 2015).

The longitudinal moduli obtained by ultrasonic testing (E_{us}) (Fig. 6) on the exposed specimens was higher than on the packed specimens by 32%, which had a higher coefficient of variation ($CV = 15\%$; 32% and 7% for A1, A2 and A3, respectively) due to the greater water content. Moreover, for the unpacked specimens, the modules were considered statistically equal for the A2 and A3 condition, while for packed specimens the three moisture content conditions were statistically different.

The elastic moduli were higher in unpacked test bodies due to partial loss of moisture, causing the suction effect. According to literature, the modulus of elasticity in clay soils is influenced directly by the degree of saturation and suction, being this parameter higher in soils with lower moisture content (Adem & Vanapalli, 2015; Vanapalli & Adem, 2014).

Furthermore, the velocity is influenced directly by the moisture content, as verified in other researches (Bui *et al.*, 2014a; Cardoso *et al.*, 2017; Champiré *et al.*, 2016; Chen *et*

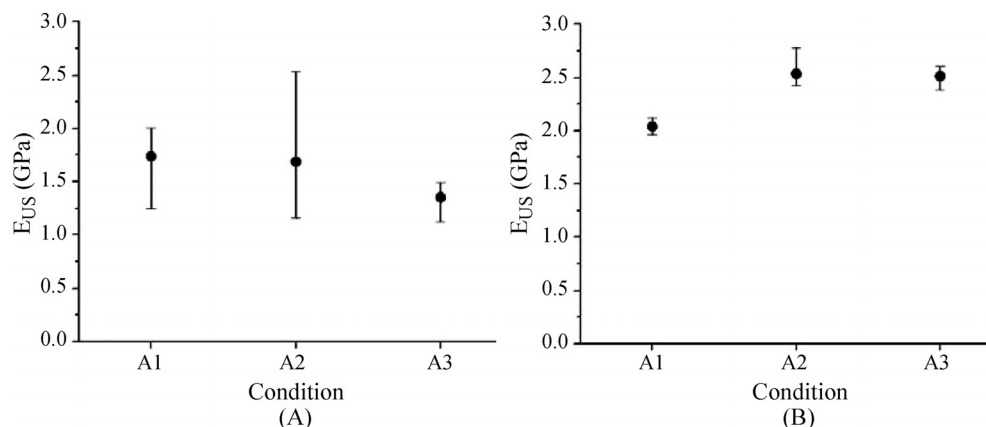


Figure 6 - Elastic modulus obtained by ultrasonic testing for the packed (A) and unpacked (B) specimens.

al., 2017; Dongqing *et al.*, 2016; Sarro *et al.*, 2017), being higher in specimens with lower moisture content. Therefore, since the E_{us} is calculated from the velocity, the value of the modulus being higher for these specimens was expected.

We compared our results for the modulus with results from the literature to highlight the importance of this study (Table 2).

The elastic modulus obtained by ultrasonic testing for unpacked specimens (Fig. 6b) presented similar values to those obtained by Wang *et al.* (2006) and Christ & Park (2009), being 2.75 and 2.5 GPa, respectively. However, these authors used frozen materials in their research. Other authors found in the literature cannot be compared with this research because they studied a different type of soil (sandy).

The values obtained by Bui *et al.* (2014a) were lower than those obtained by other authors for the modulus of

elasticity, the behavior was similar to that of the present study, where the modulus was higher for unpacked (dry) samples than for packed (wet) samples.

3.3 Mechanical characterization

Unpacked specimens presented greater compressive strength (F_c) when compared with packed specimens (Fig. 7). A possible explanation for this is that soils with higher saturation have lower resistance (Caputo, 1988; Pinto, 2006). Teixeira *et al.* (2015) and Bandeira (2009) also observed this behavior, their research having been performed on sandy and clayey soil, respectively. Ferreira & Freire (2005) used silty soil and obtained a compressive strength of 2.60 MPa.

The static elastic modulus (E_{st}) (Fig. 8) presented the same behavior as those obtained by ultrasonic testing (Fig. 6a), *i.e.*, the values of unpacked specimens were ap-

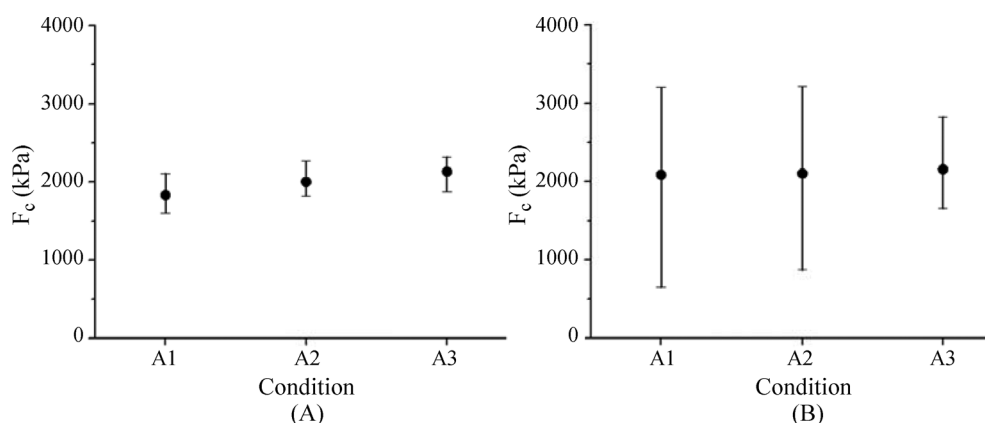


Figure 7 - Simple unconfined compression strength of packed (A) and unpacked (B) specimens.

Table 2 - Summary of elastic modulus values obtained by other authors.

Author	Material	Elastic Modulus (GPa)
Nondestructive testing (E_{us})		
Ferreira <i>et al.</i> (2013)	Sandy	1.66
Hoffmann & Gonçalves (2010)	Sandy	1.14
Christ & Park (2009)	Silty	2.50
Milani (2008)	Sandy (soil-cement)	5.70
Wang <i>et al.</i> (2006)	Clayey	2.75
Destructive testing (E_{st})		
Champiré <i>et al.</i> (2016)	Sandy	1.20-2.80
Lombillo <i>et al.</i> (2014)	Sandy	0.36
Bui <i>et al.</i> (2014a)	Sandy	0.58-0.18 ¹ 0.95-0.39 ²
Miccoli <i>et al.</i> (2014)	Sandy	2.20

¹For 2% and 11%, respectively, of sand-silt soil.

²For 3% and 8% moisture, respectively, of a silt-clay soil.

proximately 55% greater than those exposed. However, E_{US} (Fig. 6a) and E_{ST} (Fig. 8) showed similarities, with values between 1.25 and 2.50 GPa.

Miccolli *et al.* (2014) determined the static modulus of mini-walls of compacted soil blocks and obtained $E_{ST} = 2.2$ GPa. Although we used a different soil from that research (sandy), the values are within the same range. Champiré *et al.* (2016) studied specimens molded with three types of sandy soil and obtained values between 1.2 and 2.8 GPa.

We must emphasize that the values found in the literature are very different from those mentioned above, which is due to the plastic behavior of the soil and the conditions of the test. Although the results of Bui *et al.* (2014a) are not consistent with our results, the behavior observed by the author was the same, the modulus being greater for dry specimens when compared with moist specimens.

Therefore, the need for research in this area is evident, considering the scarcity of elastic modulus values for both destructive and nondestructive tests.

3.4. Statistical analysis

The correlation coefficients (R) between compressive strength (F_c) and static elastic modulus (E_{ST}) were high for both storage conditions, with R equal to 0.97 and 0.99 for the unpacked and packed condition, respectively (Table 3).

In this case, the static modulus of the unpacked condition is directly proportional to the increase in resistance. For the packed condition, it is inversely proportional.

The same occurs when the static and ultrasonic modulus are correlated, with R equal to 0.98 for both storage conditions, being directly proportional for the unpacked specimens and inversely proportional for the packed specimens. This behavior is consistent since the modulus, as well as velocity, tends to be smaller the greater the moisture content.

4. Conclusion

The ultrasonic testing allows to infer resistance and elasticity properties of compacted soil, considering the high correlations obtained between these parameters. Nevertheless, to validate the use of the technique in determining the elastic constants as a whole, including the shear modulus and Poisson's ratio, it is necessary to obtain these parameters with triaxial tests, verifying the correlation between them.

Further study is required on the influence of moisture in the ultrasound test, since this factor directly influences the mechanical behavior of the material when compacted. Even so, the test allowed us to detect differences in moisture in specimens, indicating the potential of the technique in compaction control.

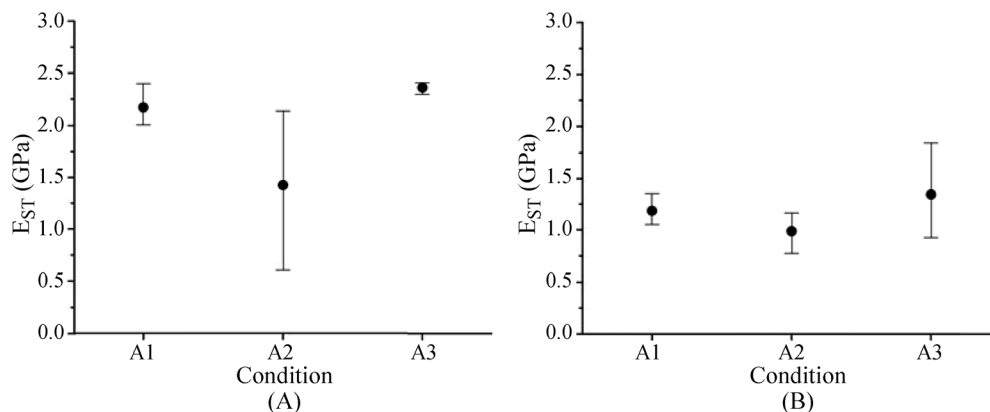


Figure 8 - Static Moduli for the unpacked (A) and packed (B) specimens.

Table 3 - Correlations obtained between the static modulus, dynamic modulus, and compressive strength.

Parameters	R	R^2	Equation	p-value
Unpacked				
$F_c - E_{ST}$	0.97	0.95	$E_{ST} = 0.0033F_c - 4.679$	0.005
$E_{ST} - E_{US}$	0.98	0.96	$E_{US} = 2.6296E_{ST} - 3.6484$	0.003
Packed				
$F_c - E_{ST}$	0.99	0.98	$E_{ST} = -0.0023F_c + 5.6647$	0.000
$E_{ST} - E_{US}$	0.98	0.96	$E_{US} = -2.0462E_{ST} + 4.1091$	0.003

Acknowledgments

The authors thank Espaço da Escrita - Coordenadoria Geral da Universidade - UNICAMP - for the language services provided.

References

- ABNT (1992). NBR 12770: Solo Coesivo - Determinação da Resistência à Compressão Não Confinada - NBR 12770. Associação Brasileira de Normas Técnicas - ABNT, Rio de Janeiro, RJ, Brazil, 4 p.
- ABNT (2008). Concreto - Determinação do Módulo Elástico de Elasticidade à Compressão - NBR 8522. Associação Brasileira de Normas Técnicas - ABNT, Rio de Janeiro, RJ, Brazil, 20 p.
- ABNT (2016a). Amostras de Solo - Preparação Para Ensaios de Compactação e Ensaios de Caracterização - NBR 6457. Associação Brasileira de Normas Técnicas, Rio de Janeiro, RJ, Brazil, 8 p.
- ABNT (2016b). Solo - Análise Granulométrica - NBR 7181. Associação Brasileira de Normas Técnicas, Rio de Janeiro, Brazil, 12 p.
- ABNT (2016c). Solo - Ensaio de Compactação - NBR 7182. Associação Brasileira de Normas Técnicas, Rio de Janeiro, RJ, Brazil, 9 p.
- Adem, H.H.; & Vanapalli, S.K. (2015). Prediction of the modulus of elasticity of compacted unsaturated expansive soils. *International Journal of Geotechnical Engineering*, 9(2):163-175.
- Andrianatrehina, S.R.; Taibi, S.; & Boutonnier, L. (2018). Bearing capacity, small-strain stiffness and air permeability of non-standard compacted soils related to suction. *European Journal of Environmental and Civil Engineering*, 22(11):1399-1415.
- Bandeira, R.F. (2009). Resistência Mecânica e Velocidade Ultrassônica Para Um Material Terroso. M.Sc. Dissertation, Department of Architecture, Federal University of Minas Gerais, Belo Horizonte, 89p.
- Bauer, L.A.F. (2000). *Materiais de Construção*. v. 1, 5th ed. LTC, Rio de Janeiro, 488 p.
- Bernat-Maso, E.; Teneva, E.; Escrig, C.; & Gil, L. (2017). Ultrasound transmission method to assess raw earthen materials. *Construction and Building Materials*, 156:555-564.
- Bucur, V. (2006). *Acoustics of Wood*. 2nd ed. Springer, France, 394 p.
- Bucur, V.; & Archer, R.R. (1984). Elastic constants for wood by an ultrasonic method. *Wood Science and Technology*, 18:255-265.
- Bui, Q.-B.; & Morel, J.-C. (2009). Assessing the anisotropy of rammed earth. *Construction and Building Materials*, 23(9):3005-3011.
- Bui, Q.B.; Morel, J.-C.; Hans, S.; & Walker, P. (2014a). Effect of moisture content on the mechanical characteristics of rammed earth. *Construction and Building Materials*, 54:163-169.
- Bui, T.T.; Bui, Q.B.; Limam, A.; & Maximilien, S. (2014b). Failure of rammed earth walls: From observations to quantifications. *Construction and Building Materials*, 51:295-302.
- Cai, Y.; Dong, Q.; Wang, J.; Gu, C.; & Xu, C. (2015). Measurement of small strain shear modulus of clean and natural sands in saturated condition using bender element test. *Soil Dynamics and Earthquake Engineering*, 76:100-110.
- Caputo, H.P. (1988). *Mecânica dos Solos e Suas Aplicações*. v. 1, 6th ed., LTC, Rio de Janeiro, 234p.
- Cardoso, S.M.; Assis, G.M. de; Sarro, W. de S.; & Ferreira, G.C. dos S. (2017). Caracterização de misturas de solo e areia descartada de fundição. Proc. 6th International Workshop - Advances in Cleaner Production, São Paulo, SP, available at <http://www.advancesincleanerproduction.net>.
- Champiré, F.; Fabbri, A.; Morel, J.C.; Wong, H.; & McGregor, F. (2016). Impact of relative humidity on the mechanical behavior of compacted earth as a building material. *Construction and Building Materials*, 110:70-78.
- Chen, J.; Wang, H.; & Yao, Y. (2016). Experimental study of nonlinear ultrasonic behavior of soil materials during the compaction. *Ultrasonics*, 69:19-24.
- Chen, Y.; Uchimura, T.; Irfan, M.; Huang, D.; & Xie, J. (2017). Detection of water infiltration and deformation of unsaturated soils by elastic wave velocity. *Landslides*, 14(5):1715-1730.
- Choo, H.; Jun, H.; & Yoon, H. K. (2018). Porosity estimation of unsaturated soil using Brutsaert equation. *Soil Dynamics and Earthquake Engineering*, 104:33-39.
- Christ, M.; & Park, J.B. (2009). Ultrasonic technique as tool for determining physical and mechanical properties of frozen soils. *Cold Regions Science and Technology*, 58(3):136-142.
- Cultrone, G.; Sebastián, E.; Cazalla, O.; Nechar, M.; Romero, R.; & Bagur, M. G. (2001). Ultrasound and mechanical tests combined with ANOVA to evaluate brick quality. *Ceramics International*, 27(4):401-406.
- Dias, I.D.M. (2007). Estudo de Solos Tropicais Para Uso em Pavimentação a Partir de Ensaios Triaxiais Estáticos. M.Sc. Dissertation, Department of Civil Engineering, University of São Paulo, São Paulo, 139 p.
- Dongqing, L.I.; Xing, H.; Feng, M.; & Yu, Z. (2016). The Impact of Unfrozen Water Content on Ultrasonic Wave Velocity in Frozen Soils. *Procedia Engineering*, 143:1210-1217.
- Ferreira, G.C. dos S.; Gonçalves, R.; Hoffmann, M.; Sarro, W. de S.; & André Campanho. (2013). Determinação de propriedades de solo compactado utilizando ensaios de ultrassom. Proc. 12ª Conferência sobre Tecnologia de

- Equipamentos, Abendi, Porto de Galinhas, PE, available in CD-ROM.
- Ferreira, G.C. dos S.; Sarro, W. de S.; Hoffmann, M.; & Gonçalves, R. (2014). Influência das camadas de compactação em inspeções de painéis monolíticos de solo-cimento por ultrassom. Proc. Congresso Nacional de Ensaio Não Destrutivo e Inspeção - ConaEnd2014, Abendi, São Paulo, SP, available in CD-ROM.
- Ferreira, R. de C.; & Freire, W.J. (2005). Desempenho físico-mecânico de minipainéis de terra crua tratada com aditivos químicos. Engenharia Agrícola, 25(3):585-597.
- Gonçalves, R.; Giaccon Junior, M.; & Lopes, I.M. (2011a). Determining the concrete stiffness matrix through ultrasonic testing. Engenharia Agrícola, 31(3):427-437.
- Gonçalves, R.; Trinca, A.J.; & Cerri, D.G.P. (2011b). Comparison of elastic constants of wood determined by ultrasonic wave propagation and static compression testing. Wood and Fiber Science, 43(1):64-75.
- Gonçalves, R.; Trinca, A.J.; & Pellis, B.P. (2014). Elastic constants of wood determined by ultrasound using three geometries of specimens. Wood Science and Technology, 48(2):269-287.
- Hammam, A.H.; & Eliwa, M. (2013). Comparison between results of dynamic & static moduli of soil determined by different methods. Housing and Building National Research Center, 9(2):144-149.
- Hoffmann, M.V.; & Gonçalves, R. (2010). Análise da qualidade da taipa de pilão por meio de ondas ultrasônicas. Proc. III Congresso de Arquitetura e construção com terra no Brasil, Terra Brasil 2010, Campo Grande, MS, CD-ROM.
- International Atomic Energy Agency (2002). Guidebook on Non-Destructive Testing of Concrete Structures. IAEA, Training Course Series, Vienna, 17:231.
- Jeong, S.W.; Locat, J.; Torrance, J.K.; & Leroueil, S. (2015). Thixotropic and anti-thixotropic behaviors of fine-grained soils in various flocculated systems. Engineering Geology, 196:119-125.
- Kohlhauser, C.; & Hellmich, C. (2012). Determination of Poisson's ratios in isotropic, transversely isotropic, and orthotropic materials by means of combined ultrasonic-mechanical testing of normal stiffnesses: Application to metals and wood. European Journal of Mechanics - A/Solids, 33:82-98.
- Lombillo, I.; Villegas, L.; Fodde, E.; & Thomas, C. (2014). In situ mechanical investigation of rammed earth: Calibration of minor destructive testing. Construction and Building Materials, 51:451-460.
- Luong, J.; Destain, M.F.; & Mercatoris, B.C.N. (2014). Characterisation of structural properties of soil using ultrasonic waves. American Society of Agricultural and Biological Engineers Annual International Meeting, ASABE 2014, v. 6, pp. 4582-4593.
- Maillard, P.; & Aubert, J.E. (2014). Effects of the anisotropy of extruded earth bricks on their hygrothermal properties. Construction and Building Materials, 63:56-61.
- Mansour, M. Ben; Ogam, E.; Fellah, Z.E.A.; Cherif, A.S.; Jelidi, A.; & Ben, S. (2016). Characterization of compressed earth blocks using low frequency guided acoustic waves. The Journal of the Acoustical Society of America, 139(5):2551-2560.
- Markov, A.M.; Markov, M.G.; Jarillo, G.R.; & Sadovnychiy, S.N. (2014). Acoustic Reverberation in a logging tool - Borehole - Saturated. Physics of the Solid Earth, 50(2):289-295.
- Miccoli, L.; Müller, U.; & Fontana, P. (2014). Mechanical behaviour of earthen materials: A comparison between earth block masonry, rammed earth and cob. Construction and Building Materials, 61:327-339.
- Miccoli, L.; Oliveira, D.V.; Silva, R.A.; Müller, U.; & Schueremans, L. (2015). Static behaviour of rammed earth: experimental testing and finite element modelling. Materials and Structures, 48:3443-3456.
- Milani, A.P. da S. (2008). Avaliação Física, Mecânica e Térmica do Material Solo-Cimento-Cinza de Casca de Arroz e seu Desempenho como Parede Monolítica. Ph.D. Dissertation, Department of Agricultural Engineering, University of Campinas, Campinas, 175 p.
- Motalleb Nejad, M.; Manahiloh, K.N.; & Momeni, M.S. (2017). Random-effects regression model for shear wave velocity as a function of standard penetration test resistance, vertical effective stress, fines content, and plasticity index. Soil Dynamics and Earthquake Engineering, 103:95-104.
- Oh, W.T.; & Vanapalli, S.K. (2016). Influence of Poisson's Ratio on the Stress vs. Settlement Behavior of Shallow Foundations in Unsaturated Fine-Grained Soils. Soils and Rocks, 39(1):71-79.
- Otálvaro, I.F.; Neto, M.P.C.; & Caicedo, B. (2015). Compressibility and microstructure of compacted laterites. Transportation Geotechnics, 5:20-34.
- Pegah, E.; Liu, H.; & Dastanboo, N. (2017). Evaluation of the lateral earth pressure coefficients at-rest in granular soil deposits using the anisotropic components of S-wave velocity. Engineering Geology, 230:55-63.
- Pietruszczak, S.; & Krucinski, S. (1989). Description of anisotropic response of clays using a tensorial measure of structural disorder. Mechanics of Materials, 8(2-3):237-249.
- Pinto, C. de S. (2006). Curso Básico de Mecânica dos Solos (16 Aulas) - 3rd ed. Oficina de Textos, São Paulo, 354 p.
- Qasrawi, H.Y. (2000). Concrete strength by combined non-destructive methods simply and reliably predicted. Cement and Concrete Research, 30(5):739-746.

- Romero, E. (2013). A microstructural insight into compacted clayey soils and their hydraulic properties. *Engineering Geology*, 165:3-19.
- Sarro, W. de S.; Ferreira, G.C. dos S.; Cardoso, S.M.; & Assis, G.M. de. (2017). Influência dos transdutores no ensaio de ultrassom aplicado a solo compactado. 14^a Conferência sobre tecnologia de equipamentos, Abendi, Rio de Janeiro, CD-ROM.
- Sarro, W. de S. (2017) Constantes Elásticas de Solo Compactado a Partir do Ensaio de Ultrassom. M.Sc. Dissertation, Department of Technology, University of Campinas, 87 p.
- Sarro, W. de S.; Ferreira, G.C. dos S.; & Galletto, A. (2015). Técnica de ultrassom aplicada na inspeção de edificações construídas em solo compactado. Proc. 57^o Congresso Brasileiro do Concreto, CBC2015, IBRACON, Bonito, MS, CD-ROM.
- Seng, S.; & Tanaka, H. (2012). Properties of very soft clays: A study of thixotropic hardening and behavior under low consolidation pressure. *Soils and Foundations*, 52(2):335-345.
- Teixeira, I.; Sarro, W. de S.; Cardoso, S.M.; Macedo, G.; & Ferreira, G.C. dos S. (2015). Influência da granulometria e umidade nas propriedades de solos a partir de ensaios destrutivos e não destrutivos. Proc. XXIX Congresso Nacional de Pesquisa em Transporte da ANPET, ANPET, Ouro Preto, pp. 196-207.
- Vanapalli, S.K.; & Adem, H.H. (2014). Elasticity moduli of expansive soils from dimensional analysis. *Geotechnical Research*, ICE publishing, 1(2):60-72.
- Vázquez, C.; Gonçalves, R.; Bertoldo, C.; Baño, V.; Vega, A.; Crespo, J.; & Guaita, M. (2015). Determination of the mechanical properties of *Castanea sativa* Mill. using ultrasonic wave propagation and comparison with static compression and bending methods. *Wood Science and Technology*, 49(3):607-622.
- Wang, D.Y.; Zhu, Y.L.; Ma, W.; & Niu, Y.H. (2006). Application of ultrasonic technology for physical-mechanical properties of frozen soils. *Cold Regions Science and Technology*, 44(1):12-19.
- Yang, H.; Zhou, Z.; Wang, X.; & Zhang, Q. (2015). Elastic Modulus Calculation Model of a Soil-Rock Mixture at Normal or Freezing Temperature Based on Micro-mechanics Approach. *Advances in Materials Science and Engineering*, 2015:1-10.
- Yu, C.; Ji, S.; & Li, Q. (2016). Effects of porosity on seismic velocities, elastic moduli and Poisson's ratios of solid materials and rocks. *Journal of Rock Mechanics and Geotechnical Engineering*, 8(1):35-49.

Geotechnical Behavior and Soil-Fiber Interaction of Clayey Soil Mixed with Randomly Dispersed Coconut Fibers

A.I. Oliveira Júnior, J.F.T. Jucá, J.A. Ferreira, L.C. Guilherme

Abstract. This study aims to experimentally analyze the influence of the addition of different amounts of short coconut fibers on the geotechnical properties of tropical clay soil. Samples with 0, 0.5, 1, and 2 wt% of fiber in regard to the dry weight of soil were analyzed. Compaction, direct shear, compressibility, hydraulic conductivity, scanning electron microscopy (SEM), and energy dispersive spectroscopy (EDS) tests were performed on samples. The best results for the direct shear test were presented by the sample with 1 wt% of fiber. For the compressibility, the results improved proportionally to the added content of coconut fiber. Samples with less than 1 wt% did not show any significant changes in the hydraulic conductivity test; the hydraulic conductivity remained of the order of magnitude of 10^{-7} cm/s. The SEM and EDS analyses revealed the existence of bonds between the particles of clay and coconut fibers surface. The geotechnical behavior of the mixes with 0.5 and 1 wt% was improved because of this bond between the matrix and reinforcement phase.

Keywords: clayey soil-coconut fiber bond, compressibility, hydraulic conductivity, reinforced soil, shear strength.

1. Introduction

Clay soils have many applications in geotechnical engineering projects, most of them concerning their low hydraulic conductivity coefficient. For instance, they are vastly used for building contaminant barriers and landfill layers. Furthermore, for these types of practical applications, besides the hydraulic conductivity, the material should also present proper mechanical properties and low compressibility. These aspects are important and should not be neglected because the material is subjected to certain loads that may break it apart. Moreover, highly compressible materials can deform exaggeratedly, which may compromise the integrity of a compacted layer.

Gathering materials that combine all these crucial characteristics is the biggest challenge because of certain limitations, such as the lifespan of deposits or distance between deposits and application sites. Therefore, it is necessary to resort to different alternatives, such as the development of new materials that are both sustainable and possess similar or even better characteristics than conventional materials.

Geotechnical materials can be developed by reinforcing soil with short and randomly spread fibrous materials (Kumar & Sharma, 2018). This technique has proven its efficiency, especially with regard to the mechanical behavior of the resulting material. Many studies reported that the inclusion of fibers in a soil matrix, primarily with fine grains, raises the shear resistance of the material (Donato *et al.*, 2004; Babu & Vasudevan, 2008; Maliakal & Thiyyak-

kandi, 2013; Mohamed, 2013). However, better understanding of how this technique can affect other geotechnical properties of the soil-fiber compound is required.

The performance of a soil-fiber mixture depends not only on the individual properties of the constituents, but also on the compatibility between the fibers and soil. The interface between reinforcement and matrix constitutes the contact area of the elements in the blend and is essential for the transmission of mechanical tensions from the matrix to the reinforcement (Tang *et al.*, 2010). Therefore, the bond between fibers and soil is indispensable for improving the properties of the composite. According to Donato *et al.* (2004), clay soil matrices have reasonable bonding to fiber surfaces because of the format, size, and load distribution of the clay minerals. Rosário *et al.* (2011) found that vegetal fibers present predominantly polar surface energy, making them suitable for reinforcing matrices with polar electrostatic nature.

In Brazil, fibrous residues coming from green coconut (*Cocos nucifera*) are in the spotlight because of the great production and volume of discarded material. Approximately 85% of coconut weight, which is averagely 1.5 kg, is contained in its shell (Corradini *et al.*, 2009), which is constituted of a voluminous fibrous material with low degradation rate. Generally, these residues are inadequately discarded, causing environmental pollution, reducing the lifespan of landfills, and hosting microorganisms, which can transmit diseases. Actually, the recovery of waste to raise the useful life of landfills and to reduce negative environmental impacts is one of the main issues that

Antônio Italcly de Oliveira Júnior, Ph.D. Student, Departamento de Engenharia Civil, Universidade Federal de Pernambuco, Recife, PE, Brazil, e-mail: antonioitalcly@hotmail.com.

José Fernando Thomé Jucá, Ph.D., Full Professor, Departamento de Engenharia Civil, Universidade Federal de Pernambuco, Recife, PE, Brazil, e-mail: jucah@ufpe.br.

Janilson Alves Ferreira, Ph.D. Student, Departamento de Ciência dos Materiais, Universidade Federal de Pernambuco, Recife, PE, Brazil, e-mail: janilsonengmat@gmail.com.

Lais Chaves Guilherme, M.Sc. Student, Departamento de Engenharia Civil, Universidade Federal de Pernambuco, Recife, PE, Brazil, e-mail: laiscguilherme@hotmail.com.

Submitted on June 22, 2018; Final Acceptance on July 8, 2019; Discussion open until December 31, 2019.

DOI: 10.28927/SR.422127

several researchers have been trying to solve. Therefore, using the discarded coconut shells as reinforcement for soils can contribute to minimize some of these issues.

This study aims to experimentally analyze the best proportion of compacted clay soil and coconut fiber mixtures for applying it as a geotechnical material. Therefore, it is necessary to understand the effects of addition of different contents of randomly spread short coconut fibers in clay soil on the compaction, shear strength, and compressibility in different flooding conditions, as well as on the hydraulic conductivity. In addition, the elemental composition and structure of the interface formed between soil and fiber at the microscopic scale were investigated.

2. Materials and Experimental Program

2.1. Materials

The soil used was brought from the deposit of Barreiras, located in the Metropolitan Region of Recife (MRR), Pernambuco, Brazil. The soil was dried in the air and then disintegrated in the laboratory. The physical properties of the soil are listed in Table 1, and its chemical composition is presented in Table 2. All the data were obtained experimentally in laboratory.

Coconut fibers were acquired already processed by a productive community in Brazil. Currently, the technology used to benefit the residues of coconut bark and to obtain coconut fibers involves using machinery. The technological process is performed in the following steps. First, the equipment crushes whole barks or cuts through a roll of fixed knives that crush the mesocarp. Second, the crushed material is conveyed to a horizontal rotary press, which removes excess moisture from the material; at the end of this step, disaggregated fiber with liquid extract of the bark of the green coconut are obtained. Finally, the pressed material is classified; namely, long fibers are separated from short fibers and powder in a sorting apparatus, which uses fixed helical hammers and a perforated sheet. In this study,

Table 1 - Clayey soil physical properties.

Soil properties	Value
Particle density (g/cm^3)	2.618
Liquid limit (%)	49
Plastic limit (%)	31
Plasticity index (%)	18
USCS classification	CL
Boulder (%)	1
Sand (%)	37
Silt (%)	22
Clay (%)	40
Activity index	0.45

Table 2 - Clayey soil chemical composition.

Compound	Value
pH	5.7
Ca (cmol/dm^3)	0.7
Mg (cmol/dm^3)	0.4
Al (cmol/dm^3)	0.9
K (cmol/dm^3)	0.2
Na (cmol/dm^3)	0.5
P (cmol/dm^3)	0.01
C.O. (g/kg)	2.62
M.O. (g/kg)	4.09
N (g/kg)	0.2
Relation C/N	13.1
Fe (g/kg)	0.04

short fibers were used, because they do not have as much applicability as long fibers.

Chemical composition and some physical and mechanical properties of the fibers are presented in Table 3. All the data were obtained experimentally in the laboratory using the methods described by Satyanarayana *et al.* (2007).

2.2. Sample preparation

Compounds with 0, 0.5, 1.0, and 2.0 wt% of coconut fiber in relation to the dry weight of clay soil were studied. These values were chosen in accordance with the experiments documented in academic papers related to reinforcing soils with fibers (Prabakar and Sridhar, 2002; Mohamed, 2013); another reason was evaluation of the effect of doubled percentages of coconut fiber mass in the mixtures.

Table 3 - Physical and mechanical properties and chemical compounds of the coconut fibers.

Properties/compounds	Value
Density (g/cm^3)	1.27
Average diameter (μm)	250
Average length (mm)	22
Tensile strength (MPa)	110
Young's modulus (MPa)	2550
Chemicals	
α - Cellulose (%)	42.51
Hemicellulose (%)	15.36
Lignin (%)	41.02
Ashes (%)	2.65
Extracts (%)	3.32

The mixtures were prepared on a metallic tray, where the fibers were randomly added in small portions to the soil. Then, the mixtures were revolved using a spatula for homogenizing the material. These processes were repeated until all the fiber content was incorporated into the matrix. After that, cylindrical samples with a diameter of 10 cm and height of 12.7 cm were molded with respect to the compaction in their respective dry densities and optimum moisture content, corresponding to the values obtained in the Proctor Compaction Test, which uses the Proctor Compaction Energy, as stated by the NBR 7182 Standard (ABNT, 1988).

2.3. Experimental program

2.3.1. Shear strength test

The shear strength parameters for different composites were obtained through the direct shear test following the ASTM D3080 standard (ASTM, 2004). The samples were molded from the compacted specimens in the dry unit weight and optimum moisture content corresponding to each mixture. The tests were performed using vertical normal stresses of 50, 100, and 200 kPa. The horizontal displacement rate used in the test was 0.483 mm/min. When the stress-horizontal displacement curve did not show well-defined peak values, the shear stress peak or maximum value was adopted as the rupture point, which makes possible to obtain the shear strength, cohesion (c), and friction angle (ϕ) parameters.

The tests were conducted under non-flooded and flooded conditions. In the non-flooded condition, the samples were sheared immediately after molding. In the flooded condition, the samples were inserted into the test equipment, and water was added until the box holder was completely filled; then, the setup was left for 24 h, before the flooded test was carried.

2.3.2. Compressibility test

The compressibility parameters for different mixtures were obtained using a fixed ring-type oedometer cell with drainage at the top and bottom of a sample, as the NBR 12007 standard procedures suggest (ABNT, 1990). The samples were molded from the compacted specimens using metal rings with area of 40 cm² and height of 2 cm. The test was performed using one-dimensional compression press.

The test was performed under non-flooded and flooded conditions. For the flooded condition, water was injected into the samples at the base of the cell immediately after applying a 10-kPa load. Samples were loaded in stages of 10, 20, 40, 80, 160, 320, 640, and 1280 kPa, and the loads were held for 24 h in both scenarios. After applying the loads, the height variation of the samples was measured with strain gauges with a sensitivity of 0.01 mm at 6 s, 15 s, 30 s, 1 min, 2 min, 4 min, 8 min, 15 min, 30 min, 1 h, 2 h, 4 h, 8 h, and 24 h. After the maximum load was reached, it was discharged in stages of 640, 160, 40, and 10 kPa. Then,

the curves of the logarithm of the applied stress vs. void ratio were plotted, and the compressibility parameters were obtained using these plots.

2.3.3. Hydraulic conductivity test

The hydraulic conductivity tests were performed for different mixtures according to the procedures established in ASTM D5084-10 (ASTM, 2010). The hydraulic conductivity was measured using a flexible wall permeameter on samples with dimensions of 12.5 cm in height and 10.0 cm in diameter. The samples were compacted with the optimum moisture content and dry unit weight corresponding to each mixture. A hydraulic gradient of 100 kPa was used to generate water percolation in the samples; then, the flow measurements were taken. Systems composed of porous stone and filter paper were used at the top and bottom of the samples to prevent loss of sample particles during water percolation. At the end of the tests, the samples were exhumed for analysis of their internal integrity. The tests were repeated until three values were obtained with $\pm 10\%$ difference from each other (minimum of three and maximum of five replicates for each sample). The coefficient of saturated hydraulic conductivity of the samples was defined as the average of flow measurements.

2.3.4. Soil-fiber interface analysis

Scanning electron microscopy (SEM) analysis was performed on the surfaces of the fibers present on the shear rupture plane of the samples with different coconut fiber contents. This analysis was carried out to evaluate the microstructural interaction between the matrix and reinforcement and to understand the influence of the interface between the different phases of the blend on the geotechnical performance of the reinforced soil.

The used samples were subjected to metallization vacuum of 10⁻⁵ bar in the Department of Fundamental Chemistry of the Federal University of Pernambuco; then, they were analyzed with a scanning electron microscope belonging to the Laboratory of the Mechanical Engineering Department of the same institution. In addition to microscopic analysis, elemental microanalysis of the soil-fiber contact zone of the samples was performed on the same equipment using the X-ray energy dispersion spectroscopy (EDS) technique. This analysis aimed to characterize the interfacial chemical composition of different mixtures.

3. Results and Discussion

3.1. Compaction characteristics

The compaction curves of pure soil and mixtures are shown in Fig. 1. It should be noted that the addition of fibers reduced the dry unit weight and increased the optimum moisture content. It suggests that the increase of the fiber content resulted in blends with larger porosity.

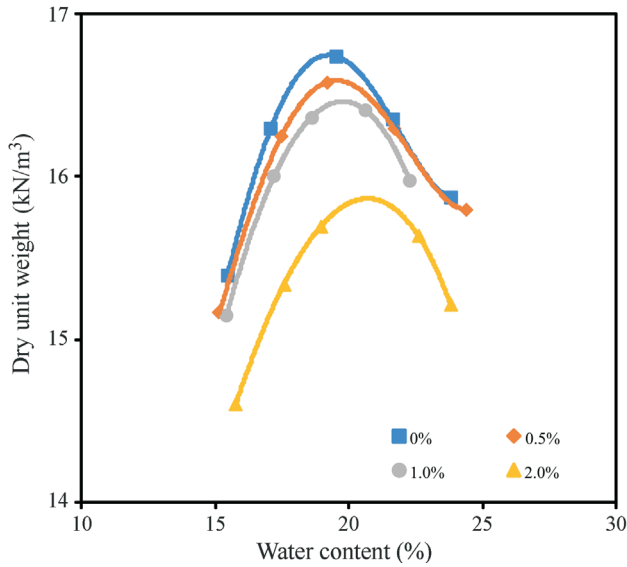


Figure 1 - Compaction curves of natural soil and soil-fiber mixtures.

The compaction parameters, maximum dry unit weight, and optimum moisture content for pure soil and different mixtures are presented in Table 4. The optimum moisture content of natural soil was 19.2%. However, the optimum moisture content of soil-fiber mixtures varied between 19.4% (mixture with 0.5 wt% of fiber) and 20.5% (mixture with 2 wt% of fiber), which is 0.2% and 1.3% more than the value of water content obtained for the natural soil, respectively. The maximum dry unit weight value for the natural soil was 16.80 kN/m³. For the mixtures, the maximum dry unit weight varied between 16.60 kN/m³ (mixture with 0.5 wt% of fiber) and 15.84 kN/m³ (mixture with 2 wt% of fiber), which is 0.2 and 0.96 kN/m³ less than the value obtained for the natural soil, respectively. Prabakar & Sridhar (2002) observed similar reduction of the maximum dry unit weight and increase of the optimum moisture content with increasing fiber content in the mixture by evaluating the addition of up to 1 wt% of randomly distributed sisal short fibers in a clay soil classified as CL by USCS from Bhopal in India. Mohamed (2013) also verified the reduction of maximum dry unit weight with the increase of the fiber content by evaluating the random inclusion of up to 1.5 wt% of hay fibers in clay soil, which

Table 4 - Compaction parameters of natural soil and soil-fiber mixtures.

Fiber content (%)	Optimum moisture content (%)	Maximum dry unit weight (kN/m ³)
0	19.2	16.80
0.5	19.4	16.60
1	19.6	16.43
2	20.5	15.84

agrees with the results obtained in this work. Meanwhile, reduction of the optimum moisture content of the mixtures with up to 1 wt% of fiber and increase of the optimal moisture content of the mixtures with up to 1.5 wt% of fiber were observed.

3.2. Shear strength

The shear stress-horizontal displacement curves obtained for natural and reinforced soils with different fiber contents (0.5, 1, and 2 wt%) in non-flooded and flooded conditions at normal stresses of 50, 100, and 200 kPa are shown in Figs. 2, 3, and 4, respectively.

The inclusion of coconut fibers in clay soil in both flood conditions increased the peak strength at all the adopted normal stress levels. The increase in peak strength was more pronounced for mixtures with 0.5 and 1 wt% of the fiber content. Furthermore, it is noted that for the higher levels of normal stress (Figs. 3 and 4), the peak strength

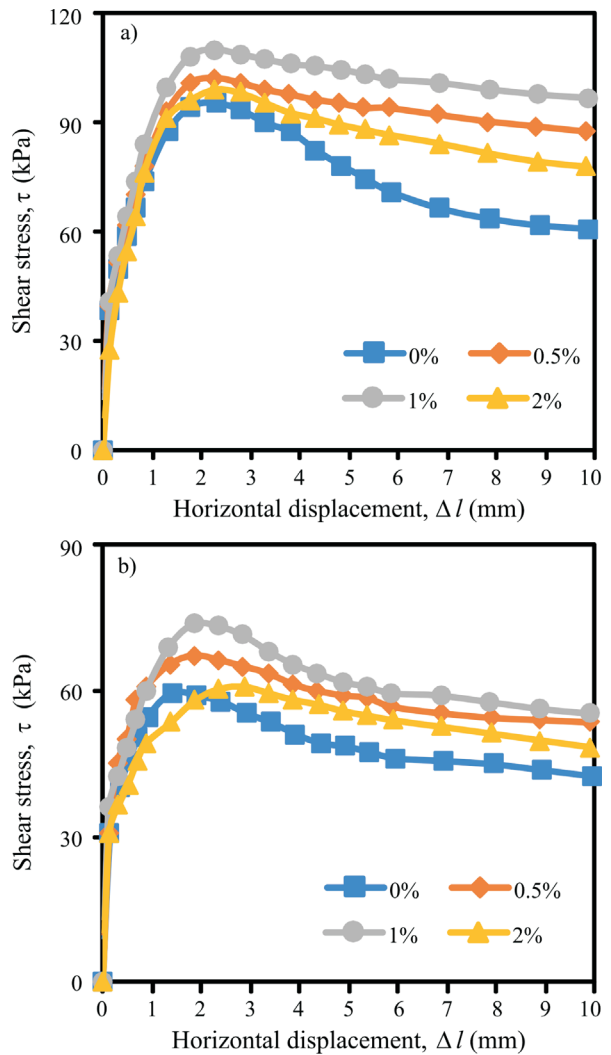


Figure 2 - Shear stress-horizontal displacement curves of natural soil and soil-fiber mixtures for normal stress of 50 kPa in non-flooded (a) and flooded (b) conditions.

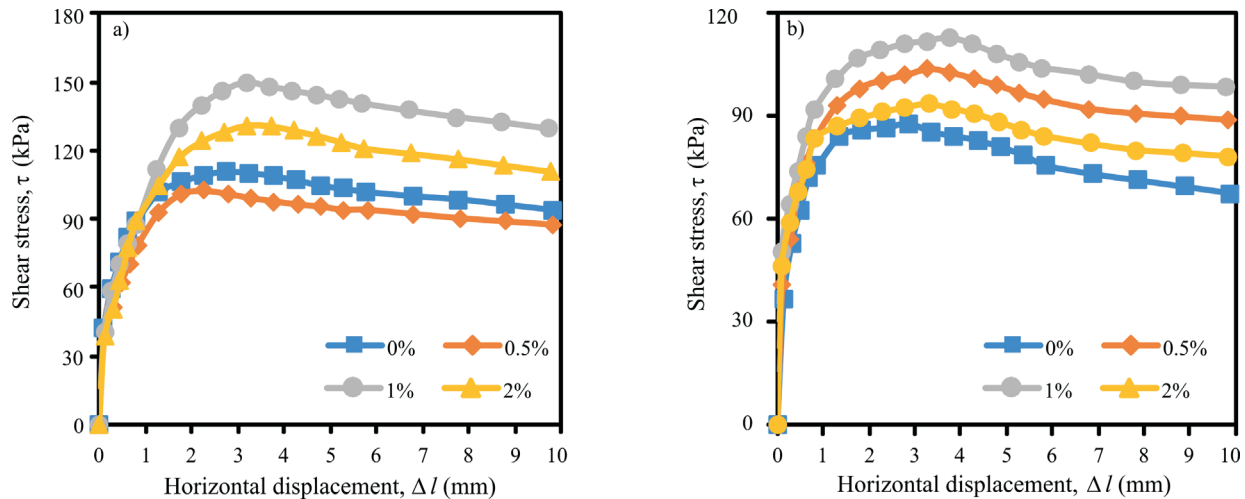


Figure 3 - Shear stress-horizontal displacement responses of natural soil and soil-fiber mixtures for normal stress of 100 kPa in non-flooded (a) and flooded (b) conditions.

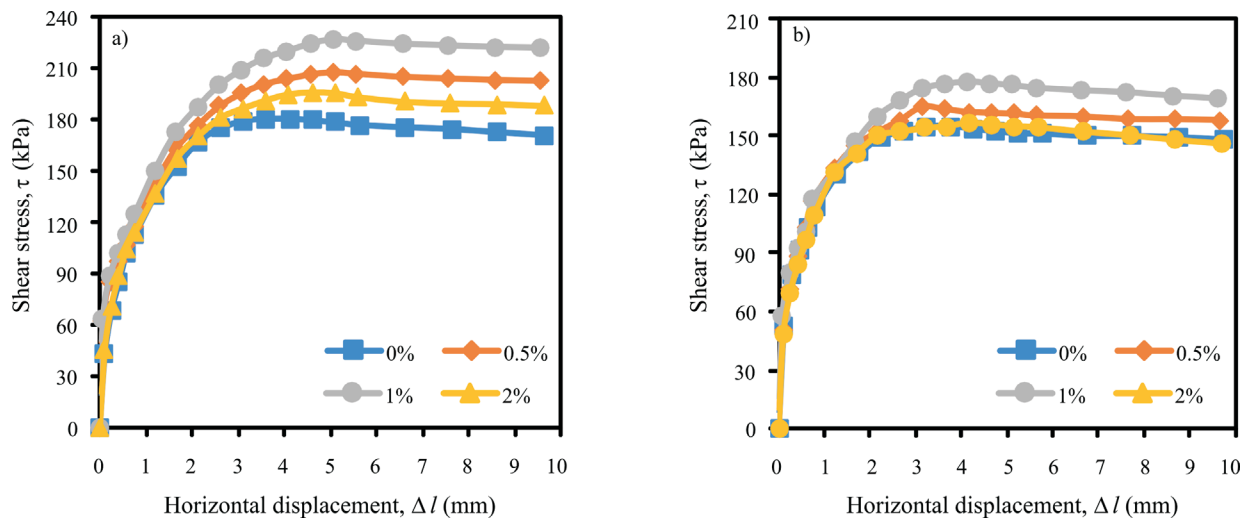


Figure 4 - Shear stress-horizontal displacement responses of natural soil and soil-fiber mixtures for normal stress of 200 kPa in non-flooded (a) and flooded (b) conditions.

gains were more evident. It was also found that with the addition of fiber and increase of the applied normal stress, there was a reduction of the post-peak strength drop. This effect was also more pronounced in the mixtures with 0.5 and 1 wt% of reinforcement. The rise of the peak strength and the decline of the post-peak drop in fiber-reinforced soils were also observed in other matrices reinforced with different types of fiber (Consoli *et al.*, 2007; Maliakal & Thyyakkandi, 2013; Mohamed, 2013; Onyejekwe & Gha-taora, 2014; Tang *et al.*, 2016).

Natural soil is fragile at the breakpoint for low levels of normal stress (Fig. 2). However, this behavior is reduced as the normal stress levels increase (Figs. 3 and 4). The reinforced mixtures with different levels of coconut fibers showed less fragile rupture behavior, which agrees with the results obtained by Tang *et al.* (2016). It occurred because

the inclusion of fibers increased the ductility and toughness of the material, especially for the 0.5 and 1 wt% contents; in these cases, the area below the shear stress vs. horizontal deformation curve is higher compared with the material with 2 wt% of fiber. In addition, there is a certain similarity between the shear stress-horizontal displacement curves of natural soil and different mixtures at levels up to 1 mm of horizontal deformation in all flood conditions and levels of normal stress adopted in the test. This suggests that regardless of the flood condition, certain deformation of the matrix is required for the fiber reinforcement to take a noticeable effect. Presumably, from this point, the matrix-reinforcement assembly contributes simultaneously to the shear strength of the soil-fiber composite. As a result, the increase in shear strength observed in the curves of the mixtures occurs.

The obtained results enabled the analysis of how the addition of fibrous material influenced the shear strength parameters of the soil. Using the Mohr-Coulomb linear criterion the cohesion (c) and friction angle (ϕ) parameters of each sample were obtained, as shown in Table 5.

In general, it can be seen that in both test conditions, the inclusion of coconut fibers influenced more on the cohesion intercept than on the friction angle. The natural soil had the cohesion and friction angle of 60.4 kPa and 30.5° (non-flooded) and 25.9 kPa and 32.7° (flood condition), respectively. Among the mixtures, the 1-wt% content of coconut fibers provided the highest shear strength parameter values, namely, 81.2 kPa cohesion and 32.7° friction angle in the non-flooded condition and 41.3 kPa cohesion and 34.6° friction angle in the flooded condition. Thus, the 34.4% cohesion increase and 7.5% angle of friction increase were observed in the non-flooded condition, and 59.5% cohesion increase and 5.8% angle of friction increase were observed in the flooded condition compared with natural soil.

The blend with 0.5 wt% of coconut fibers presented intermediate values of the shear strength parameters with approximately 76.4 kPa cohesion and 31.3° friction angle for the non-flooded condition and 36.7 kPa cohesion and 32.9° friction angle for the flooded condition. Compared with natural soil, there were 26.5% increase in the cohesion and 2.6% increase in the angle of friction for the non-flooded condition, and 41.7% increase in the cohesion and 0.6% increase in the angle of friction for the flooded condition.

The mixture with 2 wt% of coconut fiber presented the lowest values of the shear strength parameters with approximately 71.3 kPa cohesion and 30.1° friction angle for the non-flooded condition and 29.3 kPa cohesion and 32.7° friction angle for the flooded condition. Compared with natural soil, there were 18.0% increase in the cohesion and 1.3% reduction in the angle of friction for the non-flooded condition and 13.1% increase in the cohesion and unchanged angle of friction for the flooded condition.

Therefore, the optimum ratio between clay soil and short coconut fibers was found to be 1 wt% of reinforcement material for the shear strength test. Presumably, the mixtures with up to 1 wt% of coconut fiber content can be

used as a geotechnical material for construction systems that are usually made up of compacted clay soils, such as base layers and landfill covers. However, it is important to verify the variability of the shear strength parameters and mechanical performance over time, even though coconut fibers show low degradation rates.

According to Donato *et al.* (2004), the increase in shear strength of reinforced soils is more significant in clay materials, because there is a greater probability of matrix-reinforcement adhesion due to the greater amount of contact points between the fibers and soil particles. In this sense, the mixtures with 0.5 and 1 wt% of coconut fibers probably presented more contact between fibers and clay particles. Meanwhile, in the mixture with 2 wt% of fibrous material more fiber-fiber contacts may occur, compromising matrix-fiber adhesion and generating greater probability of sliding. This can explain why the mixtures with 0.5 and 1 wt% of the reinforcement material showed better mechanical performances, cohesion, and friction angle values than the 2-wt% coconut fiber blend.

Comparing these results with other studies that used fibers to reinforce matrices of compacted clay soils classified as CL by the Unified Soil Classification System, it was noticed that the coconut fiber reinforcement showed a higher proportion of optimal mixture. For example, Prabhakar & Sridhar (2002) analyzed clay mixtures and sisal fibers and obtained better shear strength parameters using 0.75 wt% of fibrous material. The content of 1 wt% presented lower performance than the other contents analyzed by the authors. Coconut fibers have higher lignin content than sisal fibers (Satyanarayana *et al.*, 2007); therefore, coconut fibers present greater flexibility. It is likely that because of this feature, coconut fibers accommodate more elements in the matrix without compromising matrix-reinforcement adhesion.

Tang *et al.* (2007) evaluated the mixtures of clay soil and polypropylene fibers and found that the best mechanical performance and shear strength parameters were obtained with 0.25-wt% fiber content. Vegetable fibers have higher porosity than synthetic fibers, which favors higher mechanical adhesion because of the penetration of the matrix into the pores of the fibers. In addition, unlike synthetic fibers, plant fibers are polar in nature, which favors adhesion by electrostatic attraction between the matrix and reinforcing elements. This may have contributed to higher optimum coconut fiber content than the analyzed clay matrix.

3.3. Compressibility

The vertical stress vs. void ratio plots obtained for natural soil and mixtures with different fiber contents for the non-flooded and flooded conditions are shown in Fig. 5.

The addition of fiber in the clay soil matrix in both flood conditions increased the slope of the virgin compression line; the highest slope was observed for the mixture

Table 5 - Shear parameters of the natural soil and soil-fiber mixtures in the non-flooded and flooded conditions.

Fiber content (%wt)	Non-flooded			Flooded		
	c (kPa)	ϕ (°)	R^2	c (kPa)	ϕ (°)	R^2
0	60.4	30.5	0.9729	25.9	32.7	0.9989
0.5	76.4	31.3	0.9879	36.7	32.9	0.9981
1	81.2	32.7	0.9934	41.3	34.6	0.9977
2	71.3	30.1	0.9989	29.3	32.7	0.9989

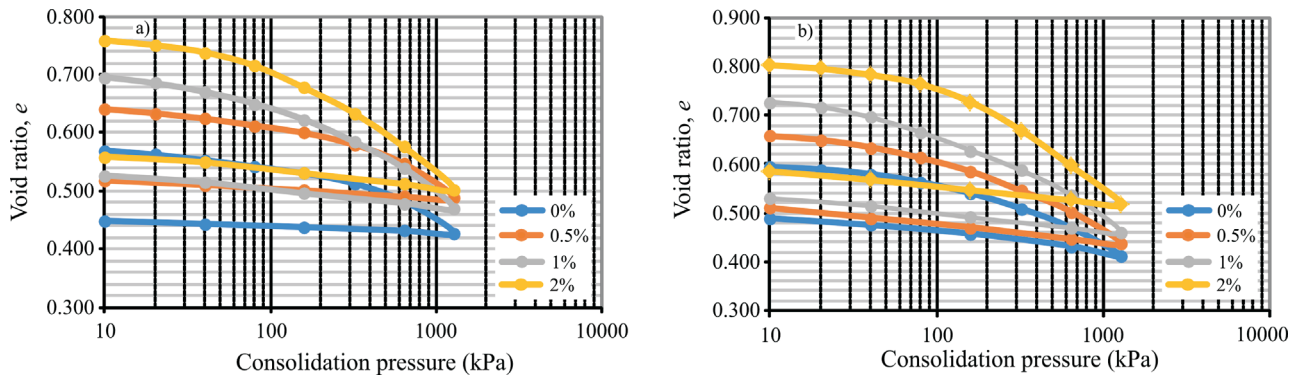


Figure 5 - Consolidation curves of natural soil and soil-fiber mixtures in the non-flooded (a) and flooded (b) conditions.

with 2-wt% content of fibrous material. This suggests that the addition of fibers increased the compressibility of the mixtures. A directly proportional relationship between fiber content and compressibility was observed; namely, the higher the fiber content was, the greater the slope of the virgin compression line became. Morandini & Schneider (2017) evaluated the influence of polypropylene fibers on matrices of lateritic soil and bentonite clay and observed similar behavior. These results may be related to the fact that the addition of fibers reduces the density of the material, which was verified by the compaction parameters, providing an increment in the initial void ratio of the soil and consequently increasing the compressibility of the composite.

The addition of fibers also increased the volumetric variation between the initial and final void ratios of the samples. The vertical tension vs. void ratio curves of the natural soil and mixture with 0.5 wt% of coconut fiber have similar shapes with more evident stiffness drop from the vertical tension of 300 and 200 kPa in the non-flooded condition (Fig. 5a). The curves of the mixtures with 1 and 2 wt% of coconut fiber exhibited different shapes from the others, with a stiffness drop more evident from 80 kPa tension (Fig. 5a). This suggests that the addition of fibers increases the virgin compression portion and reduces the vertical stress over the densification compared with natural soil. It is verifiable that the increase of the volumetric variation with the addition of fiber, when comparing the initial and final indicators of sample void ratio, was more significant in the flooded condition. The vertical stress vs. soil void ratio curves in the flooded condition show more evident stiffness drop from the 100 kPa point of vertical stress (Fig. 5b). In the cases of mixtures with 0.5, 1, and 2 wt% of coconut fiber, the stiffness drops are evident from the vertical tension of 20 kPa (Fig. 5b). This suggests that besides the addition of fiber, the flood condition also contributes to increasing the portion of virgin compression and reduction of the vertical tension over densification compared with natural soil.

The compression index (C_c) and decompression index (C_s) obtained through the curves of Fig. 6 are presented

in Table 6. They were obtained by the relationship between the differences of the initial and final logs and the initial and final void ratio values. The inclusion of coconut fibers increased the compression and decompression indices of the clay matrix; these gains were more significant for the decompression index in both flood conditions.

The compression index increased with the increase of the fiber content of the mixtures; it took the values of 0.182, 0.196, 0.228, and 0.241 for the coconut fiber contents of 0, 0.5, 1, and 2 wt%, respectively, for the non-flooded condition. In the flooded condition, the obtained values of C_c were 0.195, 0.218, 0.256, and 0.261 for the fiber contents of 0, 0.5, 1, and 2 wt%, respectively.

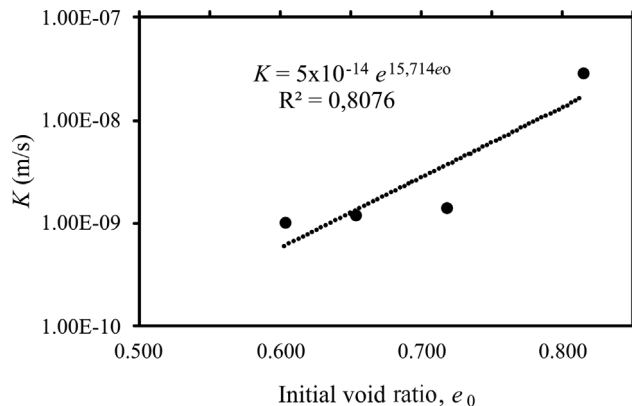


Figure 6 - K_{water} vs. initial void ratio of natural soil and soil-fiber mixtures.

Table 6 - Compressibility parameters of natural soil and soil-fiber mixtures in the non-flooded and flooded conditions.

Fiber content (%wt)	Non-flooded		Flooded	
	C_c	C_s	C_c	C_s
0	0.182	0.009	0.195	0.029
0.5	0.196	0.016	0.218	0.033
1	0.228	0.032	0.256	0.039
2	0.241	0.031	0.261	0.035

It was found that in the mixture with 0.5 wt% of coconut fibers the compression index increased by 8% and 12% for the non-flooded and flooded conditions, respectively. For the mixture with 1 wt% of coconut fibers, the compression index increased by approximately 25% in the non-flooded condition and 31% in the flooded condition. In the mixture with 2 wt% of coconut fibers, the observed gains in the compression index were 32% in the non-flooded condition and 34% in the flooded condition. Thus, depending on the applied stress level, ratio between the materials, and flooding condition, the addition of coconut fibers in the clay soil can provide approximately 30% more deformation by primary compression.

As for the decompression index, the values obtained in the non-flooded condition were 0.009 for the natural soil, 0.016 for the blend with 0.5 wt% of fiber, 0.032 for 1 wt% of fiber, and 0.030 for 2 wt% of fiber. In the flooded condition, these values were 0.029, 0.033, 0.039, and 0.035 for contents of 0, 0.5, 1, and 2 wt% of coconut fiber, respectively. This indicates that fibers increase the potential for soil expansion due to stress relief. In the non-flooded condition, the decompression index increased by approximately 78%, 256%, and 94% for the blends with 0.5, 1, and 2 wt% of coconut fibers, respectively, compared with natural soil. In the flooded condition, the decompression index increased by 14%, 34%, and 6% for the mixtures with 0.5, 1, and 2 wt% of coconut fibers, respectively. The content of 1 wt% of coconut fibers showed major influence on the potential of deformation by tension relief, especially in the non-flooded condition. Therefore, for the compressibility, the optimal ratio between clay soils and randomly distributed short coconut fibers was not found. This open question may become a limitation of the application of these mixtures as geotechnical materials.

3.4. Hydraulic conductivity

The results of the saturated hydraulic conductivity tests of natural soil and mixtures with different levels of coconut fibers are presented in Table 7.

Natural soil had a coefficient of hydraulic conductivity of 1.01×10^{-9} m/s, which is practically similar to that of the mixtures with 0.5 and 1 wt% of coconut fibers with approximately 1.20×10^{-9} m/s (approximately 19% more than natural soil) and 1.43×10^{-9} m/s (approximately 42% more than natural soil), respectively. Meanwhile, the mixture with 2 wt% of coconut fibers showed the coefficient of hydraulic conductivity of 2.87×10^{-8} m/s (approximately 2742% more than natural soil), which is higher by an order of magnitude than the coefficient of hydraulic conductivity of natural soil. These results agree with Miller & Rifai (2004), who evaluated mixtures of clay soil (classified as CL) and polypropylene fibers and observed changes of the order of magnitude of hydraulic conductivity of the mixture with 1 wt% of fiber content.

Table 7 - Initial void ratio and hydraulic conductivity of natural soil and soil-fiber mixtures.

Fiber content (%)	e_0	K_{water} (m/s)	Variation from the natural soil (%)
0	0.603	1.01×10^{-9}	-
0.5	0.653	1.20×10^{-9}	19
1	0.718	1.43×10^{-9}	42
2	0.814	2.87×10^{-8}	2742

It is believed that for the 2-wt% coconut fiber blend, the reason for the hydraulic conductivity increase is similar to that affecting the mechanical performance of this blend, namely, the loss of soil-fiber adhesion. The amount of fiber in this blend increases the fiber-fiber contacts, which creates macropores and increases the hydraulic conductivity. Figure 6 shows the behavior of hydraulic conductivity as a function of the initial void ratio of natural soil and soil-fiber mixtures. It is possible to observe that the hydraulic conductivity increases with the increase of the initial void ratio. This suggests that the structure of a material has significant influence on the hydraulic conductivity and may be responsible for the results obtained for the hydraulic conductivity of the soil-fiber mixtures.

According to the hydraulic conductivity results, mixtures with up to 1 wt% of coconut fiber can be used as a geotechnical material of construction systems, considering that the coconut fiber in these proportions does not significantly influence the hydraulic conductivity compared with natural soil. According to USEPA (2007), the final landfill cover layer must have a hydraulic conductivity lower than the bottom layer or be less than 10^{-7} m/s. According to this criterion, for example, even the 2-wt% fiber blend can be considered as a suitable material for cover layers of landfills. However, as previously reported, it is important to note that although coconut fibers possess low degradation rate, tests must be carried out to verify the behavior of hydraulic conductivity over time to verify its adequate application in mixtures as a geotechnical material.

3.5. Soil-fiber interface analysis

The micrographs made for the mixtures with different coconut fiber content are presented in Fig. 7. In general, no ruptured fibers were observed, indicating that the elements adequately supported the adopted stress levels. Such a behavior was also observed by Anagnostopoulos *et al.* (2013) when analyzing micrographs of clayey soil (CL) and polypropylene fiber mixtures.

Clay particles agglomerate around fibers, providing embedding in the matrix. This inlay is most evident in blends with 0.5 and 1 wt% of fiber (Figs 7a, 7b, and 7c). This behavior favors the transmission of mechanical stresses from the matrix to the fibers, resulting in the improve-

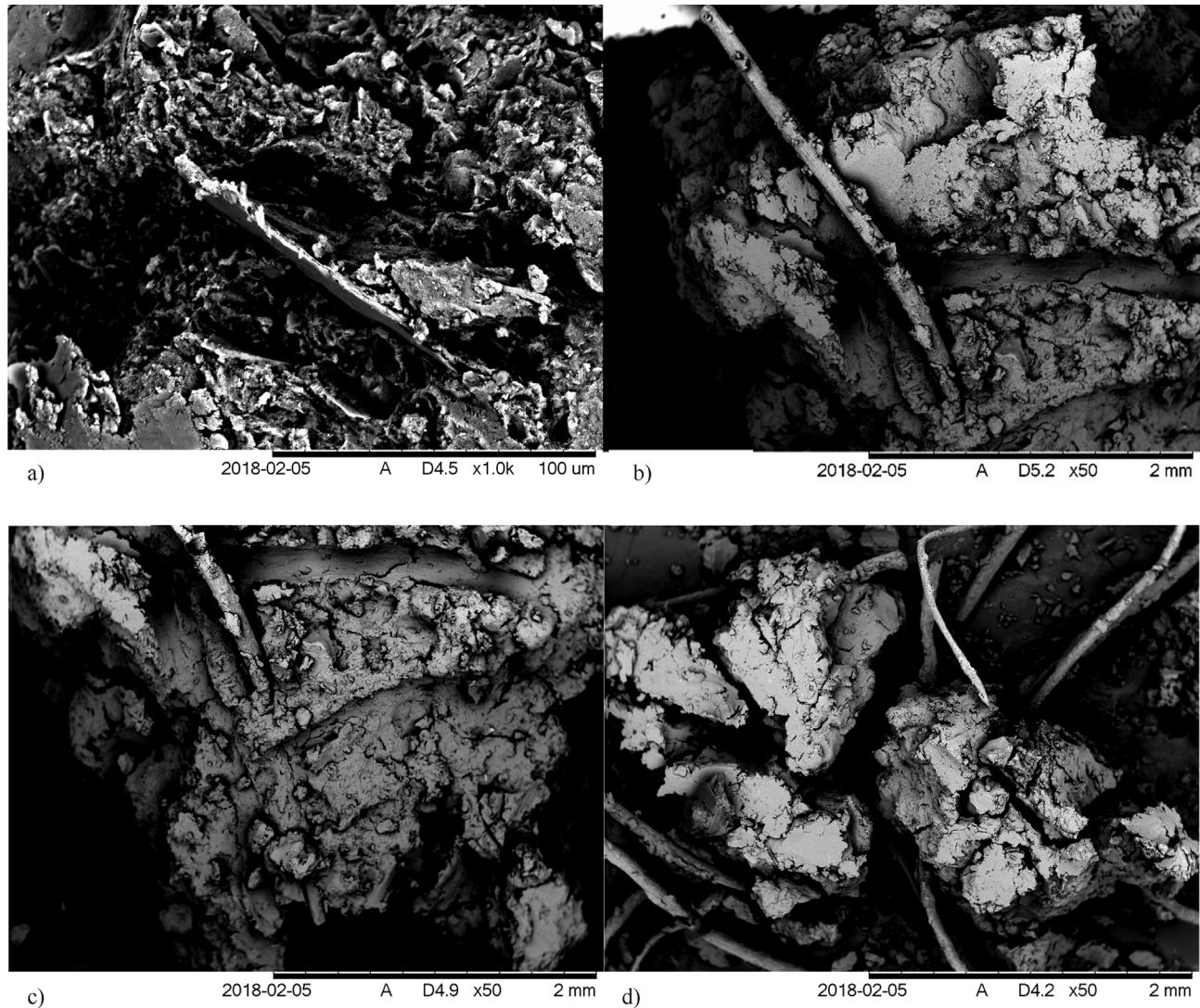


Figure 7 - SEM images of the blends with different percentages of coconut fiber: a) 1000 \times magnification of the mixture with 0.5 wt% of fibers; b) 50 \times magnification of the mixture with 0.5 wt% of fibers; c) 50 \times magnification of the mixture with 1 wt% of fibers; and d) 50 \times magnification of the mixture with 2 wt% of fibers.

ment of the shear strength of the soil-fiber assembly. In addition, it leads to the formation of the structure, which provides lower compression indices and hydraulic conductivity compared with the 2-wt% mix. Although the distribution of coconut fibers was random, in Fig. 7d, it can be seen that there may be a tendency for agglomeration of fibers in the 2-wt% blend, causing reduced interaction between soil and fibers. It, in turn, increases the fiber-fiber contacts, which compromise matrix adhesion to the reinforcement. Moreover, it can possibly create fragile points with greater compressibility, which can generate a rough surface with many localized settlements in layers compacted with these proportions.

Through the images shown in Fig. 8, it was established that the clay particles remained adherent to the surface of the fibrous material after shearing the samples. It

indicates that there is strong interfacial bonding owing to good compatibility between the matrix and reinforcement.

Some of the possible mechanisms for adhesion of the particles to the fiber surface are the mechanical adhesion and adhesion by electrostatic attraction between matrix and fiber. The mechanical adhesion occurs in the consolidation stage of the shear test. Because of the applied normal stress, local plastic deformations occur in the fiber creating cavities filled by the matrix, which provide an anchorage on the fiber surface (Tang *et al.*, 2007, Tang *et al.*, 2010). Moreover, during the compacting process of the blends, smaller particles are pressed to penetrate the pores of the fiber causing mechanical adhesion (Moraci & Gioffre, 2006; Anagnostopoulos *et al.*, 2013). The electrostatic attraction occurs because vegetal fibers usually possess polar surface energy. If the matrix has nonpolar nature, there will be little

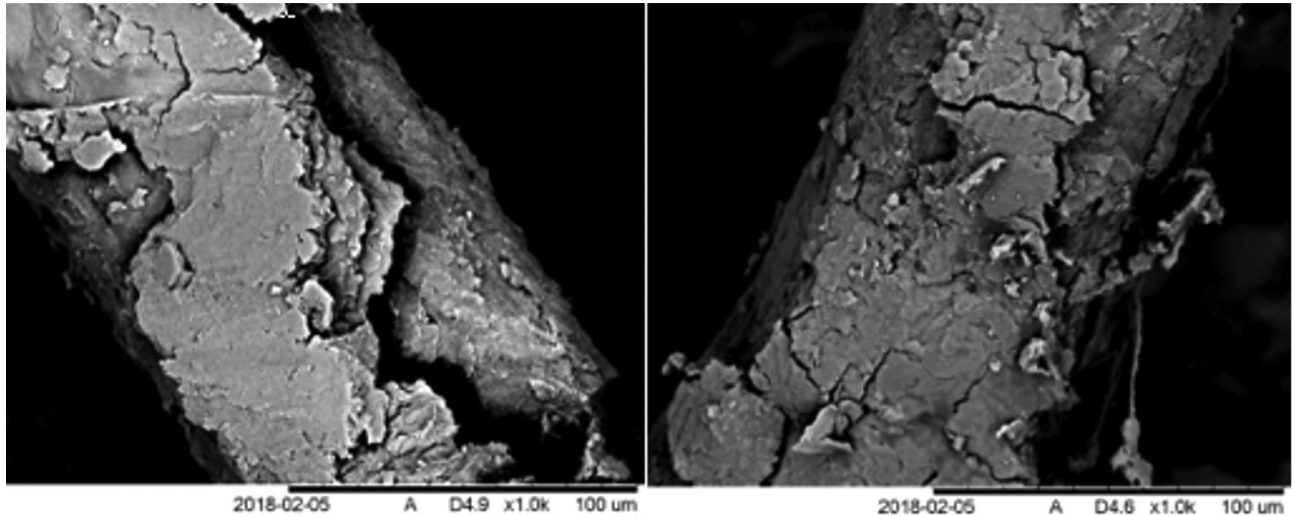


Figure 8 - Images of clay soil adherent to the surface of expanded fibers in 1000 \times .

electrostatic adhesion to the fiber surface. Conversely, if the composite matrix is polar, adhesion will occur because of the electrostatic attraction between the materials.

Clay soils are formed by various minerals, whose type and quantity influence the electrical nature of the material. Clay particles are constituted by thin lamellae that are generally negatively charged at the surface and positively at the edges, favoring the occurrence of electrostatic interactions (Macedo *et al.*, 2008). In this sense, the charge distribution in the clay particles and polar surface energy of the fibers should favor the electrostatic adhesion between the clay soil matrix and the coconut fiber surface.

The elementary analysis performed in the soil-fiber interfacial zone for the mixtures with 0.5, 1, and 2 wt% of fiber is presented in Fig. 9. The mixtures with better soil-fiber adhesion (up to 1 wt% of fiber) showed similar contents of oxygen, carbon, aluminum, silicon, iron, nitrogen, and sulfur. The soil-fiber interface of the 0.5-wt% fiber blend had 37.9% oxygen, 18.8% carbon, 18.1% aluminum, 17.8% silicon, 4.2% iron, 1.8% nitrogen, and 1.3% sulfur (Fig. 9a). The soil-fiber interface of the 1-wt% fiber blend had 38.6% oxygen, 18.3% carbon, 18.9% aluminum, 17.7% silicon, 3.9% iron, 1.5% nitrogen, and 1.2% sulfur (Fig. 9b). Meanwhile, the mixture with 2 wt% of fiber in which the soil-fiber bond was reduced, had 32.9% oxygen, 49.7% carbon, 7.1% aluminum, 7.8% silicon, 1.6% iron, and 0.8% sulfur (Fig. 9c).

The clay minerals present in the soil are composed of hydrated Al, Fe, and Mg silicates with the crystalline structure in layers (Coelho *et al.*, 2007). Furthermore, Macedo *et al.* (2008) found that red clay soils, such as the one used in the mixtures, usually show a predominance of SiO_2 , Al_2O_3 , and Fe_2O_3 . Therefore, the higher values of oxygen, aluminum, silicon, and iron observed in the compounds with 0.5 and 1 wt% of fibers are associated with the higher amounts of clay minerals present at the soil-fiber interface of these

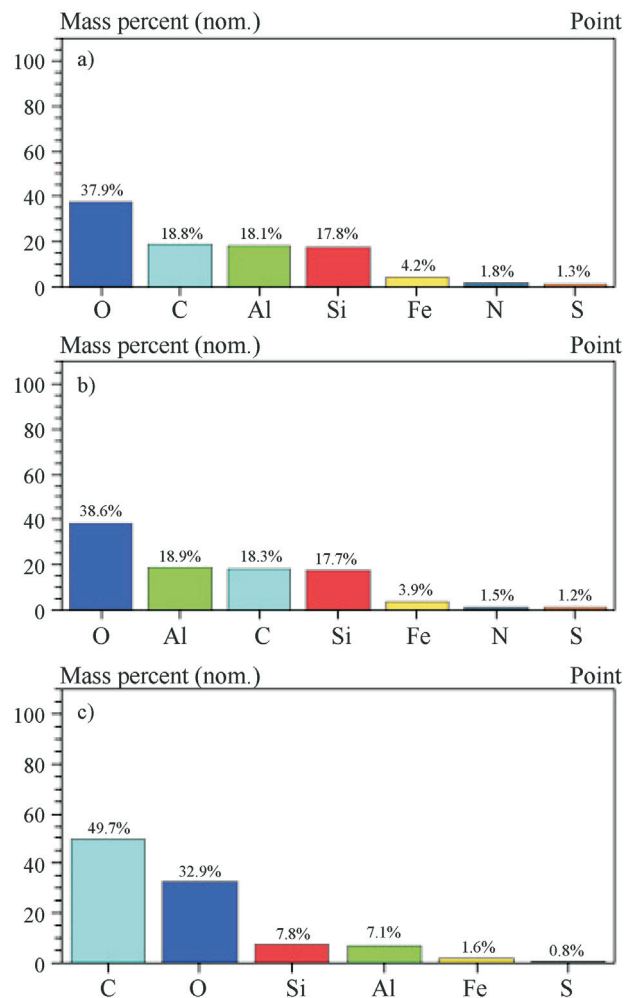


Figure 9 - Elemental analysis of the soil-fiber interface obtained by the EDS technique: a) mixture with 0.5 wt% of fiber; b) mixture with 1 wt% of fiber; and c) mixture with 2 wt% of fiber.

mixtures after the direct shear test of the samples. These results indicate that the clay particle content adhered in the interfacial zone with the coconut fiber was higher in the mixtures with up to 1 wt% of fiber, which confirms that the soil-fiber interaction in these mixtures is greater. Meanwhile, Corradini *et al.* (2009) reported that the cellulose chains of coconut fibers are polysaccharides formed of carbon, oxygen, and hydrogen. Therefore, the higher carbon content and lower oxygen, aluminum, silicon, and iron contents observed in the 2-wt% fiber blend are related to the higher vegetal tissue presence and lower presence of clay minerals in the soil-fiber interface of this mixture. This result indicates that in the 2-wt% fiber mixture, the amount of clay particles attached to the coconut fiber in the interfacial zone was lower because of the higher amount of fibers; it confirms that for this fiber content fiber-fiber contacts prevail, which compromises the matrix-reinforcement bond of the composite.

4. Conclusions

Based on the results obtained in this research, it can be concluded that the addition of different quantities of short coconut fibers randomly distributed in a clay soil matrix has significant influence on the compaction, shear strength, compressibility, and hydraulic conductivity. In particular, the following conclusions can be drawn:

1. The compaction test revealed that the optimum moisture content increases and the maximum dry unit weight reduces with the increase of the added fiber content;
2. The shear strength of the blends improved with content of up to 1 wt% of coconut fibers. In this range of content, there is a rise in the peak strength, reduction in the post-peak strength drop, and increment in the cohesion and friction angle parameters, regardless of the test flood condition;
3. The compressibility of the mixtures increased directly proportional to the coconut fiber content. The addition of coconut fiber has negatively affected the compressibility and therefore the addition of coconut fiber is not indicated as a geotechnical material. The main effects observed in the addition of coconut fibers to the soil were the increases of the compressibility curves slope, primary compression portion, and compression and decompression indices in both flood conditions.
4. Mixtures with less than 1 wt% of fiber did not show significant changes in hydraulic conductivity, which remained of the same order of magnitude of natural soil of 10^{-7} cm/s. However, for the mixtures with greater fiber content, the hydraulic conductivity sharply increased by approximately one order of magnitude.
5. SEM images indicate that clay particles adhere to the surface of coconut fibers, explaining the behavior observed in the geotechnical properties of the studied mixtures. The main effects of coconut fiber addition at a microscopic scale were the loss of adhesion verified in the 2-wt% blend due to the tendency of localized fiber agglomeration.
6. EDS performed at the interfacial zone of the mixtures with 0.5 and 1 wt% of fiber suggested that there was a greater amount of aluminum and iron oxides from the clay minerals in the soil-fiber contact, confirming that there is greater matrix-reinforcement interaction for these mixing ratios. The analysis performed in the 2-wt% fiber blend indicated a reduction in the supply of clay minerals and greater amount of vegetal tissue, indicating the predominance of fiber contacts, which confirms the weakened matrix-reinforcement adhesion observed in this proportion.

Acknowledgments

The authors thank the departments of Fundamental Chemistry and Mechanical Engineering of the Federal University of Pernambuco for the support in the accomplishment of the microscopic analysis and in the determination of the properties of the coconut fiber.

References

- ABNT (1990). Solo - Ensaio de Adensamento Unidimensional - NBR 12007. Associação Brasileira de Normas Técnicas - ABNT, Rio de Janeiro, RJ, Brazil, 15 p.
- ABNT (1988). Solo - Ensaio de Compactação Utilizando Energia de Compactação Normal - NBR 7182. Associação Brasileira de Normas Técnicas - ABNT, Rio de Janeiro, RJ, Brazil, 10 p.
- Anagnostopoulos, C.A.; Tzetzis, D. & Berketis, K. (2014). Shear strength behaviour of polypropylene fibre reinforced cohesive soils. *Geomechanics and Geoenvironmental Engineering*, 9(3):241-251.
- ASTM (2004). Standard Test Method for Direct Shear Test of Soils Under Consolidated Drained Conditions - D3080-04. ASTM International, West Conshohocken, PA, USA, 7 p.
- ASTM (2010). Standard Test Methods for Measurement of Hydraulic Conductivity of Saturated Porous Materials Using a Flexible Wall Permeameter - D5084-10. ASTM International, West Conshohocken, PA, USA, 8 p.
- Babu, G.L.S. & Vasudevan, A.K. (2008). Strength and stiffness response of coir fibre reinforced tropical soils. *Journal of Materials in Civil Engineering*, 20(9):571-577.
- Coelho, A.C.V.; Santos, P.S. & Santos, H.S. (2007). Special clays: what they are, characterization and properties. *New Chemistry*, 30(1):146-152.
- Consoli, N.C.; Heineck, K.S.; Casagrande, M.D.T. & Coop, M.R. (2007). Shear strength behavior of fiber-reinforced sand considering triaxial tests under distinct stress paths. *Journal of Geotechnical and Geoenvironmental Engineering*, 133(11):1466-1469.

- Corradini, E.; Rosa, M.F.; Macedo, B.P.; Paladin, P.D. & Mattoso, L.H.C. (2009). Chemical composition, thermal and mechanical properties for cultivars of immature coconut fibers. *Brazilian Journal of Fruticulture*, 31(3):837-846.
- Donato, M.; Foppa, D.; Ceratti, J.A.P. & Consoli, N.C. (2004). Polypropylene fibers as reinforcement for geotechnical materials. *Soils and Rocks*, 27(2):161-179.
- Kumar, J.S. & Sharma, P. (2018). Geotechnical properties of pond ash mixed with cement kiln dust and polypropylene fiber. *Journal of Material in Civil Engineering*, 30(8):04018154.
- Macedo, R.S.; Menezes, R.R.; Neves, G.A. & Ferreira, H.C. (2008). Study of clays used in red ceramics. *Ceramics*, 54(332):411-417.
- Maliakal, T. & Thiyyakkandi, S. (2013). Influence of randomly distributed coir fibers on shear strength of clay. *Geotechnical and Geological Engineering*, 31(2):425-433.
- Miller, C.J. & Rifai, S. (2004). Fiber reinforcement for waste containment soil liners. *Journal of Environmental Engineering*, 130(8):891-895.
- Mohamed, A.E.M.K. (2013). Improvement of swelling clay properties using hay fibers. *Construction and Building Materials*, 38:242-247.
- Moraci, N. & Gioffre, D.A. (2006). A simple method to evaluate the pullout resistance of extruded geogrids embedded in a compacted granular soil. *Geotextiles and Geomembrances*, 24(2):116-128.
- Morandini, T.L.C. & Schneider, V.C. (2017). Compressibility of lateritic soil, bentonite and fibre mixtures for liners proposals. *Holos Environment*, 17(1):66-78.
- Onyejekwe, S. & Ghataora, G.S. (2014). Effect of fiber inclusions on flexural strength of soils treated with non-traditional additives. *Journal of Materials in Civil Engineering*, 26(8):04014039.
- Prabakar, J. & Sridhar, R.S. (2002). Effect of random inclusion of sisal fibre on strength behaviour of soil. *Construction and Building Materials*, 16(2):123-131.
- Rosário, F.; Pachekoski, W.M.; Silveira, A.P.J.; Santos, S.F.; Savastano Júnior, H. & Casarin, S.A. (2011). Virgin and recycled polypropylene composites reinforced with sisal by-product. *Polymers*, 21(2):90-97.
- Satyanarayana, K.G.; Guimaraes, J.L. & Wypych, F. (2007). Studies on lignocellulosic fibers of Brazil. Part I: Source, production, morphology, properties and applications. *Composites Part A: Applied Science and Manufacturing*, 38(7):1694-1709.
- Tang, C.S.; Shi, B. & Zhao, L.Z. (2010). Interfacial shear strength of fiber reinforced soil. *Geotextiles and Geomembranes*, 28(1):54-62.
- Tang, C.S.; Shi, B.; Gao, W.; Chen, F. & Cai, Y. (2007). Strength and mechanical behavior of short polypropylene fiber reinforced and cement stabilized clayey soil. *Geotextiles and Geomembranes*, 25(3):194-202.
- Tang, C.S.; Wang, D.Y.; Cui, Y.J.; Shi, B. & Li, J. (2016). Tensile strength of fiber-reinforced soil. *Journal of Materials in Civil Engineering*, 28(7):04016031.
- USEPA (2007). Inventory of U.S. Greenhouse Gas Emissions and Sinks: 1990-2005. USEPA, report 430-R-07-002, available in <https://www.epa.gov/ghgemissions/us-greenhouse-gas-inventory-report-archive>.

List of Symbols

- CL: clay of low compressibility
c: cohesion
 ϕ : friction angle
e: void ratio
C_c: compression index
C_s: decompression index
K_{water}: hydraulic conductivity
e₀: initial void ratio
O: oxygen
C: carbon
Al: aluminum
Si: silicon
Fe: iron
N: nitrogen
S: sulfur

Geological-Geotechnical Characterization of Slopes Belonging to the Serra do Mar Paranaense, Brazil

A.A.M. González, L.B. Passini, R.B. Boszczowski, A.C.M. Kormann, A.P. Fiori

Abstract. An extensive campaign of field and laboratory tests were performed on samples of residual soils and colluviums present in the morphosculptural sub-unit comprising Serra do Mar Paranaense located in Southern Brazil. The geotechnical investigations included the physical characterization, *in situ* hydraulic conductivity and the mechanical behavior of the soils, by means of conventional direct shear tests, smooth interface direct shear tests, and CIU triaxial tests. The results showed that both the superficial colluvium and residual soils found along this stretch have similar granulometry, generally classified as silty sand soils, with *in situ* hydraulic conductivity of around 10^{-4} cm/s. Grain size curves show less dispersion in the case of residual soils compared with colluvial soils. The residual and colluvial soils had average peak and residual friction angles of 32° and 26° , respectively, with variations and differences attributed to the complex variety of the lithotype present in the region. Regarding cohesive intercept, a greater disparity was found in the results; however, these results corresponded to the literature. These results are relevant because they provide a framework to evaluate the stability of road slopes, together with other pertinent information, such as slope declivities and layers, water table, suction parameters and rain scenarios, both in specific cases within or close to the region, and in areas of similar geological material.

Keywords: colluvial soils, residual soils, Serra do Mar, shear strength, smooth interface, soil strength parameters.

1. Introduction

Serra do Mar is a mountain range encompassing approximately 1,500 km of the East/South coast of Brazil, going from the state of Rio de Janeiro to the North of the state of Santa Catarina (Ceri *et al.*, 2018; Vieira *et al.*, 2018). The range is classified into three large geomorphological compartments: Plains Compartment, Mangrove Compartment and Mountain Ranges and Hills Compartment, characterized by a diversity of lithological types, including granites, schists, gneisses and migmatites (Massad, 2010).

According to Listo & Vieira (2015) and Vieira *et al.* (2018), the Mountain Ranges and Hills compartment of the Serra do Mar is one of the main geomorphologic compartments frequently affected by mass movements of the shallow landslide type. Among the events that have occurred over time, the following have been significant: Caraguatatuba in 1967, Cubatão in 1985, Ilhota, Gaspar and Luís Alves (state of Santa Catarina) in 2008, Angra dos Reis in 2010 and in the mountain regions of Rio de Janeiro and Paraná in 2011. Listo & Vieira (2015) state that Serra do Mar is one of the most important reliefs of Brazil, both in geomorphologic terms when described as a function of its

genesis and evolution, and by its strategic importance, in connecting the largest import and export harbors of the South and Southeast regions, as the port of Santos, the busiest in South America (Vieira *et al.*, 2018). As such, it has a dense network of communication and important service routes supporting economic development, for example: roads, railways, water pipelines, gas pipelines, transmission lines, urban installations and energy industries (Ceri *et al.*, 2018). Thus, a varied research has been and is being performed in this region, from which several questions have arisen, for example, if the results from the models will be more efficient with the use of geotechnical values collected *in situ* (Listo & Vieira, 2015).

The occurrence of different soil types throughout the study area and the need to obtain a better understanding of the geological-geotechnical behavior of the region, reflect the importance of the experimental study of the predominant materials. Based in this context and in the absence of geotechnical information about those materials, this paper presents the geological-geotechnical characterization of a stretch of Serra do Mar, based on results obtained from samples from the superficial colluvial and residual soils of migmatite and granite found in the region. Characterization

Andrés Miguel González Acevedo, Ph.D., Post-Doctoral Researcher, Programa de Pós-Graduação em Engenharia de Construção Civil, Universidade Federal do Paraná, Curitiba, PR, Brazil, e-mail: andresmgonzaleza@gmail.com.

Larissa de Brum Passini, Ph.D., Associate Professor, Programa de Pós-Graduação em Engenharia de Construção Civil, Universidade Federal do Paraná, Curitiba, PR, Brazil, e-mail: larissapassini@hotmail.com.

Roberta Bomfim Boszczowski, Ph.D., Associate Professor, Departamento de Construção Civil, Universidade Federal do Paraná, Curitiba, PR, Brazil, e-mail: roberta.bomfim@ufpr.br.

Alessander Christopher Morales Kormann, Ph.D., Associate Professor, Programa de Pós-Graduação em Engenharia de Construção Civil, Universidade Federal do Paraná, Curitiba, PR, Brazil, e-mail: alessander@ufpr.br.

Alberto Pio Fiori, Ph.D., Full Professor, Programa de Pós-graduação em Geologia, Universidade Federal do Paraná, Curitiba, PR, Brazil, e-mail: fiori@ufpr.br.

Submitted on July 17, 2018; Final Acceptance on July 8, 2019; Discussion open until December 31, 2019.

DOI: 10.28927/SR.422139

tests for determination of physical parameters of soils is the primary and fundamental stage for several analyses, such as determining the prediction of both mechanical and hydraulic behavior in engineering, mining and environmental processes, as well as susceptibility analyses for the determination of areas at risk of mass movements.

Some studies have described the geological and geotechnical characteristics of the soils found along the Serra do Mar in order to obtain parameters as internal friction angle, cohesive intercept, granulometric distribution, hydraulic conductivity and structural features (Mendes *et al.*, 2006; Furlan *et al.*, 2011; Mendes *et al.*, 2015; Sestrem *et al.*, 2015; Advincula, 2016; González *et al.*, 2017; González, 2017; Cerri *et al.*, 2018; Vieira *et al.*, 2018; Trevizolli, 2018) looking to increase the knowledge about the region.

Other studies and researches focused on contributing to the understanding of the surface and subsurface dynamics of water at the Serra do Mar (Mendes *et al.*, 2006; Soares *et al.*, 2012; Mendes *et al.*, 2015; Oliveira *et al.*, 2016; Trevizolli, 2018, Picanço *et al.*, 2019).

The sub superficial layer of the natural slopes from Serra do Mar is unsaturated. After the dry season, infiltration capacity is high and rainfall events can cause significant effects on the distribution of soil matric suction (Bicalho *et al.*, 2015). During the rainy season, the infiltration of rainfall into the ground develops positive pore pressures by raising the water table and reducing suction levels. Consequently, the soil shear strength decreases, caused by the increase of natural moisture content and unit weight in an global stability analysis for shallow slides, like thin layer sliding (Ortigão & Sayão, 2004), being one of the causes that explain the occurrence of slope instability at Serra do Mar (Victorino, 2015; Sestrem *et al.*, 2015; González *et al.*, 2017).

The series of tests presented in this paper is part of a research with the main objective of compiling geotechnical data, in order to allow a later evaluation of the stability of road slopes along the stretch of BR-376/PR in the Serra do Mar Paranaense, through the identification of the common type of mass movement and the elaboration of susceptibility and safety factor (FS) maps.

2. Geological Background

Lithotypes present in the area of interest include characteristic rocks of the Atlantic Orogenic Belt (Gneiss-Migmatitic Complex), areas of colluvium and talus deposits (MINEROPAR, 2005). Among the lithotypes of the Gneiss-Migmatitic Complex, defined by Siga Jr. *et al.* (1995) as the Atuba Complex, are associations of stromatic migmatite with biotite-hornblende-gneiss paleosome, mica-quartz-schist, ultrabasite, metabasite and amphibolite; ophthalmic migmatites with biotite-gneiss paleosome, biotite-hornblende-gneiss and hornblende-gneiss with local quartzites; biotite-gneisses; ocellar gneisses, interdigitated with stromatic migmatites with the occurrence of

banded and leucocratic gneisses and feldspathic schist; undifferentiated migmatites with amphibolites and quartz-feldspathic veins associated with migmatites “*dent de cheval*”, local pegmatite and aplo-granites; norites, enderbites, charno-enderbites, gneisses, meta-quartz-diorites, meta-diorites, metagabros, including serpentinites and steatites; foliated granite suite, undifferentiated metasomatic granites or anatexia.

MINEROPAR (2002) defines the Complex as a set of stromatic migmatites, granite gneisses, granite gneisses and pebbles, meta-ultrabasic rocks, metabasites, amphibolites and quartzites. There are frequent intercalations of amphibolite bodies, sometimes with garnetiferous or magnesium schists, from centimetric lenses to metric bodies. Features related to the second phase of migmatization are common, with pink mobilizates (K-feldspate), either consistent or not with the gneiss banding. The association of norites, enderbites, charno-enderbites, and others corresponds more properly to a granulite complex. Two calcium-alkaline trends were identified inside this set: one tonalite (norite enderbite) and the other norite-jotunite-opdalite-charnockitic. In metamorphic terms, a recrystallization event in the order of 800 °C within the granite facies was identified in this sector of the Complex. The granite foliate, anatexitic and metasomatic is inserted in the Gneiss-Migmatitic Complex due to the close relation with the embedded migmatites, in contrast to the granitoid rocks of the Granitic-Gneiss Complex, which is considered intrusive.

In the area of interest, there are also some granitic bodies, defined in the literature as belonging to the Alkali-Granites Suite of Upper Proterozoic - Paleozoic age, with different dimensions, ranging from small stocks to batholiths. It is locally named “Granito de Morro Redondo”, a regional toponym. These massifs are characterized by alkaline nature, equigranular texture and isotropy, in contrast to the pronounced foliation of gneisses and imbedded migmatites, where contact is normally made through fault zones (MINEROPAR, 2002).

Regarding the colluvium areas of the quaternary age, Angulo (2004) described them as sediments associated with the Serra do Mar slopes, in which no evidence of transport by low viscosity flows was observed. It is described by the author as predominantly fine sediments, with variable proportions of sand and pebbles, usually without structures. Pebbles may be dispersed in the matrix or concentrated in levels or lines (stonelines), with the frequent occurrence of more than one superimposed colluvium with different texture or color characteristics. According to Angulo (2004), colluviums seem to have been originated by slow mass movement processes, involving weathering processes, however, the lines of pebbles and buried soils attest to the complexity of their evolution.

In the description of these sediments and deposits of quaternary age, Angulo (2004) refers to the deposits of talus as sediment accumulations that frequently occur in the

foothills of the steep slopes and whose deposition surfaces create ramps of strong inclination. These ramps are predominantly characterized by debris fall process with no evidence of fluvial processes. In some cases, the ramps described had ravines, with parallel and non-radial patterns, such as in fans. The distribution of the lithotypes is presented in Fig. 1.

The relief, with strongly corrugated morphology in this environment, favors the occurrence of residual soils in the upper third portion of the slopes, conditioned by the incipient pedogenesis development associated to the action of the surface runoff. Thus, these soils have characteristics linked with the original material, represented by variable granite lithotypes, migmatites and gneisses (Furlan *et al.*, 2011; Cerri *et al.*, 2018). The colluvial soils, on the other hand, may be found in the lower two-thirds of the slopes, where they gain depositions from upwind and upstream erosive processes.

3. Material and Methods

The area of study in this paper includes the segment of BR-376/PR within Serra do Mar (Fig. 2). The area extends approximately 32 km and begins in the city of São José dos Pinhais (a city belonging to the metropolitan region of Curitiba, State of Paraná), and continues until just before the border of the State of Santa Catarina, between kilometers 649 and 681 of BR-376/PR. The area includes

relief units from the First Plateau Paranaense and the morphosculptural sub-unit of the Serra do Mar Paranaense. The study of hydrographic basins supplies relevant information to the research, for further analysis of rainfall distribution at slope stability (Soares *et al.*, 2012; Vilanova, 2015; Gonzalez, 2017; Cerri *et al.*, 2018; Vieira *et al.*, 2018).

3.1. Geotechnical investigation program

The strategy for choosing the points of geotechnical investigation was initially defined by the identification of the different geologic units, described in the geologic map (Fig. 1) and in field visits. Existing reports and geotechnical projects also helped in the identification and previous localization of the depots of colluvial soils and landfill areas. The location of the investigation points (Fig. 3) was limited to the area next to the borders of road BR-376/PR, between km 660 and 680, due to the difficulty of access caused by the dense vegetation and rough topography, characteristics of Serra do Mar.

The elevation range was defined by eight classes, with intervals of 200 m between each one, beginning with < 200 m, 200 m-400 m, 400 m-600 m, 600 m-800 m, 800 m-1000 m, 1000 m-1200 m, 1200 m-1400 m and > 1400 m, with a distribution of 1.6%, 8.7%, 10.7%, 18.4%, 47.4%, 7.4%, 4.7% and 1.1% for each class, respectively. On the basis of EMBRAPA (2006) classification, and con-

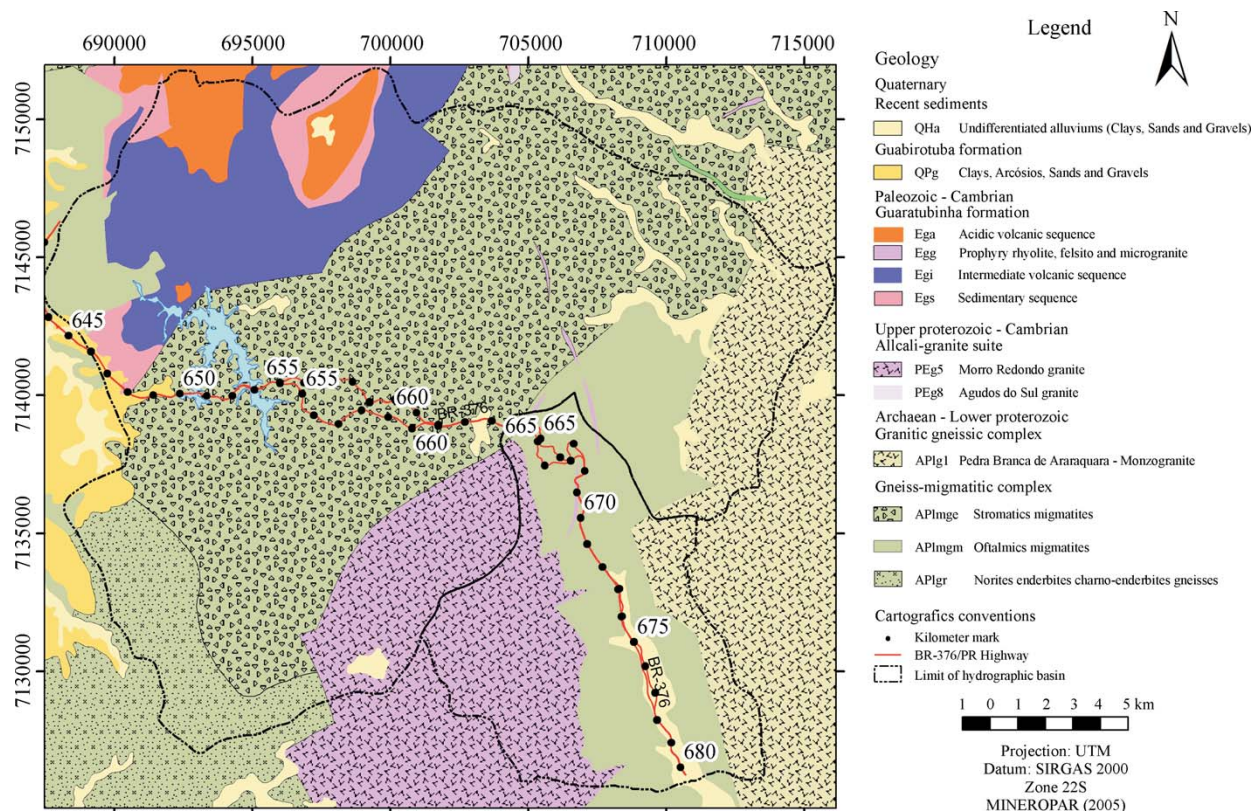


Figure 1 - Geologic map with the main lithotypes (Modified from MINEROPAR, 2005).

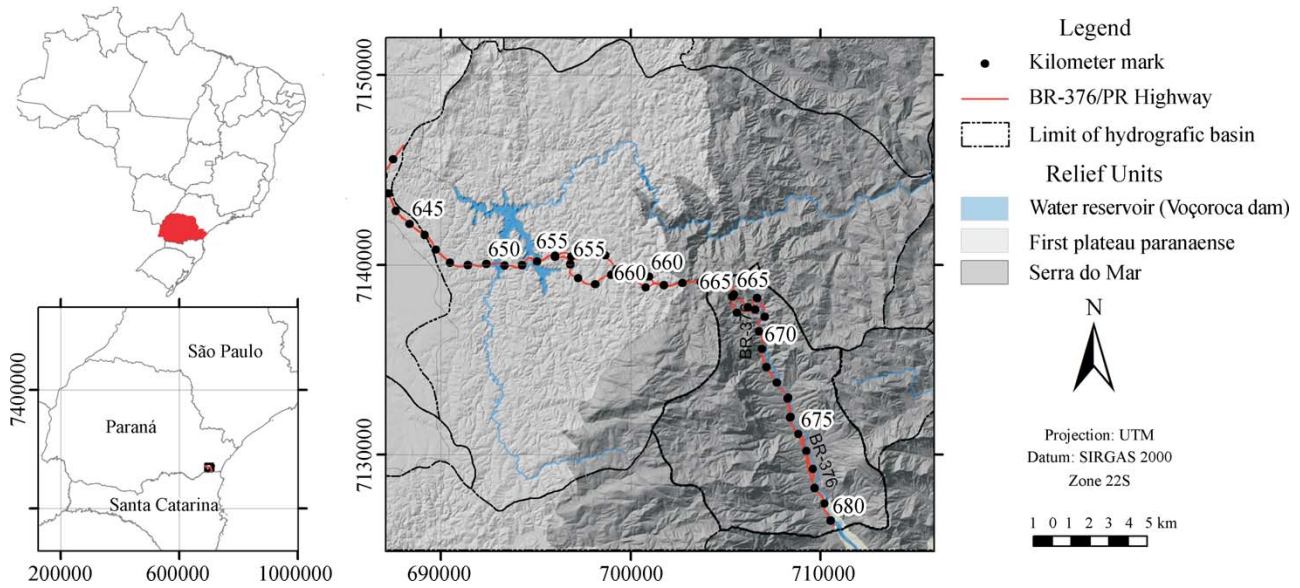


Figure 2 - Location of the study area in Serra do Mar, State of Paraná, Brazil.

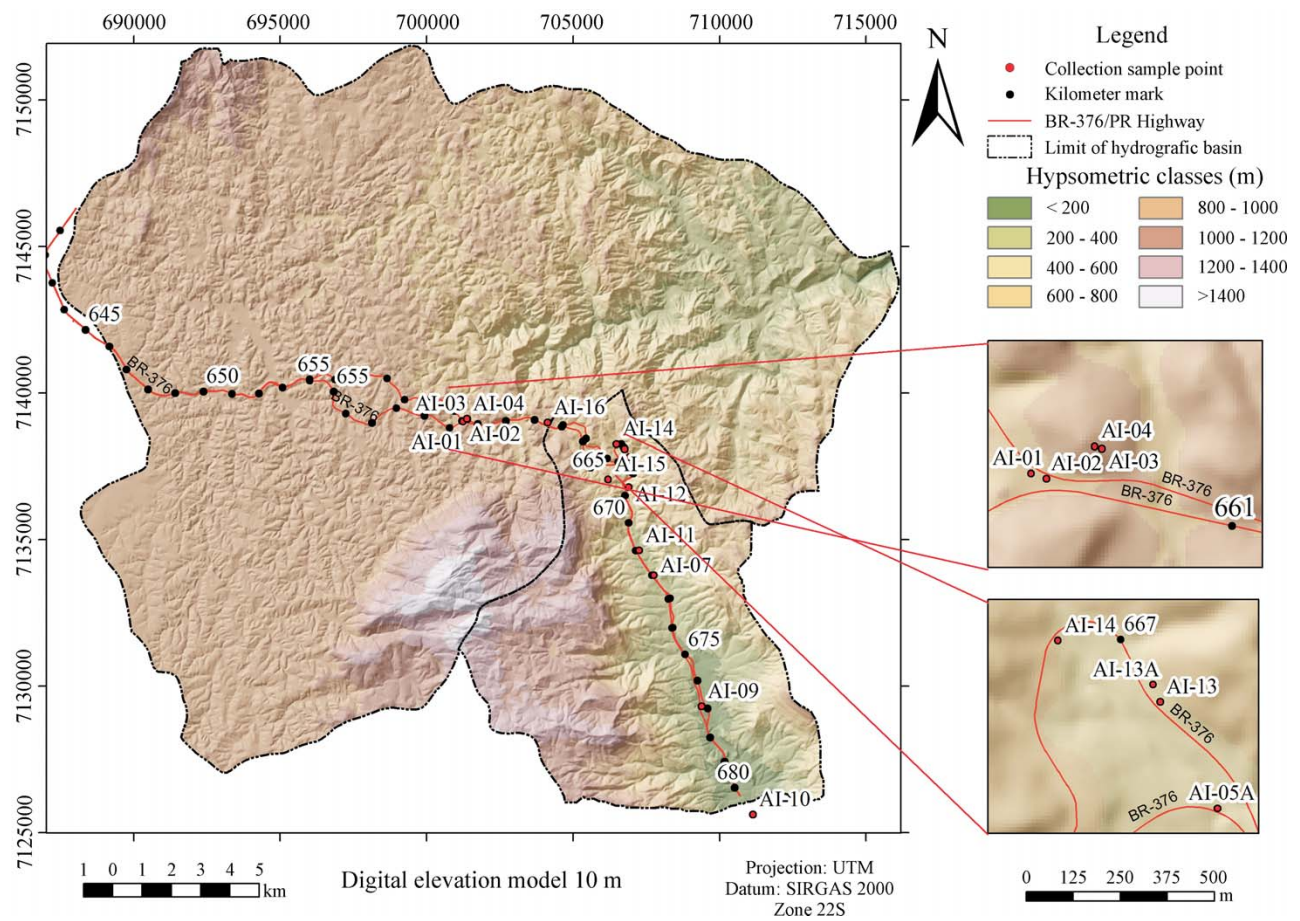


Figure 3 - Location of undisturbed samples.

Considering the slopes declivity, the area presented 45.1% of the area as Strongly Wavy, 22.1% as Wavy, 19.4% as Hilly, 7.5% as Softly Wavy, 3.6% as Steep and 2.4% as Plane.

The geotechnical investigation was distributed along the large area of study in order to increase its representativeness (Fig. 3). The soil has a process of natural forma-

tion, making its properties strongly dependent on the geological processes acting in their genesis and, therefore, the parameters defined for each type of soil carry some intrinsic variability due to the heterogeneity of the material. The undisturbed samples were obtained by excavation, avoiding roots and organic material. No signals of wall instability of the excavations were noticed at any point. Then, blocks received paraffin in all their surroundings and were involved with fabric, receiving paraffin once again. Such procedures follow standard NBR 9604 (ABNT, 1986), which tries to preserve the natural moisture conditions and to ensure the physical integrity of the sample. Before being moved from the wells, the blocks were packed in wood boxes and the voids filled with sawdust. The collection procedure involved also the identification of the caps of the boxes. Besides this procedure, from the bottom of each well approximately 3 kg of deformed material were taken, in order to proceed with geotechnical characterization tests.

3.2. Field and laboratory tests

Information of location and type of material sampled along the studied stretch are found in Table 1. The elevation and UTM coordinates were obtained via navigation GPS with precision indicated by the manufacturer of approximately 5 m. In addition, for relative location of the material sampled, data of the approximate km of the track were inserted. With regard to the location of the road where the sampling was made, it was classified as N for the track in direction North and S for the track in direction South, being LS for left side and RS for right side of the road, as well as the UTM coordinates (Zone 22S), along with the respective values of East (E) and South (S) and the depth of the disturbed and undisturbed samples to be used in the tests. The depths of sampling were defined based on field visits, in which land scars of ancient mass movements and the com-

mon type of appearance were identified, and were classified as translational and subsurface (González, 2017).

The 11 (eleven) samples were submitted to geotechnical characterization (moisture content, granulometric analysis, Atterberg Limits and particle density) and 5 of them were selected to carry out conventional direct shearing tests (with measurement of mechanical strength for specific and residual deformations), and another 4 samples to carry out consolidated undrained triaxial compression tests (CIU).

In places where samples were retrieved, permeability *in situ* tests were also carried out using a mini disk infiltrometer type. The *modus operandi* of the test consists basically in verifying the volume of water that infiltrates the soil in a given interval of time along with a given suction. For this, the upper and lower chambers of the test setup are filled with water, the upper chamber controlling the applied suction and the lower being used as a graduated reservoir to determine the water infiltrating the soil (Victorino, 2015).

Fatehnia *et al.* (2014) describe that the area measured by this type of method is small because of limitations of the disk size of the infiltrometer and small depth of the test. However, it is mainly used for determining the hydraulic properties of the superficial layer of the soil. Moreover, contrary to other devices that only measure the flow under submerged or saturated conditions (such as, for example, the double-ring permeameter), the tension disk infiltrometer is able to measure the non-saturated hydraulic conductivity of the soil. In order to measure the hydraulic conductivity of the soil, a negative potential (suction) must be made over its surface. In the current study, the depth of measurement was defined in 2.0 m (at the depth of the undisturbed samples) due to the low thickness of the potential failure plane.

The soil mechanical strength parameters were determined via direct shear and triaxial compression tests car-

Table 1 - Information about points of geotechnical investigation.

Sample ID	km	Road	Side	Origin of soil	Elevation (m)	UTM Coordinates		Depth (m)
						E (m)	S (m)	
AI-01	659	S	LS	Residual	804	0701199	7139033	1.5
AI-02	659	S	RS	Colluvium	809	0701199	7139033	1.0
AI-03	659	N	RS	Residual	800	0701387	7139099	2.3
AI-04	659	N	RS	Residual	818	0701368	7139105	1.0
AI-07	672	S	RS	Residual	311	0707750	7133769	1.2
AI-09	676	S	LS	Colluvium	178	0709382	7129296	0.9
AI-13	668	N	RS	Colluvium	582	0706740	7138096	1.5
AI-13A	668	N	RS	Residual	601	0706721	7138133	1.0
AI-14	667	N	RS	Residual	618	0706474	7138248	1.3
AI-15	666	N	RS	Residual	652	0706169	7137050	1.0
AI-16	664	N	RS	Residual	829	0704124	7138979	0.8

ried out at the Laboratory of Soils of the Institute of Technology for Development (LACTEC). The geotechnical characterization was performed at the Laboratory of Materials and Structures (LAME) of the Federal University of Paraná (UFPR).

Direct shear tests were conducted according to the British Standards BS 1377 - part 7 (BSI, 1990a). Three shearing apparatus were used: two of model L02900 from Wille Geotechnik and one model Shear Trac II made by Geocomp. The test specimens were trimmed in square rings of 100 mm side and approximately 20 mm height. After trimming, the specimen was slowly extruded into the shear box, a setting load was applied, and the soil was submerged in water (under inundation). A consolidation pressure was then applied (30, 60 and 90 kPa) during a minimum period of 24 h. Settlement readings were taken as a function of time to allow appropriate calculation of consolidation coefficients ($c_v = 2.2 \times 10^{-5}$ to 6.2×10^{-4} cm²/s for 30 kPa; 8.7×10^{-5} to 2.3×10^{-3} cm²/s for 60 kPa and 2.5×10^{-4} to 3.9×10^{-3} cm²/s for 90 kPa) and to ensure that the sample has reached equilibrium prior to the start of shearing. The shearing rate was defined from parameters of consolidation as proposed by Gibson and Henkel (1954, cited by Head, 1981), allowing to perform the test in drained conditions. The shearing rate adopted for all tests was 0.07 mm/min.

Skempton (1964), cited by Kanji (1998) evaluated the use of parameters of peak or residual strength for determining the safety factor of slopes. Kanji (1998) considers that this choice should be based in the level of stress and deformation of the slope, also considering geotechnical and geologic aspects, such as the presence of joints and fissures, degree of weathering and development of progressive failure. The author concluded that the presence of fissures and joints may lead to a progressive failure until the material reaches residual strength, suggesting, thus, the adoption of residual strength values in these cases.

Kanji (1998) proposed a simple test for obtaining residual strength parameters whose procedure consisted in molding clay soils until their liquid limit and shearing them over a polished (smooth) surface. The main difference between this procedure and the conventional one is that the lower half of the shear box is filled with polished rock, making the soil sample slide over it. The author suggests that using this technique the particles of soil become oriented in the interface. Advincula (2016) uses the test specimen trimmed from the undisturbed block; however, in order to create the polished interface, a thin steel wire was used for cutting the sample directly in the polished surface and to evaluate the residual shearing strength.

Based on Kanji (1998) and Advincula (2016), for the residual strength test of this research, the soil was molded directly in the undisturbed block and sheared over a polish surface that consisted in a granite block with dimensions of 100 mm × 100 mm × 20 mm. This interface was placed in the lower part of the shear box, in order to assess the resid-

ual shear strength of the sample. This test integrates both methods previously described, taking the best procedure from each one.

Regarding triaxial tests, they were executed using a Wille Geotechnik shearing apparatus, model UL60, according to British Standards BS 1377 - part 8 (BSI, 1990b). Triaxial shear tests were performed using cylindrical soil specimens of 50 mm in diameter by 100 mm in height. The complete saturation of triaxial specimens was achieved by employing two methods: percolation of water and application of back pressure. Back pressure in the order of 350 kPa was enough for *B* pore pressure parameter to reach the minimum of 0.95 (BSI, 1990b). For the shearing stage the effective compression pressures were between 15 kPa and 90 kPa with an axial displacement rate of 6.3×10^{-2} mm/min.

The definition of the shear strength parameters of the saturated soil depended upon the failure criteria used to determinate it. Among the most commonly used methods, are applied: peak diverting tension (maximum deviation tension), constant inclination, maximum ratio of the principal stresses (σ'_1/σ'_3), stress path and specific deformation (residual strength).

Both direct shear tests and triaxial tests were performed with saturated samples considering that this is the worst scenario, and better control conditions are possible during the tests (Advincula, 2016; González, 2017; Trevi-zolli, 2018).

4. Results and discussion

4.1. Geological aspects

Through information obtained from field work compared with information available in the literature about the area of interest, it was verified that:

Along the studied stretch of the road, residual soils were found with more frequency and greater thickness from half way up the slope to the top of the corrugated reliefs. Two main soil types have been identified that are related to this rock matrix: residual soils of migmatites/gneisses and residual soils from granite.

The residual soils of migmatites/gneisses are the most abundant and are characterized by the predominance of diverse colors (yellows, reds and whites). They are predominantly silty, compact and have low permeability and plasticity. This type of soil is frequently in the presence of relict structures from the parent material, characterized by a whitish color, which comes from concentrations of felsic materials, such as feldspar and quartz. More reddish and yellowish coloration levels are due to greater concentrations of mafic minerals in the matrix rock, such as micas of biotite type, and amphiboles.

Although the geologic map of the region indicates a distance between the presence of granites and the area of study, outcrops of this lithotype were observed during site visits, on slopes adjacent to BR-376/PR highway, which

were then mapped in addition to weathered residual soils. The residual soils of granite were characterized by lighter colors evidence of clay of kaolin type, resulting from the alteration of feldspars. The presence of colluvial soil was marked by dark grey color, lack of structure and thickness of approximately 50 cm. A layer of organic soil was also found, about 20 cm thick, and dark in color.

The residual soils from granite had lack of relict structures in the form of levels of different colorations, white to reddish. The relict structure observed in some cases is characterized by a differentiated granulometric aspect, given by the weathering alteration of feldspars of clear colors and of mafic minerals of reddish colors, oriented according to an incipient foliation that may be both of metamorphic and magmatic origin, having mineral granulometry from medium to coarse (ALS, 2014).

Most colluvial soils are characterized by the reddish, brownish or yellowish color, like bricks, of silt-sandy matrix and without evidence of relict structures from the matrix rock. They appear over residual soils, in some cases being very clear the transition between both, especially by a sudden change of coloration. They are located mainly in the more flattened tops or in the lower portions of the strands and have very irregular thickness (ALS, 2014).

The definition of colluvium soils is given as the material composed of blocks and/or grains of any dimension, transported by gravity and accumulated in the base or at a small distance of steeper slopes or rocky cliffs (Lacerda & Sandroni, 1985). This type of soil is often found in areas situated in the lower third of slopes and mountains, where the relief is strongly corrugated and makes no reference to the origin of the soil. Depending of transport factors, it may involve more than one type of material.

Contacts between colluviums and residual soils of migmatite are more accentuated in outcrops. Between horizons A and B (colluvium soils), the sudden change of coloration marks the transition between them. The transition from colluvium for residual soil (horizons C) is more subtle, marked by the change from a material without structure, or massive, to a material with relict structure, inherited from the matrix rock. Besides, the disperse whitish colors indicates the presence of weathered feldspars, in the case of residual soil, feature not verified in colluvium soil.

In more restricted places of Serra do Mar Paranaense, inside the interest area of this study, there are alluviums associated with the main channels in the section of the medium rivers course such as the “São João”, among others. Those alluviums cover an extensive region of Guaratuba, in the portion of the coastal plain, in the riverbeds of “São João, Cubatão, Cartãozinho and Canavieiras” rivers. They are constituted by sediments of river deposition, predominating sand and riverbeds of gravel, which may be associated with depots of meadow and slope. The meadow depots appear in restricted areas along some draining, characterized by unconsolidated sediments, of small thickness, con-

stituted by silts and clays, partly turfy and with sand of different granulometry. Inside those depots may also appear gravel riverbeds, of Holocene age, where predominate quartz and quartzite pebbles, well selected and rounded, indicating effective transport (ALS, 2014).

4.2. Characterization tests

Characterization tests encompassed obtaining the soil natural moisture content, Atterberg Limits and the particle density of soil samples collected in field, representing the surface material composing the hillside. Also, *in situ* hydraulic conductivity tests were performed at the bottom of the well of the undisturbed soil samples collected in the field. Results from characterization tests are shown in Table 2. Except for samples AI-13 and AI-16, classified respectively as clayey sand and silty gravel soil, the other samples were classified as silty sand, according to USCS (ASTM, 2017).

According to the plasticity chart relating liquid limit (LL) vs. plasticity index (PI) (Fig. 4), most of the samples have behavior belonging to silty soils (below line A) and all samples had liquid limit (LL) under 50% (left of line B), being, therefore, classified as soils with low compressibility and low to average plasticity. Line A distinguishes clay soils (placed above) from silty soils (placed below). Line B, describing the degree of compressibility of soils, separates the materials with liquid limit lower and greater than 50%.

Only sample (AL-07) of residual soil from migmatite exhibited behavior belonging to clay soils (over line A), al-

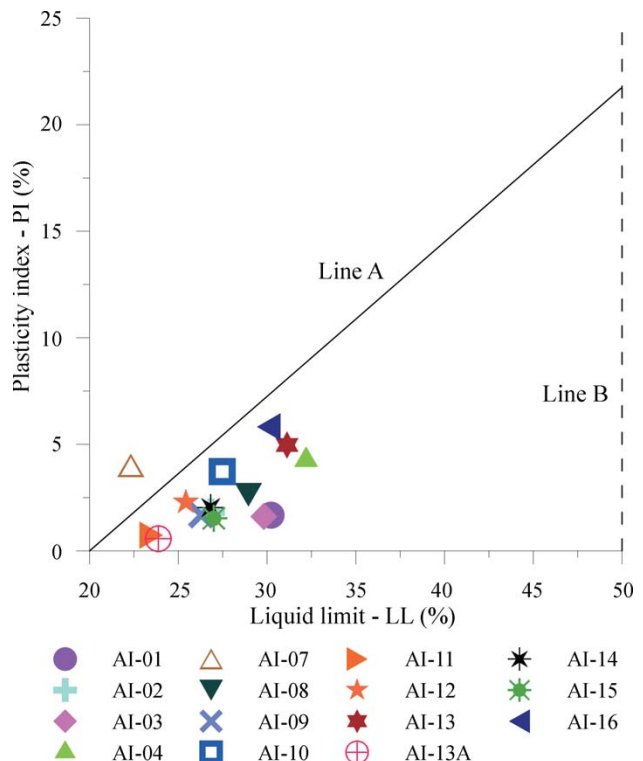


Figure 4 - Plasticity chart.

though the amount of clay present in the granulometric distribution was 3.8%. Granulometrics classification, Atterberg Limits and the particle density results are coincident between them, which indicates accuracy in the procedures. When compared by means of granulometric and the plasticity chart classification as silty sand soils, the behav-

ior corresponds to silt of low compressibility and low plasticity.

Results of granulometric analysis are presented in Table 3, which displays the percentage of material retained in each granulometric range.

The granulometric analysis of residual soil from migmatite showed that the soil lies in a well-defined range with

Table 2 - Values obtained by soil characterization tests.

Sample ID	Natural moisture (%)	Liquid limit (%)	Plastic limit (%)	Particle density (g/cm ³)	USCS classification
AI-01	25.6	30.2	28.5	2.773	Silty sand
AI-02	19.3	26.8	24.6	2.645	Silty sand
AI-03	23.5	29.8	28.2	2.694	Silty sand
AI-04	26.6	32.2	27.8	2.804	Silty sand
AI-07	19.2	22.3	18.3	2.680	Silty sand
AI-09	27.4	26.3	22.9	2.645	Silty sand
AI-10	22.8	27.5	20.5	2.637	Silty sand
AI-11	18.9	23.5	22.7	2.626	Silty sand
AI-13	30.6	31.1	26.1	2.693	Clayey sand
AI-13A	20.5	23.9	21.1	2.699	Silty sand
AI-14	22.9	26.8	24.8	2.677	Silty sand
AI-15	25.2	27.0	25.5	2.666	Silty sand
AI-16	23.1	30.1	24.3	2.634	Silty gravel

Table 3 - Granulometric analysis of soil samples.

Soil	Sample ID	Soil classification (USCS)	Gravel (2.0 mm < % < 60 mm)	Sand (0.06 mm < % < 2.0 mm)	Silt (2 µm < % < 0.06 mm)	Clay (% < 2 µm)
Residual from migmatite	AI-01	Silty sand	0.0	32.1	63.3	4.6
	AI-07	Silty sand	2.2	38.4	55.7	3.8
	AI-13A	Silty sand	4.6	34.9	56.4	4.1
	Average		1.6	32.7	61.1	4.6
	Standard deviation		1.9	4.7	6.3	1.6
Colluvium	AI-02	Silty sand	0.4	37.6	55.3	6.7
	AI-09	Silty sand	4.4	23.8	60.0	11.8
	AI-13	Clayey sand	0.1	20.4	48.8	30.7
	Average		0.3	29.0	52.1	18.7
	Standard deviation		0.2	12.2	4.6	17.0
Residual from granite	AI-03	Silty sand	1.2	32.3	59.2	7.3
	AI-04	Silty sand	0.1	25.6	71.1	3.2
	AI-14	Silty sand	0.1	35.1	54.3	10.5
	AI-15	Silty sand	0.2	38.1	56.5	5.2
	AI-16	Silty gravel	32.8	25.3	27.0	15.0
	Average		9.4	30.6	49.5	10.6
	Standard deviation		15.7	7.1	15.2	4.1

predominance of silty material (Fig. 5). The average amount of silt in samples is equal to 61.1%, with a standard deviation of 6.3%. The fraction of sand in samples was 32.7% on average, with standard deviation of 4.7%. The fractions of gravel and clay represented a small portion of the soils with averages of 1.6% and 4.6% respectively, and standard deviations of 1.9% and 1.6% respectively. The particle density was approximately 2.717 g/cm³ and standard deviation of 0.049 g/cm³. The natural moisture content of these samples was 21.8% with standard deviation of 3.4%.

Samples AI-14 and AI-15 related with the residual soils from granite showed very close granulometric distribution and consistence index (Fig. 6). In contrast, sample AI-16 had a predominance of gravel (32.8%) and high liquid limit, probably associated with the greater concentration of clay (15.0%). For all samples (residual and colluvial soils) the liquid limit (LL) had average of 27.3%, with 3.5% standard deviation and the plastic limit (PL) had average of 26.1% with 1.8% standard deviation. The particle density was approximately 2.695 g/cm³ and standard deviation of 0.065 g/cm³, with a moisture content in natural condition of 24.2% and standard deviation of 1.6%.

The granulometric distribution of colluviums showed greater dispersion when compared with residual soils

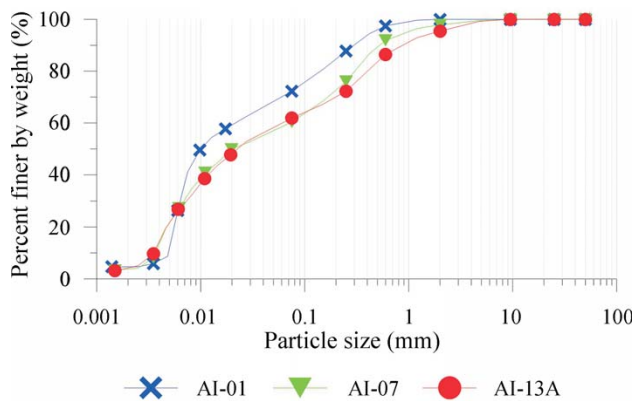


Figure 5 - Granulometric curves related to migmatite residual soil.

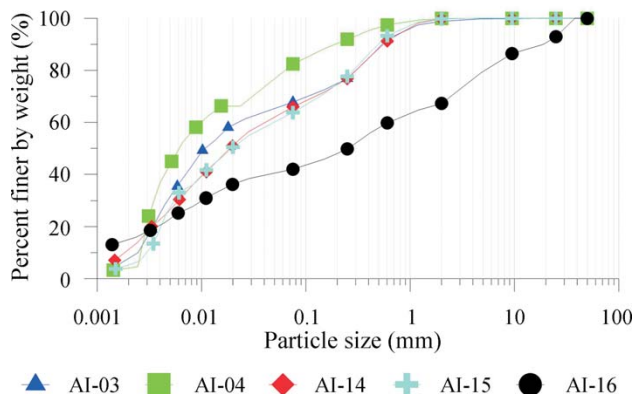


Figure 6 - Granulometric curves related to granite residual soil.

(Fig. 7). While in the sample of colluvium soil AI-02 predominated the occurrence of silty sand material, sample AI-13 had a significant percentage of clay of approximately 30.7%. A small amount of gravel was found in the two samples. The greater liquid limit (LL) corresponding to samples of colluvium material was found in sample AI-13 (31.1%), which may be explained by the clay portion present in the material. The average value for plastic limit (PL) was 24.5%, for particle density was 2.661 g/cm³ (with standard deviation of 0.028 g/cm³), and for natural moisture content was 25.8% (with standard deviation of 5.8%).

4.3. In situ permeability tests

By means of *in situ* permeability test of superficial soil, made at the bottom of the sampling wells of the undisturbed samples, average values of hydraulic conductivity around 10⁻⁴ cm/s were obtained, with minimum value of 3.1 × 10⁻⁵ cm/s and maximum value of 1.0 × 10⁻³ cm/s, getting as result coefficients defining a low degree of permeability, according to Terzaghi & Peck (1967). Such average of hydraulic conductivity is found in the interval defined by Casagrande & Fadum (1940), corresponding to very fine sand and silt. According to Lambe & Whitman (1969), those values correspond to sandy clay. For Pinto (2006), this value of hydraulic conductivity is considered characteristic of clay and fine sand. Das (2007) defines these values of hydraulic conductivity as belonging to clay or silt. Therefore, the value of the hydraulic conductivity obtained is found adequate for soils of the studied site, classified as silty sand, according to the USCS granulometric analysis.

Vieira *et al.* (2018) used in their investigation values of 10⁻⁴ and 10⁻³ cm/s obtained with Guelph Permeameter in three land scars in an experimental basin located in the Serra do Mar (Copebrás basin, São Paulo State), either in colluvial soil or in migmatite saprolite's of the Embu Complex and Costeiro Complex. According to the authors, two types of regolith above an intensely fractured bedrock were observed: colluvial soil with depths about 1.0 m, formed by pedogenesis over transported material, with a sandy-clayey texture matrix and partially weathered bedrock; and sapro-

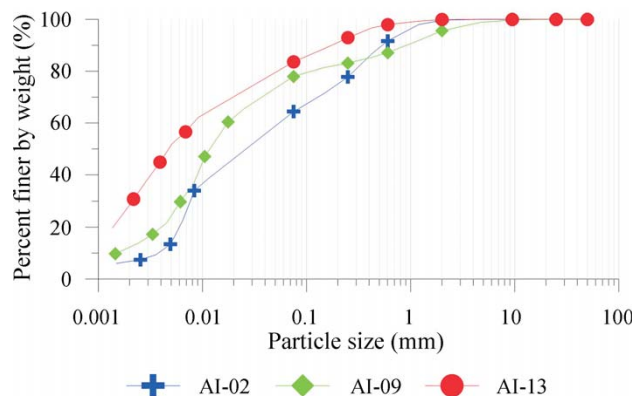


Figure 7 - Granulometric curves related to coluvium soil.

lite (about 3.0 to 4.0 m depth), more sandy than the overlying horizon, with evidence of structures inherited from bedrock.

Trevizolli (2018) studied the *in situ* permeability in a slope located at Serra do Mar, km116 in Barra do Turvo - State of São Paulo, using Guelph Permeameter. The author obtained a hydraulic conductivity of 10^{-5} cm/s for the superficial soil of the slope. The soil of the slope investigated was classified as colluvium and residual soil from Migmatite rock, with granulometric analysis resulting in clayey sand and clayey sand with gravel, respectively.

Therefore, comparing the results found here with previous research (Vieira *et al.*, 2018; Trevizolli, 2018), the soil particle size resulting from the weathering of migmatite is partially similar to the other regions at Serra do Mar with similar lithotypes, generating hydraulic conductivity between 10^{-5} and 10^{-3} cm/s for this soil.

4.4. Mechanical behavior tests

Conventional and smooth interface direct shear tests were performed for obtaining parameters of peak and residual strength, in both cases under inundation, in addition to triaxial CIU test (Fig. 8).

Based on the shearing stress-horizontal displacement response shown in Fig. 9 from conventional and smooth interface direct shear tests, the failure mode of the test specimens happened in a ductile way, in other words, with no peak (Fig. 9). This characteristic is typical of the behavior of sandy soils with void ratio greater than critical, in other words, loose sands.

Table 4 and Table 5 show a summary of shear strength results: friction angle (ϕ') and cohesive intercept (c'), normal stress, degree of saturation initial (i) and final (f) from conventional direct shear tests and smooth interface method.

The determination of the parameters of maximum shear strength of the soils considered a horizontal displace-

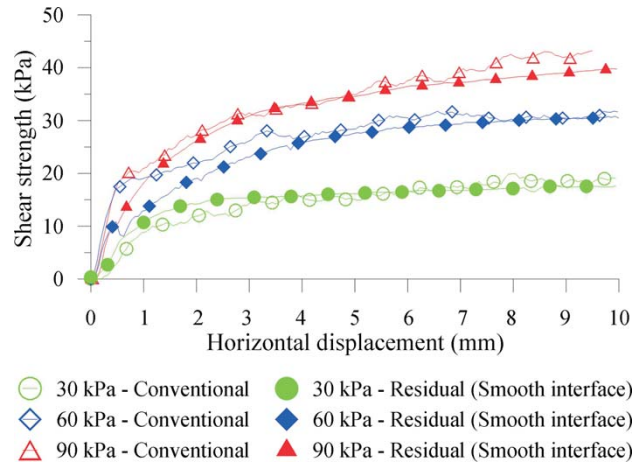


Figure 9 - Shear strength vs. horizontal displacement for migmatite residual soil (AI-01).

ment of 8 mm, which was established considering the shear stress-displacement response. For this displacement value, the shear stress is nearly constant. For residual strength test (smooth interface) larger values of horizontal displacement were required (11 mm) in order to reach constant values of shear stress (Tchalenko, 1970; Suzuki, 2004; Advincula, 2016; González, 2017; Trevizolli, 2018).

For colluvium soils, the cohesive intercept was greater than that observed for the residual soil from migmatite, and similar to that of the residual soil from granite.

Skempton (1985, cited by Kanji 1998) interpreted the residual strength of soils as a function of their fraction of clay (grains smaller than $2 \mu\text{m}$). The author concludes in its work that, for soils with percentage of clay over 50%, the angles of residual friction found are lower and have great differences between peak and residual values. On the other hand, when the percentage of clay is smaller than 25%, residual values much closer to the peak strength values are found. This trend was verified in the present research.



Figure 8 - Conventional direct shear (left) and triaxial CIU (right).

Table 4 - Parameters of soil strength from conventional direct shear tests.

Material	Sample ID	Normal stress (kPa)	Degree of saturation (i) (%)	Conventional direct shear strength test			Degree of saturation (f) (%)
				Displac. (mm)	c' (kPa)	ϕ' (°)	
Residual soil from migmatite	AI-01	30; 60; 90	60	8.0	6.5	27.9	91
	AI-13A	30; 60; 90	90	8.0	0.0	38.3	100
Colluvium	AI-02	30; 60; 90	70	8.0	8.2	26.0	93
	AI-09	30; 60; 90	80	8.0	14.8	37.9	100
	AI-13	30; 60; 90	90	8.0	11.7	31.8	100
Residual soil from granite	AI-14	30; 60; 90	60	8.0	14.2	28.1	87

Table 5 - Parameters of soil strength from direct shear with smooth interface method.

Material	Sample ID	Normal stress (kPa)	Degree of saturation (i) (%)	Direct shear strength method of smooth interface			Degree of saturation (f) (%)
				Displac. (mm)	c' (kPa)	ϕ' (°)	
Residual soil from migmatite	AI-01	30; 60; 90	60	11.0	0.0	25.6	92
Colluvium	AI-02	30; 60; 90	70	11.0	0.0	26.8	93
	AI-09	30; 60; 90	80	11.0	11.8	18.6	100
	AI-13	30; 60; 90	90	11.0	0.0	24.4	100

Therefore, sample AI-13 that has 30.7% of clay had difference of 7.4° between the friction angle obtained in the conventional shearing test and the smooth interface test, while sample AI-01, with 4.6% of clay fraction, had a difference of 2.3° between those two tests.

Sample AI-09, pertaining to colluvium soil, had a difference of 19.3 degrees between the conventional direct shearing test (37.9°) and the residual strength by smooth interface (18.6°), showing inconsistent result and too low for residual friction angle.

In sample AI-13A, the presence of relict structures was identified. This characteristic has a tendency of conditioning the failure surface and having strength parameters under or over the ones defined in the conventional direct shear test, depending on the position of structures and weakness plans about the shear surfaces in the shear box.

By comparing the present results with other researches, the behavior failure mode in a ductile way (no peak) was also observed in the study of Advincula (2016) on the determination of peak and residual strength of colluvium tropical Brazilian soils in the State of Rio de Janeiro, for normal stresses from 25 kPa to 200 kPa. Although those are colluviums soils, Advincula (2016) studied a sample of residual soil from migmatite, which exhibited peak in failure at the conventional direct shear test. For colluvium soils, the values of both residual and peak friction angles obtained by the cited author were between 22.5° and 37.4°, with values of cohesive intercept between 0.0 and 9.5 kPa for residual strength and 0.8 and 19.8 kPa for peak strength.

In the sample of residual soil from migmatite, the peak friction angle was 36.4° with a cohesive intercept of 36.5 kPa, while the corresponding residual values were 15.3° and 7.0 kPa, respectively. The author attributes the decrease of strength from peak to residual values, to the presence of mica in the mineral composition (Rigo *et al.*, 2006; Advincula, 2016).

Trevizolli (2018) performed conventional and smooth interface direct shear tests (at normal stresses from 50 kPa to 200 kPa) in colluvium and residual soils (under inundation) from Migmatite rock at Serra do Mar slope in Barra do Turvo - State of São Paulo. The author found failure mode in a ductile way (no peak). The values of both residual and peak friction angle obtained by the cited author were between 17.8° and 30.2°, with values of cohesive intercept between 4.7 and 16.8 kPa.

Suzuki (2004) performed conventional direct shear tests (at normal stresses from 25 kPa to 400 kPa) in colluvium and residual soils (under inundation) from Serra do Mar at Morretes - State of Paraná. The author also found failure mode in a ductile way (no peak) for most samples tested. The resistance parameters varied between 2.0 and 21.0 kPa for cohesive intercept and 28.3° to 34.6° for friction angle.

By means of triaxial tests, it was verified that the behavior of soil not always had a defined peak and, in some tests, the material was identified with a strain-hardening behavior, without a well-defined failure (Fig. 10). Thus, for processing results according to the material behavior, dif-

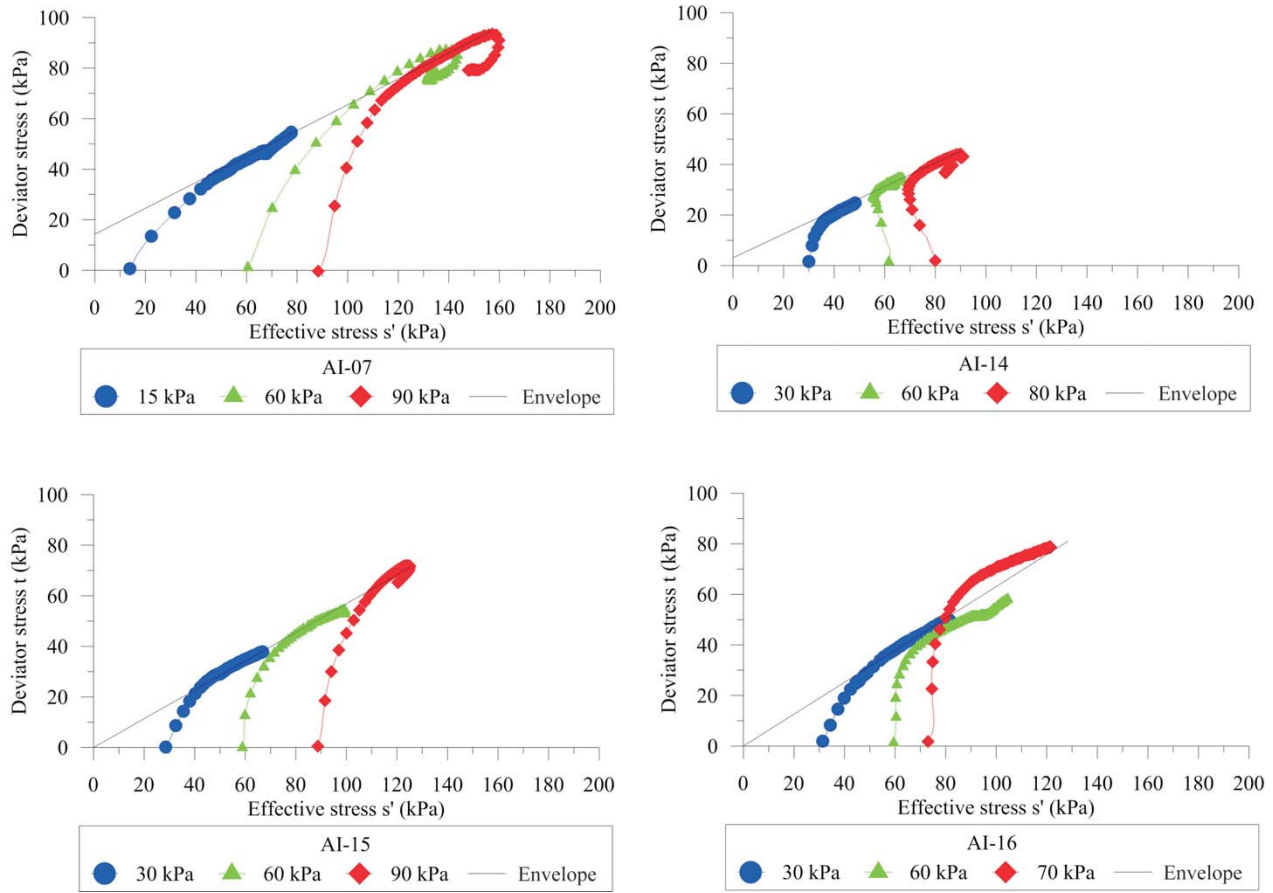


Figure 10 - Stress path curves obtained through Triaxial CIU test in samples (a) AI-07; (b) AI-14; (c) AI-15 e (d) AI-16.

ferent failure criteria were used. Triaxial tests presented a strain-hardening behavior, so the criteria of maximum rate of the principal stresses (σ'_1/σ'_3) and stress paths were applied.

The results obtained with CIU triaxial tests are presented in Table 6, as well as the values of degree of saturation initial (i) and final (f), the value of *B* pore pressure parameter and the failure criteria applied.

Contrary to that presented in the conventional direct shearing test, the residual soil from migmatite subjected to

triaxial test showed higher values of cohesive intercept, while the samples of residual soils from granite showed lower values. The friction angle showed no significant variation in the studied soils.

Generally, when comparing the results obtained from conventional direct shear tests with results from CIU triaxial tests, the values of internal friction angle were concordant, for all samples tested here (residual and colluvium soil). The minimum value of the friction angle determined from the conventional direct shear test was around 26.0°

Table 6 - Parameters of soil strength obtained with triaxial tests.

Material	Sample	Degree of saturation (i) (%)	<i>B</i> pore pressure parameter	Degree of saturation (f) (%)	Failure criteria	<i>c'</i> (kPa)	ϕ' (°)
Residual soil from migmatite	AI-07	65	1.00	100	σ'_1/σ'_3	12.7	33.3
					Stress path	14.3	32.2
	AI-14	63	0.97	99	σ'_1/σ'_3	1.6	28.9
					Stress path	3.1	27.8
Residual soil from granite	AI-15	58	0.96	99	σ'_1/σ'_3	0.5	35.1
					Stress path	0.0	34.8
	AI-16	81	0.98	99	Stress path	0.0	43.2

and the maximum value around 38.3° , with average of approximately 31.7° . In the CIU triaxial test, the minimum value found was 27.8° and the maximum value of 43.2° , with average of approximately 33.6° . Consequently, the average peak friction angle of 32° was adopted as being a conservative value for a regional approach.

Results obtained in tests of residual shear of smooth interface (for residual soil from migmatite and colluvium) presented minimum values, around 18.6° , showing inconsistent result and too low for residual friction angle, and maximum around 26.8° . Thus, the average residual friction angle of approximately 26° was assumed.

Results regarding the cohesive intercept showed more disparity (for all samples: residual and colluvium soil), with values being obtained by means of direct shear tests (ranging from 0.0 kPa to 14.8 kPa, with average equal to 9.2 kPa) similar in magnitude of minimum and maximum to the ones obtained by means of CIU triaxial tests (ranging from 0.0 kPa to 14.3 kPa, however with average equal to approximately 4.6 kPa).

In the detailed analysis of sample AI-14 (Residual soil from Granite), in which direct shear and CIU triaxial test were carried out, a small difference in the friction angle was observed. In direct shear test, the friction angle was 28.1° and from CIU triaxial test was 28.7° . The cohesive intercept was significantly disparate, being 14.2 kPa for conventional direct shear and 1.6 kPa for CIU triaxial test.

Values of cohesive intercept obtained in CIU triaxial tests for granite residual soils were closer to the results obtained in direct shear tests of smooth interface (0 kPa). The triaxial test carried out with migmatite residual soils showed greater values of cohesive intercept (average of 13.5 kPa), being different from the results obtained with samples of granite residual soils, which showed values between 0.0 and 3.1 kPa, with average of 1.0 kPa.

Once again, comparing the present results with other references about CIU triaxial tests in Brazilian tropical soils, Advincula (2016) obtained values of friction angle in colluvium soils between 29.5° and 31.1° and cohesive intercept between 6.4 kPa and 11.8 kPa.

With respect to residual soils, Carvalho (2012) performed triaxial CIU tests in migmatite residual soil in the state of Rio de Janeiro, obtaining as results values of friction angle of 21.5° and cohesive intercept of 105.8 kPa. It must be noted that as the pressures applied by Carvalho (2012) are between 25 and 500 kPa, the values of friction angle and cohesive intercept analogous to tests described in this paper could not be correlated. However, analyzing only effective stresses of 25, 75 and 150 kPa from the work of Carvalho (2012), the value of cohesive intercept and friction angle were 74.2 kPa and 27.7° , respectively, being more coherent with the results of the present research, however with a greater cohesive intercept.

In order to have knowledge about the results of shearing strength in residual terms, Bressani *et al.* (2001) presented a review of several references for different types of Brazilian tropical soils, which made possible to observe that the average angle of residual friction is 25° (excluding results from residual basalt soil, grey and red clay listed) and cohesive intercept has a lower value, around 0 kPa.

Tonus (2009), based on data presented by Dell'Avanzi *et al.* (2007) from triaxial CIU and CID tests, direct shear and ring shear tests, presented a summary of the parameters of peak strength found for different lithostratigraphic units, whose granulometric descriptions are similar to the ones observed in the current research. From statistical analysis, the author obtained friction angles between 29° and 36° (average of 32°) and cohesive intercept between 13 and 29 kPa (average of 21 kPa) for residual soils. With respect to colluvium soils, the friction angle ranged between 25° and 31° (average of 28°) and the cohesion between 6 and 21 kPa (average of 14 kPa). Those results have high coefficient of variation, with values around 20% for the friction angle and of 95% for cohesive intercept.

Regarding the high degree of variation for parameters of peak friction angle and cohesive intercept, a similar trend was observed in the study presented by Mezzomo & Bertuol (2013). By means of retro-analysis made in soils (residual and colluvium) of several slopes along the Serra do Mar, those researchers obtained an average friction angle of 25° and average cohesive intercept of 10 kPa, with coefficient of variation of 12% and 72%, respectively.

Generally, when compared with data found in literature, the results obtained with both direct shear tests and CIU triaxial tests carried out in this research are coherent and similar considering the variability of the material found in the region (Table 7).

The comparison of the shear strength parameters obtained by two different methods (CIU triaxial tests and conventional direct shear tests) is very interesting because of the differences between the apparatus applied and the principles. In CIU triaxial tests the soil fails along planes of weakness, while in direct shear tests the soil rupture occurs in a pre-established plane. (Lambe & Whitman, 1969; Pinto, 2006; Das, 2007).

At Serra do Mar, where the occurrence of mass movements with shallow-type landslide is common, as typical of the geological-geotechnical context of the region, conventional direct shear tests to obtain shear strength parameters are simple, with low cost and fast execution time comparing with CIU triaxial tests. In addition, they are useful as well as representative of the field conditions: plane slip surface at low confining stresses.

Furthermore, in these slopes progressive failure frequently occurs and, therefore, residual shear parameters are relevant as entry parameters in landslide susceptibility analysis. One more time, direct shear tests with smooth in-

Table 7 - Summary of some results from shear strength parameters of Serra do Mar soils.

Authors	Source of results	Type of soil	Friction angle (ϕ')	Cohesive intercept (c')
Present research	Direct shear tests	Residual and Colluvium	18.6°-38.3°	0.0-14.8 kPa
	CIU triaxial tests	Residual and Colluvium	27.8°-43.2°	0.0-14.3 kPa
Bressani <i>et al.</i> (2001)	Shearing strength in residual terms	Brazilian tropical soils	25°	0.0 kPa
Suzuki (2004)	Direct shear tests	Residual and Colluvium	28.3°-33.0°	2.0-21.0 kPa
Tonus (2009)	CIU and CID triaxial tests, Direct shear and ring shear tests	Residual	29°-36°	13.0-29.0 kPa
		Colluvium	25°-31°	6.0-21.0 kPa
Carvalho (2012)	CIU triaxial tests for high confining stress	Residual	21.5°	105.8 kPa
Carvalho (2012)	CIU triaxial tests for low confining stress	Residual	27.7°	74.2 kPa
Mezzomo & Bertuol (2013)	Retro-analysis	Residual and Colluvium	25.0°	10.0 kPa
Advincula (2016)	Direct shear tests	Residual	15.3°-36.4°	7.0-36.5 kPa
Advincula (2016)	Direct shear tests	Colluvium	22.5°-37.4°	0.0-19.8 kPa
Advincula (2016)	CIU triaxial tests	Colluvium	29.5°-31.1°	6.4-11.8 kPa
Trevizolli (2018)	Direct shear tests	Residual and Colluvium	17.8°-30.2°	4.7-16.8 kPa

terface can be applied to obtain those parameters, as was done in this paper.

5. Conclusions

This paper examined geological-geotechnical characteristics of slopes belonging to a segment of BR- 376/PR, within Serra do Mar in Southern Brazil.

The classification of colluvium soils and superficial granite and migmatite residual soils were, in part, similar with regard to both characteristics and granulometry: predominantly silty sand, with mean value of particle density of 2.691 g/cm³, plasticity index on average equal to 3.2% and natural moisture of 23%. The *in situ* hydraulic conductivity obtained was around 10⁻⁴ cm/s in the superficial layer of the soil, characterized as the potential failure surface.

Different from what can be found in the literature about residual soils present in the region of study, namely that migmatite residual soils and granite residual soils are clayey soils, this research observed great amounts of silt and sand and low amount of clay (in average, for all samples, 53% of silt, 8% of clay and 32% of sand). This difference among the described information may be the consequence of the variation of the composition that the lithotypes of this complex have and because these residual soils are younger. Granulometric curves had a similar trend among residual soils, while colluvial soils had a greater dispersion in the granulometric distribution, confirming the heterogeneity of the material when transported and the difference of material weathered *in situ*. Colluvium and resid-

ual areas were hard to limit, this being one of the main limitations of the research.

This finding is observed when comparing results from the characterization of those materials, made by means of granulometric analysis, Atterberg Limits and particle density, as well as from parameters of mechanical strength, obtained by means of conventional direct shear test and smooth interface tests, and of CIU triaxial tests, which were analogous.

Concerning parameters of mechanical strength, the residual and colluvial soils found in the studied area (a portion of Serra do Mar) showed average peak and residual friction angle of 32° and 26°, respectively. For cohesive intercept a greater disparity of results was obtained, but also according to literature.

Therefore, the soils found along the studied area, even if different with respect to the geological material defining their genesis, have similar physical characteristics as well as mechanical behavior. Such results, together with other relevant parameters (*e.g.*, slope declivities and layers, groundwater level, rainfall records, suction records and soil retention curve), may be used as input data for future studies, such as in the evaluation of the stability of road slopes, either in individual cases or in regional scale, in nearby areas or having a similar context of geologic material.

Acknowledgments

The authors would like to thank the Federal University of Paraná (UFPR), the support of the Technological Development Resources - RDT, of the Concessionaire Ar-

teris S.A., under the control of the National Agency of Ground Transportation - ANTT, for making possible the accomplishment of this research project.

References

- ABNT (1986). Abertura de Poço e Trincheira de Inspeção em Solo, com Retirada de Amostras Deformadas e Indeformadas - NBR 9604. Associação Brasileira de Normas Técnicas - ABNT, Rio de Janeiro, RJ, Brazil, 9 p.
- Advincula, M.R.E. (2016). Avaliação do Efeito de Aumento de Poropressão nas Características de Resistência de Três Solos Tropicais. Ph.D. Thesis. Pontifícia Universidade Católica do Rio de Janeiro, Rio de Janeiro, 278 p.
- Angulo, R.J. (2004). Mapa do cenozoico do litoral do Estado do Paraná. Boletim Paranaense de Geociências, 55:25-42.
- ALS, Autopista Litoral Sul (2014). Riscos geológico-geotécnicos em taludes rodoviários: Desenvolvimento de uma metodologia de mapeamento e gerenciamento integrado de informações para a BR-376, trecho da Serra do Mar (PR-SC). Recursos para Desenvolvimento Tecnológico - RDT. ANTT.
- ASTM (2017). Standard Practice for Classification of Soils for Engineering Purposes (Unified Soil Classification System) - D2487-17. ASTM International, West Conshohocken, PA, USA, 10 p.
- Bicalho, K.V.; Vivacqua, G.P.D.; Cui, Y.-J.; Froumentin, M.; Mercadier, D. & Tang, A.M. (2015). Experimental investigation of soil-atmosphere interaction in an instrumented embankment constructed with two treated clays. *Soils and Rocks*, 38(2):149-162.
- BSI (1990a). British Standard Methods of test for soils for civil engineering purposes. Part 7. Shear strength tests (total stress) - BS 1377: Part 7. British Standards Institution - BSI, London, UK, 56 p.
- BSI (1990b). British Standard Methods of test for soils for civil engineering purposes. Part 8. Shear strength tests (effective stress) - BS 1377: Part 8. British Standards Institution - BSI, London, UK, 38 p.
- Bressani, L.A.; Bica, A.V.D.; Pinheiro, J.B. & Rigo, M.L. (2001). Residual shear strength of some tropical soils from Rio Grande do Sul. *Solos e Rochas*, 23(2):103-113.
- Carvalho, T.M.O. (2012). Desenvolvimento de um Sistema de Medição de Variação de Volume Total de Amostras Não Saturadas em Ensaio Triaxiais e Avaliação da Influência da Técnica de Saturação no Comportamento Tensão Deformação-Resistência de Solos Residuais. Ph.D. Thesis, Pontifícia Universidade Católica do Rio de Janeiro, Rio de Janeiro, 401 p.
- Casagrande, A. & Fadum, R.E. (1940). Notes on soil testing for engineering purposes. Harvard University, Graduate School of Engineering, 268 p.
- Cerri, R.I.; Reis, F.A.G.V.; Gramani, M.F.; Rosolen, V.; Luvizotto, G.L.; Giordano, L.C. & Gabelini, B.M. (2018). Assessment of landslide occurrences in Serra do Mar mountain range using kinematics analyses. *Environmental Earth Sciences*, 77:325.
- Das, B.M. (2007). Introduction to Geotechnical Engineering. Wadsworth Publishing Co Inc, Belmont, California, 636 p.
- Dell'Avanzi, E.; Kormann, A.C.M. & Nascimento, N.A. (2007). Readequação do projeto OSPAR km 72. Relatório Técnico apresentado à TRANSPETRO. Universidade Federal do Paraná, Curitiba.
- EMBRAPA (2006). Sistema Brasileiro de Classificação de Solos. EMBRAPA - Empresa Brasileira de Pesquisa Agropecuária, Brasília, DF, Brazil, 306 p.
- Fatehnia, M.; Tawfiq, K. & Abichou, T. (2014). Comparison of the methods of hydraulic conductivity estimation from mini disk infiltrometer. *Electronic Journal of Geotechnical Engineering*, 19:1047-1063.
- Furlan, A.; Bonotto, D.M. & Gumiere, D.J. (2011). Development of environmental and natural vulnerability maps for Brazilian coastal at São Sebastião in São Paulo State. *Environmental Earth Sciences*, 64:659-669.
- Gibson, R.E. & Henkel, D.J. (1954). Influence of duration of test at constant rate of strain on measured "drained" strength. *Geotechnique*, 4:6-15.
- González, A.A.M. (2017). Simulação Geológico-Geotécnica para Avaliação de Estabilidade de Taludes a Partir de Técnicas de Geoprocessamento. Ph.D. Thesis, Universidade Federal do Paraná, Curitiba, 243 p.
- González, A.A.M.; Passini, L.B. & Kormann, A.C.M. (2017). Rainfall effects on pore pressure changes in a coastal slope of the Serra do Mar in Santa Catarina. *Soils & Rocks*, 40(3):263-278.
- Head, K.H. (1981). Manual of Soil Testing. Volume 2: Permeability, Shear Strength and Compressibility Test. 1st ed. ELE International Limited, London, 747 p.
- Kanji, M.A. (1998). Determinação de FI residual de Solos Argilosos por Ensaio de Cisalhamento Direto de Interface Lisa. In: Proc. XI Congresso Brasileiro de Mecânica dos Solos e Engenharia Geotécnica, COBRAMSEG, Brasília, p. 713-719.
- Lacerda, W.A. & Sandroni, S. (1985). Movimentos de massa coluviais. Mesa Redonda sobre aspectos geotécnicos de encostas. Clube de Engenharia, Rio de Janeiro, p. 1-19.
- Lambe, T.W. & Withman, R.V. (1969). Soil Mechanics. John Wiley & Son, New York, 553 p.
- Listo, F.L.R. & Vieira, B.C. (2015). Influência de parâmetros geotécnicos e hidrológicos na previsão de áreas instáveis a escorregamentos translacionais rasos utilizando o modelo TRIGRS. *Revista Brasileira de Geomorfologia*, 16(3):485-500.

- Massad, F. (2010). *Obras de Terra: Curso Básico de Geotecnica*. 2ª ed. Editora Oficina de Textos, São Paulo, 216 p.
- Mendes, R.M.; Orlando, P.G. & Marinho, F.A.M. (2006). Propriedades geotécnicas de solos residuais não saturados da Serra do Mar. In: Proc. XIII Congresso Brasileiro de Mecânica dos Solos e Engenharia Geotécnica, XIII COBRAMSEG, Curitiba, v. 1, pp. 355-360.
- Mendes, R.M.; Marinho, F.A.M. & Valério Filho, M. (2015). Capacidade de retenção de água em solos da Serra do Mar, SP. *Revista do Instituto Geológico*, 36(1):21-34.
- Mezzomo, S.M. & Bertuol F. (2013). Rodovia BR-376/PR - Banco de dados dos parâmetros de resistência ao cisalhamento obtidos através de retroanálise. In: Proc. VI Conferência Brasileira de Estabilidade de Encostas, COBRAE, Angra dos Reis, p. 30-35.
- MINEROPAR, Minerais do Paraná S/A. (2002). Relatório do Mapeamento das Cartas de Geologia do Paraná na área de abrangência do Programa Pró-Atlântica. In: SEMA. CARTAS GEOLOGIA (Sul). Curitiba, CD-ROM.
- MINEROPAR, Minerais do Paraná S/A. (2005). Mapa Geológico, Folha de Curitiba. MINEROPAR, Paraná. Escala: 1:250.000 colorido.
- Oliveira, N.S.; Rotunno, O.C.; Marton, E. & Silva, C. (2016). Correlation between rainfall and landslides in ova Friburgo, Rio de Janeiro - Brazil: A case study. *Environmental Earth Sciences*, 75:1358.
- Ortigão, J. A. R & Sayão, A.S.F.J. (2004). *Handbook of slope stabilization*. Springer.478 p.
- Picanço, J.; Mesquita, M.J. & Melo, L.L. (2019). Geotechnical and mineralogical properties of granite regolith related to nucleation mechanisms of debris flows in tropical areas. *International Journal of Erosion Control Engineering*, 11(3):54-62
- Pinto, C.S. (2006). *Curso Básico de Mecânica dos Solos com Exercícios Resolvidos*. 3ª ed. Oficina de Textos, São Paulo, 368 p.
- Rigo, M.L.; Pinheiro, R.J.B.; Bressani, L.A.; Bica, A.V.D.B. & Silveira, R.M. (2006). The residual shear strength of tropical soils. *Canadian Geotechnical Journal*, 43(4):431-447.
- Sestrem, L.P.; Kormann, A.C.M.; Pretto, J.H.F. & Marinho, F.A.M. (2015). Precipitation influence on the distribution of pore pressure and suction on a coastal hillside. *Soils & Rocks*, 38(1):81-92.
- Siga Jr., O.; Basei, M.A.; Neto, J.M.; Machiavelli, A. & Harara, O.M.O. (1995). O complexo Atuba: um cinturão Paleoproterozóico intensamente retrabalhado no Neoproterozóico. *Boletim. Instituto de Geociências, Série Científica*, 26:69-98.
- Skempton, A.W. (1964) Long term stability of clay slopes. *Geotechnique*, 14:77-107.
- Soares, P.V.; Pereira, S.Y.; Simoes, S.J.C.; Bernardes, G.P.; Barbosa, S.A. & Trannin, I.C. (2012). The definition of potencial infiltration areas in Guaratinguetá watershed, Paraíba do Sul basin, Southeastern Brazil: an integrated approach using physical and land-use elements. *Environ Earth Sci*. 67:1685-1694.
- Suzuki, S. (2004) Propriedades Geomecânicas de Alguns Solos Residuais e Coluviais ao Longo do Oleoduto Curitiba-Paranaguá. Dissertação de Mestrado, Universidade Federal do Rio de Janeiro, Rio de Janeiro, 329 p.
- Tchalenko, J.S. (1970). Similarities between shear zones of different magnitudes. *Geological Society of America Bulletin*, 81:1625-1640.
- Terzaghi, K. & Peck, R.B. (1967). *Mecânica de Suelos en la Ingeniería Práctica*. 2nd ed., Editorial “ El Ateneo” S.A., Buenos Aires, 750 p.
- Tonus, B.P.A. (2009). Estabilidade de Taludes: Avaliação dos Métodos de Equilíbrio Limite Aplicados a uma Encosta Coluvionar e Residual da Serra do Mar Paranaense. M.Sc. Dissertation, Universidade Federal do Paraná, Curitiba, 147 p.
- Trivazolli, M.N.B. (2018). Proposta de Modelo para Avaliação de Risco de Deslizamentos Baseado em Cenários de Eventos Pluviométricos: Aplicação em um Talude da Serra do Mar no Trecho PR/SP. M.Sc. Dissertation, Universidade Federal do Paraná, Curitiba, 197 p.
- Victorino, M.M. (2015). Influência das Chuvas nas Propressões e Estabilidade dos Taludes Rodoviários de um Trecho da BR 376 na Serra do Mar Paranaense. M.Sc. Dissertation, Universidade Federal do Paraná, Curitiba, 124 p.
- Vieira, B.C.; Fernandes, N.F.; Filho, O.A.; Martins, T.D. & Montgomery, D.R. (2018). Assessing shallow landslide hazards using TRIGRS and SHALSTAB models, Serra do Mar, Brazil. *Environmental Earth Sciences*, 77:260.
- Vilanova, M.R.N. (2015). Long-term rainfall trends in Serra da Mantiqueira Environmental Protection Area, southeast Brazil. *Environmental Earth Sciences*, 73:4779-4790.

Investigating the Differences between Various Deterministic Liquefaction Correlation Methods

E. El Kahi, M. Khouri

Abstract. In order to manage the risks associated with an earthquake, a particular attention should be given to reduce and resist the effects caused by the earthquake such as soil liquefaction. Several evaluation procedures have evolved over the last four decades, since the use of the simplified method suggested by Seed & Idriss in 1971. However, these procedures present various differences among them. The target of this article is to investigate the differences between the three deterministic liquefaction correlations presented by Seed *et al.* and those that were published more recently by Cetin *et al.* and Idriss & Boulanger. A case study of a petroleum site located in the south of Saudi Arabia is utilized for this comparison. This site is representative of the sites located in that area. Based on SPT (Standard Penetration Test) measurements, results reveal the impact of these differences on cyclic resistance and cyclic stress ratios (CRR and CSR) and on the safety factor (FS). In addition, results reveal a comparison between the considered methods in terms of economical, conservative and moderate for the considered case. Also, a step by step procedure is suggested for engineers and designers to follow when evaluating the liquefaction potential of a certain site.

Keywords: cyclic resistance and stress ratios, deterministic evaluation, soil liquefaction potential, SPT measurements.

1. Introduction

Following many earthquakes that have occurred through history, the studies carried out have always sought to identify the phenomena induced by these earthquakes which cause the amplification of the damage (Luo *et al.*, 2018; Morgenstern, 2018). One of these phenomena, which mainly concerns sandy soils, is liquefaction (Salgado & Prezzi, 2014). Many examples of earthquakes can be given where liquefaction was a major cause of both damage and loss of life.

Liquefaction is defined as the transformation of a granular material from a solid to a liquefied state as a consequence of increased pore-water pressure and reduced effective stress (Souza *et al.*, 2012). In fact, when a large earthquake occurs, seismic waves travel from the source to the ground surface, and can result in major damage affecting soils, structures and people (Pytlík & Van Baars, 2016). Liquefaction depends on soils characteristics, their composition and various indicators that distinguish these soils from each other. Researchers have tried to quantify seismic soil liquefaction initiation risk through the use of both deterministic and probabilistic techniques based on laboratory test results and/or correlations of in situ “index” tests with field case history performance data (Kiyota *et al.*, 2016; Wang & Li, 2015; De Vallejo, 2012).

In 1971, a simplified procedure was developed by Seed & Idriss based on empirical evaluation of field observations and laboratory test data. This procedure for assessing earthquake cyclic liquefaction potential of soils has two

essential components: first, the development of a framework for analyzing historical experiences; second, the development of a suitable in situ index to represent the liquefaction resistance characteristics.

Many correlations were published to evaluate liquefaction since the development of Seed & Idriss method; these new methods give more accurate results, like the correlations developed by Seed *et al.* in 1985, which was adopted with slight modification by Youd *et al.* (2001), Cetin *et al.* (2004, 2012, 2016) and Idriss & Boulanger (2004, 2008, 2012).

However, as shown in Fig. 1, there are significant differences between the methods of Seed *et al.*, Cetin *et al.* and Idriss & Boulanger. The Cetin *et al.* correlations of the cyclic resistance ratio, adjusted for a magnitude $M = 7.5$ and a vertical effective stress $\sigma'_v = 1$ atm, are significantly lower than Seed *et al.* and Idriss & Boulanger correlations.

This paper focuses on the evaluation of the differences between the three main deterministic liquefaction correlations suggested by Seed *et al.* (1985) (modified by Youd *et al.* (2001)), Cetin *et al.* (2004, 2012, 2016) and Idriss & Boulanger (2004, 2008, 2012) through a case study of a “petroleum” site located in the south of Saudi Arabia. Also, a step by step procedure is suggested to evaluate the liquefaction potential.

Elio El Kahi, M.Sc., Ph.D. Student, Ecole des Mines de Nancy, GeoRessources Laboratory, Université de Lorraine, Nancy, France, e-mail: elio.el-kahi@univ-lorraine.fr.
Michel Khouri, Ph.D., Associate Professor, Faculté de Génie, Branche II, Université Libanaise, Roumieh, Lebanon, e-mail: mkhuri@ul.edu.lb.
Submitted on November 21, 2018; Final Acceptance on May 24, 2019; Discussion open until December 31, 2019.
DOI: 10.28927/SR.422155

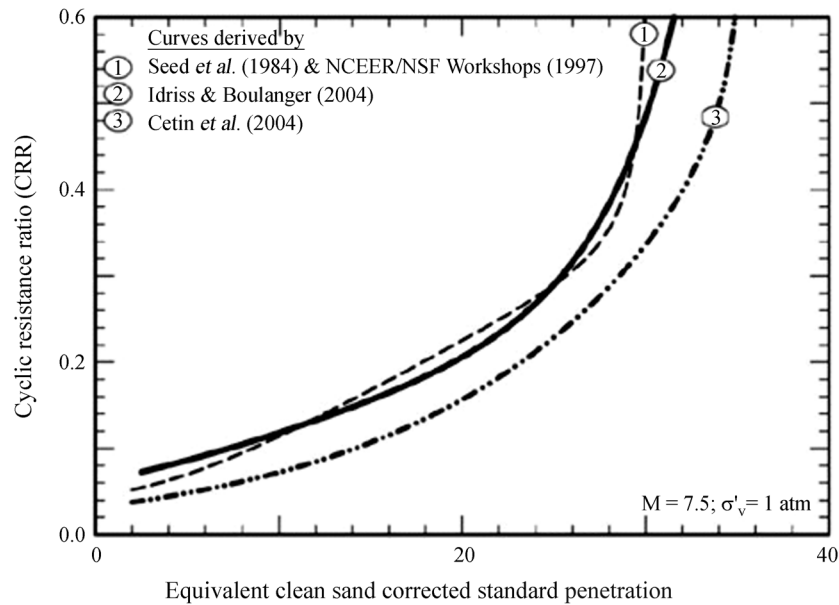


Figure 1 - Liquefaction correlations for $M = 7.5$ and $\sigma'_v = 1$ atm developed by Seed *et al.* (1985) compared with Cetin *et al.* (2004) and Idriss & Boulanger (2004) correlations.

2. Liquefaction Evaluation Methods

2.1. Determination of the cyclic stress ratio (CSR)

To determine the soil liquefaction potential, the cyclic stress ratio (CSR) has to be determined. Seed & Idriss, in 1971, defined the CSR as the average cyclic shear stress τ_{av} developed on the horizontal surface of soil layers due to vertically propagating shear waves, normalized by the initial vertical effective stress σ'_{v0} to incorporate the increase in shear strength due to increase in effective stress. By appropriately weighting the individual stress cycles based on laboratory test data, Seed & Idriss found that a reasonable amplitude to use, for the “average” or equivalent uniform stress, τ_{av} , is about 65% of the maximum shear stress. Consequently, their work resulted in a simplified evaluation procedure where the evaluation of the cyclic stress ratio (CSR) is presented in Eq. 1:

$$CSR = \frac{\tau_{av}}{\sigma'_{v0}} = 0.65 \frac{a_{max}}{g} \frac{\sigma_{v0}}{\sigma'_{v0}} r_d \quad (1)$$

where a_{max} represents the peak horizontal acceleration at the ground surface generated by the earthquake, g is the acceleration of gravity, σ_{v0} is the total vertical overburden stress and r_d is the stress reduction coefficient.

The stress reduction coefficient r_d is defined as the ratio of cyclic stresses for a flexible soil column to the cyclic stresses for a rigid soil column. It is influenced by the soil stiffness and flexibility. According to Fig. 2, Seed & Idriss assumed that its determination depends upon the depth below the ground surface. Based on the average values of Seed & Idriss (1971) that were adopted by Seed *et al.*

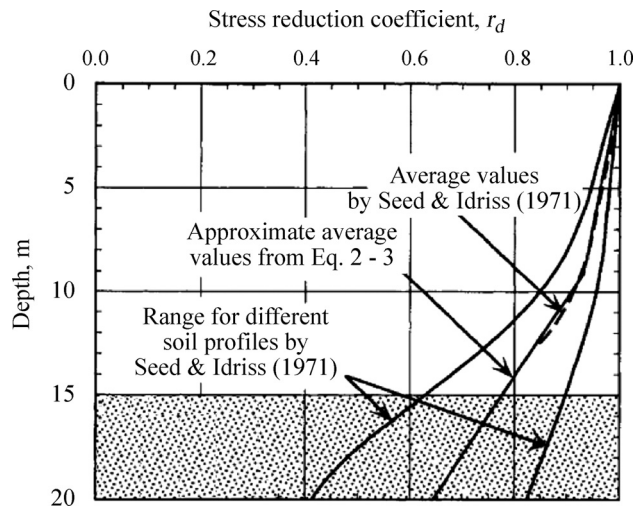


Figure 2 - Stress reduction coefficient r_d vs. depth curves developed by Seed & Idriss (1971) with added mean-value lines plotted from Eqs. 2 and 3.

(1985), Eqs. 2 and 3 were proposed to determine the value of r_d , where z is the depth in meters. However, due to the variability of the soil properties, in particular its flexibility (ElKahi *et al.*, 2018), the r_d value is variable. It can vary in a certain range around the mean value obtained by the application of Eqs. 2 and 3.

However, Cetin *et al.* (2012) used a probabilistic relationship to determine the r_d factor (Eqs. 4 and 5) that is divided into two parts (for $z < 20$ m and for $z \geq 20$ m), where $\sigma_{e_{r_d}}$ (Eqs. 6 and 7) is the standard deviation which is assumed to be zero in the deterministic approach, and $V_{s,12}^*$ is the site shear wave velocity for the top 12 m. Cetin *et al.*

(2012) assumed that the correct way to estimate $V_{s,12}^*$ is to calculate apparent travel time through each sub-layer down to a depth of 12 m, and then divide the total travel time by the distance travelled. If H_i is the height of a soil layer and $V_{s,i}$ is the shear wave velocity of the layer then $V_{s,12}^*$ is given in Eq. 8. If the site stiffness is difficult to estimate properly, $V_{s,12}^*$ can be taken between 150-200 m/s, limiting the wave velocity between 120 m/s and 250 m/s for soft and stiff sites respectively.

On the other hand, Idriss & Boulanger (2012) suggested that the use of Eq. 9 would provide a sufficient

degree of accuracy for engineering applications and recommended that these equations (Eqs. 9, 10 and 11) be used in lieu of the figure originally published by Seed & Idriss (1971) shown in Fig. 2, or any of the equations that have been derived over the past 30 years based on this figure.

Seed *et al.*:

$$r_d = 1.0 - 0.00765z \quad \text{for } z \leq 9.15 \text{ m} \quad (2)$$

$$r_d = 1.174 - 0.0267z \quad \text{for } 9.15 \text{ m} < z \leq 23 \text{ m} \quad (3)$$

Cetin *et al.*:

$$r_d = \left[\frac{1 + \frac{-23.013 - 2.949a_{\max} + 0.999M + 0.0525V_{s,12}^*}{16.258 + 0.201e^{0.341(-z + 0.0785V_{s,12}^* + 7.586)}}}{1 + \frac{-23.013 - 2.949a_{\max} + 0.999M + 0.0525V_{s,12}^*}{16.258 + 0.201e^{0.341(0.0785V_{s,12}^* + 7.586)}}} \right] \pm \sigma_{e_{r_d}} \quad \text{for } z < 20 \text{ m} \quad (4)$$

$$r_d = \left[\frac{1 + \frac{-23.013 - 2.949a_{\max} + 0.999M + 0.0525V_{s,12}^*}{16.258 + 0.201e^{0.341(-20 + 0.0785V_{s,12}^* + 7.586)}}}{1 + \frac{-23.013 - 2.949a_{\max} + 0.999M + 0.0525V_{s,12}^*}{16.258 + 0.201e^{0.341(0.0785V_{s,12}^* + 7.586)}}} \right] - 0.0046(z - 20) \pm \sigma_{e_{r_d}} \quad \text{for } z \geq 20 \text{ m} \quad (5)$$

$$\sigma_{e_{r_d}} = z^{0.85} \cdot 0.0198 \quad \text{for } z < 12 \text{ m} \quad (6)$$

$$\sigma_{e_{r_d}} = 12^{0.85} \cdot 0.0198 \quad \text{for } z \geq 12 \text{ m} \quad (7)$$

$$V_{s,12}^* = \frac{12}{\sum_{i=1}^n \frac{H_i}{V_{s,i}}} \quad (n \text{ is the number of soil layers}) \quad (8)$$

Idriss & Boulanger

$$\ln(r_d) = \alpha(z) + \beta(z)M \quad \text{for } z \leq 34 \text{ m} \quad (9)$$

$$\alpha(z) = -1.012 - 1.126 \sin\left(\frac{z}{11.73} + 5.133\right) \quad (10)$$

$$\beta(z) = 0.106 + 0.118 \sin\left(\frac{z}{11.28} + 5.142\right) \quad (11)$$

Consequently, Fig. 3 recapitulates the cyclic stress ratio (CSR) procedure for the three methods, where the reduction coefficient r_d calculation constitutes the main difference between them. As shown in this figure, to evaluate the cyclic stress ratio (CSR), three steps are required: (a) a_{\max} , σ'_{v0} and σ'_{v0} evaluation; (b) the reduction coefficient r_d evaluation and (c) CSR evaluation. The reduction coefficient r_d is the only parameter that differs between the three methods where every method presents its own equation to determine r_d . This coefficient depends upon the depth; it is directly proportional to the CSR evaluation (Eq. 1). A simple mathematical application of Eqs. 2-9 shows that r_d decreases with the increase in depth. Consequently, the assessment of the cyclic stress ratio (CSR) is usually determined for reasonable depths below the ground surface (Youd *et al.*, 2001).

2.2. Determination of the soil liquefaction resistance

The resistance to the liquefaction phenomenon is revealed through the cyclic resistance ratio (CRR) (Seed & Idriss, 1971). It represents the maximum cyclic stress ratio CSR at which a given soil can resist liquefaction. It is usually determined through several field tests including the standard penetration test (SPT), the cone penetration test (CPT), shear-wave velocity measurements (V_s), and the Becker penetration test (BPT) (Youd *et al.*, 2001).

This study focuses on the estimation of the CRR based on SPT results. In fact, SPT is generally preferred because of its wide use and its precision in the detection of the variability of soil deposits (Kayen *et al.*, 1992). In addition, for the last decades, the conditions for the evaluation of

Steps for evaluating the

cyclic stress ratio (CSR):

1 - a_{\max} , σ'_{v0} & σ'_{v0} evaluation

Geotechnical report, Field test (SPT) results

2 - Reduction coefficient r_d evaluation

Seed <i>et al.</i>	Cetin <i>et al.</i>	Idriss & Boulanger
Equations (2) and (3)	Equations (4) and (5)	Equation (9)

3 - CSR estimation

Equation (1)

Figure 3 - Diagram representing the cyclic stress ratio (CSR) evaluation procedure for the three methods.

liquefaction resistance based on SPT results have been reliable (Youd *et al.*, 2001). To manifest these conditions, Seed *et al.* (1985) have plotted the CSR curves *vs.* the SPT blow counts $(N_1)_{60}$, as shown in Fig. 4. These counts are normalized to a pressure of 100 kPa and a 60% hammer energy efficiency.

The curve plotted in Fig. 4 is approximated by Eq. 12, where $(N_1)_{60}$ is considered the same as the clean sand value $(N_1)_{60cs}$ for fines content $FC < 5\%$.

Equation 12 is valid for $(N_1)_{60} < 30$. For $(N_1)_{60} \geq 30$, clean granular soils are too dense to liquefy and are classed as non-liquefiable. For Cetin *et al.* (2004), Eq. 13 calculates CRR for a given probability of liquefaction. In this equation, the correction for fines content is built into the equa-

tions for P_L and CRR where P_L is the probability of liquefaction in decimals, FC is expressed as an integer range $5 \leq FC \leq 35$, Φ is the standard cumulative normal distribution, and $\Phi^{-1}(P_L)$ is the inverse of the standard cumulative normal distribution. The deterministic analysis is done for a probability of liquefaction of 50% and a factor of safety of 1.

Elsewhere, the equivalent clean sand value $(N_1)_{60cs}$ is used by Idriss & Boulanger (2004) to estimate the CRR as per Eqs. 15 and 16.

Seed *et al.*:

$$CRR = \frac{1}{34 - (N_1)_{60}} + \frac{(N_1)_{60}}{135} + \frac{50}{[10 \cdot (N_1)_{60} + 45]^2} - \frac{1}{200} \quad (12)$$

Cetin *et al.*:

$$CRR = \exp \left(\frac{(N_1)_{60} (1 + 0.004 FC) - 29.53 \ln(M) - 3.70 \ln \frac{\sigma'_v}{P_a} + 0.05 FC + 16.85 + 2.70 \Phi^{-1}(P_L)}{13.32} \right) \quad (13)$$

$$P_L = \Phi \left(\frac{(N_1)_{60} (1 + 0.004 FC) - 13.32 \ln(CSR_{eq}) - 29.53 \ln(M) - 3.70 \frac{\sigma'_v}{P_a} + 0.05 FC + 16.85}{2.70} \right) \quad (14)$$

Idriss & Boulanger:

$$CRR = \exp \left(\frac{(N_1)_{60cs}}{14.1} + \left(\frac{(N_1)_{60cs}}{126} \right)^2 - \left(\frac{(N_1)_{60cs}}{23.6} \right)^3 + \left(\frac{(N_1)_{60cs}}{25.4} \right)^4 - 2.8 \right) \quad \text{for } (N_1)_{60cs} < 37.5 \quad (15)$$

$$(N_1)_{60cs} < 37.5 \quad (16)$$

$$CRR = 2 \quad \text{for } (N_1)_{60cs} > 37.5$$

The N values obtained from the SPT are corrected for the following correlation factors: overburden C_N , rod length C_R , non-standard sampler C_S , borehole diameter C_B , and hammer energy efficiency C_E , resulting in a $(N_1)_{60}$ value:

$$N_{60} = N C_E C_B C_R C_S \quad (17)$$

$$(N_1)_{60} = N_{60} C_N \quad (18)$$

The equations used to calculate the correction factors (C_E , C_B , C_R and C_S) are summarized in Table 1 (Cetin *et al.*, 2004).

Most of the corrections to the SPT N value are somewhat minor however, the corrections for the use of different hammer systems have a large impact. For this reason, it is recommended to measure the transferred energy efficiency of the driller-rig-hammer system and determine a correction factor that is based on a standard energy ratio of 60%. In addition, energy measurements should be done on a periodic basis in order to verify that the rigs are functioning properly under different environmental conditions such as different weather conditions and at different times of day so that operator fatigue can be considered. Also, testing

should be accomplished in several borings in varying soil conditions so that the effect of type of soil on energy measurements can be determined (Cetin *et al.*, 2004).

Table 1 - SPT correction factors (Cetin *et al.*, 2004).

Factor	Equipment variable	Term	Correction
Energy ratio	Donut Hammer	C_E	0.5-1.0
	Safety Hammer		0.7-1.2
	Automatic Hammer		0.8-1.3
Borehole diameter	65 mm-115 mm	C_B	1.0
	150 mm		1.05
	200 mm		1.12
Rod length	< 3 m	C_R	0.75
	3 m-4 m		0.80
	4 m-6 m		0.85
	6 m-10 m		0.95
	10 m-30 m		1.00
Sampling Method	Standard sampler	C_S	1.0
	Sampler without liner		1.0-1.3

2.2.1. C_N factor

The overburden correction factor C_N adjusts N to the N_1 value that would be measured at the same depth if the effective overburden stress was 1 atm. To evaluate this factor, Eq. 19 was adopted by Seed *et al.* (1985) and Cetin *et al.* (2004) correlations, while Idriss & Boulanger (2012) proposed Eq. 20 to determine the C_N factor:

Seed *et al.* and Cetin *et al.*:

$$C_N = \left(\frac{Pa}{\sigma'_{v0}} \right)^{0.5} \tag{19}$$

Idriss & Boulanger:

$$C_N = \left(\frac{Pa}{\sigma'_{v0}} \right)^{0.784 - 0.0768\sqrt{N_{60}}} \tag{20}$$

2.2.2. Fines content

CRR curves plotted in Fig. 4 that separate the liquefaction/non-liquefaction cases, are conservative. These curves depend upon the soil fines content and the grain characteristics which have a significant influence on liquefaction resistance, and the increase of fines content causes an increase of CRR. Consequently, $(N_1)_{60}$ value has to be corrected for fines content FC and adjusted to an equivalent clean sand value $(N_1)_{60CS}$. A number of equations have been proposed to consider the influence of the fines content. Two factors α and β were introduced, as presented in Eq. 21, to consider the impact of the fines content based on Seed *et al.* (1985). However, Cetin *et al.* (2012) used another factor

C_{FINES} as per Eq. 28, while Idriss & Boulanger (2008) introduced $\Delta(N_1)_{60}$ and suggested Eq. 30.

Seed *et al.*:

$$(N_1)_{60CS} = \alpha + \beta(N_1)_{60} \tag{21}$$

$$\alpha = 0 \text{ for } FC \leq 5\% \tag{22}$$

$$\alpha = \exp \left(1.76 - \left(\frac{190}{FC} \right)^2 \right) \text{ for } 5\% < FC < 35\% \tag{23}$$

$$\alpha = 5.0 \text{ for } 35\% \leq FC \tag{24}$$

$$\beta = 1.0 \text{ for } FC \leq 5\% \tag{25}$$

$$\beta = \left(0.99 - \left(\frac{FC^{1.5}}{1000} \right) \right) \text{ for } 5\% < FC < 35\% \tag{26}$$

$$\beta = 1.2 \text{ for } 35\% \leq FC \tag{27}$$

Cetin *et al.*:

$$(N_1)_{60CS} = (N_1)_{60} C_{FINES} \tag{28}$$

$$C_{FINES} = (1 + 0.004FC) + 0.05 \frac{FC}{(N_1)_{60}} \tag{29}$$

for $5\% \leq FC \leq 35\%$

Idriss & Boulanger:

$$(N_1)_{60CS} = (N_1)_{60} + \Delta(N_1)_{60} \tag{30}$$

$$\Delta(N_1)_{60} = \exp \left(1.63 + \frac{9.7}{FC + 0.01} - \left(\frac{15.7}{FC + 0.01} \right)^2 \right) \tag{31}$$

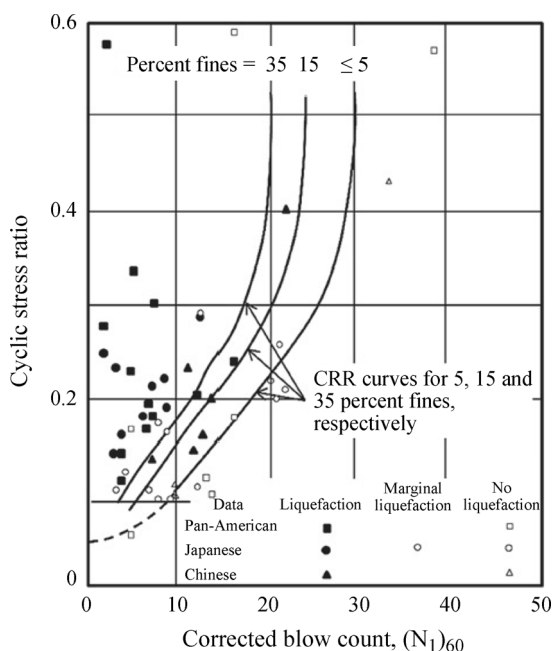


Figure 4 - SPT clean-sand base curve for magnitude 7.5 earthquakes with data from liquefaction case histories (Youd *et al.*, 2001).

Consequently, Fig. 5 recapitulates the soil liquefaction resistance evaluation procedure, where the correction of the SPT blow counts is essential in this evaluation. This correction varies according to the considered method and it is influenced by the overburden correction factor C_N and the consideration of the fines content effect. On one hand, results of several tests indicate considerable scatter of results with no apparent correlation of C_N with soil type or gradation. On the other hand, laboratory tests noted an apparent increase of CRR with increased fines content. Whether this increase is caused by an increase of liquefaction resistance or by a decrease of penetration resistance is not clear. However, approximate corrections for the influence of fines content (FC) on CRR are essential for evaluating the soil liquefaction (Youd *et al.*, 2001). These differences are added to the difference in the estimation of CRR which is different for every method; this will directly affect the evaluation of the factor of safety.

2.3. Determination of the factor of safety

2.3.1. MSF

The curves of liquefaction / non-liquefaction that represent the cases where liquefaction occurred or not (Fig. 4), were taken from field measurements of earthquakes with

Steps for evaluating the Soil liquefaction resistance:

1 - Normalized $(N_1)_{60}$ evaluation
Geotechnical report, Field test (SPT) results & Equation (18)

2 - Overburden correction factor C_N evaluation

Seed <i>et al.</i>	Cetin <i>et al.</i>	Idriss & Boulanger
Equation (19)	Equation (19)	Equation (20)

3 - Clean sand $(N_1)_{60cs}$ (Fines Content FC) evaluation

Seed <i>et al.</i>	Cetin <i>et al.</i>	Idriss & Boulanger
Equation (21)	Equation (28)	Equation (30)

4 - CRR estimation

Seed <i>et al.</i>	Cetin <i>et al.</i>	Idriss & Boulanger
Equation (12)	Equation (13)	Equations (15) and (16)

Figure 5 - Diagram representing the soil liquefaction resistance evaluation procedure for the three methods.

magnitudes that were around 7.5 (Seed & Idriss, 1971). Consequently, the clean-sand base or CRR curves in Fig. 4, are related only to 7.5 magnitude earthquakes. To adjust these curves to magnitudes smaller or larger than 7.5, Seed *et al.* (1985) introduced correction factors termed magnitude scaling factors (MSFs). These factors are used to scale the CRR base curves vs. $(N_1)_{60}$ plots upward or downward.

To illustrate the influence of magnitude scaling factors on calculated hazard, the equation of the factor of safety against liquefaction is written in terms of CRR, CSR, and MSF as follows:

$$FS = \left(\frac{CRR_{7.5}}{CSR} \right) MSF \tag{32}$$

The MSF has been questioned by many researchers; various revisions and reassessments have been proposed. However, Eq. 32 proposed by Idriss provides a fair approximation that gives reasonable risks for any given application. Consequently, Eq. 32 is highly recommended by the geotechnical engineering community.

To evaluate this factor, Seed & Idriss (1971) developed a set of MSF from average numbers of loading cycles for various earthquake magnitudes and laboratory test results. This set was reevaluated and defined in Eq. 33 and adopted by Seed *et al.* (1985); however, Cetin *et al.* (2004) and Idriss & Boulanger (2004) proposed other equations (Eqs. 34 and 35 respectively) to calculate MSF.

Seed *et al.*:

$$MSF = 10^{2.24 / M^{2.56}} \tag{33}$$

Cetin *et al.*:

$$MSF = (7.5 / M)^{2.217} \tag{34}$$

Idriss & Boulanger:

$$MSF = 6.9 \exp(-M / 4) - 0.058 \leq 1.8 \tag{35}$$

2.3.2. Correction factors K_σ and K_α

The simplified procedure was developed and validated only for some particular cases that have a low shear stress, and for depths less than 15 m with lower overburden pressures. Consequently, various correction factors were proposed in order to generalize the simplified procedure. In fact, correction factors K_σ (overburden correction factor) and K_α (ground slope correction factor) were developed by Seed *et al.* (1985) to extrapolate the simplified procedure to deeper soils and to larger overburden pressure and static shear stress.

So, the FS equation is extended to include K_σ and K_α as follows:

$$FS = \left(\frac{CRR_{7.5}}{CSR} \right) MSF \cdot K_\sigma \cdot K_\alpha \tag{36}$$

K_σ depends upon the effective confining pressure. It can be determined from Figs. 6 and 7.

Also, the relative density D_r of soil is used in the calculation of the overburden correction factor K_σ . Seed *et al.* and Cetin *et al.* use Eq. 37 to determine D_r while Idriss & Boulanger (2004) proposed Eq. 38:

Seed *et al.* and Cetin *et al.*:

$$(N_1)_{60} = 41 D_r^2 \tag{37}$$

Idriss & Boulanger:

$$D_r = \sqrt{\frac{(N_1)_{60}}{46}} \tag{38}$$

On the other hand, K_α can be determined from Fig. 8. In fact, the curves shown in Fig. 8 were recommended by

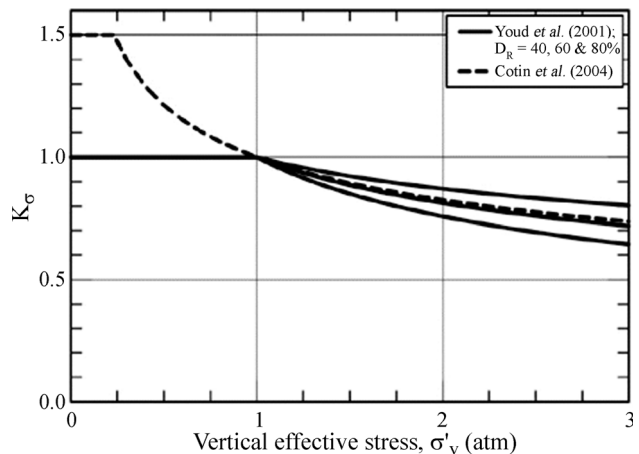


Figure 6 - K_σ values recommended by Youd *et al.* (2001) for $D_r = 40\%$, 60% , and 80% , and used by Cetin *et al.* (2004).

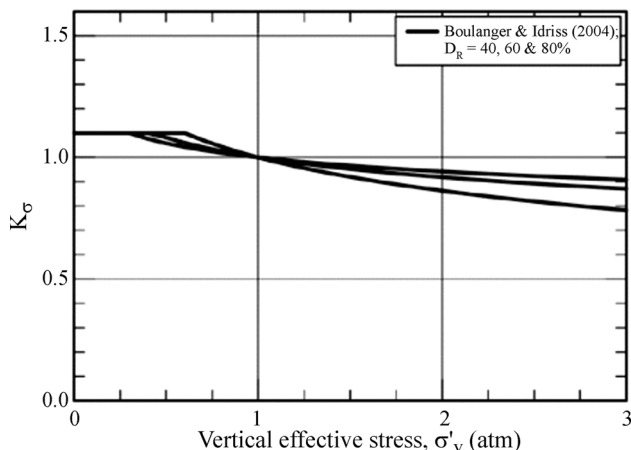


Figure 7 - $K\sigma$ values recommended by Idriss & Boulanger (2008) for $D_R = 40\%$, 60% , and 80% .

Youd *et al.* (2001), and are to be used for research purposes. To generate values for $K\alpha$, Harder & Boulanger (1997) normalized the static shear stress τ_{st} acting on a plane with respect to the effective vertical stress σ'_{v0} yielding the parameter α :

$$\alpha = \left(\frac{\tau_{st}}{\sigma'_{v0}} \right) \tag{39}$$

Consequently, liquefaction is predicted to occur if the factor of safety (FS), defined as the ratio of cyclic resistance ratio over cyclic stress ratio, is less than or equal to 1. However, to consider the effect of various elements on FS, correction factors (MSF, $K\sigma$ and $K\alpha$) are summarized and presented in Fig. 9. Since these factors are usually applied to depths greater than those verified for the simplified procedure, Youd *et al.* (2001) suggests that special expertise is generally required for their application.

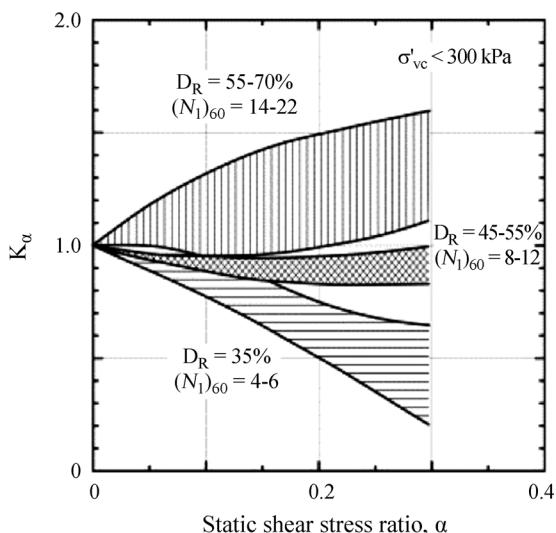


Figure 8 - $K\alpha$ -Values determined by Harder & Boulanger (1997).

3. Step by Step Procedure to Determine the Soil Liquefaction Potential According to the Different Deterministic Methods

The soil liquefaction is determined by applying the following methodology:

- (1) Define the following soil parameters using a geotechnical report:
 - (a) Peak horizontal acceleration at the ground surface (a_{max}).
 - (b) Earthquake magnitude (M).
 - (c) Ground water table (GWT).
 - (d) SPT blow counts results (N).
 - (e) Total and effective vertical overburden stresses (σ_{v0} and σ'_{v0}).
- (2) Evaluate the cyclic stress ratio (CSR):
 - (a) Eqs. 2, 3, 4, 5 and 9 to consider the reduction coefficient (r_d).
 - (b) Eq. 1 to calculate the cyclic stress ratio (CSR).
- (3) Evaluate the soil liquefaction resistance:
 - (a) Eqs. 18, 19 and 20 to correct N -SPT values for the following correlation factors: overburden C_N , rod length C_R , non-standard sampler C_S , borehole diameter C_B , and hammer energy efficiency C_E to give the normalized SPT values $(N_1)_{60}$.
 - (b) Eqs. 21, 28 and 30 to consider the influence of the fines content (FC), giving an equivalent SPT clean sand value $(N_1)_{60cs}$.
 - (c) Eqs. 12, 13, 15 and 16 to calculate the cyclic resistance ratio (CRR).
- (4) Estimate the soil liquefaction safety factor:

For regular depth soils

 - (a) Eqs. 33, 34 and 35 to adjust magnitudes by the magnitude scaling factor (MSF).

Steps for evaluating the

Soil liquefaction safety factor:

1 - Magnitude Scaling Factor (MSF) evaluation

Seed <i>et al.</i>	Cetin <i>et al.</i>	Idriss & Boulanger
Equation (33)	Equation (34)	Equation (35)

2 - Relative Density (DR) & Other Correction Factors $K\sigma$ & $K\alpha$ evaluation

Seed <i>et al.</i>	Cetin <i>et al.</i>	Idriss & Boulanger
Equation (37) Figure 6	Equation (37) Figure 6	Equation (38) Figure 7

3 - Factor of Safety (FS) estimation

Equation (36)

Figure 9 - Diagram representing the factor of safety evaluation procedure for the three methods.

(b) Eq. 32 to calculate the factor of safety (FS).

For deeper soils

(c) For deeper soils and larger overburden pressures, calculate the soil relative density D_r and use Figs. 6, 7 and 8 to determine the overburden and the ground slope correction factors ($K\sigma$ and $K\alpha$).

(d) Eq. 36 to determine the factor of safety (FS).

4. Case Study: Jazan Site in Saudi Arabia

A geotechnical report of a petroleum construction site, Jazan, in Saudi Arabia, was provided by the civil engineering department of the International EPC company, Petrofac.

4.1. Description of the project

As per the geotechnical report, ‘*The project site is located in Jazan. As shown in Fig. 10, it is located in the southwestern part of Saudi Arabia and found between the escarpment of the Asir Mountains in the east and the Red Sea coast in the west. The plain of Jazan is part of the almost 2,000 km long marginal corridor following the Border Mountains of the Arabian Peninsula.*

Many volcanic intrusions, dyke swarms and flows which occurred during the development of the Red Sea rift are characteristic in the Jazan Plain. Several small volcanic cinder cones, which are still in a good state of preservation, confirm that volcanic activity has continued to recent geologic time.

South Tank Farm Area is very close to sea and a total of eighty (80) boreholes were drilled in this area. The project site was mostly covered with silty SAND (SM) to SILT (ML)/ SILTY CLAY (CL-ML)/ CLAY (CL).

The project area on the west coast is classified under seismic zone-2B concerning seismic activities.’

4.2. Calculation tool

To calculate the liquefaction potential for the project site, this study uses the ‘‘GeoLogismiki’’ software LiqIT and then validates the results by an analytical methodology. LiqIT is a software used for the assessment of soil liquefac-

tion based on commonly used field data. The calculation procedure (as shown in Figs. 3, 5 and 9) includes the evaluation of the soil ‘‘strength’’ expressed through CRR, according to the available field data, the estimation of the induced seismic load expressed through CSR, and the calculation of the factor of safety against liquefaction.

It should be noted that the results of the three considered methods were developed according to engineering judgment taking into consideration the uncertainties involved.

4.3. Site characterization

In order to investigate the liquefaction potential, various factors have to be pre-defined. These values are indicated in the geotechnical report.

- (1) Peak Ground Acceleration (PGA) value of 0.10 g is considered for the analysis (PGA in %g = 10 for the considered site in Jazan).
- (2) Earthquake Magnitude of 5.5 is taken from the earthquake magnitude record of the Saudi eastern province.
- (3) Ground Water Table (GWT) is at 7 m depth.
- (4) Results of the SPT field test are stated in Table 2 and soil stresses are presented in Fig. 11.

4.4. Cyclic stress ratio (CSR)

Every method presents its own equation to determine the reduction coefficient r_d . As shown in Fig. 12, Seed *et al.* and Idriss & Boulanger relationships produce relatively low differences compared to Cetin *et al.* which can significantly affect the evaluation of the liquefaction for some particular depths.

Based on Fig. 3, r_d is the only parameter that differs in the evaluation of CSR among the three considered methods. Consequently, the difference shown in Fig. 12 directly affects the CSR evaluation shown in Fig. 13. Seed *et al.* results are higher than Idriss & Boulanger and Cetin *et al.*; the latter method gives the lowest results.

4.5. Soil liquefaction resistance

Various correction factors were applied to the N blows count of the SPT test to evaluate CRR. These factors consider the rod length, the non-standard sampler, the borehole diameter, the hammer energy efficiency, the overburden stress, the fines content, etc. These corrections differ from one procedure to another. A comparison of the various SPT blows corrected values for the three considered methods is shown in Fig. 14.

Results show the impact of the correction factors:

- (1) To pass from N to N_{60} the factors that have to be considered are C_E , C_B , C_R and C_S . These factors have limited variability. However, to pass from N_{60} to $(N_1)_{60}$, the overburden correction factor C_N has to be considered. This factor usually decreases with the increasing values of σ'_v (Eqs. 19 and 20) and becomes lower than 1.



Figure 10 - Project location.

Table 2 - SPT field test results.

Depth (m)	Field N SPT (blows/30 cm)	Unit weight (kN/m ³)	Fines content (%)	σ_v (kPa)	u (kPa)	σ'_v (kPa)	Depth (m)	Field N SPT (blows/30 cm)	Unit weight (kN/m ³)	Fines content (%)	σ_v (kPa)	u (kPa)	σ'_v (kPa)
0.75	7	15.00	77.00	11.25	0.00	11.25	15.00	16	15.00	98.00	225.00	78.48	146.52
1.50	6	15.00	77.00	22.50	0.00	22.50	16.50	19	15.00	98.00	247.50	93.20	154.31
2.25	8	15.00	77.00	33.75	0.00	33.75	18.00	21	15.00	98.00	270.00	107.91	162.09
3.00	7	15.00	77.00	45.00	0.00	45.00	19.50	28	15.00	98.00	292.50	122.63	169.88
3.75	9	15.00	77.00	56.25	0.00	56.25	21.00	32	15.00	98.00	315.00	137.34	177.66
4.50	12	16.00	77.00	72.00	0.00	72.00	22.50	40	16.00	18.00	360.00	152.06	207.95
6.00	11	16.00	77.00	96.00	0.00	96.00	24.00	30	16.00	18.00	384.00	166.77	217.23
7.50	12	16.00	77.00	120.00	4.91	115.10	25.50	27	16.00	18.00	408.00	181.49	226.52
9.00	15	16.00	19.00	144.00	19.62	124.38	27.00	26	16.00	18.00	432.00	196.20	235.80
10.50	15	16.00	19.00	168.00	34.34	133.67	28.50	27	16.00	18.00	456.00	210.92	245.09
12.00	13	15.00	98.00	180.00	49.05	130.95	30.00	29	16.00	18.00	480.00	225.63	254.37
13.50	15	15.00	98.00	202.50	63.77	138.74							

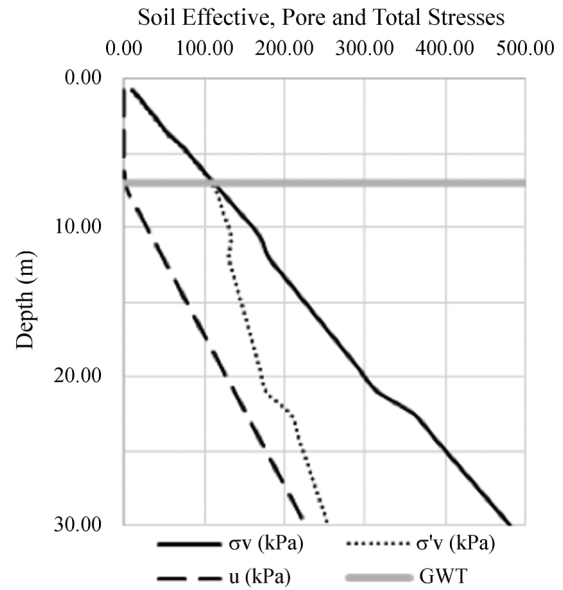


Figure 11 - Soil stresses (σ'_v , σ_v , u) (GWT at 7 m depth).

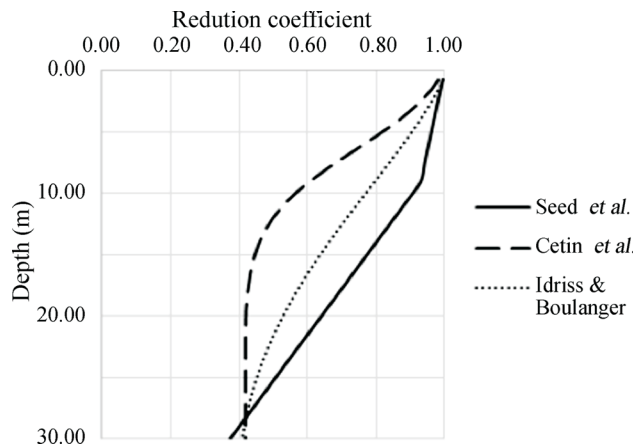


Figure 12 - Comparison of the reduction coefficient graphs for each method.

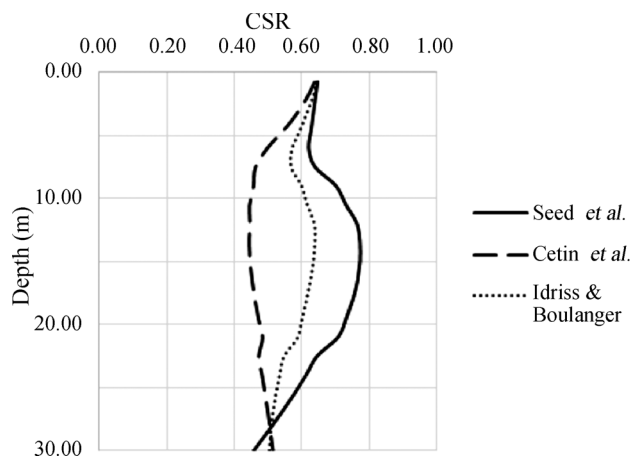


Figure 13 - Comparison of the CSR graphs for each method.

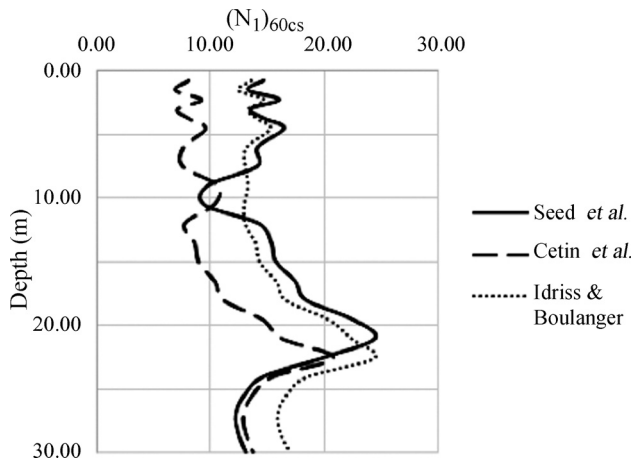


Figure 14 - Comparison of the corrected blow count $(N_1)_{60cs}$ graphs for each method.

This is clearly shown in Fig. 15, where for all cases the curves decrease with the increasing values of σ'_v .

- (2) Since the evaluation of the fines content FC is based on different processes for every method, then by considering this factor, a difference between $(N_1)_{60cs}$ curves is shown in Fig. 14.

On the other hand, CRR for the three methods is calculated according to Eqs. 12, 13, 15 and 16. As shown in Fig. 16, Idriss & Boulanger and Seed *et al.* results are comparable while Cetin *et al.* results are significantly lower for the site considered. This clearly validates the studies developed in the literature and presented in Fig. 1 where Cetin *et al.* method gives lower resistance than the other two methods.

4.6. Factor of safety

After calculating the two fundamental parameters CSR and CRR for the three methods, the calculation of the factor of safety becomes direct, just by comparing these two parameters and considering the MSF ($MSF_{Seed} = 2.21$; $MSF_{Cetin} = 1.99$ and $MSF_{IB} = 1.69$), the $K\sigma$ and $K\alpha$ factors.

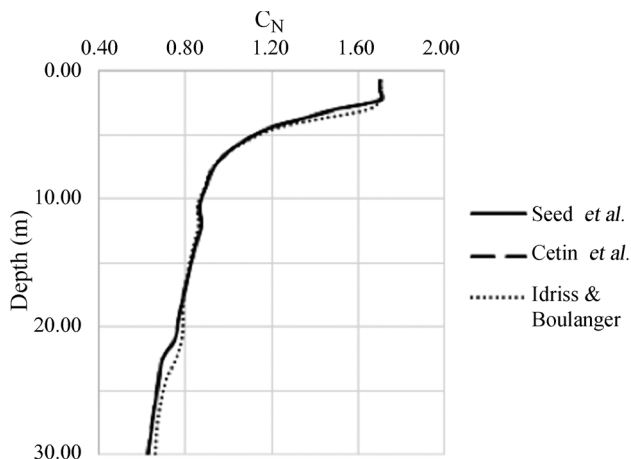


Figure 15 - Comparison of the C_N graphs for each method.

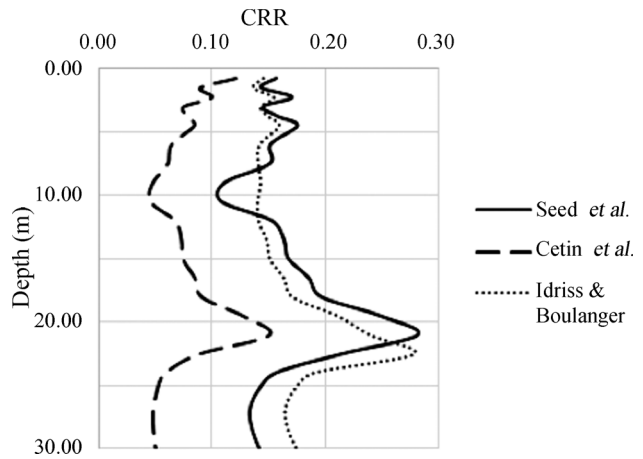


Figure 16 - Comparison of CRR graphs for each method.

For the three methods considered, Fig. 17 shows that an earthquake-induced liquefaction is not expected to occur in the Jazan petroleum site ($FS > 1$). However, the minimum safety factor obtained is around 1.4 which may be considered as unsafe by some designers for some particular cases due to the uncertainty related to the evaluation of the design conditions and related soil parameters that is considerably large.

Results show that Cetin *et al.* method provides the lowest FS values revealing conservative results, while Idriss & Boulanger method provides the highest results, where the FS can surpass 7 at some depths. The difference in the three methods has reached over 100% at some depths under the ground. In fact, this difference is non-linear; it is around 10-15% for $z = 2$ m; it reaches around 75% for $z = 5$ m, particularly between Cetin *et al.* and Seed *et al.*; it is about 30% for the range of 10-20 m depth, however, it may reach more than 300% for high depths ($z = 30$ m).

On the other hand, even if Seed *et al.* method delivers some comparable results with the Idriss & Boulanger method, Seed *et al.* seems to deliver relatively moderate results for this case.

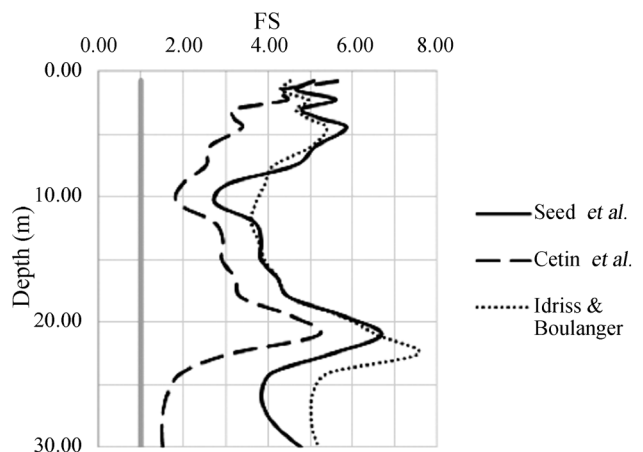


Figure 17 - Comparison of FS graphs for each method.

Finally, the difference between the three methods is significant for high depths ($z > 22$ m). This is caused by the uncertainty related to the application of the simplified procedures for high depths where other problematical considerations have to be investigated.

5. Conclusions

This paper compares three deterministic liquefaction correlations presented by Seed *et al.*, Cetin *et al.* and Idriss & Boulanger. A case study of a site located in the south of Saudi Arabia is considered, the petroleum site of Jazan, which can be considered as representative of the south of Saudi Arabia area. The civil engineering department of the International EPC company, Petrofac, has supported this study by delivering a geotechnical report of the site. This report provides all the necessary information needed to examine the soil liquefaction potential, with all the required parameters for the three methods. Based on SPT results of tests executed on site, the three methods were evaluated and a step by step analytical method is realized with the assistance of LiqIT software.

The calculation of CRR, CSR and FS was developed as per the three methods and the following conclusions can be made:

- (1) For the Jazan case study, the procedure of Cetin *et al.* leads to lower FS compared to Idriss & Boulanger.
- (2) For the considered case, the procedure of Cetin *et al.* can be considered as a conservative procedure and leads to relatively non-economical results of the factor of safety FS.
- (3) In this particular case, the procedure of Idriss & Boulanger gives high values for FS; on one hand, it is an economical solution and on the other it can be considered less safe.
- (4) Between the three procedures, Seed *et al.* is the one that gives relatively moderate results.
- (5) For a depth $z > 22$ m, the difference between the three methods becomes significant. This difference can be linked to the fact that the applications of the simplified procedures are not verified for high depths and require more complex conditions that need to be considered.
- (6) All the procedures show that the liquefaction potential in the Jazan site in the south of Saudi Arabia is relatively minor, and no serious precaution actions for liquefaction need to be taken in the future; in any event, a specialized engineering judgment is always recommended.

In summary, for the petroleum site of Jazan, an earthquake-induced liquefaction is not expected to occur. However, there is a significant difference between the investigated deterministic liquefaction correlations methods for this case study. Even though Seed *et al.* is considered as the moderate method in this case, these results may vary in case a different location is considered due to the uncertainties re-

lated to the design conditions and related soil parameters that affect the overall liquefaction potential assessment.

Acknowledgments

The work presented in this paper was supported by the civil engineering department of the International EPC company, Petrofac, which has supported this study by delivering a geotechnical report of the site.

References

- Cetin, K.O.; Seed, R.B.; Kayen, R.E.; Moss, R.E.S.; Bilge, H.T.; Ilgac M. & Chowdhury, K. (2016). Summary of SPT based field case history data of Cetin (2016) database, Ankara: Soil Mechanics & Foundation Engineering Research Center.
- Cetin, K.O.; Unutmaz, B. & Jeremic, B. (2012). Assessment of seismic soil liquefaction triggering beneath building foundation systems. *Soil Dynamics and Earthquake Engineering*, 43:160-173.
- Cetin, K.O.; Seed, R.B.; Kiureghian, A.D.; Tokimatsu, K.; Harder, L.F.; Kayen, R.E. & Moss, R.E.S. (2004). SPT-based probabilistic and deterministic assessment of seismic soil liquefaction potential. *Journal of Geotechnical and Geoenvironmental Engineering*, 130(12):1314-1340.
- De Vallejo, L.I.G. (2012). Design with geo-hazards: An integrated approach from engineering geological methods. *Soils and Rocks*, 35(1):3-28.
- EIKahi, E.; Khouri, M.; Deck, O.; Rahme, P. & Mehdi-zadeh, R. (2018). Studying the Influence of Uncertainties on the Transmission of Ground Movements Affecting the Soil-Structure Interaction. 10^{èmes} journées Fiabilité des Matériaux et des Structures, Bordeaux.
- Harder, L.F. & Boulanger, R.W. (1997). Application of $K\sigma$ and $K\alpha$ correction factors. Proc., NCEER Workshop on Evaluation of Liquefaction Resistance of Soils, National Center for Earthquake Engineering Research, SUNY, Buffalo, pp. 167-190.
- Idriss, I.M. & Boulanger, R.W. (2012). Examination of SPT-based liquefaction triggering correlations. *Earthquake Spectra*, 28(3):989-1018.
- Idriss, I.M. & Boulanger, R.W. (2008). *Soil Liquefaction During Earthquakes*. Earthquake Engineering Research Institute, Oakland.
- Idriss, I.M. & Boulanger, R.W. (2004). Semi-empirical procedures for evaluating liquefaction potential during earthquakes. *Soil Dynamics and Earthquake Engineering*, 26:115-130.
- Kayen, R.E.; Mitchell, J.K.; Seed, R.B.; Lodge, A.; Nishio, S. & Coutinho, R. (1992). Evaluation of SPT, CPT, and shear wave-based methods for liquefaction potential assessment using Loma Prieta data. Technical Report NCEER. US National Center for Earthquake Engineering Research (NCEER).

- Kiyota, T.; Ikeda, T.; Yokoyama, Y. & Kyokawa, H. (2016). Effect of in-situ sample quality on undrained cyclic strength and liquefaction assessment. *Soils and Foundations*, 56(4):691-703.
- Luo, Y.; Ampuero, J.P.; Miyakoshi, K. & Irikura, K. (2018). Surface Rupture Effects on earthquake moment-area scaling relations. *Pure and Applied Geophysics*, 174(9):3331-3342.
- Morgenstern, N.R. (2018). Geotechnical risk, regulation, and public policy. *Soils and Rocks*, 41(2):107-129.
- Pytlik, R. & Van Baars, S. (2016). Shear strength and stiffness degradation of geomaterials in cyclic loading. *Soils and Rocks*, 39(3):273-283.
- Salgado, R. & Prezzi, M. (2014). Penetration rate effects on cone resistance: insights from calibration chamber and field testing. *Soils and Rocks*, 37(3):233-242.
- Seed, H.B. & Idriss, I.M. (1971). Simplified procedure for evaluating soil liquefaction potential. *Journal of the Soil Mechanics and Foundations Division*, 97(9):1249-1273.
- Seed, H.B.; Tokimatsu, K.; Harder, L.F. & Chung, R.M. (1985). The influence of SPT procedures in soil liquefaction resistance evaluations. *Journal of Geotechnical Engineering*, 111(12):1425-1445.
- Souza, J.M.S.; Danziger, B.R. & Danziger, F.A.B. (2012). The influence of the relative density of sands in SPT and CPT correlations. *Soils and Rocks*, 35(1):99-113.
- Wang, W.M. & Li, X.F. (2015). Correlation analysis of liquefaction characteristic parameters with liquefaction based on real testing data. *Advanced Materials Research*, 1065:292-295.
- Youd, T.L.; Idriss, I.M.; Andrus, R.D.; Arango, I.; Castro, G.; Christian, J.T.; Dobry, R.; Finn, W.D.L.; Harder, L.F.; Hynes M.E.; Ishihara K.; Koester, J.P.; Liao, S.S.C. & Marcuson, W.F. (2001). Liquefaction resistance of soils: summary report from the 1996 NCEER and 1998 NCEER/NSF Workshops on Evaluation of Liquefaction Resistance of Soils. *Journal of Geotechnical and Geoenvironmental Engineering*, 127(10):1061-1090.

Soil Classification System from Cone Penetration Test Data Applying Distance-Based Machine Learning Algorithms

L.O. Carvalho, D.B. Ribeiro

Abstract. Most work from the literature dedicated to soil classification systems from cone penetration test (CPT) data are based on simple two-dimensional charts. One alternative approach is using machine learning (ML) to produce new soil classification systems or to reproduce existing ones. The available studies within this research field can be considered limited, once most of them do not include more than two inputs within their analysis and are applicable only to specific regions. In this context, the aim of this work is to use distance-based ML techniques to replicate two chart-based methods from the literature. Up to five input feature combinations are tested, with the objective of discussing geotechnical aspects of soil classification systems. Results are compared using the statistical test of Friedman with the post-hoc statistics of Nemenyi and the signed-rank statistical test of Wilcoxon. The used dataset can be considered diversified because it contains 111 CPT soundings from several countries. Results show that the used ML techniques maintain reasonable accuracy when inputs are substituted and when incomplete data is used, which can lead to cost reduction in real engineering projects. It is important to notice that these observations would not be possible by using the replicated soil classification systems alone.

Keywords: cone penetration test, distance-based algorithms, machine learning, soil classification system.

1. Introduction

Most available systems for soil classification from CPT data use two-dimensional charts divided into regions which represent different soil types. Initially, these charts were based on soil type (grain size and plasticity) and used raw CPT data, like cone resistance and lateral friction (Begemann, 1965). Nonetheless, later studies produced better classification methods by focusing on soil behavior and by proposing normalizations for CPT data (Douglas, 1981; Robertson *et al.*, 1986). Some popular classification methods make use of two charts instead of one, combining three normalized variables in pairs. In this context, some work propose normalizations to include the influence of depth and overburden (Robertson, 1990). Nevertheless, these methods are not accurate for offshore soils (Jefferies & Davies, 1991) due to the dilative behavior of highly overconsolidated clays commonly found in deep water soils (Robertson, 1991). This limitation is supported by experimental data (Jefferies & Davies, 1991; Ramsey, 2002). Thus, these methods fail to distinguish stiff or dense granular soils from overconsolidated clay (Schneider *et al.*, 2008). Different normalizations and charts were proposed to address this problem (Schneider *et al.*, 2008; Schneider *et al.*, 2012). Nonetheless, Robertson (2016) affirms that soil classification systems that use charts may not be reliable for structured soils, meaning aged or cemented, like some offshore soils. He also recommends to consider soils

structured if a modified normalized small-strain rigidity index K_G^* is above 330, although some geotechnical judgment is required.

Another possible approach for soil classification systems from CPT data is based on the use of statistics and ML techniques. Most authors interested in solving general geotechnical problems use artificial neural networks (ANN) to predict values of interest such as soil parameters (Goh, 1995; Goh, 1996; Schaap *et al.*, 1998; Juang & Chen, 1999; Kumar *et al.*, 2000; Juang *et al.*, 2002; Juang *et al.*, 2003; Hanna *et al.*, 2007). Nevertheless, one can find work using support vector machines (SVM) (Goh & Goh, 2007), decision trees (DT) (Livingston *et al.*, 2008) and random forests (RF) (Kohestani *et al.*, 2015). For soil classification systems there are two main approaches, one is replicating existing soil classification systems and the other is trying to propose new ones. Most work in this research field are dedicated to the latter approach, using data clustering (Hegazy & Mayne, 2002; Facciorusso & Uzielli, 2004; Liao & Mayne, 2007; Das & Basudhar, 2009; Rogiers *et al.*, 2017). Usually, among the few work that investigate replicating existing soil classification systems such as Robertson charts (Arel, 2012), the only ML technique tested is ANN (Kurup & Griffin, 2006; Reale *et al.*, 2018). Nonetheless, there is a study that compares different ML techniques when replicating existing systems for soil classification (Bhattacharya & Solomatine, 2006), although the used

Lucas Orbolato Carvalho, M.Sc., Departamento de Geotecnia, Divisão de Engenharia Civil, Instituto Tecnológico de Aeronáutica, São José dos Campos, SP, Brazil, e-mail: lucasorbol.carvalho@gmail.com.

Dimas Betioli Ribeiro, Associate Professor, Departamento de Geotecnia, Divisão de Engenharia Civil, Instituto Tecnológico de Aeronáutica, São José dos Campos, SP, Brazil, e-mail: dimas@ita.br.

Submitted on March 12, 2018; Final Acceptance on July 8, 2019; Discussion open until December 31, 2019.

DOI: 10.28927/SR.422167

dataset is restricted to few CPT soundings which are all taken from the same location. Other work related to classifying soil with ML are Bilski & Rabarjioely (2009), Rao *et al.* (2016) and Chandan & Thakur (2018).

In this work, two chart-based soil classification systems proposed by Robertson (1991) and Robertson (2016) are replicated using distance-based ML techniques. These techniques were elected among other options for their simplicity and because there is a lack in the literature for this type of approach. The objective is to investigate and discuss geotechnical aspects of soil classification systems that can not be disclosed by using the original Robertson methods. First, the stratigraphic profiles of 111 CPT soundings taken within several countries are obtained using a student version of CPeT-IT v2.0.2.5 software (Ioannides & Robertson, 2016), which employs Robertson charts in a soil classification system. Next, the so-called k-nearest neighbor (KNN) and distance-weighted nearest-neighbor (DWNN) ML techniques are used to replicate Robertson (1991) and Robertson (2016) charts. For each ML technique and each classification method, 33 input feature combinations are tested and all results are compared using the Friedman statistical test (Friedman, 1937) with the Nemenyi post-hoc statistics (Nemenyi, 1963) and the Wilcoxon statistical test (Wilcoxon, 1945). The proposed discussions produced several original contributions, like showing that:

1. Distance-based ML techniques are capable of reproducing Robertson soil classification systems with good accuracy;
2. Reasonable accuracy can be obtained without normalizations proposed in the literature for the CPT data;
3. Including soil age as an input feature contributes for distinguishing between soil classes.

2. Soil Classification Systems

In this work, two soil classification systems available within a student version of CPeT-IT software are replicated using distance-based ML techniques. The objective of this section is to present the theory that sustains each of these methods.

2.1. Influenced by soil type (IST)

The first replicated method is based on the work of Robertson (1991). Although it was idealized to be oriented towards a behavioral classification, the labels assigned to classes are inspired by conventional soil type classes, showing even some compatibility with real soil types (Kurup & Griffin, 2006). For this reason, this method is here considered influenced by soil type, being referred to as IST throughout this text. It adopts nine possible soils types, within which two are said to be heavily overconsolidated or cemented. The IST classes are in Table 1.

The initial inputs used by CPeT-IT to classify soil with the IST method are raw CPT data, named cone resistance q_c (MPa), lateral friction f_s (kPa), pore pressure mea-

sured behind the cone tip u_2 (kPa) and depth z (m). These values are used to obtain the input features originally considered by Robertson (1990), named normalized cone resistance Q_{t1} (Eq. 1), normalized friction ratio F_r (Eq. 2) and normalized excess pore pressure B_q (Eq. 3). The cone resistance normalization was later updated to Q_m (Schneider *et al.*, 2008), resulting in the charts presented in Figs. 1a and 1b. Beside the nine classes predicted within these charts, an additional class 0 is used for misclassified soils.

To obtain the normalized values, first the raw cone resistance q_c is replaced by the total cone resistance q_t , to compute the pore pressure assisting cone penetration. Next step is estimating the soil unit weight γ (kN/m³) (Lunne *et al.*, 2002; Mayne *et al.*, 2010; Mayne, 2014), which is used to obtain the total overburden pressure σ_{v0} (kPa) and the effective overburden pressure σ'_{v0} (kPa). If the water table is not known, it can be estimated by fitting a straight line in the chart $z \times u_2$ (Fig. 2) when a drained penetration is observed. The water table depth is then used to compute the equilibrium pore pressure u_0 , which is used to determine the excess pore pressure $u_2 - u_0$.

Given these estimations, the following normalizations are obtained:

$$Q_{t1} = \frac{q_t - \sigma_{v0}}{\sigma'_{v0}} \quad (1)$$

$$F_r = \frac{f_s}{q_t - \sigma_{v0}} \quad (2)$$

$$B_q = \frac{u_2 - u_0}{q_t - \sigma_{v0}} \quad (3)$$

Nevertheless, work from the literature state that the exponent n of σ'_{v0} ($n = 1$ in Eq. 1) should vary from 0.5 for sands to 1 for clays (Zhang *et al.*, 2002). To calculate n , one can consider its correlation with the classification index I_c (Robertson, 2009):

$$I_c = [(3.47 - \log Q_{tq})^2 + (\log F_r + 1.22)2]^{0.5} \quad (4)$$

The normalized cone resistance Q_m is then given by:

Table 1 - IST classes.

1) Sensitive, fine grained
2) Organic soils – peats
3) Clays – clay to silty clay
4) Silt mixtures – clayey silt to silty clay
5) Sand mixtures – silty sand to sandy silt
6) Sands – clean sand to silty sand
7) Gravelly sand to sand
8) Very stiff sand to clayey sand
9) Very stiff, fine grained

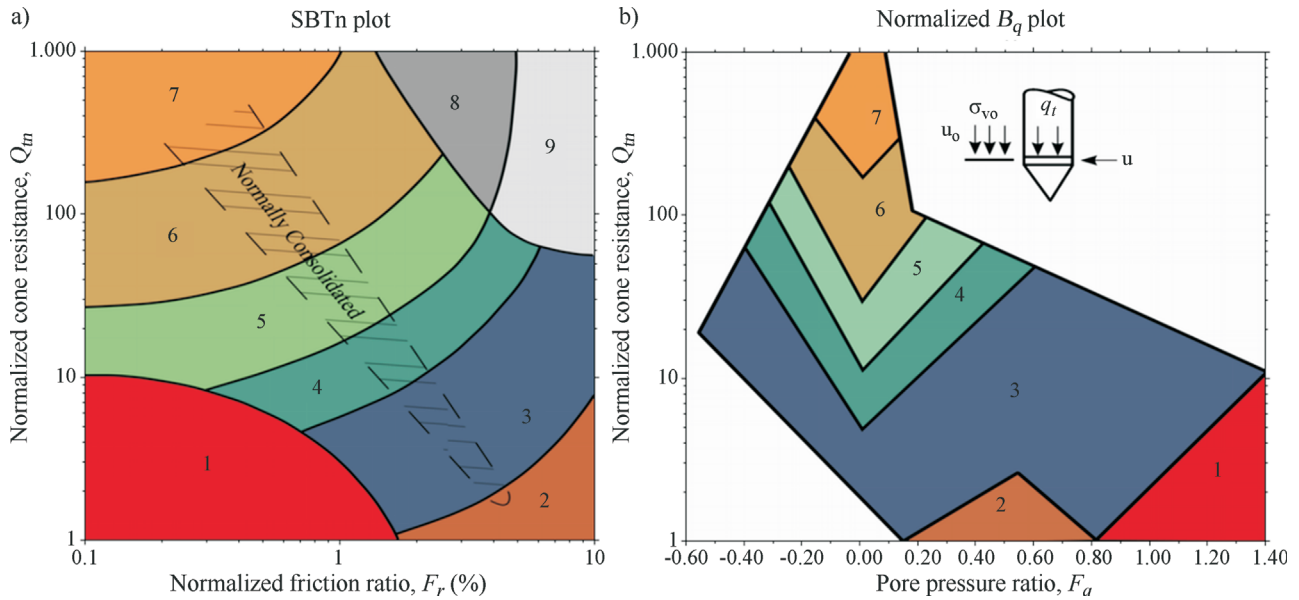


Figure 1 - a) $Q_m \times F_r$ chart from Robertson (1991) updated by Robertson (2009). b) $Q_m \times B_q$ chart from Robertson (1991) updated by Robertson (2009).

$$Q_m = \left(\frac{q_t - \sigma_{v0}}{p_a} \right) \left(\frac{p_a}{\sigma'_{v0}} \right)^n \quad (5)$$

and the exponent n can be written as:

$$n = 0.381I_c + 0.05 \left(\frac{\sigma'_{v0}}{p_a} \right) - 0.15 \quad (6)$$

where $p_a = 0.1$ MPa is a reference pressure.

The CPeT-IT software uses only the $Q_m \times F_r$ chart to generate the soil classification system outputs. Soil is considered misclassified and is labeled with class 0 if the values obtained for Q_m and F_r are not within the ranges presented in this chart.

2.2. Focused on soil behavior only (FSB)

The system proposed by Robertson (2016) establishes a full behavioral-oriented soil classification, which is why it is here considered more focused on soil behavior and named FSB throughout this text. FSB method includes seven classes (Table 2).

One can observe that the three main soil types are sand-like, clay-like and transitional. Each of these soil types is divided into contractive or dilative. A seventh class

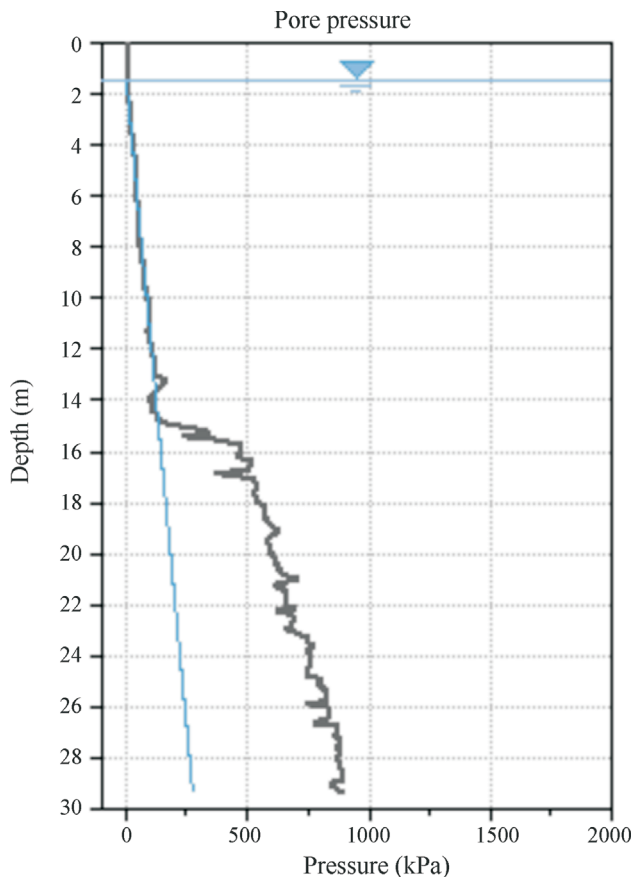


Figure 2 - Excess pore pressure.

Table 2 - FSB classes.

- | |
|---|
| 1) CCS: Clay-like – Contractive – Sensitive |
| 2) CC: Clay-like – Contractive |
| 3) CD: Clay-like – Dilative |
| 4) TC: Transitional – Contractive |
| 5) TD: Transitional – Dilative |
| 6) SC: Sand-like – Contractive |
| 7) SD: Sand-like – Dilative |

is reserved for contractive clays that have high sensitivity to disturbance, which can be related to the friction ratio using the expression $S_f = 7.1/F_r$ (Robertson, 2009). If sensitivity is greater than 3, which corresponds to $F_r < 2\%$, then the clay is considered sensitive. The upper limit for the normalized cone resistance for sensitive clays is defined as 10 because they are soft.

Likewise for the IST system, q_c, f_s, u_2 and z are the initial inputs used by CPeT-IT to classify soil with the FSB system. Nonetheless, in this case the soil classification system is based on the charts shown in Figs. 3 and 4, which use the normalized cone resistance Q_m , the normalized friction ratio F_r and the normalized excess pore pressure U_2 (Schneider *et al.*, 2008) as inputs. The FSB method also includes a class 0 for misclassified soil, which is identified if Q_m, F_r or U_2 are not within the ranges presented in the charts and if the class given by both charts is not the same.

The excess pore pressure normalization U_2 is obtained as:

$$U_2 = \frac{u_2 - u_0}{\sigma'_{v0}} \quad (7)$$

The curves that separate soil classes are inspired by Schneider *et al.* (2008) and Schneider *et al.* (2012). The $Q_m \times F_r$ chart has closely circular curves in the IST method, while in Robertson (2016) the curves have hyperbolic shapes as suggested by Schneider *et al.* (2012). The $Q_m \times U_2$

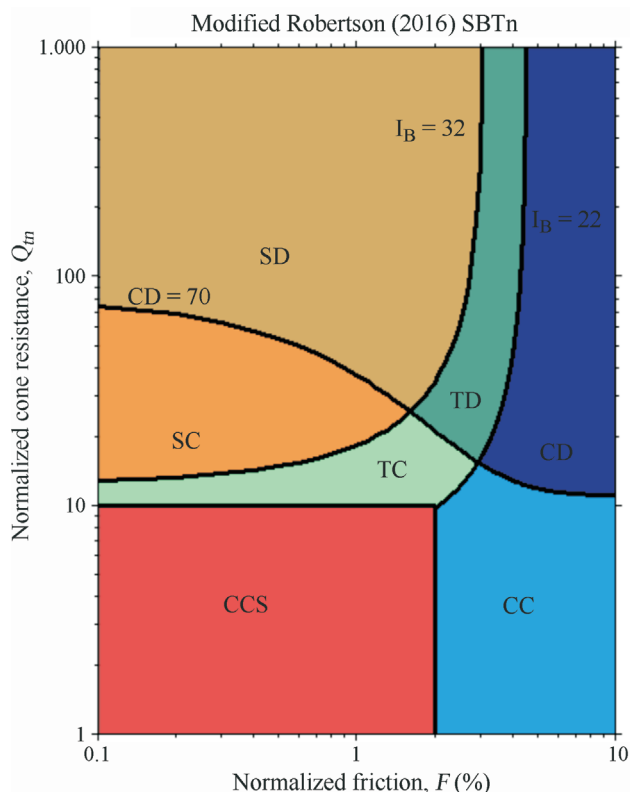


Figure 3 - $Q_m \times F_r$ chart from Robertson (2016).

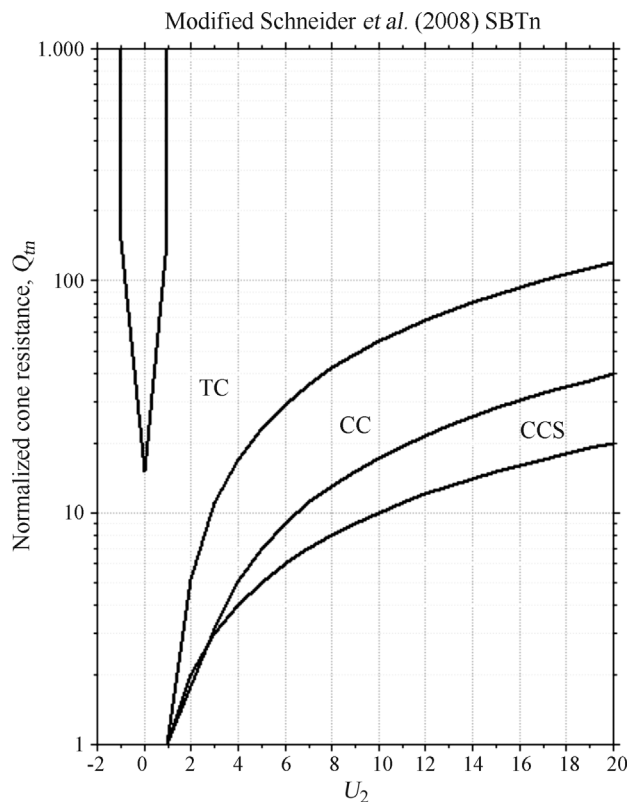


Figure 4 - $Q_m \times U_2$ chart from Robertson (2016).

chart was taken from Schneider *et al.* (2008) with minor changes, containing the classes originally proposed there.

3. Distance-Based Techniques

In this work, distance-based ML techniques are used to replicate the soil classification systems described in Section 2. These ML techniques have the advantage of using an approach similar to the chart-based methods to be replicated, representing soil examples as points in a space composed by the input features. It also uses the hypothesis that, if two soil examples produce close points, they are similar. One way of measuring the distance between points is with the Euclidean metric. Considering a pair (x_i, x_j) of objects in a d -dimensional feature space, the distance between them is given by:

$$dist(x_i, x_j) = \sqrt[p]{\sum_{l=1}^d |x_i^l - x_j^l|^p} \quad (8)$$

The distance-based ML algorithms used in this work predict the class of an unknown example using a dataset of examples whose classes are known. The simplest strategy is detecting which known example produces a point that is the nearest neighbour of the point that represents the unknown example. It is then assigned to the unknown example the same class of its nearest neighbor (Cover & Hart, 1967).

It is also possible to use an arbitrary number k of nearest neighbors and decide the class of the unknown example by voting, which corresponds to the k -nearest neighbors (KNN) technique. Tests can be performed to calibrate which k leads to best predictive performance. In this work, only odd values of k are tested starting from one, increasing k until decreasing predictive performance is observed.

It is also possible to weight the votes, so that closer neighbors are more valued than farther ones. In this case, the technique is named distance-weighted nearest neighbor (DWNN) (Dudani, 1976). One specific way for defining these weights is by using Gaussian weighting, which is defined by the following expression (Hechenbichler & Schliep, 2004):

$$w(dist) = \frac{1}{\sqrt{2\pi}} e^{-\frac{1}{2}dist^2} \quad (9)$$

where $dist$ is the distance value. In this work, the KNN and the DWNN with Gaussian weighting are used and compared to replicate the soil classification systems presented in Section 2.

4. Methodology

4.1. Datasets description

The ML programs used in this work require a dataset of known examples to predict new examples. This dataset can be formatted as a table, where each line represents a different soil example. Input features are represented as columns and the last column contains the output feature. Table 3 presents a sample with 10 soil examples (lines), within a 0.45 m soil layer. In this sample, the inputs are raw CPT data and the output is the corresponding IST soil class, obtained using the CPeT-IT software. This program is also used to produce other input-output combinations for the ML techniques, as described with more detail in Section 4.3.

Thirty eight of all CPT soundings used to compose the datasets were sent directly by Professor P.K. Robertson.

Table 3 - Sample of soil examples.

z (m)	Inputs			Output
	q_c (MPa)	f_s (kPa)	u_2 (kPa)	IST Class
13.00	16.93	55.84	120.32	6
13.05	16.53	46.32	124.47	6
13.10	10.14	36.69	129.95	6
13.15	7.13	24.76	146.66	6
13.20	4.92	22.80	158.69	6
13.25	3.90	21.47	163.42	5
13.30	3.28	21.46	159.58	5
13.35	2.73	23.89	153.03	5
13.40	3.70	33.80	148.37	5

They are the same ones used in Robertson (2016) to produce the FSB method, which is described in Section 2.2. Once detailed information about these soundings can be found in the original reference, only a brief description about them is presented in Table 4.

The first column of Table 4 gives a general description of the soil types within the CPT soundings. The second identifies where soundings were taken and the third gives the geological age when the soil was deposited. The last column presents a discrete ordered variable named “class of geology” (CG), considering the most recent age 1 and the other numbered sequentially to the oldest. The information from these 38 soundings plus the variable CG compose the here named geological dataset. The objective of including CG, as an input feature in some of the studies presented in Section 5, is investigating if information about geological age can help differentiate one soil class from the other.

Another 73 CPT soundings were obtained from the website of Professor P.W. Mayne, whose information is summarized in Table 5. Further detail about the soundings can be found on the website. All these soundings were taken within the United States of America and more specific information about location is presented in the table. Information about geological age was not available for these soundings, so they are not included in studies that make use of the variable CG. These soundings grouped with the ones sent by Robertson compose the here named complete dataset, totalizing 111 CPT soundings. All CPT data used in this dataset were taken in intervals of 2 to 5 cm, the pore pressure was measured behind the cone tip (u_2) and the raw cone tip resistance q_c was corrected to q , using CPeT-IT.

4.2. Data preprocessing

In this work, all CPT data were used to classify soil using the CPeT-IT software, which was later replicated using the methods described in Section 3. The accuracy of the final results depends on the quality of the used datasets, which can be improved with data preprocessing.

The first problem is that distance-based ML techniques are sensitive to data scale. When the distance between points is calculated, the importance of input features that vary within large ranges tends to be emphasized, while the ones with low variation tend to be ignored. The solution adopted here is normalizing all input features to the interval [0, 1].

Another issue is that data taken within CPT soundings can contain noise, which is here defined as any variable becoming severely different from what it was supposed to be. Noise can have several causes, like sensor errors, formatting problems and human mistakes. The main noise types are missing data and outliers, which are here defined as distorted or corrupted values. CPeT-IT is unable to classify most noisy examples, assigning class 0 in both IST and FSB methods or no class whatsoever. Once the ML

Table 4 - Geological dataset (Robertson, 2016) (Classification in terms of geology age – GC).

General soil type	Identification	Geological age	CG
Mixed Soils	UBC, Canada	Holocene	2
	Venice Lagoon, Italy	Holocene	2
	Ford Center, USA	Pleistocene	4
	San Francisco, USA	Late Pleistocene	3
	Tailings, USA	Recent	1
	UBC KIDD, Canada	Holocene	2
	UBC KIDD, Canada (2)	Holocene	2
Soft Clay	Bothkennar, RU	Holocene	2
	Burswood, Perth, Australia	Holocene	2
	Onsoy, Norway	Holocene	2
	Amherst, USA	Late Pleistocene	3
	San Francisco Bay, USA	Holocene	2
	San Francisco Bay, USA (2)	Holocene	2
Soft Rock	Newport Beach, USA	Miocene	5
	LA Downtown, USA	Miocene	5
	Newport Beach, USA (2)	Miocene	5
Stiff Clay	Madingley, UK	Cretaceous	6
	Houston, USA	Pleistocene	4

Table 5 - Number of CPTs and test location from P.W. Mayne database (acquired in years 2000 – 2003).

Location	Number of soundings
Gosnell, Arkansas	1
Lenox, Tennessee	1
Memphis, Tennessee	16
Dexter, Missouri	6
Mooring, Tennessee	6
Marked Tree, Arkansas	19
Collierville, Tennessee	1
Meramec, Missouri	4
Opelika, Alabama	4
Wilson, Arkansas	4
Wolf, Wyoming	7
Wyatt, Missouri	4
Total	73

techniques presented in Section 3 are here used to replicate CPeT-IT, these errors tend to be also replicated.

Although it is difficult to completely eliminate noise from the datasets, it is desirable to reduce them as much as possible in order to avoid classification errors. In this work,

dataset cleaning was first performed manually, removing the noisy examples that could be easily identified. This procedure was then complemented by an automatic cleaning procedure that makes use of the box-plots of the input features, as illustrated in Fig. 5.

In the box-plot, the base of the rectangle represents the first quartile Q_1 and the top of the rectangle represents the third quartile Q_3 . The whiskers above and below the rectangle represent the interval $[Q_1 - 1.5 \times IQ, Q_3 + 1.5 \times IQ]$, where $IQ = Q_3 - Q_1$. Values outside this range (white circles) are identified as potential outliers. Preliminary tests have shown that removing all potential outliers affects accuracy, which indicates that relevant information is being eliminated. To solve this problem, the Edit Nearest Neighbor technique (Wilson, 1972) is used in this work as a second criterion to decide if each potential outlier will be, in fact, removed. This technique compares the potential outlier with its nearest neighbor and removes it only if the classes given by CPeT-IT do not match.

This procedure is illustrated in Fig. 6 for two input features, where the white dot represents the potential outlier and the black dots represent other known examples from the dataset. The numbers close to each dot represent the class assigned by CPeT-IT. One can observe that, in this example, the classes of the potential outlier and its nearest

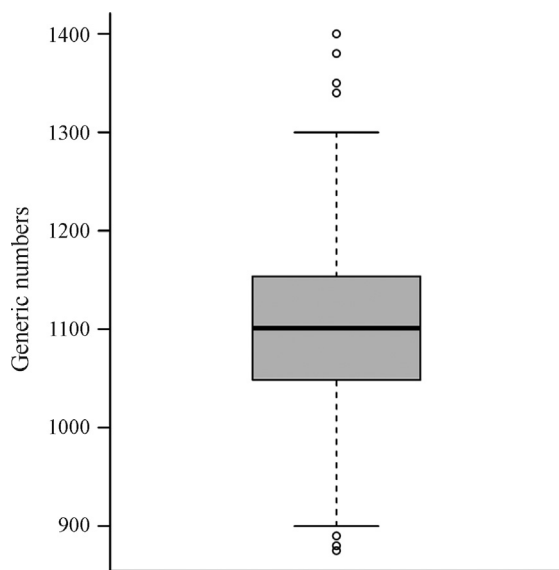


Figure 5 - Box-plot example using generic numbers. The rectangle represents ordinate values within the 1st and 3rd quartiles and the circles represent outliers.

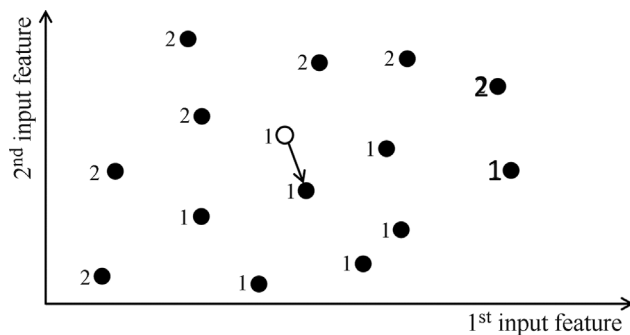


Figure 6 - Edit nearest neighbor technique, with two possible classes (1 and 2) and black dots representing known examples. The unknown example (white) is labeled with the class of its nearest neighbor.

neighbor are the same. This means that this potential outlier will be maintained.

The next issue to be evaluated is if the number of examples within each soil class is balanced, considering both IST and FSB methods. Severe unbalance can compromise the accuracy of distance-based ML techniques because they tend to focus majority classes and ignore minority classes. The distribution of examples among classes can be checked using histograms, as presented in Figs. 7a and 7b for the complete dataset and Figs. 7c and 7d for the geological dataset.

One can observe that the classes are, in fact, imbalanced, which is expected for real CPT soundings. In this work, data imbalance is prevented by eliminating examples of majority classes and creating new artificial examples for minority classes. Preliminary results have shown that ran-

dom elimination does not affect predictive performance, which can be explained by the fact that CPT data contains redundancies due to several data items being taken within each soil layer.

To create new artificial examples for minority classes, the SMOTE (Chawla *et al.*, 2002) technique was used. For better distribution within the input feature space, it is here proposed to estimate each d -dimensional new artificial object from $d + 1$ original examples. This corresponds to the vertex number of a d -dimensional simplex. The maximum between 1000 and two times the number of elements of the minority class was stipulated as the final number of elements of each class for the balanced dataset. Once class 0 of the IST method could not be well represented within the geological dataset even with the use of SMOTE, examples of this class were completely removed from the geological dataset.

4.3. General strategy

Two ML algorithms are tested and compared, the classical KNN and the Gaussian DWNN, with respect to their capacity for replicating the IST and FSB soil classification systems. This comparison is made using several input feature combinations, including three basic sets:

- First set: depth z (m), corrected cone resistance q_i (MPa), lateral friction f_s (kPa) and pore pressure behind the cone tip u_2 (kPa);
- Second set: depth z (m), normalized cone resistance Q_{n1} , normalized lateral friction F_r (%) and normalized pore pressure B_q ;
- Third set: depth z (m), normalized cone resistance Q_{n2} , normalized lateral friction F_r (%) and normalized pore pressure U_2 .

The first set contains only non-normalized parameters, the second contains inputs of the IST method combined with depth and the third contains inputs of the FSB method combined with depth. For the main analysis, all combinations of two, three and four input features within each set were tested, although not all of them are presented in Section 5. Additional selected input feature combinations are tested in three complementary studies.

In order to generate statistically relevant comparisons, a 10-fold cross-validation procedure (Stone, 1974) was applied to evaluate classification accuracy. The procedure starts by randomly separating the dataset into ten partitions or folds with approximately the same size, maintaining the same proportion between classes observed in the complete dataset. At each cross-validation round, one partition is left for testing, one partition (chosen at random) is chosen as a validation set and the remaining partitions compose the training set. The validation set is used to calibrate the best number of neighbors k to be used in the distance-based algorithms.

For each cross-validation round, the average of the accuracies per class are taken. This avoids disregarding mi-

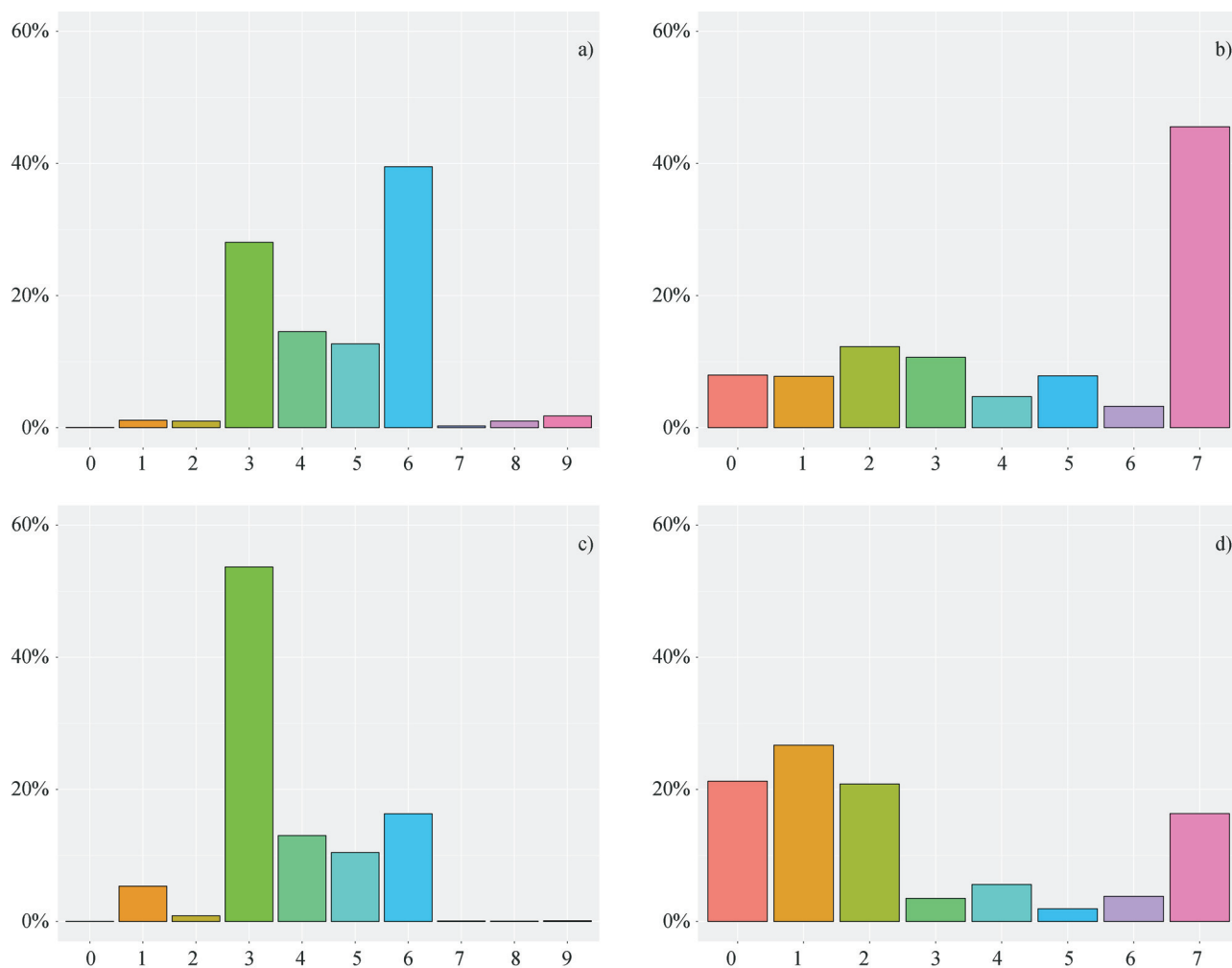


Figure 7 - Histograms. (a) For IST classes and the complete dataset. (b) For FSB classes and the complete dataset. (c) For IST classes and the geological dataset. (d) For FSB classes and the geological dataset.

nority classes in the performance evaluation. After all folds are used for testing, a mean and a standard deviation accuracy performance are computed. For comparing the results of the experiments, the Friedman statistical test (Friedman, 1937) with the Nemenyi post-hoc statistics (Nemenyi, 1963) and the Wilcoxon statistical test (Wilcoxon, 1945) are used, based on the 10 accuracies recorded (per test fold).

5. Results and Discussion

A total of 132 classification results were generated to produce the comparisons presented in this main analysis: 2 replicated classification methods (IST and FSB described in Section 2) \times 33 input feature combinations \times 2 distance-based classification algorithms. The units used for the input features are z (m), q_r (MPa), f_s (kPa), u_2 (kPa), F_r (%) and the other ones are dimensionless. Each predicted soil class is compared to the one originally given by CPeT-IT to compute accuracy. Tables present the mean and stan-

dard deviation accuracy obtained within the 10-fold cross-validation procedure described in Section 4.3.

Combinations that presented best performance with KNN for replicating IST outputs are presented in Table 6. Once the first combination uses the original IST inputs and outputs, it was expected that it would lead to the highest mean accuracy among all. Nonetheless, results of the Friedman statistical test with the Nemenyi post-hoc statistics show a statistical equivalence between the first two combinations in Table 6. Thus, the last two combinations shown in Table 6 can be considered of lower performance. This

Table 6 - Best KNN predictive results for replicating IST.

Inputs	Elected k	Mean	SD
$Q_m F_r$	1	96.52	0.57
$Q_m F_r U_2$	3	94.70	0.96
$Q_m z F_r$	1	93.49	0.67
$Q_m z F_r U_2$	1	92.54	1.12

shows that including more features among the original ones does not contribute to improve performance in this case.

The same comparison is proposed for the combinations that lead to the best performance with the Gaussian DWNN technique for replicating IST outputs, which are presented in Table 7. One can observe that results are very close to those presented in Table 6, reinforcing the same conclusions.

Considering now the classical KNN technique for replicating FSB outputs, the best feature combinations are presented in Table 8. In this case, the Friedman statistical test with the Nemenyi post-hoc statistics show that last two feature combinations are equivalent and statistically better than the first two. One can observe that, as expected, the best combination for this case include all three original FSB inputs, named Q_m , F_r and U_2 . However, associating depth to these features contributed to improve performance, even with the biasing due to the way in which the outputs were generated.

In the end, the feature combinations that produced best performance for the Gaussian DWNN technique for replicating FSB outputs are presented in Table 9. One can observe that the results are very close to the ones from Table 8, reinforcing that using original FSB inputs leads to good accuracy and that including depth among these features contributes to improve performance.

Table 7 - Best DWNN predictive results for replicating IST.

Inputs	Elected k	Mean	SD
$Q_m F_r$	1	96.52	0.57
$Q_m F_r U_2$	1	94.63	0.98
$Q_m z F_r$	1	93.49	0.67
$Q_m z F_r U_2$	1	92.63	1.02

Table 8 - Best KNN predictive results for replicating FSB.

Inputs	Elected k	Mean	SD
$Q_m F_r$	7	88.79	0.40
$Q_m z F_r$	1	91.86	0.28
$Q_m F_r U_2$	3	92.97	0.46
$Q_m z F_r U_2$	1	93.83	0.55

Table 9 - Best DWNN predictive results for replicating FSB.

Inputs	Elected k	Mean	SD
$Q_m F_r$	7	88.90	0.40
$Q_m z F_r$	1	91.86	0.28
$Q_m F_r U_2$	1	93.02	0.38
$Q_m z F_r U_2$	1	93.83	0.55

Concerning more general observations, both tested ML techniques presented good performance for replicating both soil classification systems. With respect to the non-normalized inputs, good performance can be observed when they are associated with depth. For IST and both ML techniques, for example, accuracy is around 70% when only q_t and f_s are used as input features, but rises close to 90% when z is included. These observations suggest that proposing a soil classification system that uses only raw CPT data would be feasible if depth is included. Nevertheless, one should notice that confirming this hypothesis would require further studies.

Another general observation concerns evaluating which classification technique is better, comparing the classical KNN and the Gaussian DWNN. The Wilcoxon test was employed for this task adopting a p-value of at most 5%. Comparing all combinations, results show that the Gaussian DWNN presents better predictive performance than the classical KNN.

6. Conclusions and Recommendations

In this work, distance-based ML techniques are used to replicate systems for soil classification from CPT data. It is important to notice that the proposed discussions and obtained conclusions would not be possible by using the original soil classification systems alone, because these original methods do not allow changing input features. It was the flexibility of the ML techniques that made possible to evaluate if raw inputs without normalizations have enough information for reproducing the original methods accurately, for example.

The main advantages of the proposed approach are the ease of applying it to different datasets and little adaptation required for it to be associated with other ML techniques. The use of distance-based techniques can also be considered advantageous for its simplicity, once accurate results were obtained. Thus, the presented method can be considered rigorous compared to other work from the literature that make use of ML applications in geoscience, which do not present a data analysis as detailed as in Section 4.

A total of 132 tests were performed to draw the discussions and conclusions presented and in all of them the mean accuracy is above 85%, which can be considered reasonable within geotechnical applications. Notice the good results obtained using raw parameters, which suggests that would make sense to dismiss some types of data normalization that are proposed in the literature for soil classification systems. Reducing data normalization is advantageous because any data transformation proposed to the original dataset tend to diminish its original information, specially if the original number of input features is reduced. Results presented here are not sufficient to affirm that using raw parameters would lead to greater performance, nonetheless

they can justify future studies about this issue. Other conclusions to be pointed out are:

- Highest accuracies were obtained when using the original IST inputs and outputs;
- Including depth as an input increased accuracy, in most cases;
- Gaussian DWNN is better than the classical KNN, considering the Wilcoxon test with a p-value of at most 5%.

Future studies that can be conducted include applying and comparing different ML techniques to this same problem, discussing other geotechnical issues about soil classification systems that can not be exposed using distance-based techniques. Another possible investigation is applying clustering techniques to the problem, taking advantage of the ease of increasing dimensionality to test several normalized and non-normalized feature combinations. Thus, CPT data can be associated with data from other in situ experiments like the standard penetration test or the flat dilatometer test, exploring the problem with even higher dimensionality.

Acknowledgments

To Peter K. Robertson and Paul W. Mayne for making available the dataset used in this work. This research did not receive any specific grant from funding agencies in the public, commercial, or not-for-profit sectors.

Computer Code Availability

The codes produced to generate all results presented in this paper can be downloaded from the following link: <https://github.com/Orbolato/KNN.git>.

References

- Arel, E. (2012). Predicting the spatial distribution of soil profile in Adapazari/Turkey by artificial neural networks using CPT data. *Computers and Geosciences*, 43:90-100.
- Begemann, H.K.S. (1965). The friction jacket cone as an aid in determining the soil profile. *Proc. 6th Int. Conf. on Soil Mech. and Found. Engrg., ICSMFE, Montreal*, v.1, pp. 8-15.
- Bhattacharya, B. & Solomatine, D.P. (2006). Machine learning in soil classification. *Neural Networks*, 19(2):186-195.
- Bilski, P. & Rabarijoely, S. (2009). Automated soil categorization using CPT and DMT investigations. *Proc. 2nd Int. Conf. on New Developments in Soil Mechanics and Geotechnical Engineering, Nicosia, North Cyprus*, v. 1, pp. 1-8.
- Chandan, T.R. (2018). Recent trends of machine learning in soil classification: A review. *International Journal of Computational Engineering Research (IJCER)*, 8(9):25-32.
- Chawla, N.V.; Bowyer, K.W.; Hall, L.O. & Kegelmeyer, W.P. (2002). SMOTE: Synthetic minority over-sampling technique. *Journal of Artificial Intelligence Research*, 16:321-357.
- Cover, T.M. & Hart, P.E. (1967). Nearest neighbor pattern classification. *IEEE Transactions on Information Theory*, 13(1):21-27.
- Das, S.K. & Basudhar, P.K. (2009). Utilization of self-organizing map and fuzzy clustering for site characterization using piezocone data. *Computers and Geotechnics*, 36(1-2):241-248.
- Douglas, B.J. (1981). Soil classification using electric cone penetrometer. In *Symp. on Cone Penetration Testing and Experience, Geotech. Engrg. Div., American Society of Civil Engineers, New York, NY*, pp. 209-227.
- Dudani, S.A. (1976). The distance-weighted *k*-nearest-neighbor rule. *IEEE Transactions on Systems, Man, and Cybernetics*, SMC-6(4):325-327.
- Facciorusso, J. & Uzielli, M. (2004). Stratigraphic profiling by cluster analysis and fuzzy soil classification from mechanical cone penetration tests. *Proc. ISC-2 on Geotechnical and Geophysical Site Characterization. Rotterdam*, v. 1, pp. 905-912.
- Friedman, M. (1937). The use of ranks to avoid the assumption of normality implicit in the analysis of variance. *Journal of the American Statistical Association*, 32(200):675-701.
- Goh, A.T. (1995). Modeling soil correlations using neural networks. *Journal of Computing in Civil Engineering*, 9(4):275-278.
- Goh, A.T. (1996). Neural-network modeling of CPT seismic liquefaction data. *Journal of Geotechnical Engineering*, 122(1):70-73.
- Goh, A.T. & Goh, S.H. (2007). Support vector machines: Their use in geotechnical engineering as illustrated using seismic liquefaction data. *Computers and Geotechnics*, 34(5):410-421.
- Hanna, A.M.; Ural, D. & Saygili, G. (2007). Neural network model for liquefaction potential in soil deposits using Turkey and Taiwan earthquake data. *Soil Dynamics and Earthquake Engineering*, 27(6):521-540.
- Hechenbichler, K. & Schliep, K. (2004). Weighted *k*-nearest-neighbor techniques and ordinal classification. *Collaborative Research Center 386, Discussion Paper 399*.
- Hegazy, Y.A. & Mayne, P.W. (2002). Objective site characterization using clustering of piezocone data. *Journal of Geotechnical and Geoenvironmental Engineering*, 128(12):986-996.
- Ioannides, J. & Robertson, P.K. (2016). CPeT-IT v.2.0 – CPT interpretation software. URL: <https://geologismiki.gr/>, accessed on July 26th 2019.
- Jefferies, M.G. & Davies, M.P. (1991). Soil classification by the cone penetration test: Discussion. *Canadian Geotechnical Journal*, 28(1):173-176.
- Juang, C.H. & Chen, C.J. (1999). CPT-based liquefaction evaluation using artificial neural networks. *Computer-*

- Aided Civil and Infrastructure Engineering, 14(3):221-229.
- Juang, C.H.; Yuan, H.; Lee, D.H. & Lin, P.S. (2003). Simplified cone penetration test-based method for evaluating liquefaction resistance of soils. *Journal of Geotechnical and Geoenvironmental Engineering*, 129(1):66-80.
- Kohistani, V.R.; Hassanlourad, M. & Ardakani, A. (2015). Evaluation of liquefaction potential based on CPT data using random forest. *Natural Hazards*, 79(2):1079-1089.
- Kumar, J.K.; Konno, M. & Yasuda, N. (2000). Subsurface soil-geology interpolation using fuzzy neural network. *Journal of Geotechnical and Geoenvironmental Engineering*, 126(7):632-639.
- Kurup, P.U. & Griffin, E.P. (2006). Prediction of soil composition from CPT data using general regression neural network. *Journal of Computing in Civil Engineering*, 20(4):281-289.
- Liao, T. & Mayne, P.W. (2007). Stratigraphic delineation by three-dimensional clustering of piezocone data. *Georisk*, 1(2):102-119.
- Livingston, G.; Piantedosi, M.; Kurup, P. & Sitharam, T.G. (2008). Using decision-tree learning to assess liquefaction potential from CPT and V_s . *Proc. of the 4th Geotechnical Earthquake Engineering and Soil Dynamics Congress*, Sacramento, California, v. 1, pp. 1-10.
- Lunne, T.; Robertson, P.K. & Powell, J.J. (2002). *Cone Penetration Testing in Geotechnical Practice*. Taylor & Francis Group, London and New York.
- Mayne, P.W.; Peuchen, J. & Bouwmeester, D. (2010). Soil Unit Weight Estimated from CPTu in Offshore Soils. Gourvenec & White (eds.) *Front Offshore Geotech*, Taylor & Francis Group, London, pp. 371-376.
- Mayne, P.W. (2014). Interpretation of geotechnical parameters from seismic piezocone tests. *Proc. of 3rd International Symposium on Cone Penetration Testing, CPT14*, Las Vegas, Nevada, v. 1, pp. 1-27.
- Nemenyi, P.B. (1963). *Distribution-Free Multiple Comparisons*. Ph.D. Thesis, Princeton University.
- Ramsey, N. (2002). A calibrated model for the interpretation of cone penetration tests (CPTs) in North Sea quaternary soils. *Proc. of Offshore Site Investigation and Geotechnics Diversity and Sustainability*, Society of Underwater Technology, London, v. 1, pp. 1-16.
- Rao, A.; Janhavi, U.; Abhishek, G.N.; Manjunatha & Beham, R.A. (2016). Machine learning in soil classification and crop Detection. *International Journal for Scientific Research & Development*, 4(1):792-794.
- Reale, C.; Gavin, K.; Libric, L. & Juric-Kacunic, D. (2018). Automatic classification of fine-grained soils using CPT measurements and Artificial Neural Networks. *Advanced Engineering Informatics*, 36:207-215.
- Robertson, P.K.; Campanella, R.G.; Gillespie, D. & Greig, J. (1986). Use of Piezometer Cone Data. Clemence, S.P. (ed.) *Use of In Situ Tests in Geotechnical Engineering*. American Society of Civil Engineers, New York, pp. 1263-1280.
- Robertson, P.K. (1990). Soil classification using the cone penetration test. *Canadian Geotechnical Journal*, 27(1):151-158.
- Robertson, P.K. (1991). Soil classification using the cone penetration test: Reply. *Canadian Geotechnical Journal*, 28(1):176-178.
- Robertson, P.K. (2009). Interpretation of cone penetration tests - a unified approach. *Canadian Geotechnical Journal*, 46(11):1337-1355.
- Robertson, P.K. (2016). Cone penetration test (CPT)-based soil behaviour type (SBT) classification system - an update. *Canadian Geotechnical Journal*, 53(12):1910-1927.
- Rogiers, B.; Mallants, D.; Batelaan, O.; Gedeon, M.; Huysmans, M. & Dassargues, A. (2017). Model-based classification of CPT data and automated lithostratigraphic mapping for high-resolution characterization of a heterogeneous sedimentary aquifer. *Plos One*, 12(5):e0176656.
- Schaap, M.G.; Leij, F.J. & Van Genuchten, M.T. (1998). Neural network analysis for hierarchical prediction of soil hydraulic properties. *Soil Science Society of America Journal*, 62(4):847-855.
- Schneider, J.A.; Randolph, M.F.; Mayne, P.W. & Ramsey, N.R. (2008). Analysis of factors influencing soil classification using normalized piezocone tip resistance and pore pressure parameters. *Journal of geotechnical and geoenvironmental engineering*, 134(11):1569-1586.
- Schneider, J.A.; Hotstream, J.N.; Mayne, P.W. & Randolph, M.F. (2012). Comparing CPTU $Q - F$ and $Q - \Delta u_2/\sigma'_{v0}$ soil classification charts. *Geotechnique Letters*, 2(4):209-215.
- Stone, M. (1974). Cross-validatory choice and assessment of statistical predictions. *Journal of the Royal Statistical Society: Series B (Methodological)*, 36(2):111-133.
- Wilcoxon, F. (1945). Individual comparisons by ranking methods. *Biometrics bulletin*, 1(6):80-83.
- Wilson, D.L. (1972). Asymptotic properties of nearest neighbor rules using edited data. *IEEE Transactions on Systems, Man, and Cybernetics*, SMC-2(3):408-421.
- Zhang, G.; Robertson, P.K. & Brachman, R.W. (2002). Estimating liquefaction-induced ground settlements from CPT for level ground. *Canadian Geotechnical Journal*, 39(5):1168-1180.

List of Symbols

- B_q : normalized excess pore pressure
 CG: class of geology
 d : feature space dimensionality
 $dist$: distance between points
 F_s : normalized friction ratio
 f_s : lateral friction

I_c : classification index
 IQ : interquartile range
 k : number of nearest neighbors
 n : exponent of σ_{v0}'
 p_a : reference pressure
 Q_1 : first quartile
 Q_3 : third quartile
 q_c : cone resistance
 q_t : total cone resistance
 Q_n : normalized cone resistance
 Q_m : updated normalized cone resistance

R_f : friction ratio
 SD : standard deviation
 S_s : sensitivity
 u_0 : equilibrium pore pressure
 u_2 : pore pressure measured behind the cone tip
 U_2 : updated normalized excess pore pressure
 w : Gaussian weighting
 x_i, x_j : points representing objects
 z : depth
 γ : soil unit weight
 σ_{v0} : total overburden pressure
 σ_{v0}' : effective overburden pressure

An Alternative Method to Estimate the Effective Energy During Pile Driving Based on Set and Elastic Rebound Records

A. Querelli, F. Massad

Abstract. Although the dynamic load test technique has been developed for a long time, it became very popular in Brazil over the last 20 years (especially after the publication of Brazilian standard NBR6122, in 2010). However, the site quality control of driven piles in respect to the resistant capacities remains with the practical application of the so-called “dynamic formulas”. Most of the established formulations use a key parameter of the driving event: the driving system efficiency, whose calibration is performed with dynamic monitoring. However, assuming a single value for the efficiency in order to extrapolate it to non-tested piles of the site requires a much more careful analysis of the test than that which has been carried out in practice. The aim of this paper is to discuss the issues involving the efficiency assessment based on the dynamic test and to propose an alternative method of estimating the effective energy during driving through measurements of set and elastic rebound. The method application was verified in comparison with 692 dynamic test records (526 in concrete and 166 in steel piles) of twelve sites spread across seven different locations in Brazil.

Keywords: driven piles, dynamic testing, PDA, effective energy, efficiency, elastic rebound, set.

1. Introduction

In order to control the resistant capacity of driven piles, the Brazilian practice is based on two different approaches: by sampling or the universal one. The sampling approach is limited to a small number of piles. It consists in performing pile load tests, sometimes static, but mostly dynamic. The universal controls are the ones extended to all piles of the site. There are two of them to highlight: the set and the elastic rebound. About them, the Brazilian standard NBR6122 states: “the set and the elastic rebound must be measured in all piles” (ABNT, 2010).

The measure of set (s) refers to the permanent (plastic) displacement of the pile after a single hammer blow (ABNT, 2010). However, even the Brazilian standard itself recognizes that the magnitude of such a measure is extremely small, making it difficult to be precisely read. Aiming to make it easier, the technical community agreed to denominate as “set” the average permanent displacement of ten sequential blows of the hammer (Alves *et al.*, 2004). The set is the main tool that a site engineer has for demanding the end of driving: in Brazilian practice, a certain value of set is specified to ensure the desired resistance after driving.

The elastic rebound (K) is a dynamic measure which indicates the elastic displacements recovered in the blow. Alonso (1991) defines it as “the elastic portion of the maximum displacement of the pile”. It is composed by both the elastic shortening of the pile element itself ($C2$) and the

elastic displacement of the soil under the pile tip ($C3$), also called “toe *quake*”, as displayed by Eq. 1:

$$K = C2 + C3 \quad (1)$$

Both set and rebound can be obtained simultaneously and in a very simple and inexpensive way: a pencil is supported by a stationary reference with its tip pressed against a piece of paper attached to the pile. Then, the pile is hammered (usually ten times), resulting in a graph such as presented in Fig. 1.

In Fig. 1, the record was performed for ten strokes: the measured set (s) is 1.3 mm (average penetration) and the elastic rebound (K) is 20 mm.

The main utility of these two measurements is to estimate the pile resistant load by means of dynamic formulas. Those equations are very familiar to the technical community and still widely used as tools for design and quality control of driven piles. These formulas are intended to obtain the mobilized resistance by means of: a) the elastic rebound (K), b) the set (s) and c) the effective applied energy, considering all sources of loss.

There are several criticisms regarding dynamic formulas. Fellenius (2018), for example, stated: “basing a pile design today on a dynamic formula shows unacceptable ignorance and demonstrates incompetence”. It is a tough, but reasonable assertion: because of the inherent uncertainties and scatter, the dynamic formulas should not be the primary basis of a foundation design. Instead, some authors highlight that they could be used as auxiliary tools in the quality

André Querelli, M.Sc., Civil Engineer, Escola Politécnica, Universidade de São Paulo, São Paulo, SP, Brazil, e-mail: andre.querelli@gmail.com.
Faíçal Massad, Ph.D., Full Professor, Escola Politécnica, Universidade de São Paulo, São Paulo, SP, Brazil, e-mail: faical.massad@usp.br.
Submitted on March 12, 2019; Final Acceptance on June 2, 2019; Discussion open until December 31, 2019.
DOI: 10.28927/SR.422179

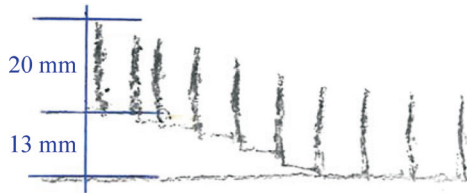


Figure 1 - Examples of set (s) and elastic rebound (K) records (not to scale).

and performance control of driven piles. Alves *et al.* (2004) mention that “the use of these formulas should be restricted to the control of the piling uniformity” and also “as an end-of-driving criterion”. As Chellis (1951) says: that calculated resistance “is only one item of design information that must be considered with other conditions in order to design the pile foundations intelligently, safely and economically”.

2. The Danish Formula

At this point, it is important to highlight the well-known “Danish Formula” in order to support the objective methodology of this paper.

It was proposed by Sorensen & Hansen (1957) based on the Engineering News Formula, published by Arthur Wellington in the 20th issue of the journal (1888) and one of the most widely used dynamic equations in the last century (Likins *et al.*, 2012).

The Danish Formula is written as:

$$R = \frac{\eta \cdot W \cdot h}{s + \frac{1}{2} \sqrt{\frac{2 \cdot \eta \cdot W \cdot h \cdot L}{A \cdot E}}} \quad (2)$$

where R is the pile static resistance, η the hammer efficiency, W the ram weight, h the drop height, s the pile penetration per blow (set), L the pile length, A the area of the pile cross section and E its dynamic modulus of elasticity (as shown in List of symbols).

Caputo (1983) said that the Danish Formula is “generally applied for steel piles”, although its developers Sorensen & Hansen did not make that kind of statement.

Something to emphasize in that formulation is the square root term in the denominator of Eq. 2. Rosa (2000) identified it as the “energy loss due to the elastic deformation of the pile”. Sorensen & Hansen (1957) defined it as the “dynamic compression of a pile with a fixed point”, S_o :

$$S_o = \sqrt{\frac{2 \cdot \eta \cdot W \cdot h \cdot L}{A \cdot E}} \quad (3)$$

In this way, it is possible to observe in Eq. 2 the “tripod” of closely related values of the driving event, which are present (implicitly or explicitly) in almost all dynamic formulas: resistance (R), permanent and elastic displacements (s , S_o) and the effectively transferred energy ($\eta \cdot W \cdot h$).

There are many other equations that are analogous to the Danish Formula, but using the elastic rebound (K) or any other form of total elastic displacement in place of S_o , as done by the Engineering News Formula (1888), the Hiley’s formula (1925) and its variation. One recent and well-known formula that matches this similarity is the complete Energy Approach Equation (Paikowsky & Chernauskas, 1992), which can be written as:

$$R = 2 \cdot K_{sp} \cdot \frac{\eta \cdot W \cdot h}{s + D} \quad (4)$$

where K_{sp} is a coefficient of energy loss by viscous damping effects and D is the maximum pile displacement after blow (sum of $s + K$).

3. Dynamic Load Test and The Brazilian Practice

Concerning the dynamic load test, this paper does not aim to discuss the one dimensional wave propagation theory nor the Case and CAPWAP analysis methods, since all of those subjects are widely explored in the technical literature. Therefore, a brief description of the test will be given, highlighting its use and functionalities.

The dynamic loading test (DLT) is one of the most used field tests for pile driving quality control and pile long term performance evaluation. It is based on the one dimensional wave propagation theory and it is standardized in Brazil by NBR13208 (ABNT, 2007).

Basically, it consists in monitoring a pile with both deformation transducers and accelerometers in response to hammer blows. The mostly used microcomputer to perform that test is called “Pile Driving Analyzer”, PDA (Beim, 2009).

After the blow, measurements of strain and acceleration are recorded by PDA and converted into two curves over time, related to pile top: one of force (F) and another of particle velocity (v) multiplied by pile impedance (Z). The force is calculated through strain (Hooke’s Law) and velocity is calculated by integrating the accelerometer measurements over time. The impedance Z is given by Eq. 5.

$$Z = \frac{E \cdot A}{c} \quad (5)$$

All of these data is readily analyzed by the Case Method and later on by the CAPWAP (Case Pile Wave Analysis Program).

Based on the Case Method analysis, assessments can be made for hammer performance, transferred energy, pile stresses, pile integrity and capacity at the time of testing. These applications have been described by many authors, including Goble *et al.* (1980), Rosa (2000), Alves & Lopes (2004), Vieira (2006), Saldívar (2008), Gonçalves *et al.* (2007), Beim (2009) and many others, which makes it challenging to try to quote them all. Some others, such as Niyama *et al.* (1984), Hussein *et al.* (1993), Rausche *et al.*

(2004), Likins & Rausche (2008), Paraíso & Costa (2010) and Tokhi (2012), for example, additionally emphasized the possibility of evaluating the increase (set-up) or decrease (relaxation) of pile resistant capacity over time.

In Brazil, the current practice of the dynamic load test consists in the procedure proposed by Aoki (1989), which is commonly named as “increasing energy load test”. It is performed after the end of driving and the applied energy during the test is gradually increased (from one blow to another) by varying the hammer drop height. The main objective of it is to obtain the maximum mobilized resistance of the pile. Gonçalves *et al.* (2007) pointed out that collecting data of increasing hammer drop heights allows finding sufficient pile displacements to fully mobilize the pile resistance.

As the test energy increases, some care should be taken with sensitive clays due to the loss of shaft resistance in soil remoulding. To overcome that problem, Valverde & Massad (2018) suggested using the concept of “maximum lateral resistance envelope”, allowing estimating the mobilized resistance along the shaft that was lost in the first blows of the test.

4. Maximum Transferred Energy and Efficiency Calibration

Among the information that results from the dynamic load test (DLT), there is one item to highlight in the present paper: the maximum transferred energy to the pile, designated in PDA as *EMX*. It is calculated through integration of the product of measured force by particle velocity in time, as shown by Eq. 6.

During the DLT, one of *EMX*'s main functions is to confirm to the operator that the effectively applied energy is appropriate to the type of test being performed (constant energy, increasing energy, etc).

$$EMX = \max \left[\int F(t) \cdot v(t) \cdot dt \right] \quad (6)$$

In addition, *EMX* also contributes to estimate the efficiency of the driving system (η), *i.e.*, the ratio between *EMX* and the nominal applied energy (product of hammer weight by drop height), as displayed by Eq. 7.

$$\eta = \frac{EMX}{W \cdot h} \quad (7)$$

The efficiency of the impact has great value, not only for instant evaluation of the driving system at the time of test, but also to support the use of dynamic formulas in the quality control of the non-tested piles of a given site.

Tavenas & Audy (1972) conducted a study on the limitations of the dynamic formulas, comprising 478 records of pile driving in non-cohesive soil and 45 static load tests. One of their conclusions was that the largest source of scatter using dynamic formulas resided in the wrong consideration of the energy (as nominal, *i.e.* ‘ $W \cdot h$ ’), without

correctly accounting for the energy losses (or an efficiency factor). And so, quoting these authors: “The usual energy estimate being proved erroneous, it is possible to conclude [...] that any pile driving formulas in which this estimate will be used will also be erroneous”.

Therefore, one of the major problems when extrapolating dynamic formulas (calibrated by sampling) to all piles of a site is the correct evaluation of the efficiency.

As mentioned by Goble & Likins (1996), the specifications of each dynamic test, *i.e.* the way it will be performed, depends on the purpose for which it is intended. Thus, the authors state: a test to estimate hammer performance requires different procedures compared to a test scheduled for static resistance evaluation.

That raises some criticism to the Brazilian methodology of increasing energy dynamic test in the estimation and adoption of a driving efficiency. The first problem is that just a few strokes are applied in this type of test: typically three to seven blows, which makes the statistical sampling for efficiency evaluation very poor.

In addition, the method requires non sequential blows (different from driving situation): a first blow is applied, then the PDA operator evaluates the calculated information, and only after a period of time, the operator requests another hammer blow to the pile driver. There are no sequential blows, which would take advantage, in terms of efficiency, of the driving “pace” and inertia. It causes some problems both for free fall and hydraulic hammers:

- In free fall hammers, the non-sequential blows require the pile driver operator to use the clutch and the hammer brake in a way that causes some random energy losses, messing with the efficiency evaluation. In a case study of increasing energy test, Rausche (1997) reported efficiency variation between 35% and 52% after a 6 blows test. He concluded that scatter was due to “crane operator effects” and hammer “alignment problems”.
- In hydraulic hammers, isolated blows are not setup automatically. For that situation, the operator needs to quickly regulate the oil pressure (increase and instantly decrease) by a manual switch. That causes the drop height not to be exactly the desired one. This situation occurs even with an experienced operator, resulting in poor efficiency evaluation.

That kind of scatter shows that the Brazilian practice of increasing energy test may be unsuitable for evaluation of the hammer efficiency (η). Thus, if an efficiency value is adopted from increasing energy test in order to extrapolate to all piles of a site, much more (unwanted) inaccuracies could be carried to the resistance estimations of dynamic formulas.

Given all those issues, this paper proposes an alternative to the adoption of a single value for the hammer efficiency. It is based on the estimation of the effectively transferred energy through the set, elastic rebound and some pile geometric and material characteristics.

5. Alternative Method for Estimating the Effective Energy

The methodology is based on some simplifying hypotheses that will be presented later, during its development, but it is anchored in two main points:

1. the idealized curve of resistance vs. displacement due to the hammer blow.
2. the Chellis formula (1951), which derives directly from Hooke's law.

The deduction starts from the equilibrium between the effective energy applied after the impact and the work done by the pile-soil set against penetration (Paikowsky, 2001).

The application of an effective energy (E_{ef}) causes two kinds of displacement: one permanent (s) and other elastic ($K = C2 + C3$). At the apex of both, the maximum static resistance (R) is mobilized by the pile-soil system. After pile rest, the elastic displacement is recovered, remaining only the set. Also, soil resistance returns to zero, resulting in the ideal graph of resistance vs. displacement (linear elastic/perfectly plastic) presented in Fig. 2.

The hatched trapezoidal area in Fig. 2 represents the total work performed by the pile-soil system against penetration. It is equal to the effective energy applied (E_{ef}) and may be calculated as:

$$E_{ef} = \frac{[s + (s + K)] \cdot R}{2} = \frac{(s + D) \cdot R}{2} \tag{8}$$

Taking into account that $E_{ef} = \eta \cdot W \cdot h$, it follows from Eq. 8 that:

$$R = \frac{2 \cdot \eta \cdot W \cdot h}{(s + D)} \tag{9}$$

On the other hand, the Chellis formula (1951) is written as:

$$R = \frac{C2 \cdot E \cdot A}{l} \tag{10}$$

Chellis (1951) defined l as the "length of pile measured from head to center of driving resistance". Thus, it can be considered as a percentage of the full pile length, as shown in Eq. 11:

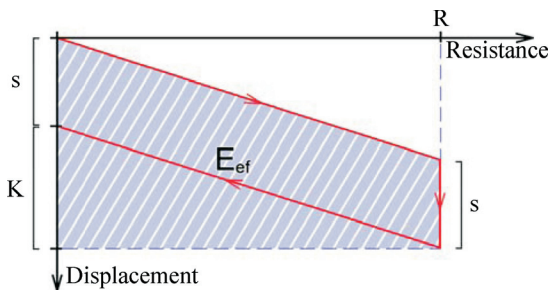


Figure 2 - Idealized curve of pile resistance vs. displacement after impact.

$$R = \frac{C2 \cdot E \cdot A}{\alpha \cdot L} \tag{11}$$

That length multiplier (α) was proposed by Velloso (1987) and it is calculated considering the distribution of pile shaft and toe resistances. Matching by the resistance (R) the previous Eqs. 9 and 11, it follows:

$$(s + D) \cdot C2 = \frac{2 \cdot \eta \cdot W \cdot h \cdot \alpha \cdot L}{E \cdot A} \tag{12}$$

The first simplifying hypothesis is that the pile set (plastic displacement) is so small compared to the elastic rebound that it will be disregarded ($s = 0$). Then, it follows that $K = D$, and the Eq. 12 could be written as shown in Eq. 13.

$$D \cdot C2 = \frac{2 \cdot \eta \cdot W \cdot h \cdot \alpha \cdot L}{E \cdot A} \tag{13}$$

$C2$ is usually obtained by measuring the elastic rebound (K) and subtracting from it the toe quake ($C3$). However, there are two major problems with that practice: a) the quake magnitude is generally unknown and b) establishing a fixed value for the quake assumes that it is invariable with the applied energy. Some authors assume it is constant, equal to 2.5 mm. That is not true: the quake is higher as the energy increases. Thus, Rosa (2000) proposed a very convenient solution: to consider $C2$ as a percentage of the maximum elastic displacement (K). Since the set was disregarded ($s = 0$), then $K = D$ and $C2$ is written as:

$$C2 = \kappa \cdot K = \kappa \cdot D \tag{14}$$

Taking that into Eq. 13:

$$D \cdot (\kappa \cdot D) = \frac{2 \cdot \eta \cdot W \cdot h \cdot \alpha \cdot L}{E \cdot A} \tag{15}$$

Then, reordering the terms:

$$D = \sqrt{\frac{2 \cdot \alpha}{\kappa}} \cdot \sqrt{\frac{\eta \cdot W \cdot h \cdot L}{E \cdot A}} \tag{16}$$

Or, considering the term $\lambda = \sqrt{2\alpha / \kappa}$, Eq. 16 may be rewritten as:

$$D = \lambda \cdot \sqrt{\frac{\eta \cdot W \cdot h \cdot L}{E \cdot A}} \tag{17}$$

Reordering the terms of Eq. 17, the effective transferred energy is given by Eq. 18.

$$E_{ef} = \eta \cdot W \cdot h = \frac{1}{\lambda^2} \cdot \frac{D^2 \cdot E \cdot A}{L} \tag{18}$$

That is the base equation of the alternative method, in which the λ coefficient is the main parameter and a function of α and κ .

In the same research that Rosa proposed the solution of considering $C2$ as a percentage of K (Rosa, 2000), the au-

thor found mean values for κ , relating it to the soil at the pile tip, as follows:

- 0.80 for pile tip over sandy soil;
- 0.70 for pile tip over silty soils or clay.

Thus, as λ depends on the distribution of pile shaft and toe resistances (α) and the soil type at the pile tip (κ), it can be described as a “site-specific” parameter that might differ from one site (and subsoil profile) to another.

Querelli & Massad (2017) briefly introduced Eq. 18, although not explicitly mentioning the λ coefficient. It could be verified that their results showed very similar λ values – 1.28 and 1.29 – for two neighboring sites located in Duque de Caxias (state of Rio de Janeiro, Brazil).

More recently, Querelli & Massad (2019) showed another case study involving the deduced methodology. They evaluated the λ coefficient for three sites in the Rio de Janeiro metropolitan area, resulting in λ values between 1.22 and 1.39.

In the case of the Danish Formula (Sorensen & Hansen, 1957), the adjustment coefficient λ implicit in the term S_o , given by Eq. 3 and analogous to Eq. 17, is $\lambda = \sqrt{2} = 1.41$ and, therefore, the ratio $1/\lambda^2 = 0.50$. Also, it can be deduced that, as the pile toe is “fixed”, $C3 = 0$, $C2 = K$ and $\kappa = 1$. Therefore, it follows that Sorensen & Hansen assumed no shaft resistance, *i.e.* $\alpha = 1$ ($l = L$).

6. Case Studies: Characterization and Method Application

Various case studies were selected in order to apply the alternative method, based on Eqs. 17 and 18. They include 12 distinct sites, at seven Brazilian locations with 244 dynamically tested piles: 161 concrete and 83 steel piles. That resulted in 692 records of dynamic load tests of increasing energy: 526 from concrete and 166 from steel piles.

The evaluated subsoils are quite diverse. For example: there are cases of piles length most through marine sedimentary clays (some with organic material), and just a few meters into compact sand (residual), as occurs in sites 2, 3, 9, 10 and 11. Sites 4 and 5 are mostly of residual clays and site 6 of residual sand (of quartz). The piles length in site 12 are mostly through residual sandy silt of gneiss.

The hammer types used in pile driving were only drop hammers for sites 2, 9 and 11 and both drop and hydraulic hammers for sites 3 and 12. There is no information about the hammer types of the other sites.

Table 1 summarizes the site locations, pile materials, amount of tests, dynamic records and cross sections.

In order to evaluate the λ values of Eq. 17, linear correlations were made between the two terms, D and $[(\eta.W.h.L)/(E.A)]^{0.5}$. As mentioned above, $D = DMX$ and $E_{ef} = \eta.W.h = EMX$, given by the dynamic load tests. Plotting those linear correlations, it follows that the angular

coefficient (slope) is equal to λ . Therefore, to get the desired effective energy (E_{ef}), it is only necessary to use Eq. 18.

6.1. Results and discussions

The linear correlations were made: a) grouping the data according to the pile material (concrete or steel); and b) for each site, alone.

6.1.1. λ coefficient by material

The plots in the form $D \times [(\eta.W.h.L)/(E.A)]^{0.5}$ for both concrete and steel piles are presented in Fig. 3 and Fig. 4.

The linear correlation through the origin gave the following values for the λ coefficient: 1.34 for concrete piles and 1.23 for steel piles. The coefficient of determination (R^2) was lower for concrete piles (0.88) than for steel piles (0.92), much because of the scatter caused by the higher λ values of sites 1 and 7 (1.71 and 1.56, respectively), which are presented separately in section 6.1.2 (Figs. 5 and 11, respectively).

Therefore, in order to propose an average equation for each material, the effective transferred energy can be calculated by Eqs. 19 and 20:

$$E_{ef} = 0.56 \cdot \frac{D^2 \cdot E \cdot A}{L} \quad (\text{concrete piles}) \quad (19)$$

$$E_{ef} = 0.68 \cdot \frac{D^2 \cdot E \cdot A}{L} \quad (\text{steel piles}) \quad (20)$$

6.1.2. λ coefficient by site

The plots in the form $D \times [(\eta.W.h.L)/(E.A)]^{0.5}$ for each site are presented in Figs. 5 to 16 with the linear correlations, where the angular coefficient is λ , and with the coefficients of determination (R^2), that in general are above 90%. Table 2 summarizes these results.

Observing the sites separately, there is greater dispersion in the mean values of λ for concrete piles, ranging from 1.23 to 1.71, with an average of 1.40 between sites and Coefficient of Variation (CV) of 12.8% (Table 2). For steel piles, the coefficient of variation drops to 7.7%, with λ ranging from 1.13 to 1.35 and averaging around 1.25 between sites (Table 2).

6.1.3. Ratio $1/\lambda^2$ by site

Table 2 also presents mean values of the term $1/\lambda^2$, from Eq. 17, which allows the estimation of the effective energy ($E_{ef} = EMX$). It can be seen that:

- for concrete piles, the value of the ratio $1/\lambda^2$ ranged from 0.34 to 0.67. The average of the sites was 0.53, with standard deviation of 0.12 and coefficient of variation of 22.6%; and

Table 1 - Summary of the studied sites.

Site	City/Location (State)	Piles material	Amount of tested piles	Amount of dynamic load test records	Cross-sections with main dimension (cm)
1	Foz do Iguaçu (PR)	Concrete	4	36	36 × SQ 16.0 / 20.0 / 23.0
2	Rio de Janeiro metropolitan area (RJ)	Concrete	26	26	10 × SQ 21.5 / 23.5 / 26.5 / 29.5 16 × STR 22.9 / 26.9 / 29.8 / 40.6
3	Rio de Janeiro metropolitan area (RJ)	Concrete	23	102	102 × SQ 19.5 / 26.5 / 29.5
4	São José dos Campos (SP)	Concrete	35	131	131 × SQ 23.0 / 26.5
5	São José dos Campos (SP)	Concrete	12	35	35 × SQ 19.5 / 23.5
6	São Paulo (SP)	Concrete	20	51	51 × H 40 / 45
7	São Paulo (SP)	Concrete	41	145	30 × HS 33 115 × CC 38 / 42
8	Aracaju (SE)	Steel	4	12	12 × HP 25 (73 kg/m)
9	Rio de Janeiro metropolitan area (RJ)	Steel	16	84	84 × HP 31 (125 kg/m)
10	Rio de Janeiro metropolitan area (RJ)	Steel	2	9	9 × RL 6.8
11	Itajaí (SC)	Steel	7	7	7 × W 25 (25 kg/m)
12	Belo Horizonte metropolitan area (MG)	Steel	54	54	54 × TB 35.6 / 50.8 / 61.0

SQ = Square; STR = Star section; H = Hexagon; HS = Solid Hexagon; CC = Cylinder centrifuged pile; HP and W = H pile; RL = Rail pile; TB = Tubular.

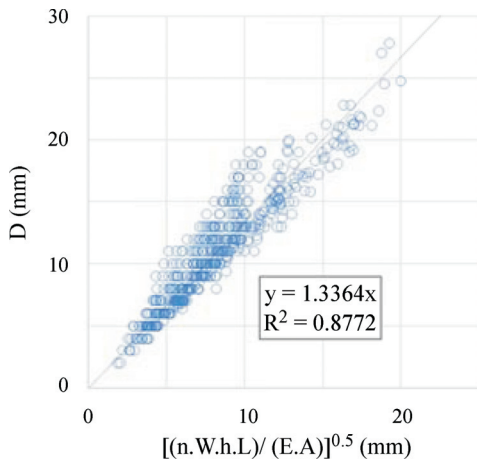


Figure 3 - All concrete piles.

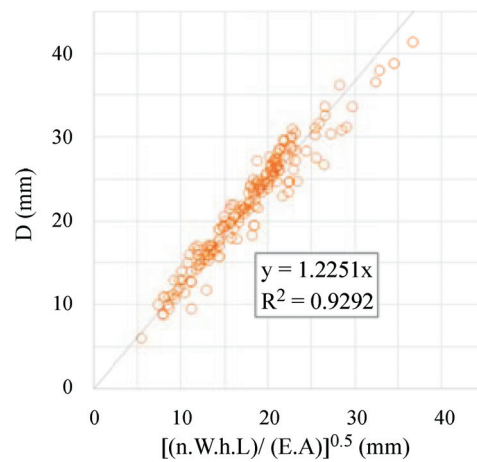


Figure 4 - All steel piles.

b) for steel piles, the average $1/\lambda^2$ value was 0.65, ranging from 0.55 to 0.78, with a standard deviation of 0.10 and a coefficient of variation of 15.6%.

These results confirm that it is possible to estimate the ratio $1/\lambda^2$ in a consistent way, allowing using the proposed methodology to estimate the effective transferred energy (E_{ef}) without needing the hammer efficiency (η). In order to

properly use the method, the analysis shows that it is recommended to perform previous calibrations of λ for each site, by means of dynamic load tests (DLT), before the beginning and even during the construction.

7. Method Limitations and Cautions

The method stands as an alternative to the assessment of hammer efficiency, since the 12-site case study validated

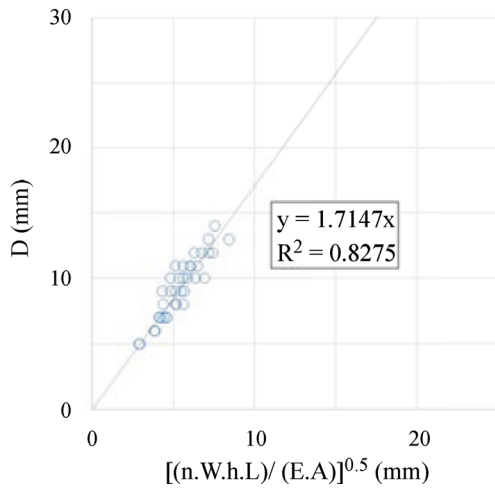


Figure 5 - Site 1 – concrete.

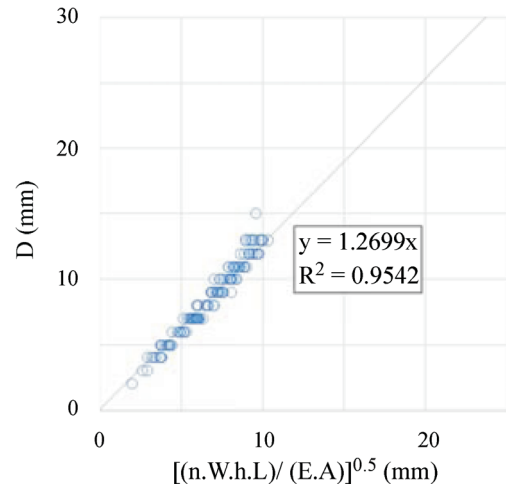


Figure 8 - Site 4 – concrete.

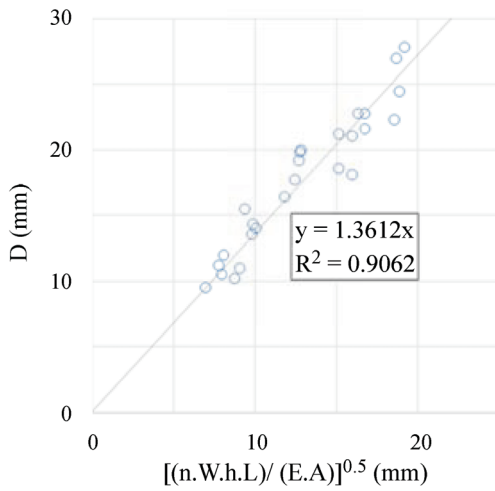


Figure 6 - Site 2 – concrete.

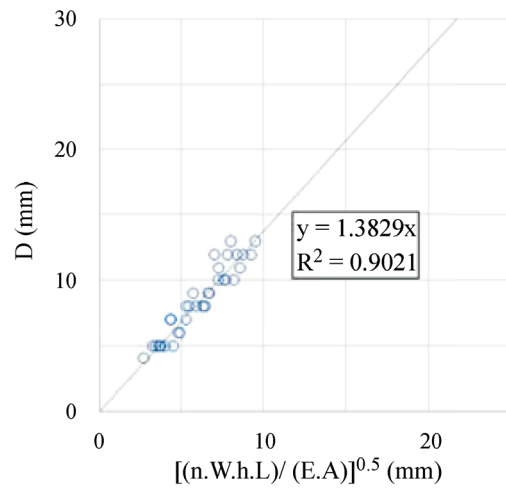


Figure 9 - Site 5 – concrete.

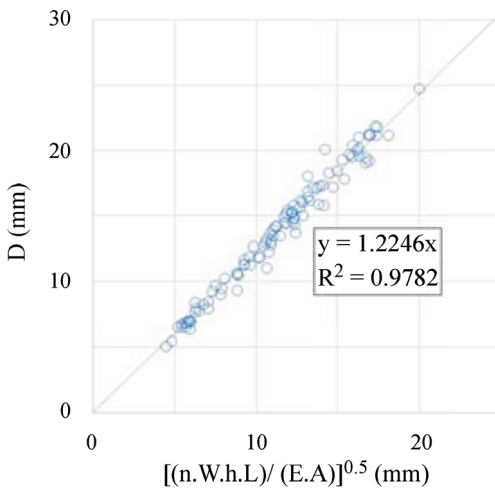


Figure 7 - Site 3 – concrete.

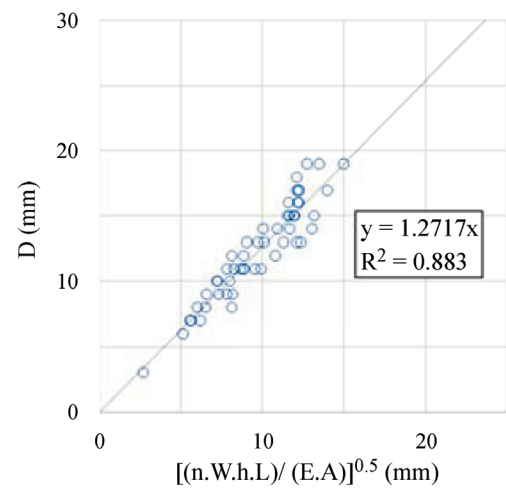


Figure 10 - Site 6 – concrete.

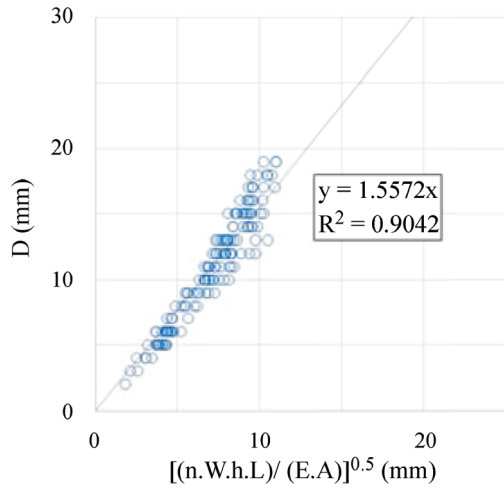


Figure 11 - Site 7 – concrete.

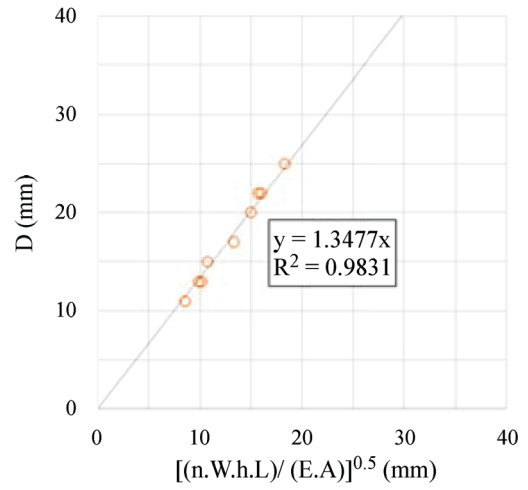


Figure 14 - Site 10 – steel.

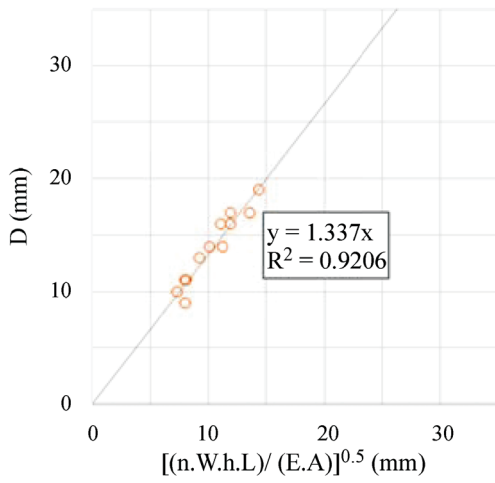


Figure 12 - Site 8 – steel.

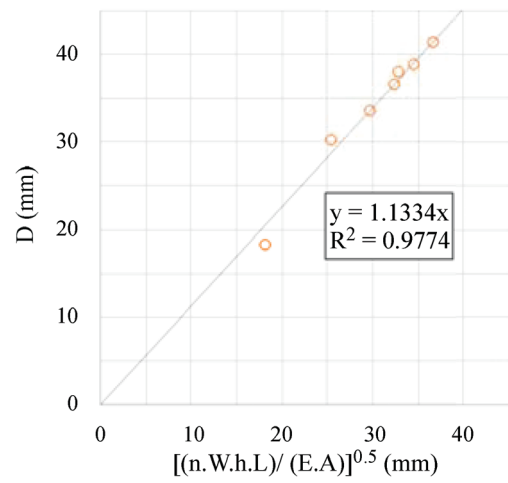


Figure 15 - Site 11 – steel.

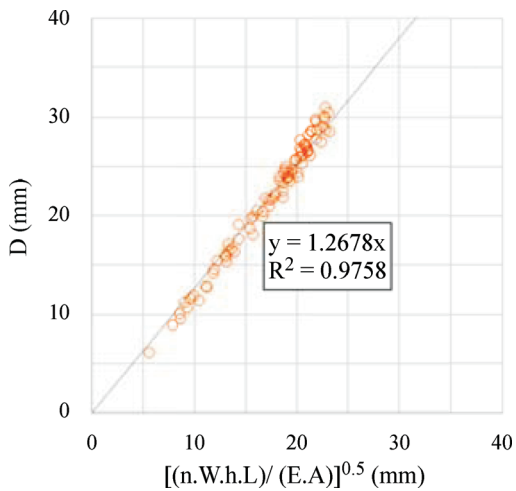


Figure 13 - Site 9 – steel.

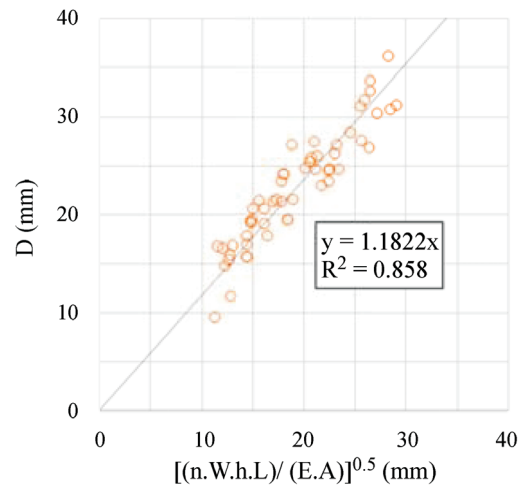


Figure 16 - Site 12 – steel.

Table 2 - Values of λ , $1/\lambda^2$ and R^2 by site.

Site	λ coefficient		ratio $1/\lambda^2$		R^2 (linear regression)
	Concrete	Steel	Concrete	Steel	
Site 1	1.71		0.34		0.83
Site 2	1.36		0.54		0.91
Site 3	1.22		0.67		0.98
Site 4	1.27		0.62		0.95
Site 5	1.38		0.52		0.90
Site 6	1.27		0.62		0.88
Site 7	1.56		0.41		0.90
Site 8		1.34		0.56	0.92
Site 9		1.27		0.62	0.98
Site 10		1.35		0.55	0.98
Site 11		1.13		0.78	0.98
Site 12		1.18		0.72	0.86
Minimum	1.22	1.13	0.34	0.55	0.83
Maximum	1.71	1.35	0.67	0.78	0.98
Average	1.40	1.25	0.53	0.65	0.92
Std. dev.	0.18	0.10	0.12	0.10	0.05
Coef. of variation	12.8%	7.7%	22.6%	15.6%	5.6%

its application. However, some limitations and cautions are presented below:

- the method was not verified for large quake (high rebound) soils;
- the range of permanent set per blow evaluated was $s \leq 7$ mm; also, in 90% (621) of the dynamic records, the permanent set per blow was $s \leq 3$ mm (hard driving);
- the method is valid when the elastic rebound (K) is much higher than the set (s), since it is one of the method's simplifying hypothesis;
- when applying it to non-tested pile, the scatter of the elastic modulus (E) should be accounted, since it has direct influence on the effective energy estimations.

8. Basic Step-By-Step Guide to the Method Application

In order to apply the proposed methodology, the following routine could be applied:

- (1) Select the sample of piles to be dynamically tested (DLT);
- (2) Perform the dynamic load tests (of increasing energy) in the selected piles, measuring the set (s) and elastic rebound (K) of each blow;
- (3) With that pile geometry and the results from the DLT, plot the graphs in the form D vs. $[(E_{ef} \cdot L)/(E \cdot A)]^{0.5}$ for all blows of the tested piles;

- (4) The calibrated and site-specific λ value could be obtained from the plot, as it is the slope of the linear correlation through the origin [0,0];
- (5) Measuring the set (s) and elastic rebound (K) of blows in non-tested piles, that calibrated λ value could be applied to Eq. 18 in order to estimate the effective transferred energy.

9. Conclusions

The proposed method to estimate the effective transferred energy is a practical and, in the authors' view, relevant contribution to quality control of driven piles, since two very simple records (s and K) are needed – besides the knowledge of the λ coefficient, calibrated through dynamic load tests of increasing energy on selected piles of a given site.

After λ calibration, it is possible to use Eq. 18 and apply the calculated effective energy (E_{ef}) to dynamic formulas, in order to estimate the resistance of non-tested piles.

There is no need to know the hammer efficiency (η), which presents huge scatter in the same site and difficulties to be calibrated to a single, fixed value (even with dynamic instrumentation). The methodology also does not require input of soil type, since it is considered in the site-calibration of the λ coefficient.

The case studies showed the importance of first calibrating the λ coefficient, since it differs from site to site and the correlations (R^2) showed to be good to excellent when

considering each site alone; the site-specific calibrated λ ranged from 1.22 to 1.71 in the concrete piles' sites and 1.13 to 1.35 for the steel piles' sites, with R^2 from 0.83 to 0.98.

Due to λ variability and the influence of both α and κ parameters (site-specific attributes), it is important to mention that if the site area is extensive, if the local subsoil is very heterogeneous or even if the pile lengths are quite different, it is strongly recommended to divide the site in regions and perform more than one calibration of λ in order to contemplate all of the local particularities. Investigations about other reasons for λ variability were outside the scope of this paper. In this sense, the influence of hammer type or pile crosssections in λ was not evaluated.

Although the proposed method dispenses the knowledge of hammer efficiency (η), as a "last but not least" comment, it is reasonable to say that engineers have to be cautious with overly simple methods when representing complex events.

References

- ABNT (2007). Estacas – Ensaio de Carregamento Dinâmico – Método de Ensaio - NBR 13208. Associação Brasileira de Normas Técnicas. Rio de Janeiro, RJ, Brazil, 12 p.
- ABNT (2010). Projeto e Execução de Fundações - NBR 6122. Associação Brasileira de Normas Técnicas. Rio de Janeiro, RJ, Brazil, 91 p.
- Alonso, U.R. (1991). Previsão e Controle das Fundações. Edgard Blucher Ltda, São Paulo.
- Alves, A.M.L. & Lopes, F. de R. (2004). Estacas de deslocamento: Tipos, aplicações e controle de execução. Proc. Seminário sobre Fundações Profundas, Porto Alegre, Brazil.
- Alves, A.M. de L.; Lopes, F. de R. & Danziger, B.R. (2004). Métodos dinâmicos para previsão e controle do comportamento de estacas cravadas. Teoria e Prática na Engenharia Civil, 4(4):12-21.
- Aoki, N. (1989). A new dynamic load test concept. Proc. XII International Conference on Soil Mechanics and Foundation Engineering, Rio de Janeiro, Brazil, v. 1, pp. 1-3.
- Beim, J.W. (2009). Aplicação da equação da onda na análise da cravação e ensaio de fundações: passado, presente e futuro. In: Engenharia de Fundações: Passado Recente e Perspectivas – Homenagem ao Prof. Nelson Aoki. Rio de Janeiro.
- Caputo, H.P. (1983). Mecânica dos Solos e Suas Aplicações, v. 2. LTC, Rio de Janeiro, 5ª ed.
- Chellis, R.D. (1951). Pile Foundations. McGraw-Hill, New York.
- Fellenius, B.H. (2018). Basics of foundation design. January 2018. Vero Beach: Pile Buck International, Inc. Available at <https://www.fellenius.net/papers.html>. Downloaded in 28 dez. 2018.
- Goble, G.G.; Rausche, F. & Likins, G.E. (1980). The analysis of pile driving - A state-of-the-art. Proc. International Seminar on the Application of Stress-Wave Theory on Piles, Stockholm, Sweden, pp. 131-161.
- Goble, G.G. & Likins, G.E. (1996). On the application of PDA dynamic pile testing. Proc. Fifth International Conference on the Application of Stress-Wave Theory to Piles, Orlando, United States, pp. 263-273.
- Gonçalves, C.; Bernardes, G. de P. & Neves, L.F. de S. (2007). Estacas Pré-Fabricadas de Concreto: Teoria e Prática, 1st ed. Author's edition, São Paulo.
- Hiley, A. (1925). A rational pile-driving formula and its application in piling practice explained. Engineering (London), v. 119(3100):657-721.
- Hussein, M.H.; Likins, G.E. & Hannigan, P.J. (1993) Pile evaluation by dynamic testing during restrike. Proc. 11th Southeast Asia Geotechnical Conference, Singapore, pp. 535-539.
- Likins, G.E.; Fellenius, B.H. & Holtz, R.D. (2012). Pile driving formulas: past and present. Proc. ASCE Geoinstitute Geo-Congress, Full-Scale Testing in Foundation Design, State of the Art and Practice in Geotechnical Engineering, Oakland, United States, pp. 25-29.
- Likins, G.E. & Rausche, F. (2008). What constitutes a good PDA test? Proc. Eighth International Conference on the Application of Stress Wave Theory to Piles, Lisbon, Portugal, pp. 403-407.
- Niyama, S.; Martins, J.A. de A.; Medeiros Jr., C. & Likins, G.E. (1984). Dynamic pile instrumentation in a calcareous sand close to PCR-2 platform, Brazil. Proc. Second International Conference on the Application of Stress Wave Theory on Piles, Stockholm, Sweden, pp. 306-312.
- Paikowsky, S.G. (2001). Load and Resistance Factor Design (LRFD) for dynamic analysis of deep foundations. Proc. 15th International Conference on Soil Mechanics and Foundation Engineering, Istanbul, Turkey, v. 2, pp. 981-984.
- Paikowsky, S.G. & Chernauskas, L.R. (1992). Energy Approach for capacity evaluation of driven piles. Proc. Fourth International Conference on the Application of Stress-Wave Theory to Piles, Rotterdam, Netherlands, pp. 21-24.
- Paraíso, S.C. & Costa, C.M.C. (2010). A eficácia do ensaio de carregamento dinâmico na avaliação do efeito de "setup" em estacas cravadas. Proc. XV Congresso Brasileiro de Mecânica dos Solos e Engenharia Geotécnica, COBRAMSEG, Gramado, Brazil.
- Querelli, A. & Massad, F. (2017). Simplified Hiley's formula calibration for precast concrete piles in Duque de Caxias. Proc. International Conference on Advances in Structural and Geotechnical Engineering, ICASGE17, Hurghada, Egypt.

- Querelli, A. & Massad, F. (2019) Proposição de um método alternativo para estimativa da energia efetiva na cravação de estacas. Proc. 9º Seminário de Engenharia de Fundações Especiais e Geotecnia, SEFE 9, São Paulo, Brazil.
- Rausche, F. (1997). Hammer Design for Drilled Shaft Testing: Two Case Studies. Notes from PDA Users Day in Cleveland, OH. Pile Dynamics, Inc, Cleveland, pp. 1-13.
- Rausche, F.; Robinson, B.R. & Likins, G.E. (2004). On the prediction of long term pile capacity from end-of-driving information. Geotechnical Special Publication, (N. 125):77-95.
- Rosa, R.L. (2000). Proposição de Modificação das Fórmulas Dinâmicas de Cravação de Chellis de Uto *et al.* a Partir de Resultados do Método Case. Master's Thesis, Universidade de São Paulo, São Paulo, 196 p.
- Saldívar, R.E.R. (2008). Retroanálise Probabilista Aplicada à Análise Dinâmica da Cravação de Estacas. Master's Thesis, Universidade de São Paulo, São Paulo, 147 p.
- Sorensen, T. & Hansen, B. (1957). Pile driving formulae – An investigation based on dimensional considerations and a statistical analysis. Proc. 4th International Conference Soil Mechanics and Foundation Engineering, London, England, p. 61-65.
- Tavenas, F. & Audy, R. (1972). Limitations of the driving formulas for predicting the bearing capacities of piles in sand. Canadian Geotechnical Journal, 9(1):47-62.
- Tokhi, H. (2012). A Practical Method for Improved Implementation of Pile Driving Formula. Master's Thesis, RMIT University, Australia, 207 p.
- Valverde, R. & Massad, F. (2018). Maximum envelope of lateral resistance through dynamic increasing energy test in piles. Soils & Rocks, 41(1):75-89.
- Velloso, P.P.C. (1987). Fundações: Aspectos Geotécnicos v. 2 e 3. Departamento de Engenharia Civil, PUC, Rio de Janeiro, 5ª ed.
- Vieira, S.H.A. (2006). Controle de Cravação de Estacas Pré-Moldadas: Avaliação de Diagramas de Cravação e Fórmulas Dinâmicas. Master's Thesis, COPPE-UFRJ, Rio de Janeiro, 122 p.

List of Symbols

- s*: Set. Permanent (plastic) displacement per blow
K: elastic rebound after the blow
C2: pile elastic displacement (structural element)
C3: Quake. Elastic displacement of the soil below pile tip
R: pile-soil's static resistance
 η : driving system efficiency / impact efficiency
W: hammer weight
h: hammer drop height
L: pile length
A: pile crosssectional área
E: dynamic elastic modulus
 S_o : dynamic elastic compression of a pile with a fixed point (Sorensen & Hansen, 1957); analogous to *K*
 K_{sp} : coefficient of energy loss in the soil by the viscous damping effect
D: maximum pile displacement after blow (sum *s* + *K*)
F: force calculated in the dynamic load test
v: particle velocity calculated in the dynamic load test
Z: pile impedance
c: wave speed
EMX: maximum transferred energy to the pile calculated in the dynamic load test (analogous to ' $\eta.W.h$ ')
F(t): force measured along time;
v(t): particle velocity measured along time
 E_{ef} : effective transferred energy to the pile (analogous to *EMX*)
l: length from pile top to the center of driving resistance
 α : pile length multiplier in order to consider the center of driving resistance
 κ : elastic rebound multiplier proposed by Rosa (2000)
 λ : site-specific adjustment coefficient
DMX: maximum pile displacement after stroke calculated in the dynamic load test (analogous to *D*)
 R^2 : coefficient of determination (linear regression)
CV: coefficient of variation (statistics)

Technical Notes

Soils and Rocks
v. 42, n. 2

Biodegradation of Biodiesel in Laboratory and Field in a Clayey Residual Soil

A. Thomé, A.W.S. Trentin, I. Cecchin, C. Reginato

Abstract. This study compared the process of biotic and abiotic degradation of biodiesel in a clayey soil in a laboratory environment (*ex situ*) and infield environment (*in situ*). The experiment carried out *ex situ* had controlled temperature and humidity, while the experiment *in situ* was directly influenced by external factors such as rainfall and temperature. The soil was collected deformed and contaminated with 4% of biodiesel in relation to dry weight (m/m). The bioreactors were molded under the same initial parameter conditions of the field. The experiment lasted for 120 days and contaminant reduction measurements were made throughout the experiment. At the end of the experiment, there was a reduction of 89% in the contaminant initially added to the soil in the *ex situ* experiment, whereas in the *in situ* experiment there was a reduction of 32%. The main conclusion is that the laboratory experiment provided better results of biodegradation, since it was possible to perform an effective control of abiotic factors, such as temperature, humidity and pH. However, these results are not representative of the actual behavior in the field.

Keywords: abiotic factors, bioremediation, leaching, natural attenuation.

1. Introduction

Monitored Natural Attenuation (MNA) is by definition a process that combines all possible reactions that may reduce a contaminant concentration in the environment, such as physical or chemical reactions and biological process. The success of a biodegradation process depends on the intrinsic ability of the system to create and maintain the conditions that promote the biodegradation of pollutants at a sufficiently high rate. (EPA, 1999; Mulligan & Yong, 2004; Bento *et al.*, 2005; Das & Chandran, 2011; Declercq *et al.*, 2012; Sihag *et al.*, 2014; Agnello *et al.*, 2016; Guarino *et al.*, 2017).

Bioremediation techniques can be categorized as *ex situ* when they occur in controlled environments, such as in laboratories, or *in situ* when they occur in the field and environmental conditions are not controlled (Frutos *et al.*, 2012; Smith *et al.*, 2015; Azubuike *et al.*, 2016). Different studies have been carried out to evaluate the effectiveness of *ex situ* bioremediation (Dott *et al.*, 1995; Pasqualino *et al.*, 2006; DeMello *et al.*, 2007; Mariano *et al.*, 2008; Owsianiak *et al.*, 2009; Aktas *et al.*, 2010; Corseuil *et al.*, 2011; Sorensen *et al.*, 2011; Borges *et al.*, 2014; Agnello *et al.*, 2016; Guarino *et al.*, 2017; Decesaro *et al.*, 2017), or *in situ* bioremediation (Dott *et al.*, 1995; Sendzikiene *et al.*, 2007; Ramos *et al.*, 2013). However, a direct comparison, with the same soil conditions and the same contaminant, of the monitored natural attenuation technique when applied

in situ and *ex situ* was not found. The influence of infiltration of water in the soil due to rainfall and the influence of the variation of ambient temperature on the biodegradation of biodiesel in residual clayey soil are not yet known. Therefore, studies seeking to understand the response of the monitored natural attenuation technique when applied *in situ* and *ex situ* environments are important for the scientific and technical remediation field.

The objective of this study is to evaluate biodegradation by monitored natural attenuation in experiments in a controlled environment (*ex situ*) and non-controlled (external) environments (*in situ*) using a simulated contamination of biodiesel in a residual clayey soil.

2. Materials and Methods

2.1. Soil

The clayey soil was obtained from the Geotechnical Experimental Site at the University of Passo Fundo, Southern Brazil. It was collected at 2 meters depth (B horizon) in an open pit, and represents a typical Brazilian basaltic residual soil. Table 1 shows the geotechnical and physical properties of the soil (ASTM, 2017a; ASTM, 2017b; ASTM, 2017c; ASTM, 2017d; ASTM, 2017e; ASTM, 2018a; ASTM, 2019). The soil is classified as an Oxisol (Streck *et al.*, 2008) and is a high plasticity clay (CH) according to the Unified Soil Classification System (ASTM, 2017f). As can be seen in Table 1, the soil has a relatively

Antônio Thomé, Dr. Eng., Professor, Programa de Pós-Graduação em Engenharia Civil e Ambiental, Universidade de Passo Fundo, Passo Fundo, RS, Brazil, e-mail: thome@upf.br.

Adan William da Silva Trentin, Ph.D. Student, Programa de Pós-Graduação em Engenharia Civil e Ambiental, Universidade de Passo Fundo, Passo Fundo, RS, Brazil, e-mail: adan_trentin@hotmail.com.

Iziquiel Cecchin, Ph. D., Lecturer, Curso de Engenharia Ambiental, Universidade de Passo Fundo, Passo Fundo, RS, Brazil. e-mail: iziquielc@gmail.com.

Cleomar Reginato, Ph. D., Associate Professor, Programa de Pós-Graduação em Engenharia Civil e Ambiental, Universidade de Passo Fundo, Passo Fundo, RS, Brazil, e-mail: cleomar@upf.br.

Submitted on August 21, 2018; Final Acceptance on July 8, 2019; Discussion open until December 31, 2019.

DOI: 10.28927/SR.422193

Table 1 - Geotechnical and physicochemical characteristics of the clayey soil.

Parameter (unit)	Value
Clay (%)	68
Silt (%)	5
Fine sand (%)	27
Liquid limit (%)	53.0
Plastic limit (%)	42.0
Particle unit weight (kN/m ³)	26.7
Natural moisture content (%)	34
Natural unit weight (kN/m ³)	16.3
Void ratio	1.2
Degree of saturation (%)	75.7
Porosity (%)	54
pH	5.4
Organic matter (%)	< 0.8
Cation exchange capacity-CEC (cmolc/dm ³)	8.6
Hydraulic conductivity (m/s)	1.39 x 10 ⁻⁵

acidic pH, high clay content and a low Cation Exchange Capacity (CEC) (ASTM, 2018b; ASTM, 2018c). These characteristics are representative of a typical soil with a predominance of clay-mineral kaolinite due to its structural conformation. X-ray diffraction analysis indicated that the clay fraction is composed of approximately 70% kaolinite and 30% oxides (Fe and Al). The organic content of the soil is low due to the greater depth at which the soil was collected (ASTM, 2014). The soil is very porous, with a high

void ratio, characteristic of residual clays, and these characteristics allow a high permeability.

2.2. Contaminant characteristics (biodiesel)

Pure soybean biodiesel (B100) was used in this study to simulate organic contamination in a typical fuel spill/leak situation. Biodiesel has a high flash point (104.2 ± 5.0 °C and 77% less particulate matter emissions when compared to regular diesel. Biodiesel also has a higher level of biodegradability and a lower volatility than regular diesel. It is insoluble in water and has a density of 889 kg/m³. Moreover, it does not contain sulphur and aromatic compounds (Silva & Corseuil, 2012; Meneghetti *et al.*, 2012; Thomé *et al.*, 2014), but contains mainly methyl esters highly hydrophobic due to the presence of long carbon chains, which results in a very low solubility in water (Wedel, 1999). Table 2 presents the main characteristics of the methyl esters present in the regular soy biodiesel.

2.3. Assembly of the experiment *ex situ* (laboratory)

The disturbed soil sample was contaminated with 4.0% biodiesel over the dry weight of soil (m/m), equivalent to a soil contamination of 40 g/kg. Previous studies in laboratory have shown that values above this value cause leaching of the contaminant (Cecchin *et al.*, 2016; Thomé *et al.*, 2017). The collected soil was dry until reaching 20% of moisture content. It was sieved in a 2 mm sieve (ASTM No.10) for homogenization, and then water was added until it reached a 30% moisture. After homogenized, the 4% of biodiesel was added, and the soil returned to the field moisture content of 34%. The experiment was set up in aluminum cylinders (24 cm in diameter and 24 cm in height), with a volume of 108 cm³ (Fig. 1). The bottom of the cylin-

Table 2 - Physicochemical properties of methyl esters of soybean oil.

Properties	Compound				
	Methyl Palmitate	Methyl Stearate	Methyl Oleate	Methyl Linoleate	Methyl Linolenate
Molecular formula	C ₁₇ H ₃₄ O ₂	C ₁₉ H ₃₈ O ₂	C ₁₉ H ₃₆ O ₂	C ₁₉ H ₃₄ O ₂	C ₁₉ H ₃₂ O ₂
Molecular mass (g mol ⁻¹)	270.46	298.51	296.49	294.49	291.46
FP (°C)	30.5 ⁽²⁾	39.0 ⁽²⁾	-20.0 ⁽²⁾	-35.0 ⁽²⁾	-52.0 ⁽³⁾
BP (°C)	415-418 ⁷⁴⁷⁽²⁾	442-443 ⁷⁴⁷⁽²⁾	218.5 ²⁰⁽²⁾	215.0 ²⁰⁽²⁾	182.0 ³⁽⁴⁾
Relative density	0.852 ⁽⁵⁾	0.850 ⁽⁵⁾	0.874	0.889	0.895 ⁽⁵⁾
Solubility Water (25 °C) (mg L ⁻¹)	Insoluble ⁽⁶⁾	Insoluble	Insoluble	Insoluble ⁽⁶⁾	Insoluble ⁽⁶⁾
Vapor pressure (atm)	4.99 × 10 ⁻⁸	5.85 × 10 ⁻⁹	9.72 × 10 ⁻⁹	1.15 × 10 ⁻⁸⁽⁷⁾	1.14 × 10 ⁻⁸⁽⁷⁾
Henry's constant	1.37 × 10 ⁻¹	2.34 × 10 ⁻¹	3.23 × 10 ⁻²	6.54 × 10 ⁻³⁽⁷⁾	1.39 × 10 ⁻³⁽⁷⁾
Log K _{ow} (25 °C)	7.38	8.35	7.45	6.82 ⁽⁷⁾	6.29 ⁽⁷⁾
Log K _{oc} (25 °C)	4.26	4.79	4.79	-	-

Note: FP: Fusion Point; BP: Boiling Point.

Source: TOXNET (2018);⁽¹⁾NIST (2018);⁽²⁾Knothe (2005);⁽³⁾Foon *et al.* (2006);⁽⁴⁾SCIENCE LAB.COM (2018);⁽⁵⁾SIGMA-ALDRICH (2018);⁽⁶⁾TGSC (2008);⁽⁷⁾Krop *et al.* (1997).

ders was filled with inert sand to level the useful volume of all cylinders used. The soil volume was calculated according to the useful area of the cylinder, considering the soil field characteristics for moisture (34%), natural unit weight (16.3 kN/m^3) and void ratio ($e = 1.19$). The total soil mass contained in each bioreactor was divided into 5 equal parts; for each part, compaction was performed within the bioreactor vessel at the natural field density. Bioreactors were assembled and kept in a laboratory with a controlled temperature of $24 \text{ }^\circ\text{C}$ during the whole time.

Samples were collected at 15, 30, 45, 60, 90 and 120 days. It was used a hollow metal rod of 1 cm in diameter (direct push) to collect the samples. The metal rod was carried to the depth at which it reached the drain. Upon removal from the test specimen, the contained soil therein was homogenized, and 15 g were separated to verify the biodiesel content at that time, in triplicate. After the samples were collected, the empty site was filled with clean sterile sand.

2.4. Assembling the experiment *in situ* (field)

The assembly of this reactor included the use of a polyethylene box with a 2 m^3 capacity. The total volume of contaminated soil used was 1.95 m^3 , with 0.75 m^3 in the layer 1 (VL1), 0.65 m^3 in layer 2 (VL2) and 0.55 m^3 in layer 3 (VL3) (Fig. 2). At the base of the reactor, a percolated drainage system was installed, providing leachate material

collected on rainy days. The molding process was similar to that of the laboratory experiment. The soil was homogenized and mixed with water until it reached 30% moisture content, and then 4% of contaminant (97.4 kg) was added and homogenized to achieve the natural soil moisture in the field, *i.e.*, 34%. Considering the large volume of soil, the soil compaction process was carried out in layers of 10 cm thickness. This was performed so that the soil density control was more efficient and became as close as possible to the natural field density (16.3 kN/m^3) and the natural void ratio ($e = 1.19$).

A 2 meter deep trench was excavated on a slope of the experimental field, and the box was placed at the bottom. At soil sampling, guide tubes were left at pre-determined points, and a backfill was performed with local natural soil (Fig. 2). Due to the large size of the bioreactor, three sampling depths were defined in relation to the natural soil surface, that is, depth 1 (D1) at 0.2 m from the bioreactor surface, depth 2 (D2) at 0.5 m, and depth 3 (D3) at 0.8 m. The soils collected at each depth were homogenized and taken to the laboratory to determine the residual contaminant content. This determination was performed in triplicate. The samplings occurred in the same period of the laboratory study (*ex situ*), that is, at 15, 30, 45, 60, 90 and 120 days. As a response variable, the percentage of contaminant reduction was evaluated over the experimental time at each depth.

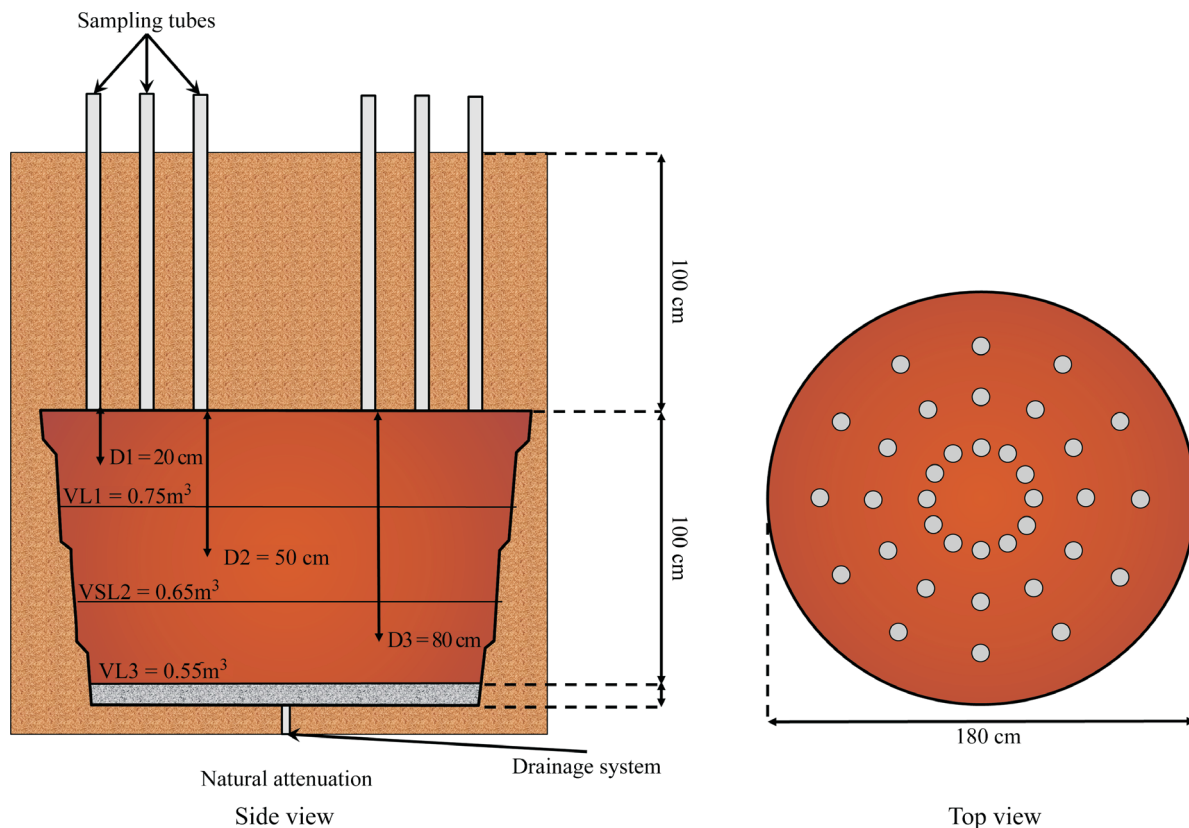


Figure 1 - Illustration of the bioreactor used in the laboratory experiment (*ex situ*).

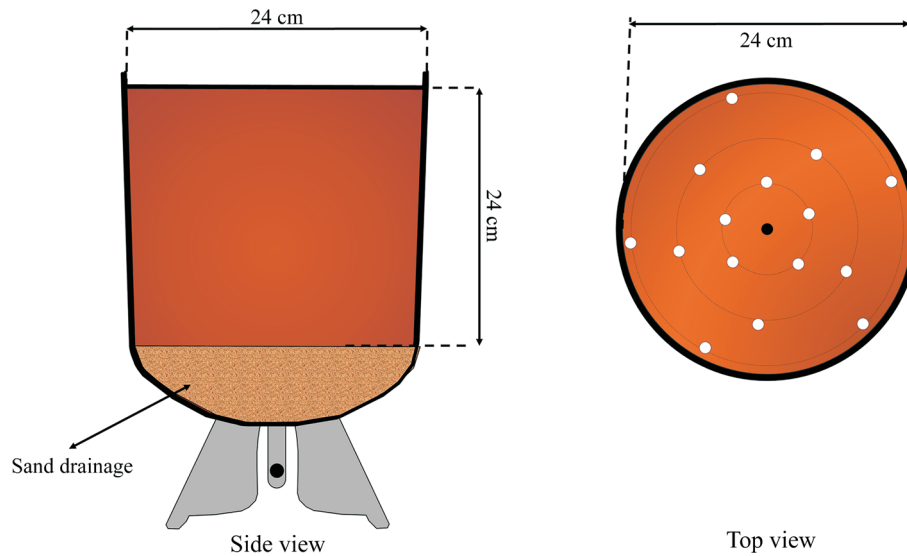


Figure 2 - Illustration of the bioreactor used in the field experiment (*in situ*).

In the case of application *in situ*, elements such as soil temperature, humidity and infiltration were not controlled. The field experiment was set up in January, which is summer in the Southern Hemisphere. By the Köppen classification, Passo Fundo (28°13'36" S, 52°23'13" W and 687 m altitude) is located in the fundamental temperate climate zone (C), presenting a humid (f) and a subtropical specific variety (Cfa). Thus, the local climate is described as humid subtropical (Cfa), with rainfall well distributed during the year, and average temperature of the hottest month exceeding 22 °C. Table 3 shows the mean, minimum and maximum temperatures and mean rainfall in the months during which the experiment was performed (EMBRAPA, 2018).

2.5. Analyses of experiments *ex situ* and *in situ*

The residual free phase contaminant content for the *ex situ* experiment and for the *in situ* experiment was determined by the quantification of oils and greases after the homogenization of soil samples. The extraction was performed using a UNIQUE® probe ultrasound, according to the methodology of USEPA 3550B.

In both experiments, the residual content of contaminant extracted was calculated by Eq. 1.

$$RC = \frac{W_{B+C} - B_w}{D_w} \quad (1)$$

onde RC = residual of contaminant present in test specimen (g/kg), D_w = quantity of soil in dry weight used in the analysis (g), B_w = weight of the beaker (g) e W_{B+C} : weight of the beaker plus the weight of the contaminant extracted from the soil (g).

3. Discussion

3.1. Evaluation of the residual content of experiment *ex situ* (laboratory)

Figure 3 shows the residual biodiesel content in the different sample periods of the experiment *ex situ*, and the data presented represent the mean of the values obtained from both bioreactors used in the experiment.

Considering the initial value of contaminant added to the soil (40 g/kg), the contents of the contaminant decreased with time. After 15 days of experiment, the residual content was 24 g/kg, which represents a decrease of 40% in the initial contamination, the same value observed in the sampling performed in the period of 30 days of experiment.

The values observed in the samplings carried out after 45 and 60 days of experiment presented the same percentage of decrease in contaminant (60%), remaining with

Table 3 - Average, minimum and maximum temperatures and average rainfall during the field experiment (*in situ*).

	January	February	March	April
Mean temperature (°C)	22.1	21.9	20.6	17.6
Higher temperature (°C)	28.3	28.0	26.7	23.7
Lower temperature (°C)	17.5	17.5	16.3	13.5
Rainfall (mm)	143.4	148.3	121.3	118.2

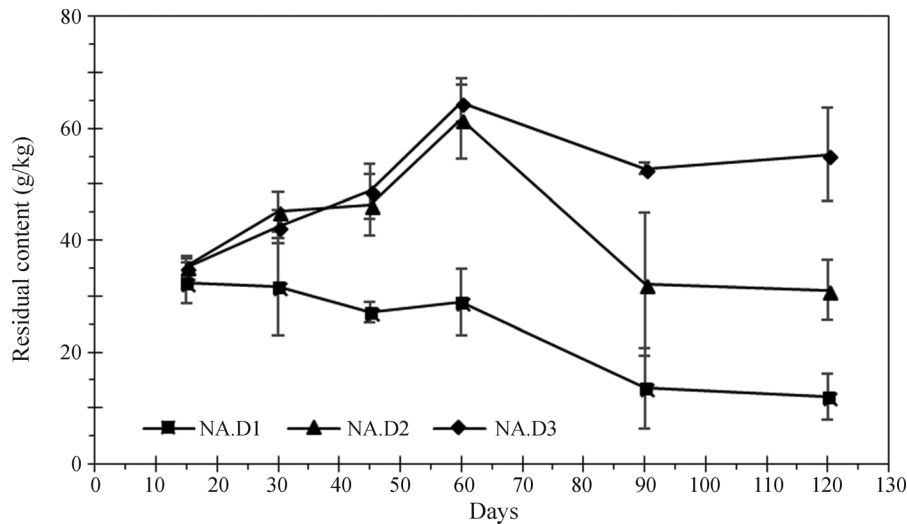


Figure 3 - Mean residual biodiesel content in the different sampling periods in the laboratory experiment.

15 g/kg of biodiesel. For the sampling performed at 90 days, the residual content decreased to 11.5 g/kg, that is, a degradation of 72.5%. After 120 days of experiment, the percentage of contaminant decreased to 4.5% and reached 89% of the degradation, that is, only 11% of the value added. This reduction is due to the action of microorganisms, since biodiesel is non-volatile at a temperature of 24 °C, and no contaminant leached through the drainage system of the bioreactor.

3.2. Evaluation of the residual content of experiment *in situ* (field)

Figure 4 shows the residual biodiesel contents at different depths during the period of the field experiment (*in situ*). As in the experiment *ex situ*, the data presented represent a mean of the values obtained at each of the depths analyzed.

Figure 4 shows that the lowest residual pollutant results during the experiment period were observed at depth 1 (NA.D1). The contaminant content at 15 days was 32 g/kg for depth 1 and 35 g/kg for depths 2 and 3. These values are below the 40 g/kg initially used in the experiment, representing an average reduction of 16% in the initial contamination. It should be noted that the field experiment was set up in January, the hottest month in the Southern Hemisphere, with an average temperature of 22.1 °C, but average maximum of 28 °C. Another fact that should be mentioned is that during the first 15 days of the experiment, no rainfall occurred. Therefore, the environmental conditions of the first 15 days of the experiment were very similar to those that occurred in the laboratory.

Between 15 and 30 days of the experiment, a 32 mm rainfall with several cloudy days and below-average temperature was observed. This rainfall and temperature influ-

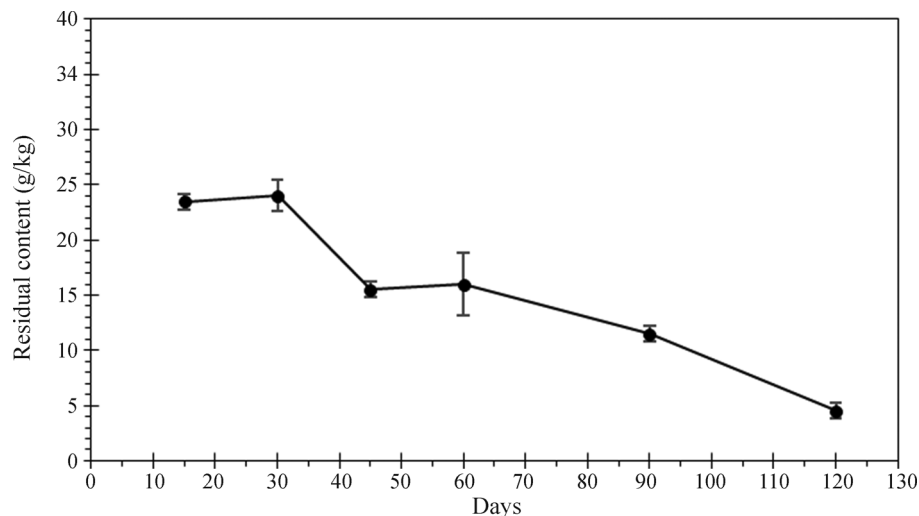


Figure 4 - Average residual biodiesel content at different depths for the field experiment.

enced greatly the results of residual content. Fig. 4 shows that at depth 1, the mean value was 30 g/kg, which is very close to that obtained at 15 days. At depth 2, the mean value was 45 g/kg, and at depth 3, the mean residual value was 42 g/kg. These values above the value initially added indicate that biodiesel leaching occurred from the upper to the lower layers. This finding becomes acceptable when we observed that the residual contents at depths 2 (NA.D2) and 3 (NA.D3), up to the 60 days of experiment, increased gradually, reaching values of 65 g/kg. It is noteworthy that, in this period, there was a total rainfall of 155 mm. A factor that draws attention is that at depth 1, the residual value remained practically constant at the measured points. We concluded that this occurred because the guide tubes were placed for sample removal, and these tubes were closed with a cap to prevent the entry of animals. This may have influenced the volume of water entering these depths, not changing the residual value. A significant decrease in contaminant was observed at this depth, reducing to 14 g/kg at 90 days and to 12 g/kg at 120 days.

The final contents observed in the experiment were 12 g/kg for depth 1, 31 g/kg for depth 2 and 55.4 g/kg for depth 3. Therefore, it can be concluded that, in a place where natural attenuation is being monitored *in situ*, precautions should be taken to prevent water from entering the soil. This may mask degradation results and, depending on where the sample was taken, it can be concluded that biodegradation has occurred. However, in fact, what occurs is contaminant leaching from upper to lower layers.

To calculate the amount of biodiesel degraded in the *in situ* experiment, the difference in volume of soil at the different depths should be considered. For depth 1 the total residual biodiesel mass was 10 kg (12 g/kg \times dry soil in layer 1), for depth 2 the biodiesel mass was 24 kg (33 g/kg \times dry soil in layer 2) and for depth 3 was 33 kg (55.4 g/kg \times dry soil in layer 3). The total amount of the biodiesel mass at the end of the experiment was 67 kg, *i.e.* 68.7% of the value initially added (97.4 kg). Therefore, it can be stated that the amount of contaminant degraded in the *in situ* experiment was 32%. The amount of contaminant obtained in the drainage liquid was negligible. Probably the geotextile placed as a separator served as a filter element for the biodiesel.

3.3. Comparison of degradation in laboratory and in field

Figure 5 shows the percentages of degradation of biodiesel after 120 days of experiment *ex situ* and *in situ*. By analyzing Fig. 5, the percent degradation in the experiment *ex situ* was 89%, while for the experiment *in situ* was 32%. The degradation in the field was 3 times lower than the laboratory degradation. This finding leads to conclude that the abiotic effects of climate directly affect the efficacy of bioremediation, making the results obtained in the field (*in situ*) worse when compared with laboratory data (*ex*

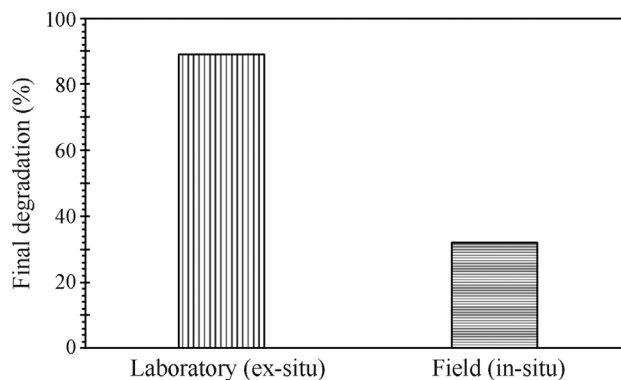


Figure 5 - Percentage degradation after 120 days of experiment *ex situ* and *in situ*.

situ). The control of the entry of water into the soil must occur in *in situ* experiments to avoid problems of erroneous analysis of results. This is because, in the case of installing a monitoring well at a fixed depth, reducing the amount of contaminant in the site can be attributed to biodegradation, whereas in fact it is due to leaching of the contaminant to deeper layers.

4. Conclusions

This study evaluated the difference in behavior of biodegradation in laboratory and in field experiments, considering the moisture and density characteristics of the residual clayey soil. From the results obtained, it was possible to reach the following conclusions:

- The conduction of the experiment in laboratory provided better results of biodegradation, since it is possible to perform an effective control of abiotic factors, such as temperature, humidity and pH. However, these results are not representative of the actual behavior in the field.
- The field experiment allowed identifying the migration and leaching of the contaminant to lower layers of the reactor, since there was a considerable reduction in the volume of contaminant in the top soil and a progressive increase in the contaminant at lower soil depths.
- At the end of the experiment, the total contaminant reduction in the field was 3 times lower than the contaminant reduction in laboratory. This leads to the conclusion that abiotic factors directly influence the efficiency of bioremediation, especially the natural attenuation.
- Waterproofing the soil surface is suggested in places where natural attenuation monitoring is carried out *in situ* to avoid leaching, thus preventing an erroneous analysis of biodegradation.

Acknowledgments

The authors would like to thank the CNPq (grants number 400646/2014-5 and 307020/2017-7), the FAPERGS, and CAPES for the fellowships and financial support granted to the research group.

References

- Agnello, A.C.; Bagard, M.; Van Hullebusch, E.D.; Esposito, G. & Huguenot, D. (2016). Comparative bioremediation of heavy metals and petroleum hydrocarbons co-contaminated soil by natural attenuation, phytoremediation, bioaugmentation and bioaugmentation-assisted phytoremediation". *Science of the Total Environment*, 563-564(1):693-703.
- Aktas, D.F.; Lee, J.S.; Little, B.J.; Ray, R.I.; Davidova, I.A.; Lyles, C.N. & Suflita, J.M. (2010). Anaerobic metabolism of biodiesel and its impact on metal corrosion. *Energy and Fuels*, 24 (5) 2924-2928.
- ASTM (2014). Standard Test Methods for Moisture, Ash, and Organic Matter of Peat and Other Organic Soils - D2974-14. ASTM International, West Conshohocken, PA, USA, 4 p.
- ASTM (2017a). Standard Test Methods for Particle-Size Distribution (Gradation) of Soils Using Sieve Analysis - D6913/D6913M-17. ASTM International, West Conshohocken, PA, USA, 34 p.
- ASTM (2017b). Standard Test Methods for Determining the Amount of Material Finer than 75- μ m (No. 200) Sieve in Soils by Washing - D1140-17. ASTM International, West Conshohocken, PA, USA, 6 p.
- ASTM (2017c). Standard Test Method for Particle-Size Distribution (Gradation) of Fine-Grained Soils Using the Sedimentation (Hydrometer) Analysis - D7928-17. ASTM International, West Conshohocken, PA, USA, 25 p.
- ASTM (2017d). Standard Test Methods for Liquid Limit, Plastic Limit, and Plasticity Index of Soils - D4318-17e1. ASTM International, West Conshohocken, PA, USA, 20 p.
- ASTM (2017e). Standard Test Method for Density of Soil in Place by the Drive-Cylinder Method - D2937-17e2. ASTM International, West Conshohocken, PA, USA, 8 p.
- ASTM (2017f). Standard Practice for Classification of Soils for Engineering Purposes (Unified Soil Classification System) - D2487-17. ASTM International, West Conshohocken, PA, USA, 10 p.
- ASTM (2018a). Standard Test Methods for Laboratory Determination of Density (Unit Weight) of Soil Specimens - D7263-09(2018). ASTM International, West Conshohocken, PA, USA, 7 p.
- ASTM (2018b). Standard Test Methods for pH of Soils - D4972-18. ASTM International, West Conshohocken, PA, USA, 6 p.
- ASTM (2018c). Standard Test Method for Measuring the Exchange Complex and Cation Exchange Capacity of Inorganic Fine-Grained Soils - D7503-18. ASTM International, West Conshohocken, PA, USA, 5 p.
- ASTM (2019). Standard Test Methods for Laboratory Determination of Water (Moisture) Content of Soil and Rock by Mass - D2216-19. ASTM International, West Conshohocken, PA, USA, 7 p.
- Azubuike, C.C.; Chikere, C.B. & Okpokwasili, G.C. (2016). Bioremediation techniques-classification based on site of application: principles, advantages, limitations and prospects. *World Journal of Microbiology and Biotechnology* 32(180):1-18.
- Bento, F.M.; Camargo, F.A.O.; Okeke, B.C. & Frankenberg, W.T. (2005). Comparative bioremediation of soils contaminated with diesel oil by natural attenuation, biostimulation and bioaugmentation. *Bioresource Technology*, 96:1049-1055.
- Borges, J.M.; Dias, J.M. & Danko, A.S. (2014). Influence of the anaerobic biodegradation of different types of biodiesel on the natural attenuation of benzene. *Water, Air and Soil Pollution*, 2146:1-10.
- Cecchin, I.; Reginatto, C.; Thomé, A.; Colla, L.M. & Reddy, K.R. (2016). Influence of physicochemical factors on biodiesel retention in clayey residual soil. *Journal of Environmental Engineering (New York)*, 142(4): 04015093.
- Corseuil, H.X.; Monier, A.L.; Gomes, A.P.N.; Chiaranda, H.S.; Rosario, M.D. & Alvarez, P.J.J. (2011). Biodegradation of soybean and castor oil biodiesel: implications on the natural attenuation of monoaromatic hydrocarbons in groundwater. *Ground Water Monitoring and Remediation*, 31:111-118.
- Das, N. & Chandran P. (2011). Microbial degradation of petroleum hydrocarbon contaminants: An overview. *Biotechnol. Res. Int.*, 2011:941810.
- Decesaro, A.; Rampel, A.; Machado, T.S.; Thomé A.; Reddy, K.R.; Margarites, A.C. & Colla, L.M. (2017). Bioremediation of soil contaminated with diesel and biodiesel fuel using biostimulation with microalgae biomass. *Journal of Environmental Engineering*, 143(4):04016091.
- Declercq, I.; Cappuyns, V. & Duclos, Y. (2012) Monitored natural attenuation (MNA) of contaminated soils: State of the art in Europe - A critical evaluation. *Science of the Total Environment* 426:393-405.
- DeMello, J.A.; Carmichael, C.A.; Peacock, E.E.; Nelson, R.K.; Arey, J.S. & Reddy, C.M. (2007). Biodegradation and environmental behavior of biodiesel mixtures in the sea: an initial study. *Marine Pollution Bulletin*, 54:894-904.
- Dott, W.; Feidieker, D.; Steiof, M.; Becker, P.M. & Kämpfer, P. (1995). Comparison of ex situ and in situ techniques for bioremediation of hydrocarbon-polluted soils. *International Biodeterioration & Biodegradation*, 16:301-313.
- Empresa Brasileira de Pesquisa Agropecuária (EMBRAPA). (2018) Laboratório de Agrometeorologia. Disponível em: <http://www.cnpt.embrapa.br/pesquisa/agromet/app/principal/agromet.php>.

- EPA, Environmental Protection Agency (1999). Use of monitored natural attenuation at superfund, RCRA corrective action, and underground storage tank sites. OSWER Dir. 1-32.
- Foon, C.S.; Liang, Y.C.; Dian, N.L.H.M.; May, C.Y.; Hock, C.C. & Ngan, M.A. (2006) Crystallisation and melting behavior of methyl esters of palm oil. *American Journal of Applied Sciences*, 3(5):1859-1863.
- Frutos F.J.G.; Pérez, R.; Escolano, O.; Rubio, A.; Gimeno, A.; Fernandez, M.D.; Carbonell, G.; Perucha, C. & Laguna, J. (2012). Remediation trials for hydrocarbon-contaminated sludge from a soil washing process: evaluation of bioremediation technologies. *Journal of Hazardous Materials*, 199:262-271.
- Guarino, C.; Spada, V. & Sciarrillo, R. (2017). Assessment of three approaches of bioremediation (natural attenuation, landfarming and bioaugmentation - assisted landfarming) for a petroleum hydrocarbons contaminated soil. *Chemosphere* 170:10-16.
- Knothe, G.; Gerpen, J.V. & Krahl, J. (2005). *The Biodiesel Handbook*. 1st Edition Champaign, Illinois, Ed. AOCS, 286 p.
- Krop, H.B.; Velzen, M.J.M.V.; Parsons, J.R. & Govers, H.A.J. (1997). n-Octanol-water partition coefficients, aqueous solubilities and Henry's Law constants of fatty acid esters. *Chemosphere*, 34(1):107-119.
- Mariano, A.P.; Tomasella, R.C.; Oliveira, L.M.; Contiero, J. & Angelis, D.F. (2008). Biodegradability of diesel and biodiesel blends. *African Journal of Biotechnology*, 7(9):1323-1328.
- Meneghetti, L.R.R.; Thomé, A.; Schnaid, F.; Prietto, P.D.M. & Cavellão, G. (2012). Natural attenuation and biostimulation of biodiesel contaminated soils from Southern Brazil with different particle sizes. *Journal of Environmental Science and Engineering B*, 1:155-162.
- Mulligan, C.N. & Yong, R.N. (2004). Natural attenuation of contaminated soils. *Environ. Int.*, 30:587-601.
- NIST, National Institute of Standards and Technology (2018). 9,12-Octadecadienoic acid (Z,Z)-, methyl ester. Available in: <http://webbook.nist.gov/cgi/cbook.cgi?ID=112-63-0&Units=SI&cMS=on>.
- Owsianiak, M.; Chrzanowski, L.; Szulc, A.; Staniewski, J.; Olszanowski, A.; Olejnik-Schmidt, A.K. & Heipieper, H.J. (2009). Biodegradation of diesel/biodiesel blends by a consortium of hydrocarbon degraders: effect of the type of blend and the addition of biosurfactants. *Bioresource Technology*, 100:1497-1500.
- Pasqualino, J.C.; Montané, D. & Salvadó, J. (2006). Synergic effects of biodiesel in the biodegradability of fossil-derived fuels. *Biomass and Bioenergy*, 30(10):874-879.
- Ramos, D.T.; Silva, M.L.B.D.; Chiaranda, H.S.; Alvarez, P.J.J. & Corseuil, H.X. (2013). Biostimulation of anaerobic BTEX biodegradation under fermentative methanogenic conditions at source-zone groundwater contaminated with a biodiesel blend (B20). *Biodegradation*, 24:333-341.
- Science Lab. Com - Chemicals and Laboratory Equipment (2018). Material Safety Data Sheet, available in http://www.sciencelab.com/xMSDS-Methyl_linolenate-8363.
- Sendzikiene, E.; Makareviciene, V.; Janulis, P. & Makareviciute, D. (2007). Biodegradability of biodiesel fuel of animal and vegetable origin. *European Journal of Lipid Science and Technology*, 109:493-497.
- Sihag, S.; Pathak, H. & Jaroli, D.P. (2014). Factors affecting the rate of biodegradation of polyaromatic hydrocarbons. *Int. J. Pure App. Biosci.* 2:185-202.
- Silva, M.L.B. & Corseuil, H.X. (2012). Groundwater microbial analysis to assess enhanced BTEX biodegradation by nitrate at a gasohol-contaminated site. *International Biodeterioration & Biodegradation*, 67:21-27.
- Smith, E.; Thavamani, P.; Ramadass, K.; Naidu, R.; Srivastava, P. & Megharaj, M. (2015). Remediation trials for hydrocarbon-contaminated soils in arid environments: Evaluation of bioslurry and biopiling techniques. *Int Biodeterior Biodegradation* 101:56-65.
- Sorensen, G.; Pedersen, D.V.; Norgaard, A.K.; Sorensen, K.B. & Nygaard, S.D. (2011). Microbial growth studies in biodiesel blends. *Bioresource Technology*, 102:5259-5264.
- Streck, E.V.; Kämpf, N.; Dalmolin, R.S.D.; Klamt, E.; Nascimento, P.C.; Schneider, P.; Giasson, E. & Pinto L.F.S. (2008). *Soils From RS-Brazil*. 2nd ed. Emater, Porto Alegre, 222 p. (in Portuguese)
- TGSC, The Good Scents Company (2018). Available in <http://www.thegoodscentscompany.com/data/rw1477771.html>.
- Thomé, A.; Cecchin, I.; Reginatto, C.; Colla, L.M. & Reddy, K.R. (2017). Biostimulation and rainfall infiltration: influence on retention of biodiesel in residual clayey soil. *Environmental Science and Pollution Research International*, 24:9594-9604.
- Thomé, A.; Reginatto, C.; Cecchin, I. & Colla, L.M. (2014). Bioventing in a residual clayey soil contaminated with a blend of biodiesel and diesel oil. *Journal of Environmental Engineering*, 140(11):06014005.
- TOXNET, Toxicology Data Network (2018). Hazardous Substances Data Bank, available in <http://toxnet.nlm.nih.gov/cgi-bin/sis/htmlgen?HSDB>.
- USEPA, United States Environmental Protection Agency (2016). Method 3550 C: Ultrasonic Extraction, available in <https://www.epa.gov/sites/production/files/2015-12/documents/3550c.pdf>.
- Von Wedel, R. (1999). *Technical Handbook for Marine Biodiesel*. 2nd ed. National Renewable Energy Laboratory, U.S. Department of Energy.

Dynamic Cone Penetrometer (DCP) Relative Density Correlations for Sands

C.J. MacRobert, G.S. Bernstein, M.M. Nchabeleng

Abstract. The dynamic cone penetrometer (DCP) is a widely used in-situ device to determine the engineering properties of soils. This paper reports a meta-analysis of laboratory calibration studies to establish a relationship between the rate of penetration and relative density for sands. Fourteen (14) different sands from different geographic and geological settings are compared. A direct relationship between the rate of penetration and relative density is proposed with a standard error in relative density predictions of 11%. A relationship incorporating the sand's median particle size is also proposed with a standard error in relative density predictions of 9%. Whilst there is good agreement between most of these studies, local conditions should be considered before adopting a proposed correlation in engineering design.

Keywords: Dynamic Cone Penetrometer (DCP), Dynamic Penetration Index (*DPI*), poorly graded sandy soil (SP), Relative Density (D_r), well graded sands (SW).

1. Introduction

The manner in which a site investigation is carried out is dictated by the cost and importance of the intended work. For many daily soil mechanics problems a simple *in-situ* test is required. These problems may include determining whether shallow or deep foundations are required, estimating allowable bearing capacities and predicting whether excessive settlements are likely. Sanglerat (1976) suggested that in many of these cases a simple static-dynamic test is suitable. One such test is the Dynamic Cone Penetrometer (DCP), a light hand operated device, in which a cone tipped rod is driven into the ground by the repetitive impact of a falling hammer.

Various standards exist for carrying out the DCP, however the same theoretical maximum specific energy is imparted per blow for most standards (Table 1). Little research has been undertaken to examine actual energies imparted by different arrangements. The efficiency of the DCP system will be influenced by user efficiency, rod length, rod weight, cone geometry and permanent rod penetration. Ayers (1990), based on California bearing ratio (CBR) correlations, suggested that 30° cones can result in higher penetration rates compared to 60° cones, particularly in dense materials. A more rigorous assessment of DCP efficiencies, as carried out by Odebrecht *et al.* (2005) on the Standard Penetration Test (SPT), would shed greater light on its use.

Results from the test are reported in two ways. The first is to record the number of blows to penetrate a specified depth. Usually this depth is 100 mm and is reported as

an N_{10} value with units of blows. The second approach is to record the depth penetrated by each blow. Typically, this is an average over a representative depth and is reported as a dynamic penetration index (*DPI* or *DN*) with units of mm/blow. The latter approach is more widely used.

Recent work on the SPT (Odebrecht *et al.*, 2005) considering energy measurements and the wave equation (Schmertmann & Palacios, 1979) has resulted in an alternative means to interpret dynamic penetration tests. This method determines the dynamic penetration resistance of respective tests and allows a direct comparison between different tests. This removes the necessity of developing empirical correlations between different tests. Correlations between engineering parameters can then be used irrespective of original test to which parameters were correlated. Schnaid *et al.* (2017) presented data showing the promising direct comparisons possible with this approach. The simplicity of the DCP test and dependence of results on user efficiency may preclude such an approach being developed for this test, however, it would be the most rigorous. Consequently, direct empirical relationships are likely to remain the state of practice for some time to come.

Various researchers have attempted to develop direct empirical relationships between DCP results and engineering parameters (Table 2). The DCP was originally developed as a tool for road design (Scala, 1956). Consequently, it is widely accepted for pavement design, particularly to determine California bearing ratio (CBR) values. Soils making up pavements are compacted heavily in thin layers resulting in heavily overconsolidated soils. Natural soils exist at a much wider range of densities limiting the DCP's

Charles John MacRobert, Ph.D., Senior Lecturer, Department of Civil Engineering, Stellenbosch University, Stellenbosch 7600, South Africa, e-mail: macrobert@sun.ac.za.
Greggory Sean Bernstein, Graduate Student, School of Civil and Environmental Engineering, University of the Witwatersrand, Johannesburg, South Africa, e-mail: 830328@students.wits.ac.za.
Mokgadi Mahlatse Nchabeleng, Graduate Student, School of Civil and Environmental Engineering, University of the Witwatersrand, Johannesburg, South Africa, e-mail: 1481246@students.wits.ac.za.
Submitted on November 30, 2018; Final Acceptance on May 14, 2019; Discussion open until December 31, 2019.
DOI: 10.28927/SR.422201

Table 1 - DCP standards.

Standard	Rod diameter (mm)	Cone angle (°)	Cone diameter (mm)	Hammer mass (kg)	Hammer fall (mm)	Specific work per blow [#] (kJ/m ²)
ASTM (2003)	16	60	20	8	575	144
Australian	16	30	20	9	510	143
South African	16	30	20	10	460	144

[#]Cross sectional area used is the plan area.

Table 2 - DCP correlations proposed in literature.

Correlation	Reference
California bearing ratio	Al-Refeai & Al-Suhaibani (1997); Ese <i>et al.</i> (1994); Gabr <i>et al.</i> (2000); Harison (1989); Kleyn (1975); Livneh (1989); Paige-Green & Pinard (2012); Smith & Pratt (1983); Van Vuuren (1969)
Unconfined compressive strength	De Villiers (1980); McElvaney & Bundadidjatnika (1991)
Standard penetration test	Ampadu <i>et al.</i> (2018); Ibrahim & Nyaoro (2011); Sowers & Hedges (1966)
Stiffness parameters	Alshibli <i>et al.</i> (2005); Lee <i>et al.</i> (2014); Mohammadi <i>et al.</i> (2008); Sawangsuriya & Edil (2005)
Shear strength parameters	Ayers (1990); Hamid (2013); Mohammadi <i>et al.</i> (2008); Rahim <i>et al.</i> (2004)
Density parameters	Azad (2008); Chennarapu <i>et al.</i> (2018); Hamid (2013); Hossain (2009); Katakiya & Parekh (2017); Salgado & Yoon (2003)

applicability in these cases. This paper compares correlations proposed in the literature for determining the relative density of sands. It will be shown that good agreement exists between some studies but not others. This disagreement is shown to be as a result of different grain mineralogy, highlighting the importance of knowing local geology.

2. Relative Density Correlation

The behaviour of non-plastic soils is closely related to relative density (D_r) given by Equation 1 (Holtz & Kovacs 1981):

$$D_r = \frac{e_{\max} - e}{e_{\max} - e_{\min}} \quad (1)$$

where e_{\max} and e_{\min} are reference void ratios determined from minimum and maximum densities respectively, and e is the soil current void ratio.

2.1. Database

A database of studies correlating D_r to either DPI or N_{10} was collected (Table 3). Studies were excluded from the meta-analysis using the following criteria. Firstly, DCP tests had to be carried out according to ASTM (2003). Secondly, tests had to have been done in containers larger than 500 mm. Chamber size relative to probe size, boundary conditions (stress or strain controlled), particle size and relative density all influence the results of chamber based correlations (Schnaid & Houlsby 1991). An explicit assess-

Table 3 - Details of calibration testing.

Study	Details of calibration chamber	Reference void ratio procedure
R1	Air dried sand was placed in a 0.5 m diameter by 1 m high calibration chamber by air pluviation and vibration. The calibration chamber was formed from 13 mm thick steel.	ASTM (2006a) ASTM (2006b)
R2	Air dried sand was placed in a 0.5 m diameter by 1 m high calibration chamber by air pluviation and vibration. The calibration chamber was formed from 13 mm thick steel.	ASTM (2006a) ASTM (2006b)
R3	Air dried sand was placed in a 1.6 m diameter by 1.5 m high calibration chamber by funnel filling, air pluviation and vibration tamping. The calibration chamber was formed from 25 mm thick glass fibre reinforced plastic.	ASTM (2006a) ASTM (2006b)
R4	Air dried sand was placed in a 0.6 m square by 0.75 m high calibration chamber filled by tamping. The calibration chamber was formed from Plexiglas.	IS 2720 (Part 14) - 1983 BIS (1983)
R5	Air dried sand was placed in a 0.7 m diameter by 0.7 m high calibration chamber in 0.1 m lifts and vibration tamping. The calibration chamber was formed from steel.	Not specified.

R1 - Azad (2008), R2 - Hossain (2009), R3 - Hamid (2013), R4 - Katakiya & Parekh (2017), R5 - Mohammadi *et al.* (2008).

ment of chamber effects has not been undertaken for the DCP, however, experimental work by Mohammadi *et al.* (2008) suggested that confining effects are reduced above a diameter of 500 mm or a chamber to probe diameter ratio of 25. Details of container boundary conditions are given in Table 3.

Details of the soils tested are given in Table 4. All soils investigated were non-plastic sands with the percentage of sand ranging between 86 and 100%. Five (5) soils had gravel fractions ranging between 4 and 14% and nine (9) had fines contents ranging between 2 and 8%. Most of the sands were poorly graded with three (3) being well graded. Particle size can have an influence on penetration results, with gravel particles in particular, potentially impeding the probe. This can result in high blow counts that are not representative of the overall consistency of the deposit. The influence of median particle size is therefore explored in this paper.

2.2. Correlation

2.2.1. Overall correlation

Data from the first four studies is plotted in Fig. 1. A logarithmic trend line was found to fit best. The average coefficient of determination (R^2) for individual data sets was on average 0.97 and the average standard error in D_r estimates for individual data sets was 3%. It is apparent that very accurate relationships between DPI and D_r can be obtained for particular sands. The best-fit line (solid line in

Fig. 1) through the entire dataset resulted in an R^2 value of 0.7 and a standard error in D_r estimates of 11% (dashed lines in Fig. 1).

Tavenas & La Rochelle (1972) estimated that the error of determining relative density was in the order of 10-22%. The error in the best-fit line is within this suggested range, suggesting that D_r estimates from DPI are within expected accuracies. It must be kept in mind that this error is based on tests done under laboratory conditions and field conditions may result in substantially larger errors. Further, the regression analysis predicts $D_r > 100\%$ for $DPI < 10$ mm/blow. This is an artefact of the statistical analysis as well as inherent error in the DCP and D_r . Practitioners using this relationship should therefore place greater emphasis on the range of D_r values predicted than the specific D_r value predicted. The DCP should only be used to obtain a qualitative estimate of relative density.

2.2.2. Influence of particle size

Some authors (Hossain 2009; Lee *et al.*, 2014) have suggested the influence of particle size can be incorporated by including the median particle size (D_{50}) as an additional prediction variable. Including D_{50} as a regression variable did result in a marginally better fit to the data (Fig. 2). For this regression an R^2 value of 0.8 and a standard error in D_r estimates of 9% were obtained. The suitability of this relationship for field use is limited as D_{50} requires laboratory determination.

Table 4 - Details of non-plastic soils.

Study	Soil names	Gravel (%)	Sand (%)	Fines ¹ (%)	C_u ²	C_c ³	D_{50} ⁴ (mm)	USCS ⁶	e_{max}	e_{min}
R1	Jamuna sand	0	95	5	2.2	1.3	0.20	SP	1.20	0.57
	Sylhet sand	0	100	0	3.2	1.1	0.50	SP	0.84	0.54
R2	Medium sand	0	100	0	2.9	1.1	0.47	SP	1.23	0.56
	Fine sand	0	100	0	2.0	0.8	0.27	SP	1.21	0.56
R3	Dune sand (1% silt)	0	99	1	2.0	0.9	0.27 ⁵	SP	0.68	0.48
	Dune sand (4% silt)	0	96	4	NP	NP	NP	SP	0.66	0.41
	Dune sand (8% silt)	0	92	8	NP	NP	NP	SP	0.63	0.33
R4	Khanpur sand	6	94	0	3.3	1.2	2.24 ⁵	SP	0.60	0.39
	Sevaliya sand	4	93	3	2.6	0.8	0.79 ⁵	SP	0.63	0.38
	Ahmedabad sand	0	95	5	2.2	1.1	0.30 ⁵	SP	0.71	0.56
	Combo 1	14	86	0	6.1	1.0	1.60 ⁵	SW	0.48	0.22
	Combo 2	9	88	3	9.4	1.0	1.31 ⁵	SW	0.51	0.20
	Combo 3	11	87	2	6.5	1.0	1.42 ⁵	SW	0.47	0.17
R5	Terrace deposits	0	98	2	1.2	1.0	0.17	SP	0.97	0.46

R1 - Azad (2008), R2 - Hossain (2009), R3 - Hamid (2013), R4 - Katakia & Parekh (2017), R5 - Mohammadi *et al.* (2008).

¹Passing 0.075 mm sieve. ² $C_u = D_{60}/D_{30}$. ³ $C_c = D_{30}^2/(D_{10} \times D_{60})$. ⁴Particle size at percentage passing shown by subscript. ⁵Interpolated from D_{60} and D_{30} . ⁶Unified Soil Classification System ASTM (2017).

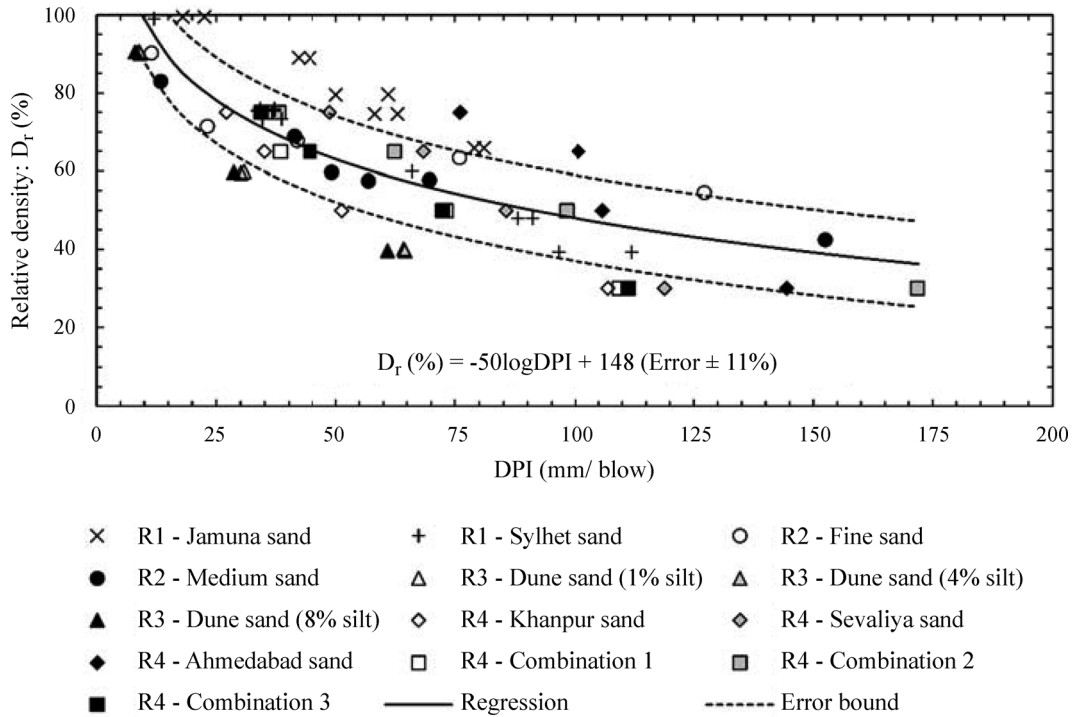


Figure 1 - DPI vs. D_r relationship.

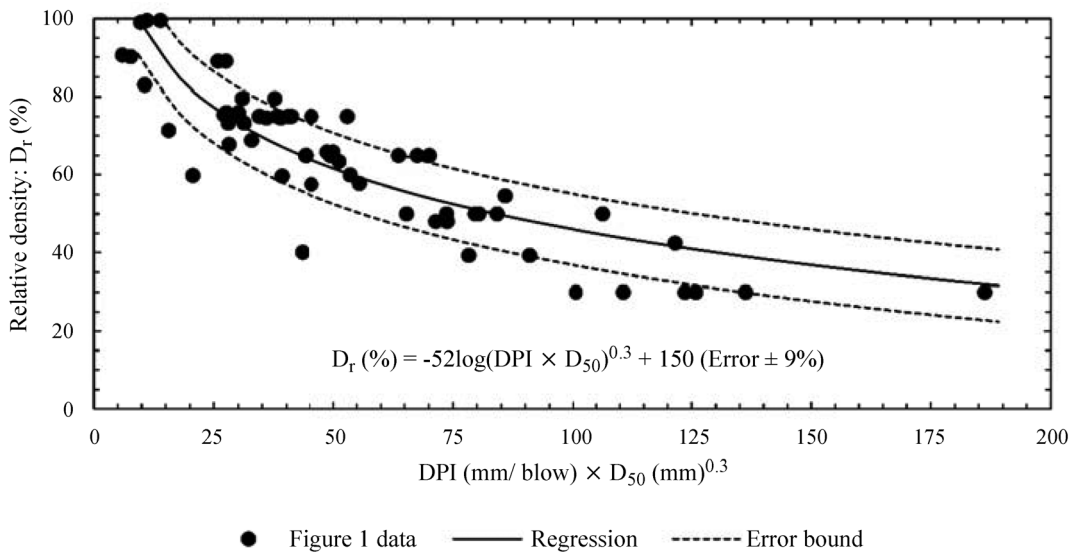


Figure 2 - DPI and D_{50} vs. D_r relationship.

Azad (2008) suggested that the fines content can be included to improve predictions. However, considering R1 – Jamuna sand, R3 – Dune sand (8% silt) and R4 – Ahmedabad sand in Fig. 1 it is evident that fines content does not have a consistent influence on D_r values at a given DPI value. Including fines content in the regression model did not improve the accuracy of predictions. Further, the influence of small fractions of gravel particles on DPI (see R4 – Khanpur sand, R4 – Sevaliya sand, R4 – Combo 1, R4 –

Combo 2 and R4 – Combo 3 in Fig. 1) appeared to be limited.

2.2.3. Influence of mineralogy

Data set R5 reported by Mohammadi *et al.* (2008) is compared to the entire data set in Fig. 3. Despite the sand tested by Mohammadi *et al.* (2008) having similar particles sizes to the other data, statistical testing shows the probability of the data set falling within the larger data set is less

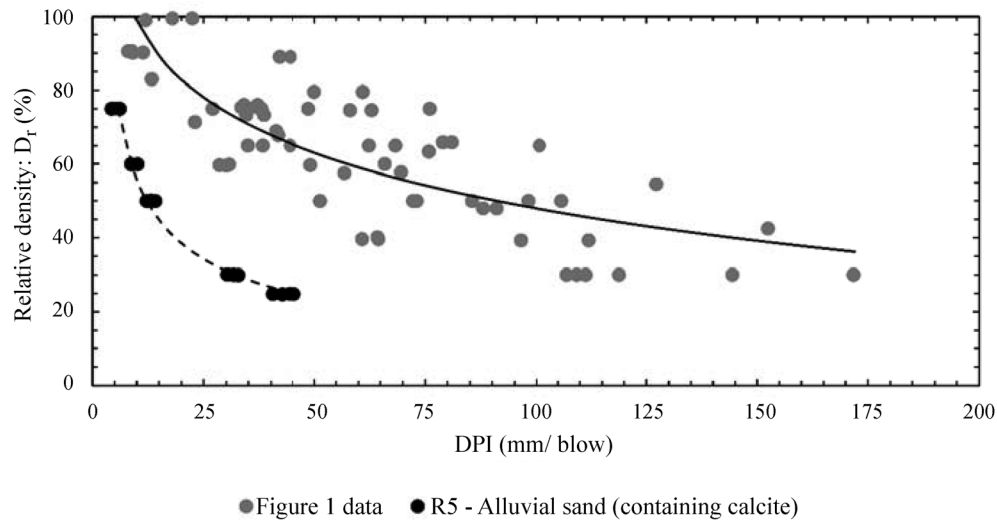


Figure 3 - Comparison of regression model to sands containing calcite.

than 0.005. According to Mohammadi *et al.* (2008), X-ray analysis has shown that the sandy samples are made of quartz, feldspar, pyroxene and calcite. It is known that calcite grains are prone to crushing during driving resulting in variable strengths (Murff, 1987; Sterianos, 1988). It is suggested that calcite crushing may be responsible for the lower DPI values reported by Mohammadi *et al.* (2008) at equivalent D_r values. Practitioners therefore need to take careful consideration of the mineralogy of sands before using correlations suggested in the literature.

3. Conclusions

A correlation was proposed between dynamic cone penetrometer penetration rates and relative density for sands. The correlation was based on testing reported in literature on thirteen (13) different sands from different geographic and geological settings. The standard error in relative density predictions was found to be 11%. Using the same database, a second correlation was proposed that incorporates the median particle size as a measure of particle size effects. The standard error in relative density predictions for this second correlation was found to be 9%.

One data set was found to be statistically inconsistent with the larger database. For this data set, penetration rates were consistently lower at equivalent relative densities. This is likely a consequence of the presence of calcite grains, which are known to be crushable. This data set was therefore excluded from the regression analysis. Local conditions should always be considered before adopting a proposed correlation in engineering design.

References

- Al-Refeai, T. & Al-Suhaibani, A. (1997). Prediction of CBR using dynamic cone penetrometer. *Journal of King Saud University-Engineering Sciences*, 9(2):191-203.
- Alshibli, K.A.; Abu-Farsakh, M. & Seyman, E. (2005). Laboratory evaluation of the geogauge and light falling weight deflectometer as construction control tools. *Journal of Materials in Civil Engineering*, 17(5):560-569.
- Ampadu, S.I.K.; Ayeh, F.F.J. & Boadu, F. (2018). Deriving SPT N-Values from DCP test results: The case of foundation design in a tropical environment. *Geotechnical and Geological Engineering*, 36(4):2517-2531.
- ASTM (2003). Standard Test Method for Use of the Dynamic Cone Penetrometer in Shallow Pavement Applications - D6951-03. ASTM International, West Conshohocken, PA, USA, 7 p.
- ASTM (2006a). Standard Test Methods for Maximum Index Density and Unit Weight of Soils Using a Vibratory Table - D4253-06. ASTM International, West Conshohocken, PA, USA, 15 p.
- ASTM (2006b). Standard Test Methods for Minimum Index Density and Unit Weight of Soils and Calculation of Relative Density - D4254-06. ASTM International, West Conshohocken, PA, USA, 9 p.
- ASTM (2017). Standard Practice for Classification of Soils for Engineering Purposes (Unified Soil Classification System) - D2487-17. ASTM International, West Conshohocken, PA, USA, 10 p.
- Ayers, M.E. (1990). Rapid Shear Strength Evaluation of in situ Granular Materials Utilizing the Dynamic Cone Penetrometer. PhD Thesis, University of Illinois at Urbana-Champaign, Urbana, Illinois.
- Azad, A.K. (2008). Development of Correlation Between Dynamic Cone Resistance and Relative Density of Various Sands. Masters Dissertation, Bangladesh University of Engineering and Technology, Dhaka, Bangladesh.
- BIS (1983). Methods of Test for Soils, Part 14 Determination of Density Index (Relative Density) of Cohesion-

- less Soils (IS 2720 (Part 14)). Bureau of Indian Standards, New Delhi, India.
- Chennarapu, H.; Garala, T.K.; Chennareddy, R.; Balunaini, U. & Venkata Narasimha Reddy, G. (2018). Compaction quality control of earth fills using dynamic cone penetrometer. *Journal of Construction Engineering and Management*, 144(9):04018086.
- De Villiers, P.J. (1980). Dynamic cone penetrometer correlation with unconfined compressive strength. University of Pretoria, Pretoria, South Africa.
- Ese, D.; Myre, J.; Noss, P. & Vaernes, E. (1994). The use of dynamic cone penetrometer (DCP) for road strengthening design in Norway. Proc., 4th International Conference on Bearing Capacity of Roads and Airfields, pp. 3-22.
- Gabr, M.A.; Hopkins, K.; Coonse, J. & Hearne, T. (2000). DCP criteria for performance evaluation of pavement layers. *Journal of Performance of Constructed Facilities*, 14(4):141-148.
- Hamid, A.M.A. (2013). Assessment of Density and Shear Strength of Eastern Saudi Sands Using Dynamic Cone Penetration Testing (DCPT). Masters Dissertation, King Fahd University of Petroleum and Minerals, Dhahran, Saudi Arabia.
- Harison, J.A. (1989). In situ CBR determination by DCP testing using a laboratory-based correlation. *Australian Road Research*, 19(4):313-317.
- Holtz, R.D. & Kovacs, W.D. (1981). *An Introduction to Geotechnical Engineering*. Prentice Hall, New Jersey.
- Hossain, M.S. (2009). Determination of Relative Density of Sands Using Dynamic Cone Resistance Data. Masters Dissertation, Bangladesh University of Engineering and Technology, Dhaka, Bangladesh.
- Ibrahim, M. & Nyaoro, D.L. (2011). Correlations of DCPT and SPT for analysis and design of foundations. Proc. 15th African Regional Conference on Soil Mechanics and Geotechnical Engineering, IOS Press, pp. 632-637.
- Katakiya, M.P. & Parekh, A.D. (2017). Effect of gradation and particle size on correlations between DCP Index (ASTM D6951 - 03) and relative density for sand. Proc. ICRISSET2017, pp. 185-191.
- Kleyn, *e.g.* (1975). *The Use of the Dynamic Cone Penetrometer (DCP)*. Transvaal Provincial Administration, Pretoria, South Africa.
- Lee, C.; Kim, K.-S.; Woo, W. & Lee, W. (2014). Soil stiffness gauge (SSG) and dynamic cone penetrometer (DCP) tests for estimating engineering properties of weathered sandy soils in Korea. *Engineering Geology*, 169:91-99.
- Livneh, M. (1989). Validation of correlations between a number of penetration tests and in situ California bearing ratio tests. *Transportation Research Record*, 1219:56-67.
- McElvaney, J. & Bundadidjatnika, I.R. (1991). Strength evaluation of lime-stabilised pavement foundations using the dynamic cone penetrometer. *Australian Road Research*, 21(1):40-52.
- Mohammadi, S.D.; Nikoudel, M.R.; Rahimi, H. & Khamchian, M. (2008). Application of the dynamic cone penetrometer (DCP) for determination of the engineering parameters of sandy soils. *Engineering Geology*, 101(3):195-203.
- Murff, J.D. (1987). Pile capacity in calcareous sands: state of the art. *Journal of Geotechnical Engineering*, 113(5):490-507.
- Odebrecht, E.; Schnaid, F.; Rocha, M.M. & Bernardes, G.d.P. (2005). Energy Efficiency for Standard Penetration Tests. *Journal of Geotechnical and Geoenvironmental Engineering*, 131(10):1252-1263.
- Paige-Green, P. & Pinard, M.I. (2012). Optimum design of sustainable sealed low volume roads using the dynamic cone penetrometer (DCP). Proc. 25th ARRB Conference: Shaping the future: Linking policy, research and outcomes, ARRB Group Ltd, pp. 1-11.
- Rahim, A.; Prasad, S. & George, K. (2004). Dynamic cone penetration resistance of soils - Theory and evaluation. *Geotechnical Engineering for Transportation Projects*, ASCE, pp. 1755-1766.
- Salgado, R. & Yoon, S. (2003). Dynamic Cone Penetration Test (DCPT) for Subgrade Assessment. Indiana Department of Transportation and the U.S. Department of Transportation Federal Highway Administration West Lafayette, Indiana.
- Sanglerat, G. (1976). The static-dynamic penetrometer - why not? *Ground Engineering*, 9(6):2.
- Sawanguriya, A. & Edil, T.B. (2005). Evaluating stiffness and strength of pavement materials. Proceedings of the Institution of Civil Engineers-Geotechnical Engineering, 158(4):217-230.
- Scala, A.J. (1956). Simple methods of flexible pavement design using cone penetrometers. Proc. Second Australian Soil Mechanics Conference, New Zealand Engineer, pp. 34-44.
- Schmertmann, J.H. & Palacios, A. (1979). Energy dynamics of SPT. *Journal of the Geotechnical Engineering Division*, 105(8):909-926.
- Schnaid, F. & Houlsby, G.T. (1991). An assessment of chamber size effects in the calibration of in situ tests in sand. *Géotechnique*, 41(3):437-445.
- Schnaid, F.; Lourenço, D. & Odebrecht, E. (2017). Interpretation of static and dynamic penetration tests in coarse-grained soils. *Géotechnique Letters*, 7(2):113-118.
- Smith, R.B. & Pratt, D.N. (1983). A field study of in situ California bearing ratio and dynamic cone penetrometer testing for road subgrade investigations. *Australian Road Research*, 13(4):285-293.
- Sowers, G. & Hedges, C. (1966). Dynamic cone for shallow in-situ penetration testing. Vane shear and cone penetration resistance testing of in-situ soils. ASTM In-

- ternational, West Conshohocken, Pennsylvania, pp. 29-38.
- Sterianos, B. (1988). Geotechnical Properties of Carbonate Soils with Reference to an Improved Engineering Classification. Masters Dissertation, University of Cape Town, Cape Town.
- Tavenas, F. & La Rochelle, P. (1972). Accuracy of relative density measurements. *Géotechnique*, 22(4):549-562.
- Van Vuuren, D.J. (1969). Rapid determination of CBR with the portable dynamic cone penetrometer. *The Rhodesian Engineer*, 7(5):852-854.

SOILS and ROCKS

An International Journal of Geotechnical and Geoenvironmental Engineering

Publication of

ABMS - Brazilian Association for Soil Mechanics and Geotechnical Engineering

SPG - Portuguese Geotechnical Society

Volume 42, N. 2, May-August 2019

Author index

Andreyko, S.S.	77	Lyalina, T.A.	77
Araújo, G.L.S.	3	MacRobert, C.J.	201
Barreto, G.A.	21	Massad, F.	179
Benetti, M.	83	Matos, Y.M.P.	21
Bernstein, G.S.	201	Menezes, L.C.P.	31
Boszczowski, R.B.	139	Nchabeleng, M.M.	201
Bressani, L.A.	99	Neto, S.A. Dantas	21
Camapum de Carvalho, J.C.	61	Oliveira Júnior, A.I.	127
Carvalho, L.O.	167	Passini, L.B.	139
Cecchin, I.	193	Pierozan, R.C.	3
Consoli, N.C.	83	Pulko, B.	93
El Kahi, E.	155	Querelli, A.	179
Ferreira, G.C.S.	117	Rebolledo, J.F.R.	61
Ferreira, J.A.	127	Reginato, C.	193
Ferreira, S.R.M.	31	Ribeiro, D.B.	167
Festugato, L.	43	Sarro, W.S.	117
Fiori, A.P.	139	Siacara, A.T.	43
González, A.A.M.	139	Silvani, C.	83
Guilherme, L.C.	127	Sousa, D.B.	31
Jucá, J.F.T.	127	Sukar, S.F.	31
Khoury, M.	155	Teixeira, C.A.	3
Kormann, A.C.M.	139	Teixeira, S.H.C.	3
León, R.F.P.	61	Thomé, A.	193
Logar, J.	93	Trentin, A.W.S.	193
		Xavier, S.C.	99



Geotechnic and Rehabilitation

TEIXEIRA DUARTE ENGENHARIA E CONSTRUÇÕES, S.A.

- **Head Office**
Lagoas Park – Edifício 2
2740-265 Porto Salvo - Portugal
Tel.: [+351] 217 912 300
Fax: [+351] 217 941 120/21/26
- **Algeria**
Parc Miremont – Rua A, Nº136 - Bouzareah
16000 Alger
Tel.: [+213] 219 362 83
Fax: [+213] 219 365 66
- **Spain**
Avenida Alberto Alcocer, nº24 – 7º C
28036 Madrid
Tel.: [+34] 915 550 903
Fax: [+34] 915 972 834
- **Angola**
Alameda Manuel Van Dunen 316/320 - A
Caixa Postal 2857 - Luanda
Tel.: [+34] 915 550 903
Fax: [+34] 915 972 834
- **Brazil**
Rua Iguatemi, nº488 – 14º - Conj. 1401
CEP 01451 - 010 - Itaim Bibi - São Paulo
Tel.: [+55] 112 144 5700
Fax: [+55] 112 144 5704
- **Mozambique**
Avenida Julyus Nyerere, 130 – R/C
Maputo
Tel.: [+258] 214 914 01
Fax: [+258] 214 914 00

BUILDING A BETTER WORLD



TPF

PLANEGE CENOR



Engineering and Architectural Consultancy

Geology, Geotechnics, Supervision of Geotechnical Works
Embankment Dams, Underground Works, Retaining Structures
Special Foundations, Soil Improvement, Geomaterials



MEMBER OF

TPF

www.tpfplanegecenor.pt



- > **Prospecção Geotécnica**
Site Investigation
- > **Consultoria Geotécnica**
Geotechnical Consultancy
- > **Obras Geotécnicas**
Ground Treatment-Construction Services
- > **Controlo e Observação**
Field Instrumentation Services and Monitoring Services
- > **Laboratório de Mecânica de Solos**
Soil and Rock Mechanics Laboratory

Certificada ISO 9001 por



Geocontrole



Parque Oriente, Bloco 4, EN10
2699-501 Bobadela LRS
Tel. 21 995 80 00
Fax. 21 995 80 01
e.mail: mail@geocontrole.pt
www.geocontrole.pt


Geocontrole
Geotecnia e Estruturas de Fundação SA



COBA



GEOLOGY AND GEOTECHNICS

Hydrogeology • Engineering Geology • Rock Mechanics • Soil Mechanics • Foundations and Retaining Structures • Underground Works • Embankments and Slope Stability
Environmental Geotechnics • Geotechnical Mapping



- Water Resources Planning and Management
- Hydraulic Undertakings
- Electrical Power Generation and Transmission
- Water Supply Systems and Pluvial and Wastewater Systems
- Agriculture and Rural Development
- Road, Railway and Airway Infrastructures
- Environment
- Geotechnical Structures
- Cartography and Cadastre
- Safety Control and Work Rehabilitation
- Project Management and Construction Supervision



PORTUGAL

CENTER AND SOUTH REGION
Av. 5 de Outubro, 323
1649-011 LISBOA
Tel.: (351) 210125000, (351) 217925000
Fax: (351) 217970348
E-mail: coba@coba.pt
www.coba.pt

Av. Marquês de Tomar, 9, 6.
1050-152 LISBOA
Tel.: (351) 217925000
Fax: (351) 213537492

NORTH REGION

Rua Mouzinho de Albuquerque, 744, 1.
4450-203 MATOSINHOS
Tel.: (351) 229380421
Fax: (351) 229373648
E-mail: engico@engico.pt

ANGOLA

Praceta Farinha Leitão, edifício nº 27, 27-A - 2º Dto
Bairro do Maculusso, LUANDA
Tel./Fax: (244) 222338 513
Cell: (244) 923317541
E-mail: coba-angola@netcabo.co.ao

MOZAMBIQUE

Pestana Rovuma Hotel. Centro de Escritórios.
Rua da Sé nº114. Piso 3, MAPUTO
Tel./Fax: (258) 21 328 813
Cell: (258) 82 409 9605
E-mail: coba.mz@tdm.co.mz

ALGERIA

09, Rue des Frères Hocine
El Biar - 16606, ARGEL
Tel.: (213) 21 922802
Fax: (213) 21 922802
E-mail: coba.alger@gmail.com

BRAZIL

Rio de Janeiro
COBA Ltd. - Rua Bela 1128
São Cristóvão
20930-380 Rio de Janeiro RJ
Tel.: (55 21) 351 50 101
Fax: (55 21) 258 01 026

Fortaleza

Av. Senador Virgílio Távora 1701, Sala 403
Aldeota - Fortaleza CEP 60170 - 251
Tel.: (55 85) 3261 17 38
Fax: (55 85) 3261 50 83
E-mail: coba@esc-te.com.br

UNITED ARAB EMIRATES

Corniche Road - Corniche Tower - 5th Floor - 5B
P. O. Box 38360 ABU DHABI
Tel.: (971) 2 627 0088
Fax: (971) 2 627 0087

Reliable solutions with **technology, quality,** and **innovation** for Civil Engineering proposes



MACCAFERRI POLIMAC

New polymeric coating with high performance
PoliMac™



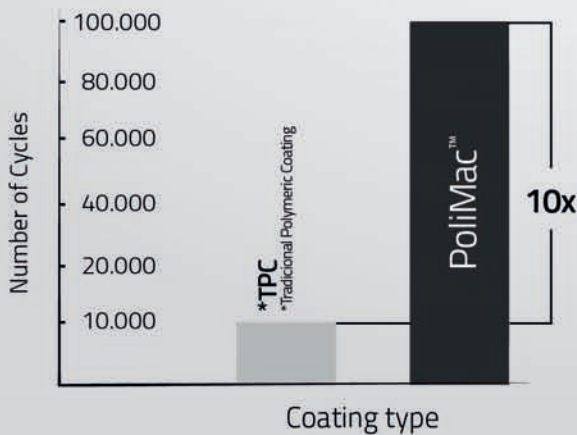
Long-life galvanising
GalMac® 4R

Intermetallic coating

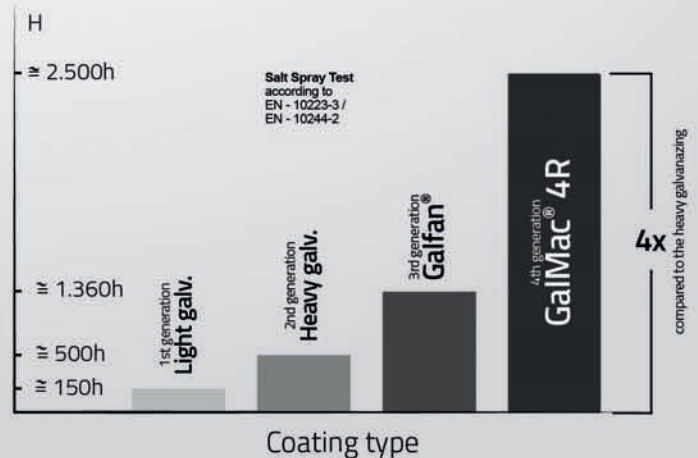
Steel wire LCC*
*Low Carbon Content



The **PoliMac™** in controlled abrasion resistance tests, it showed its excellent performance by resisting up to 100,000 cycles in the standard tests **ABNT NBR 7577** and **EN 10223-3**; about **10x more** than the traditional coating.



The **GalMac® 4R** coating complies with the main national and international standards such as: **EN 10223-3: 2013, ASTM B860** and **NBR 8964**.



Follow us on our **social media**



/maccaferri



/maccaferriatriz



@Maccaferri_BR



+MaccaferriWorld

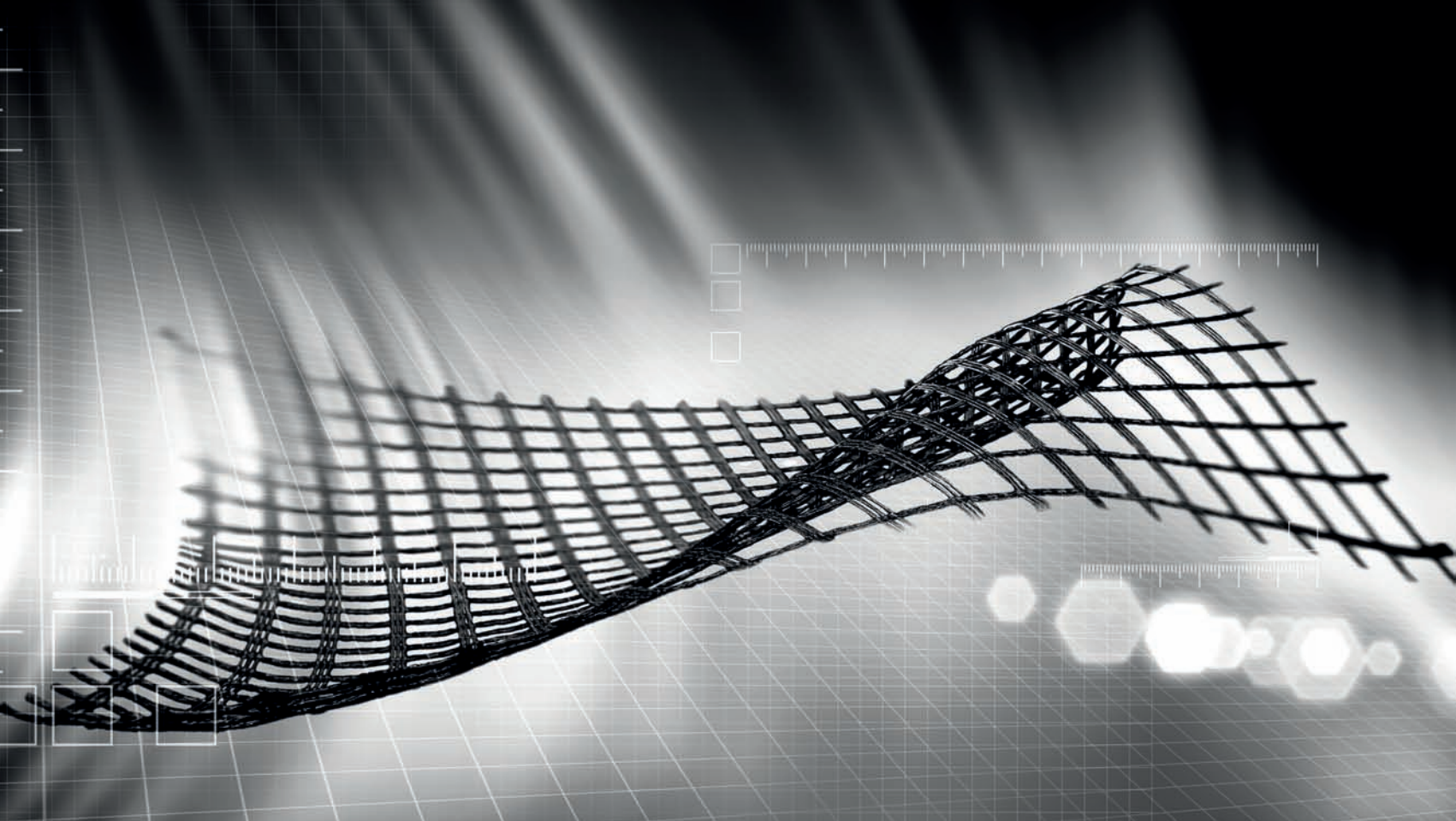


/maccaferriworld



MACCAFERRI

www.maccaferri.com/br



A strong, lasting connection.

With a history of over 150 years of pioneering in geosynthetics, we strive to create solutions for the most diverse engineering challenges.

Our business areas:



**Earthworks and
Foundations**



**Environmental
Engineering**



Roads and Pavements



Hydraulic Engineering

Talk to HUESKER Brasil:
www.HUESKER.com.br
HUESKER@HUESKER.com.br
+55 (12) 3903 9300

Follow HUESKER Brasil in social media:



HUESKER
Ideen. Ingenieure. Innovationen.

Instructions for Submission of Manuscripts

Category of the Papers

Soils and Rocks is the international scientific journal edited by the Brazilian Association for Soil Mechanics and Geotechnical Engineering (ABMS) and the Portuguese Geotechnical Society (SPG). The aim of the journal is to publish (in English) original research and technical works on all geotechnical branches.

According to its content the accepted paper is classified in one of the following categories: Article paper, Technical Note, Case Study or Discussion. An article paper is an extensive and conclusive dissertation about a geotechnical topic. A paper is considered as a technical note if it gives a short description of ongoing studies, comprising partial results and/or particular aspects of the investigation. A case study is a report of unusual problems found during the design, construction or the performance of geotechnical projects. A case study is also considered as the report of an unusual solution given to an ordinary problem. The discussions about published papers, case studies and technical notes are made in the Discussions Section.

When submitting a manuscript for review, the authors should indicate the category of the manuscript, and is also understood that they:

- assume full responsibility for the contents and accuracy of the information in the paper;
- assure that the paper has not been previously published, and is not being submitted to any other periodical for publication.

Manuscript Instructions

Manuscripts must be written in English. The text is to be typed in a word processor (preferably MS Word), **single column**, using ISO A4 page size, left, right, top, and bottom margins of 25 mm, Times New Roman 12 font, and line spacing of 1.5. All lines and pages should be numbered. The text should be written in the third person.

The first page of the manuscript must include the title of the paper followed by the names of the authors with the abbreviation of the most relevant academic title. The affiliation, address and e-mail must appear below each author's name. An abstract of 200 words follows after the author's names. A list with up to six keywords at the end of the abstract is required.

Although variations on the sequence and title of each section are possible, it is suggested that the text contains the following sections: Introduction, Material and Methods, Results, Discussions, Conclusions, Acknowledgements, References and List of Symbols. A brief description of each section is given next.

Introduction: This section should indicate the state of the art of the problem under evaluation, a description of the problem and the methods undertaken. The objective of the work should be clearly presented at the end of the section.

Materials and Methods: This section should include all information needed to the reproduction of the presented work by other researchers.

Results: In this section the data of the investigation should be presented in a clear and concise way. Figures and tables should not repeat the same information.

Discussion: The analyses of the results should be described in this section.

Conclusions: The content of this section should be based on the data and on the discussions presented.

Acknowledgements: If necessary, concise acknowledgements should be presented in this section.

References: References to other published sources must be made in the text by the last name(s) of the author(s), followed by the year of publication, similarly to one of the two possibilities below:

...while Silva & Pereira (1987) observed that resistance depended on soil density... or It was observed that resistance depended on soil density (Silva & Pereira, 1987).

In the case of three or more authors, the reduced format must be used, e.g.: Silva *et al.* (1982) or (Silva *et al.*, 1982). Two or more citations belonging to the same author(s) and published in the same year are to be distinguished with small letters, e.g.: (Silva, 1975a, b, c.). Standards must be cited in the text by the initials of the entity and the year of publication, e.g.: ABNT (1996), ASTM (2003).

Full references shall be listed alphabetically at the end of the text by the first author's last name. Several references belonging to the same author shall be cited chronologically. Some examples are listed next:

Papers: Bishop, A.W. & Blight, G.E. (1963). Some aspects of effective stress in saturated and unsaturated soils. *Geotechnique*, 13(2):177-197.

Books: Lambe, T.W. & Whitman, R.V. (1979). *Soil Mechanics*, SI Version. John Wiley & Sons, New York, 553 p.

Book with editors: Sharma, H.D.; Dukes, M.T. & Olsen, D.M. (1990). Field measurements of dynamic moduli and Poisson's ratios of refuse and underlying soils at a landfill site. Landva, A. & Knowles, G.D. (eds), *Geotechnics of Waste Fills - Theory and Practice*, American Society for Testing and Materials - STP 1070, Philadelphia, pp. 57-70.

Proceedings (printed matter or CD-ROM): Jamiolkowski, M.; Ladd, C.C.; Germaine, J.T. & Lancellotta, R. (1985). New developments in field and laboratory testing of soils. Proc. 11th Int. Conf. on Soil Mech. and Found. Engn., ISSMFE, San Francisco, v. 1, pp. 57-153. (specify if CD ROM).

Thesis and dissertations: Lee, K.L. (1965). *Triaxial Compressive Strength of Saturated Sands Under Seismic Loading Conditions*. PhD Dissertation, Department of Civil Engineering, University of California, Berkeley, 521 p.

Standards: ASTM (2003). *Standard Test Method for Particle Size Analysis of Soils - D 422-63*. ASTM International, West Conshohocken, Pennsylvania, USA, 8 p.

Internet references: Soils and Rocks available at <http://www.abms.com.br> and downloaded on August 6th 2003.

On line first publications must also bring the digital object identifier (DOI) at the end.

Figures shall be either computer generated or drawn with India ink on tracing paper. Computer generated figures must be accompanied by the corresponding digital file (.tif, .jpg, .pcx, etc.). All figures (graphs, line drawings, photographs, etc.) shall be numbered consecutively and have a caption consisting of the figure number and a brief title or description of the figure. This number should be used when referring to the figure in text. Photographs should be black and white, sharp, high contrasted and printed on glossy paper.

Tables shall be numbered consecutively in Arabic and have a caption consisting of the table number and a brief title. This number should be used when referring to the table in the text. Units should be indicated in the first line of the table, below the title of each column. Acronyms should be avoided. When applicable, the units should come right below the corresponding column heading. Additional comments can be placed as footnotes.

Equations shall appear isolated in a single line of the text. Numbers identifying equations must be flushed with the right margin. International System (SI) units must be used. The definitions of the symbols used in the

equations must appear in the List of Symbols. It is recommended that the symbols used are in accordance with Lexicon in 8 Languages, ISSMFE (1981) and the ISRM List of Symbols.

The text of the submitted manuscript (including figures, tables and references) intended to be published as an article paper or a case history should not contain more than 30 pages, formatted according to the instructions mentioned above. Technical notes and discussions should have no more than 15 and 8 pages, respectively. Longer manuscripts may be exceptionally accepted if the authors provide proper explanation for the need of the required extra space in a cover letter.

Discussion

Discussions must be written in English. The first page of a discussion should contain:

The title of the paper under discussion;

Name of the author(s) of the discussion, followed by their position, affiliation, address and e-mail. The author(s) of the discussion should refer to himself (herself/themselves) as the reader(s) and to the author(s) of the paper as the author(s).

Figures, tables and equations should be numbered following the same sequence of the original paper. All instructions previously mentioned for the preparation of article papers, case studies and technical notes also apply to the preparation of discussions.

Editorial Review

Each paper will be evaluated by reviewers selected by the editors according to the subject of the paper. The authors will be informed about the results of the review process. If the paper is accepted, the authors will be required to submit a version of the revised manuscript with the suggested modifications. If the manuscript is rejected for publication, the authors will be informed about the reasons for rejection. In any situation comprising modification of the original text, classification of the manuscript in a category different from that proposed by the authors, or rejection, the authors can reply presenting their reasons for disagreeing with the reviewer comments.

Submission

The author(s) must upload a digital file of the manuscript to the Soils and Rocks website.

Follow Up

The online management system will provide a password to the corresponding author, which will enable him/her to follow the reviewing process of the submitted manuscript at the Soils and Rocks website.

Volume 42, N. 2, May-August 2019**Table of Contents***ARTICLES*

- Progressive Mapping and Urban Growth: The Construction of Urbanization Suitability Map of Pelotas-Southern Brazil*
S.C. Xavier, L.A. Bressani 99
- Soil Elastic Modulus Determined by Ultrasound Tests*
W.S. Sarro, G.C.S. Ferreira 117
- Geotechnical Behavior and Soil-Fiber Interaction of Clayey Soil Mixed with Randomly Dispersed Coconut Fibers*
A.I. Oliveira Júnior, J.F.T. Jucá, J.A. Ferreira, L.C. Guilherme 127
- Geological-Geotechnical Characterization of Slopes Belonging to the Serra do Mar Paranaense, Brazil*
A.A.M. González, L.B. Passini, R.B. Boszczowski, A.C.M. Kormann, A.P. Fiori 139
- Investigating the Differences between Various Deterministic Liquefaction Correlation Methods*
E. El Kahi, M. Khouri 155
- Soil Classification System from Cone Penetration Test Data Applying Distance-Based Machine Learning Algorithms*
L.O. Carvalho, D.B. Ribeiro 167
- An Alternative Method to Estimate the Effective Energy During Pile Driving Based on Set and Elastic Rebound Records*
A. Querelli, F. Massad 179
- TECHNICAL NOTES*
- Biodegradation of Biodiesel in Laboratory and Field in a Clayey Residual Soil*
A. Thomé, A.W.S. Trentin, I. Cecchin, C. Reginato 193
- Dynamic Cone Penetrometer (DCP) relative density correlations for sands*
C.J. MacRobert, G.S. Bernstein, M.M. Nchabeleng 201